

Drivers of plant nutrient acquisition and allocation strategies and their influence  
on plant responses to environmental change

by

Evan A. Perkowski, B.S.

A Dissertation

In

Biological Sciences

Submitted to the Graduate Faculty  
of Texas Tech University in  
Partial Fulfillment of  
the Requirements for  
the Degree of

Doctor of Philosophy

Approved

Nicholas G. Smith, Ph.D.  
Chair of Committee

Aimée T. Classen, Ph.D.

Natasja van Gestel, Ph.D.

Lindsey C. Slaughter, Ph.D.

Dylan W. Schwilk, Ph.D.

Mark Sheridan, Ph.D.  
Dean of the Graduate School

May 2023

Copyright 2023, Evan A. Perkowski

## Acknowledgements

This dissertation was made possible by the mentorship, collaboration, and friendship of many people. I am so thankful to be surrounded by such supportive and helpful mentors, peers, and friends that have made navigating through graduate school and finishing this dissertation an enjoyable experience. Specifically, I am thankful for the incredible mentorship of my advisor and committee chair, Dr. Nick Smith, who provided invaluable insight and tools that have helped shape me into the plant ecophysiological I claim to be today. I am also indebted to my committee members, Drs. Aimée Classen, Natasja van Gestel, Dylan Schwilk, and Lindsey Slaughter, for useful feedback, invaluable support, and encouragement as I planned and implemented experiments.

I am also thankful for past and present members of the EcoHealth lab for encouragement, support, and extracurricular activities that made time inside and outside the lab enjoyable and memorable. Particular thanks go to Dr. Lizz Waring, Dr. Xiulin Gao, Helen Scott, and Risa McNellis, Billi Jean Petermann, and the late Dr. Kris Petterson, all of whom were invaluable to helping me navigate my first year. I am especially thankful for the mentorship and friendship of Dr. Lizz Waring, as our weekly coffee chats were instrumental for helping me feel welcome in Lubbock and acclimate to life as a graduate student. I am also grateful for the friendship of Billi Jean Petermann and the late Dr. Kris Petterson for their encouragement and willingness to discuss microbial symbioses over coffee on random Saturday mornings.

Additional thanks go out to Isa Beltran, Snehanjana Chatterjee, Jeff Chi-

eppa, Peter Eludini, Zinny Ezekannagha, Hannah German, Eve Gray, Monika Kelley, Azaj Mahmud, Jorge Ochoa, Brad Posch, Avery Schoenherr, Christine Vanginault, and Jose Villeda for help with experiments or for lending an ear over puzzling results. I am also thankful for collaborators Dr. Christy Goodale and Dave Frey, who provided invaluable insight for the second experimental chapter.

I would like to thank my undergraduate advisor, Dr. Janice Krumm, for continued mentorship and friendship and for insightful advice about navigating graduate school, but most of all for helping me realize my career aspirations and pushing me to pursue this endeavor. Additional thanks go out to my family, particularly my parents, partner, and dog for continued support and distractions outside the lab. The experiments included here would not have been possible without their emotional and monetary support.

This work was made possible from funding by the NSF, USDA, Braun and Gresham, PLLC., and was a contribution to the LEMONTREE (Land Ecosystem Models based On New Theory, obseRvations and ExperimEnts) project. The LEMONTREE project is funded through the generosity of Eric and Wendy Schmidt by recommendation of the Schmidt Futures programme and the Imperial College initiative on Grand Challenges in Ecosystems and the Environment. This work was also funded by graduate student research awards from Texas Tech University and the Botanical Society of America.

I have inevitably missed mentioning folks that were instrumental to the completion of these experiments and contributed to my development as a plant ecophysiological. Please know that I am grateful and appreciative of our interactions.

## Table of Contents

<b>Acknowledgements . . . . .</b>	ii
<b>Abstract . . . . .</b>	ix
<b>List of Tables . . . . .</b>	xi
<b>List of Figures . . . . .</b>	xv
<b>1. Introduction . . . . .</b>	1
<b>2. Structural carbon costs to acquire nitrogen are determined by nitrogen and light availability in two species with different nitrogen acquisition strategies . . . . .</b>	7
2.1    Introduction . . . . .	7
2.2    Methods . . . . .	11
2.2.1 <i>Experiment setup</i> . . . . .	11
2.2.2 <i>Plant measurements and calculations</i> . . . . .	12
2.2.3 <i>Statistical analyses</i> . . . . .	13
2.3    Results . . . . .	15
2.3.1 <i>Carbon costs to acquire nitrogen</i> . . . . .	15
2.3.2 <i>Whole plant nitrogen biomass</i> . . . . .	18
2.3.3 <i>Root carbon biomass</i> . . . . .	20
2.3.4 <i>Root nodule biomass</i> . . . . .	22
2.4    Discussion . . . . .	26
2.4.1 <i>Carbon costs to acquire nitrogen increase with light availability and decrease with fertilization</i> . . . . .	26
2.4.2 <i>Modeling implications</i> . . . . .	28
2.4.3 <i>Study limitations</i> . . . . .	30
2.4.4 <i>Conclusions</i> . . . . .	32
<b>3. Soil nitrogen availability modifies leaf nitrogen economies in mature temperate deciduous forests: a direct test of photosynthetic least-cost theory . . . . .</b>	34
3.1    Introduction . . . . .	34

3.2	Methods	38
3.2.1	<i>Study site description</i>	38
3.2.2	<i>Experimental design</i>	39
3.2.3	<i>Leaf gas exchange and trait measurements</i>	39
3.2.4	$A_{net}/C_i$ curve-fitting and parameter estimation	42
3.2.5	<i>Proportion of leaf nitrogen allocated to photosynthesis and structure</i>	44
3.2.6	<i>Tradeoffs between nitrogen and water use</i>	45
3.2.7	<i>Soil nitrogen availability and pH</i>	46
3.2.8	<i>Statistical analyses</i>	48
3.3	Results	50
3.3.1	<i>Leaf nitrogen content</i>	50
3.3.2	<i>Net photosynthesis and leaf biochemistry</i>	53
3.3.3	<i>Leaf nitrogen allocation</i>	56
3.3.4	<i>Tradeoffs between nitrogen and water use</i>	59
3.4	Discussion	62
3.4.1	<i>Soil nitrogen availability modifies tradeoffs between nitrogen and water use</i>	63
3.4.2	<i>Soil pH did not modify tradeoffs between nitrogen and water usage</i>	65
3.4.3	<i>Species identity explains a large amount of variation in leaf and whole plant traits</i>	66
3.4.4	<i>Implications for photosynthetic least-cost theory model development</i>	67
3.4.5	<i>Conclusions</i>	69
4.	<b>The relative cost of resource use for photosynthesis drives variance in leaf nitrogen content across a climate and soil resource availability gradient</b>	70
4.1	Introduction	70
4.2	Methods	76
4.2.1	<i>Site descriptions and sampling methodology</i>	76

4.2.2 <i>Leaf trait measurements</i>	77
4.2.3 <i>Site climate data</i>	82
4.2.4 <i>Site edaphic characteristics</i>	82
4.2.5 <i>Plant functional group assignments</i>	84
4.2.6 <i>Data analysis</i>	85
4.3 Results	88
4.3.1 <i>Cost to acquire nitrogen relative to water</i>	88
4.3.2 <i>Leaf <math>C_i:C_a</math></i>	92
4.3.3 <i>Leaf nitrogen content</i>	95
4.3.4 <i>Structural equation model</i>	99
4.4 Discussion	102
4.4.1 <i>Negative effects of leaf <math>C_i:C_a</math> on <math>N_{area}</math> are driven by reductions in <math>M_{area}</math>, not <math>N_{mass}</math></i>	102
4.4.2 <i>Soil nitrogen availability increases <math>N_{area}</math> through changes in <math>\beta</math></i>	104
4.4.3 <i>Soil moisture increases <math>N_{area}</math> by facilitating increases in soil nitrogen availability</i>	105
4.4.4 <i>Indirect effects of climate on <math>N_{area}</math> are mediated through changes in leaf <math>C_i:C_a</math> and <math>\beta</math></i>	106
4.4.5 <i>Species identity traits modify effects of the environment on <math>\beta</math>, leaf <math>C_i:C_a</math>, and <math>N_{area}</math></i>	107
4.4.6 <i>Next steps for optimality model development</i>	108
4.4.7 <i>Conclusions</i>	109
5. Optimal resource investment to photosynthetic capacity maximizes nutrient allocation to whole plant growth under elevated CO <sub>2</sub>	111
5.1 Introduction	111
5.2 Methods	116
5.2.1 <i>Seed treatments and experimental design</i>	116
5.2.2 <i>Growth chamber conditions</i>	117
5.2.3 <i>Leaf gas exchange measurements</i>	119

5.2.4 <i>Leaf trait measurements</i> . . . . .	120
5.2.5 <i>A/C<sub>i</sub> curve fitting and parameter estimation</i> . . . . .	122
5.2.6 <i>Stomatal limitation</i> . . . . .	123
5.2.7 <i>Proportion of leaf nitrogen allocated to photosynthesis and structure</i> . . . . .	123
5.2.8 <i>Whole plant traits</i> . . . . .	125
5.2.9 <i>Statistical analyses</i> . . . . .	127
5.3 Results . . . . .	129
5.3.1 <i>Leaf nitrogen and chlorophyll content</i> . . . . .	129
5.3.2 <i>Leaf biochemistry and stomatal conductance</i> . . . . .	133
5.3.3 <i>Leaf nitrogen allocation</i> . . . . .	137
5.3.4 <i>Whole plant traits</i> . . . . .	141
5.3.5 <i>Nitrogen fixation</i> . . . . .	145
5.4 Discussion . . . . .	149
5.4.1 <i>Soil nitrogen fertilization has divergent effects on leaf and whole plant acclimation responses to CO<sub>2</sub></i> . . . . .	150
5.4.2 <i>Implications for future model development</i> . . . . .	153
5.4.3 <i>Study limitations and future directions</i> . . . . .	155
5.4.4 <i>Conclusions</i> . . . . .	156
6. Conclusions . . . . .	158
References . . . . .	168
Appendix A: Supplemental material for "Structural carbon costs to acquire nitrogen are determined by nitrogen and light availability in two species with different nitrogen acquisition strategies" . . . . .	205
Appendix B: Supplemental material for "Soil nitrogen availability modifies leaf nitrogen economies in mature temperate deciduous forests: a direct test of photosynthetic least-cost theory" . . . . .	209

<b>Appendix C: Supplemental material for "The relative cost of resource use for photosynthesis drives variance in leaf nitrogen content across a climate and soil resource availability gradient" . . . . .</b>	<b>214</b>
<b>Appendix D: Supplemental material for "Optimal resource investment to photosynthetic capacity maximizes nutrient allocation to whole plant growth under elevated CO<sub>2</sub>" . . .</b>	<b>220</b>

## Abstract

Photosynthesis is the largest carbon flux between the atmosphere and is constrained by ecosystem carbon and nutrient cycle dynamics, which causes terrestrial biosphere models to be sensitive to the formulation of photosynthetic processes. Terrestrial biosphere models exhibit high divergence in simulated carbon and nitrogen fluxes under future environmental conditions, which may be due to uncertainty in the acclimation response of photosynthetic processes to environmental change. Photosynthetic least-cost theory provides a promising framework for understanding effects of climatic and edaphic factors on photosynthetic acclimation responses to changing environments. Yet, empirical tests of the theory are rare, limiting our ability to assess whether the theory is suitable for implementation in next-generation terrestrial biosphere models.

Here, I present four experiments designed to test assumptions of photosynthetic least-cost theory. Experiment chapters are flanked by a general introduction chapter and conclusions chapter. The first experimental chapter quantifies structural carbon costs to acquire nitrogen in *Glycine max* and *Gossypium hirsutum* grown under four nitrogen fertilization levels and four light availability levels in a full factorial greenhouse experiment. I find that carbon costs to acquire nitrogen in both species increase with increasing light availability and decrease with increasing fertilization, though responses to fertilization in *G. max* were markedly less than *G. hirsutum*. The second experimental chapter quantifies leaf nitrogen and photosynthetic traits in upper canopy leaves of deciduous trees growing in a 9-year nitrogen-by-sulfur field manipulation experiment. I find strong evi-

dence for nitrogen-water use tradeoffs with increasing soil nitrogen availability, evidenced through a strong negative relationship between leaf nitrogen content and leaf  $C_i:C_a$  and stronger increase in leaf nitrogen content with increasing soil nitrogen availability than leaf  $C_i:C_a$ . The third experiment investigates variance in leaf nitrogen content across a climate and soil resource availability gradient in Texan grasslands, showing that effects of soil resource availability and climate on leaf nitrogen content are driven by changes in leaf  $C_i:C_a$ . Finally, the fourth experiment quantifies leaf and whole plant acclimation responses in *G. max* grown under two atmospheric CO<sub>2</sub> levels, with and without inoculation with *Bradyrhizobium japonicum*, and across nine nitrogen fertilization treatments in a full factorial growth chamber experiment. I find that leaf acclimation responses to CO<sub>2</sub> were independent of soil nitrogen fertilization or inoculation treatment, though stimulations in whole plant growth under elevated CO<sub>2</sub> were enhanced with increasing soil nitrogen fertilization and in inoculated pots under low nitrogen fertilization.

Experiments included in this dissertation provide consistent support for patterns expected from photosynthetic least-cost theory. The use of multiple experimental approaches allowed me to examine mechanisms driving patterns expected from the theory and investigate whether these patterns occur in the field across environmental gradients. Findings from these chapters challenge common paradigms in plant ecophysiology, providing empirical evidence suggesting that including photosynthetic least-cost frameworks in terrestrial biosphere models may improve the longstanding observed divergence in simulated outcomes across terrestrial biosphere model products.

## List of Tables

2.1	Analysis of variance results exploring species-specific effects of light availability, nitrogen fertilization, and their interactions on carbon costs to acquire nitrogen, whole-plant nitrogen biomass, and root carbon biomass . . . . .	16
2.2	Analysis of variance results exploring effects of light availability, nitrogen fertilization, and their interactions on <i>G. max</i> root nodule biomass and the ratio of root nodule biomass to root biomass . . . . .	23
2.3	Slopes of the regression line describing the relationship between each dependent variable and nitrogen fertilization at each light level	24
3.1	Effects of soil nitrogen availability, soil pH, and species on leaf nitrogen content per unit leaf area, leaf nitrogen content per unit leaf mass, and leaf mass per unit leaf area . . . . .	51
3.2	Effects of soil nitrogen availability, soil pH, species, and $N_{\text{area}}$ on net photosynthesis, the maximum rate of Rubisco carboxylation, the maximum rate of RuBP regeneration, and the ratio of the maximum rate of RuBP regeneration to the maximum rate of Rubisco carboxylation . . . . .	54
3.3	Effects of soil nitrogen availability, soil pH, and species on the proportion of leaf nitrogen content allocated to photosynthesis, Rubisco, bioenergetics, and structure . . . . .	57

3.4 Effects of soil nitrogen availability, soil pH, species, and $N_{\text{area}}$ on $\chi$ , photosynthetic nitrogen use efficiency, leaf nitrogen content per unit $\chi$ , and maximum Rubisco carboxylation rate per unit $\chi$ . . . . .	60
4.1 Site locality information, sampling year, 2006-2020 mean annual precipitation, mean annual temperature, and water holding capacity	80
4.2 Effects of soil moisture, soil nitrogen availability, and plant functional group on $\beta$ . . . . .	89
4.3 Effects of soil moisture, soil nitrogen availability, and plant functional group on leaf $C_i:C_a$ . . . . .	93
4.4 Effects of soil moisture, soil nitrogen availability, plant functional group, and leaf $C_i:C_a$ on leaf nitrogen content per unit leaf area, leaf nitrogen content per unit leaf biomass, and leaf biomass per unit leaf area . . . . .	97
4.5 Structural equation model results investigating direct effects of climatic and soil resource availability on leaf nitrogen content . . . . .	100
5.1 Effects of soil nitrogen fertilization, inoculation, and $\text{CO}_2$ treatments on leaf nitrogen content per unit leaf area, leaf nitrogen content per unit leaf mass, leaf mass per unit leaf area, and chlorophyll content per unit leaf area . . . . .	131

5.2	Effects of soil nitrogen fertilization, inoculation, and CO <sub>2</sub> on the maximum rate of Rubisco carboxylation, the maximum rate of RuBP regeneration, dark respiration, the ratio of the maximum rate of RuBP regeneration to the maximum rate of Rubisco carboxylation, stomatal conductance, and stomatal limitation . . . . .	135
5.3	Effects of soil nitrogen fertilization, inoculation, and CO <sub>2</sub> on the fraction of leaf nitrogen allocated to Rubisco, bioenergetics, light harvesting proteins, photosynthesis, and structure . . . . .	139
5.4	Effects of CO <sub>2</sub> , fertilization, and inoculation on total leaf area, whole plant biomass, carbon costs to acquire nitrogen, belowground carbon biomass, and whole plant nitrogen biomass . . . . .	143
5.5	Effects of CO <sub>2</sub> , fertilization, and inoculation on root nodule biomass, plant investments in symbiotic nitrogen fixation, and percent nitrogen fixed from the atmosphere . . . . .	147
A1	Summary table containing volumes of compounds used to create modified Hoagland's solutions for each soil nitrogen fertilization treatment . . . . .	205
A2	Analysis of variance results exploring species-specific effects of light availability, nitrogen fertilization, and their interactions on the ratio of whole plant biomass to pot volume . . . . .	206
A3	Slopes of the regression line describing the relationship between each dependent variable and nitrogen fertilization at each light level	207

B1	Sample sizes of each species, abbreviated by their USDA NRCS PLANTS database code, within each plot at each site . . . . .	209
B2	Analysis of variance results exploring the linear effect of leaf temperature on net photosynthesis rate and stomatal conductance measured at 400 $\mu\text{mol mol}^{-1}$ CO <sub>2</sub> . . . . .	210
B3	Second order log-polynomial regression coefficients that described the effect of leaf temperature on net photosynthesis and stomatal conductance measured at 400 $\mu\text{mol mol}^{-1}$ CO <sub>2</sub> . . . . .	211
B4	Mean, standard error, and 95% confidence interval ranges of soil nitrogen availability estimates across all measured plots . . . . .	212
C1	List of sampled species and their plant functional group assignment	216
C2	List of sampled species and their plant functional group assignment (cont.) . . . . .	217
C3	Model selection results for soil moisture and vapor pressure deficit	218
D1	Summary table containing volumes of compounds used to create modified Hoagland's solutions for each soil nitrogen fertilization treatment . . . . .	220
D2	Summary of the daily growth chamber growing condition program	221
D3	Effects of CO <sub>2</sub> , fertilization, and inoculation on whole plant biomass: pot volume . . . . .	222

## List of Figures

2.1 Relationships between soil nitrogen fertilization and light availability on carbon costs to acquire nitrogen in <i>G. hirsutum</i> and <i>G. max</i> . . . . .	17
2.2 Relationships between soil nitrogen fertilization and light availability on whole-plant nitrogen biomass in <i>G. hirsutum</i> and <i>G. max</i> . . . . .	19
2.3 Relationships between soil nitrogen fertilization and light availability on root carbon biomass in <i>G. hirsutum</i> and <i>G. max</i> . . . . .	21
2.4 Effects of shade cover and nitrogen fertilization on root nodule biomass and the ratio of root nodule biomass to root biomass in <i>G. max</i> . . . . .	25
3.1 Effects of soil nitrogen availability and species on leaf nitrogen content per unit leaf area, leaf nitrogen content per unit leaf biomass, and leaf mass per leaf area . . . . .	52
3.2 Effects of soil nitrogen availability, species, and leaf nitrogen content on net photosynthesis, maximum Rubisco carboxylation rate, and maximum RuBP regeneration rate . . . . .	55
3.3 Effects of soil nitrogen availability, species, and leaf nitrogen content on the fraction of leaf nitrogen allocated to photosynthesis and structure . . . . .	58
3.4 Effects of soil N availability, species, and leaf N content on tradeoffs between nitrogen and water use . . . . .	61

4.1	Site locations along 2006-2020 mean annual precipitation and mean annual temperature gradients in Texas, USA. . . . .	81
4.2	Effects of soil nitrogen availability and soil moisture on the cost of acquiring and using nitrogen . . . . .	91
4.3	Effects of 4-day mean vapor pressure deficit, 2-day soil moisture (per water holding capacity), and soil nitrogen availability on leaf $C_i:C_a$ . . . . .	94
4.4	Effects of leaf $C_i:C_a$ , soil nitrogen availability, and soil moisture on leaf nitrogen content per unit leaf area, leaf nitrogen content per unit leaf biomass, and leaf mass per area. . . . .	98
4.5	Structural equation model results exploring drivers of $N_{\text{area}}$ . . . .	101
5.1	Effects of $\text{CO}_2$ , fertilization, and inoculation on leaf nitrogen per unit leaf area, leaf nitrogen content, leaf mass per unit leaf area, and chlorophyll content per unit leaf area . . . . .	132
5.2	Effects of $\text{CO}_2$ , fertilization, and inoculation on maximum rate of Rubisco carboxylation, the maximum rate of RuBP regeneration, and the ratio of the maximum rate of RuBP regeneration to the maximum rate of Rubisco carboxylation leaf mass per unit leaf area, dark respiration, stomatal conductance, and stomatal limitation .	136
5.3	Effects of $\text{CO}_2$ , fertilization, and inoculation on the relative fraction of leaf nitrogen allocated to photosynthesis and the fraction of leaf nitrogen allocated to structure . . . . .	140

5.4	Effects of CO <sub>2</sub> , fertilization, and inoculation on total leaf area, total biomass, and structural carbon costs to acquire nitrogen . . . . .	144
5.5	Effects of CO <sub>2</sub> , fertilization, and inoculation on nodule biomass, nodule biomass: root biomass, and percent nitrogen fixed from the atmosphere . . . . .	148
A1	Effects of shade cover and nitrogen fertilization on the ratio of plant biomass to rooting volume in <i>G. hirsutum</i> and <i>G. max</i> . . . . .	208
B1	Effects of leaf temperature on net photosynthesis rate and stomatal conductance values when measured at 400 μmol mol <sup>-1</sup> CO <sub>2</sub> . . .	213
C1	Model selection results exploring relevant timescales for soil moisture and vapor pressure deficit . . . . .	219
D1	Relationships between area-based leaf nitrogen content, mass-based leaf nitrogen content, and leaf mass per unit leaf area measured on the focal leaf used to generate $A_{\text{net}}/C_i$ curves and leaf nitrogen content measured on the leaf used for chlorophyll extractions . . .	223
D2	Effects of CO <sub>2</sub> , fertilization, and inoculation on the ratio of whole plant biomass to pot volume . . . . .	224

1                             **Chapter 1**  
2                             **Introduction**

3       Photosynthesis represents the largest carbon flux between the atmosphere  
4   and biosphere, and is regulated by complex ecosystem carbon and nutrient cy-  
5   cles (Hungate et al. 2003; IPCC 2021). As a result, the inclusion of robust,  
6   empirically tested representations of photosynthetic processes is critical in order  
7   for terrestrial biosphere models to accurately and reliably simulate carbon and  
8   nutrient fluxes between the atmosphere and terrestrial biosphere (Oreskes et al.  
9   1994; Smith and Dukes 2013; Prentice et al. 2015; Wieder et al. 2015). De-  
10   spite evidence that the inclusion of coupled carbon and nutrient cycles can reduce  
11   model uncertainty, widespread divergence in predicted carbon and nutrient fluxes  
12   is still apparent across model products (Friedlingstein et al. 2014; Arora et al.  
13   2020; Davies-Barnard et al. 2020). Divergence in predicted carbon and nutrient  
14   fluxes across terrestrial biosphere models may be due to an incomplete under-  
15   standing of how plants acclimate to changing environments (Smith and Dukes  
16   2013; Davies-Barnard et al. 2020), as terrestrial biosphere models are sensitive to  
17   the formulation of photosynthetic processes (Bonan et al. 2011; Ziehn et al. 2011;  
18   Booth et al. 2012; Smith et al. 2016; Smith et al. 2017; Rogers et al. 2017).

19       Many terrestrial biosphere models predict leaf-level photosynthesis through  
20   linear relationships between area-based leaf nitrogen content and the maximum  
21   rate of Ribulose-1,5-bisphosphate carboxylase/oxygenase (“Rubisco”), following  
22   the idea that large fractions of leaf nitrogen content are allocated to the con-  
23   struction and maintenance of Rubisco and other photosynthetic enzymes (Evans

24 1989). The inclusion of coupled carbon and nutrient cycles in terrestrial bio-  
25 sphere models (Shi et al. 2016; Braghieri et al. 2022) allows for the prediction  
26 of leaf nitrogen content through soil nitrogen availability, which causes models to  
27 indirectly predict photosynthetic processes through shifts in soil nitrogen avail-  
28 ability (Smith et al. 2014; Lawrence et al. 2019). While these patterns are  
29 commonly observed in ecosystems globally (Brix 1971; Evans 1989; Firn et al.  
30 2019; Liang et al. 2020), this formulation does not allow for the prediction of  
31 leaf and whole plant acclimation responses to changing environments (Smith and  
32 Dukes 2013; Rogers et al. 2017; Harrison et al. 2021), and suggests that constant  
33 leaf nitrogen-photosynthesis relationships are ubiquitous across ecosystems.

34 Photosynthetic least-cost theory (Prentice et al. 2014; Wang et al. 2017;  
35 Smith et al. 2019; Paillassa et al. 2020; Scott and Smith 2022; Harrison et al.  
36 2021) provides a framework for predicting leaf and whole plant acclimation re-  
37 sponds to environmental change. The theory, which unifies optimal coordination  
38 (Chen et al. 1993; Maire et al. 2012) and least-cost (Wright et al. 2003) theories,  
39 posits that plants optimize photosynthetic processes by minimizing the summed  
40 cost of nutrient and water use (i.e.,  $\beta$ ). The summed cost of nutrient and water  
41 use is predicted to be positively correlated with the ratio of intercellular CO<sub>2</sub> to  
42 atmospheric CO<sub>2</sub> (leaf C<sub>i</sub>:C<sub>a</sub>). Leaf C<sub>i</sub>:C<sub>a</sub> is determined by factors that influ-  
43 ence leaf nutrient demand, such as CO<sub>2</sub>, temperature, vapor pressure deficit, and  
44 light availability (Prentice et al. 2014; Wang et al. 2017; Smith et al. 2019;  
45 Stocker et al. 2020), and may change in response to changing edaphic charac-  
46 teristics through changes in  $\beta$  (Paillassa et al. 2020). Photosynthetic processes  
47 are optimized such that nutrients and water are allocated to photosynthetic en-

48 zymes to allow net photosynthesis rates to be equally co-limited by the maximum  
49 rate of Rubisco carboxylation and the maximum rate of Ribulose-1,5-bisphosphate  
50 (RuBP) regeneration (Chen et al. 1993; Maire et al. 2012). The theory indicates  
51 that costs of nutrient and water use are substitutable such that, in a given en-  
52 vironment, optimal photosynthesis rates can be achieved by sacrificing inefficient  
53 use of a relatively more abundant (and less costly to acquire) resource for more  
54 efficient use of a relatively less abundant (and more costly to acquire) resource.

55 [DWS: a ton of passive voice through here]

56 Optimality models leveraging [?? how does a model leverage something?] patterns expected from photosynthetic least-cost theory have been developed for both C<sub>3</sub> (Wang et al. 2017; Smith et al. 2019; Stocker et al. 2020) and more recently for C<sub>4</sub> species (Scott and Smith 2022). Such models show broad agreement with patterns observed across environmental gradients (Smith et al. 2019; Stocker et al. 2020; Paillassa et al. 2020; Querejeta et al. 2022; Westerband et al. 2023), and are capable of reconciling dynamic leaf nitrogen-photosynthesis relationships and acclimation responses to elevated CO<sub>2</sub>, temperature, light availability, and vapor pressure deficit (Dong et al. 2017; Dong et al. 2020; Smith and Keenan 2020; Luo et al. 2021; Peng et al. 2021; Dong et al. 2022; Dong et al. 2022; Querejeta et al. 2022; Westerband et al. 2023). Current versions of optimality models that invoke patterns expected from photosynthetic least-cost theory hold  $\beta$  constant across growing environments. As growing evidence suggests that costs of nutrient use change across resource availability and climatic gradients in species with different nutrient acquisition strategies (Fisher et al. 2010; Brzostek et al. 2014; Terrer et al. 2018; Allen et al. 2020), one might expect that  $\beta$  should

72 dynamically change across environments and in species with different nutrient  
73 acquisition strategies.

74 [DWS: Sort of fuzzy on what source of variation and “change” is... eco-  
75 typic? plastic?]

76 Despite recent recognition that patterns expected from photosynthetic  
77 least-cost theory occur across broad environmental gradients, [DWS: “despite?”]  
78 a limited number of studies have investigated how  $\beta$  varies across edaphic and  
79 climatic gradients and how variance in  $\beta$  might scale to influence leaf nutrient-  
80 water use tradeoffs (Lavergne et al. 2020; Paillassa et al. 2020). Furthermore, no  
81 previous study has investigated whether  $\beta$  varies in species with different nutrient  
82 acquisition strategies, or if changes in  $\beta$  due to changes in edaphic characteristics  
83 scale to influence leaf or whole plant acclimation responses to changing environ-  
84 ments. The lack of such studies provided motivation for the experimental chapters  
85 included in this dissertation.

86 In this dissertation, I use a combination of greenhouse, field manipula-  
87 tion, environmental gradient, and growth chamber experiments to quantify leaf  
88 and whole plant acclimation responses across various climatic and edaphic con-  
89 ditions and [DWS; species represnting?] different nutrient acquisition strategies.  
90 Together, these experiments evaluate patterns expected from photosynthetic least-  
91 cost theory and test mechanisms predicted to drive responses expected from the-  
92 ory. The empirical data collected in these experiments provide important infor-  
93 mation needed to refine existing optimality models that include photosynthetic  
94 least-cost frameworks, and could help determine whether such models are suitable  
95 for implementing in next-generation terrestrial biosphere models. While theory

96 suggests that plants acclimate across environments by minimizing the summed  
97 cost of nutrients relative to water, I chose to isolate effects of soil nitrogen avail-  
98 ability on costs of nitrogen acquisition relative to water for the sake of brevity. I  
99 acknowledge that patterns expected from theory may be modified by other nu-  
100 trients (e.g., phosphorus) or other edaphic characteristics (Smith et al. 2019;  
101 Paillassa et al. 2020; Westerband et al. 2023), and, though not included here,  
102 should also be investigated.

103 In the first experimental chapter, I re-analyze data from a greenhouse ex-  
104 periment that grew *Glycine max* and *Gossypium hirsutum* seedlings under full-  
105 factorial combinations of four light treatments and four fertilization treatments  
106 to examine effects of nitrogen and light availability on structural carbon costs to  
107 acquire nitrogen. In the second experimental chapter, I measure leaf physiological  
108 traits in the upper canopy of mature trees growing in a 9-year nitrogen-by-pH  
109 field manipulation experiment to assess whether changes in soil nitrogen availabil-  
110 ity or soil pH modify nitrogen-water use trade-offs expected from photosynthetic  
111 least-cost theory. The third experimental chapter leverages a broad precipitation  
112 and soil nitrogen availability gradient in Texan grasslands to investigate primary  
113 drivers of leaf nitrogen content. In the fourth experimental chapter, I use growth  
114 chambers to quantify leaf and whole plant acclimation responses to CO<sub>2</sub> across  
115 a soil nitrogen fertilization gradient, while also manipulating nutrient acquisition  
116 strategy by controlling whether seedlings were able to form associations with sym-  
117 biotic nitrogen-fixing bacteria.

118 Across experiments, I find strong and consistent support for patterns ex-  
119 pected from photosynthetic least-cost theory, showing that shifts in edaphic char-

120 characteristics predictably alter  $\beta$ , and that shifts in  $\beta$  facilitate changes in leaf  
121 nitrogen-water use tradeoffs and leaf nitrogen-photosynthesis relationships. I also  
122 show that costs of nitrogen acquisition vary in species with different nitrogen  
123 acquisition strategies. Finally, I show strong evidence suggesting that leaf accli-  
124 mation responses to elevated CO<sub>2</sub> are decoupled from soil nitrogen availability and  
125 inoculation with symbiotic nitrogen-fixing bacteria. It is my hope that these ex-  
126 periments will encourage future iterations of optimality models that adopt photo-  
127 synthetic least-cost frameworks to consider frameworks for implementing dynamic  
128  $\beta$  values across soil resource availability gradients and in species with different nu-  
129 trient acquisition strategies.

130 The four experimental chapters included in this dissertation are presented  
131 either as previously published journal articles or as manuscript drafts currently  
132 in preparation for journal submission. Specifically, the first experimental chapter  
133 was published in *Journal of Experimental Botany* in 2021 and the second chapter  
134 is currently in review, while the third and fourth chapters are each in preparation  
135 for journal submission. The dissertation concludes with a sixth chapter that sum-  
136 marizes experiment findings, briefly synthesizes common themes observed across  
137 experiments, and provides some suggestions for future experimentation.

138

## Chapter 2

139

140      Structural carbon costs to acquire nitrogen are determined by  
141      nitrogen and light availability in two species with different nitrogen  
              acquisition strategies

142      Perkowski EA, EF Waring, NG Smith, "Root mass carbon costs to acquire nitro-  
143      gen are determined by nitrogen and light availability in two species with different  
144      nitrogen acquisition strategies", *Journal of Experimental Botany*, 2021, Volume  
145      72, Issue 15, Pages 5766-5776, by permission of Oxford University Press

146      2.1 Introduction

147      Carbon and nitrogen cycles are tightly coupled in terrestrial ecosystems. This  
148      tight coupling influences photosynthesis (Walker et al. 2014; Rogers et al. 2017),  
149      net primary productivity (LeBauer and Treseder 2008; Thomas et al. 2013), de-  
150      composition (Cornwell et al. 2008; Bonan et al. 2013; Sulman et al. 2019), and  
151      plant resource competition (Gill and Finzi 2016; Xu-Ri and Prentice 2017). Ter-  
152      restrial biosphere models are beginning to include connected carbon and nitrogen  
153      cycles to improve the realism of their simulations (Fisher et al. 2010; Brzostek  
154      et al. 2014; Wieder et al. 2015; Shi et al. 2016; Zhu et al. 2019). Simula-  
155      tions from these models indicate that coupling carbon and nitrogen cycles can  
156      drastically influence future biosphere-atmosphere feedbacks under global change,  
157      such as elevated carbon dioxide or nitrogen deposition (Thornton et al. 2007;  
158      Goll et al. 2012; Wieder et al. 2015; Wieder et al. 2019). Nonetheless, there  
159      are still limitations in our quantitative understanding of connected carbon and  
160      nitrogen dynamics (Thomas et al. 2015; Meyerholt et al. 2016; Rogers et al.  
161      2017; Exbrayat et al. 2018; Shi et al. 2019), forcing models to make potentially  
162      unreliable assumptions.

163 Plant nitrogen acquisition is a process in terrestrial ecosystems by which  
164 carbon and nitrogen are tightly coupled (Vitousek and Howarth 1991; Delaire  
165 et al. 2005; Brzostek et al. 2014) [dWS: redundant with above]. Plants must  
166 allocate photosynthetically derived [DWS: as opposed to?] carbon belowground  
167 to produce and maintain root systems or exchange with symbiotic soil microbes in  
168 order to acquire nitrogen (Högberg et al. 2008; Högberg et al. 2010). Thus, plants  
169 have an inherent carbon cost associated with acquiring nitrogen, which can include  
170 both direct energetic costs associated with nitrogen acquisition and indirect costs  
171 associated with building structures that support nitrogen acquisition (Gutschick  
172 1981; Rastetter et al. 2001; Vitousek et al. 2002; Menge et al. 2008). [DWS: You  
173 make this sound more complicated than it is. It is just good old allocation]. Model  
174 simulations (Fisher et al. 2010; Brzostek et al. 2014; Shi et al. 2016; Allen et al.  
175 2020) and meta-analyses (Terrer et al. 2018) suggest that these carbon costs vary  
176 between species, particularly those with different nitrogen acquisition strategies.  
177 For example, simulations using iterations of the Fixation and Uptake of Nitrogen  
178 (FUN) model indicate that species that acquire nitrogen from non-symbiotic active  
179 uptake pathways (e.g. mass flow) generally have larger carbon costs to acquire  
180 nitrogen than species that acquire nitrogen through symbiotic associations with  
181 nitrogen-fixing bacteria (Brzostek et al. 2014; Allen et al. 2020).

182 Carbon costs to acquire nitrogen likely vary in response to changes in soil  
183 nitrogen availability. For example, if the primary mode of nitrogen acquisition  
184 is through non-symbiotic active uptake, then nitrogen availability could decrease  
185 carbon costs to acquire nitrogen as a result of increased per-root nitrogen up-  
186 take (Franklin et al. 2009; Wang et al. 2018). However, if the primary mode of

187 nitrogen acquisition is through symbiotic active uptake, then nitrogen availabil-  
188 ity may incur additional carbon costs to acquire nitrogen if it causes microbial  
189 symbionts to shift toward parasitism along the parasitism–mutualism continuum  
190 (Johnson et al. 1997; Hoek et al. 2016; Friel and Friesen 2019) or if it reduces  
191 the nitrogen acquisition capacity of a microbial symbiont (van Diepen et al. 2007;  
192 Soudzilovskaia et al. 2015; Muñoz et al. 2016). Species may respond to shifts in  
193 soil nitrogen availability by switching their primary mode of nitrogen acquisition  
194 to a strategy with lower carbon costs to acquire nitrogen in order to maximize  
195 the magnitude of nitrogen acquired from a belowground carbon investment and  
196 outcompete other individuals for soil resources (Rastetter et al. 2001; Menge et al.  
197 2008).

198 Environmental conditions that affect demand to acquire nitrogen to sup-  
199 port new and existing tissues could also be a source of variance in plant carbon  
200 costs to acquire nitrogen [DWS: Awkward sentence with too many prepositions.  
201 Watch out for this throughout]. For example, an increase in plant nitrogen de-  
202 mand could increase carbon costs to acquire nitrogen if this increases the carbon  
203 that must be allocated belowground to acquire a proportional amount of nitrogen  
204 (Kulmatiski et al. 2017; Noyce et al. 2019). This could be driven by a temporary  
205 state of diminishing return associated with investing carbon toward building and  
206 maintaining structures that are necessary to support enhanced nitrogen uptake,  
207 such as fine roots (Matamala and Schlesinger 2000; Norby et al. 2004; Arndal  
208 et al. 2018), mycorrhizal hyphae (Saleh et al. 2020), or root nodules (Parvin et al.  
209 2020). Alternatively, if the environmental factor that increases plant nitrogen de-  
210 mand causes nitrogen to become more limiting in the system (e.g. atmospheric

211 CO<sub>2</sub>) (Luo et al. 2004; LeBauer and Treseder 2008; Vitousek et al. 2010; Liang  
212 et al. 2016), species might switch their primary mode of nitrogen acquisition to  
213 a strategy with lower relative carbon costs to acquire nitrogen in order to gain a  
214 competitive advantage over species with either different or more limited modes of  
215 nitrogen acquisition (Ainsworth and Long 2005; Taylor and Menge 2018).

216 Using a plant economics approach, I examined the influence of plant ni-  
217 trogen demand and soil nitrogen availability on plant carbon costs to acquire  
218 nitrogen. This was done by growing a species capable of forming associations  
219 with nitrogen-fixing bacteria (*Glycine max* L. (Merr)) and a species not capable  
220 of forming these associations (*Gossypium hirsutum* L.) under four levels of light  
221 availability (plant nitrogen demand proxy) and four levels of soil nitrogen fertil-  
222 ization (soil nitrogen availability proxy) in a full-factorial, controlled greenhouse  
223 experiment. [DWS: these species come out of nowhere? Why these two? Seems  
224 random. I mean they are both rosids but otherwise? What can one learn by just  
225 growing two random species out of hundreds of thousands? You need to justify  
226 this or it is a huge surprise..]

227 I used this experimental set-up to test the following hypotheses:

228 1. An increase in plant nitrogen demand due to increasing light availability will  
229 increase carbon costs to acquire nitrogen through a proportionally larger  
230 increase in belowground carbon than whole-plant nitrogen acquisition. This  
231 will be the result of an increased investment of carbon toward belowground  
232 structures that support enhanced nitrogen uptake, but at a lower nitrogen  
233 return.

234        2. An increase in soil nitrogen availability will decrease carbon costs to acquire  
235        nitrogen as a result of increased per root nitrogen uptake in *G. hirsutum*.  
236        However, soil nitrogen availability will not affect carbon costs to acquire  
237        nitrogen in *G. max* because of the already high return of nitrogen supplied  
238        through nitrogen fixation.

239      2.2 Methods

240      2.2.1 *Experiment setup*

241      *Gossypium hirsutum* and *G. max*. were planted in individual 3 liter pots (NS-300;  
242      Nursery Supplies, Orange, CA, USA) containing a 3:1 mix of unfertilized potting  
243      mix (Sungro Sunshine Mix #2, Agawam, MA, USA) to native soil extracted from  
244      an agricultural field most recently planted with *G. max* at the USDA-ARS Lab-  
245      oratory in Lubbock, TX, USA (33.59°N, -101.90°W). The field soil was classified  
246      as Amarillo fine sandy loam (75% sand, 10% silt, 15% clay). Upon planting,  
247      all *G. max* pots were inoculated with *Bradyrhizobium japonicum* (Verdesian N-  
248      Dure™ Soybean, Cary, NC, USA) to stimulate root nodulation. Individuals of  
249      both species were grown under similar, unshaded, ambient greenhouse conditions  
250      for 2 weeks to germinate and begin vegetative growth.

251           Three blocks were set up in the greenhouse, each containing four light  
252           treatments created using shade cloth that reduced incoming radiation by either 0  
253           (full sun), 30, 50, or 80%. Two weeks post-germination, individuals were randomly  
254           placed in the four light treatments in each block. Individuals received one of four  
255           nitrogen fertilization doses as 100mL of a modified Hoagland solution (Hoagland  
256           and Arnon 1950) equivalent to either 0, 70, 210, or 630 ppm N twice per week

257 within each light treatment. Nitrogen fertilization doses were received as topical  
258 agents to the soil surface. Each Hoagland solution was modified to keep concen-  
259 trations of other macro- and micronutrients equivalent (Table A1). Plants were  
260 routinely well watered to eliminate water stress.

261 2.2.2 *Plant measurements and calculations*

262 Each individual was harvested after 5 weeks of treatment, and biomass was sepa-  
263 rated by organ type (leaves, stems, and roots). Nodules on *G. max* roots were also  
264 harvested. Except for the 0% shade cover and 630 ppm N treatment combination,  
265 all treatment combinations in both species had lower average dry biomass:pot vol-  
266 ume ratios than the 1:1 ratio recommended by Poorter et al. (2012) to minimize  
267 the likelihood of pot volume-induced growth limitation (Table A2, A3; Fig. A1).

268 All harvested material was dried, weighed, and ground by organ type.  
269 Carbon and nitrogen content ( $\text{g g}^{-1}$ ) was determined by subsampling from ground  
270 and homogenized biomass of each organ type using an elemental analyzer (Costech  
271 4010; Costech, Inc., Valencia, CA, USA). I scaled these values to total leaf, stem,  
272 and root carbon and nitrogen biomass (g) by multiplying dry biomass of each  
273 organ type by carbon or nitrogen content of each corresponding organ type. Whole  
274 plant nitrogen biomass (g) was calculated as the sum of total leaf (g), stem (g),  
275 and root (g) nitrogen biomass. Root nodule carbon biomass was not included in  
276 the calculation of root carbon biomass; however, relative plant investment toward  
277 root or root nodule standing stock was estimated as the ratio of root biomass to  
278 root nodule biomass ( $\text{g g}^{-1}$ ), following similar metrics to those adopted by Dovrat  
279 et al. (2018) and Dovrat et al. (2020).

280 Carbon costs to acquire nitrogen ( $N_{\text{cost}}$ ; gC gN<sup>-1</sup>) were estimated as the  
281 ratio of total root carbon biomass ( $C_{\text{bg}}$ ; gC) to whole-plant nitrogen biomass  
282 ( $N_{\text{wp}}$ ; gN). This calculation quantifies the relationship between carbon spent on  
283 nitrogen acquisition and whole plant nitrogen acquisition by using root carbon  
284 biomass as a proxy for estimating the magnitude of carbon allocated toward ni-  
285 trogen acquisition. This calculation therefore assumes that the magnitude of root  
286 carbon standing stock is proportional to carbon transferred to root nodules or my-  
287 corrhizae, or lost through root exudation or turnover. The assumption has been  
288 supported in species that associate with ectomycorrhizal fungi (Hobbie 2006; Hob-  
289 bie and Hobbie 2008), but is less clear in species that acquire nitrogen through  
290 non-symbiotic active uptake or symbiotic nitrogen fixation. It is also unclear  
291 whether relationships between root carbon standing stock and carbon transfer to  
292 root nodules are similar in magnitude to carbon lost through exudation or when  
293 allocated toward other active uptake pathways. Thus, because of the way mea-  
294 surements were calculated, proximal values of carbon costs to acquire nitrogen are  
295 underestimates.

296 2.2.3 *Statistical analyses*

297 I explored the effects of light and nitrogen availability on carbon costs to acquire  
298 nitrogen using separate linear mixed-effects models for each species. Models in-  
299 cluded shade cover, nitrogen fertilization, and interactions between shade cover  
300 and nitrogen fertilization as continuous fixed effects, and also included block as a  
301 random intercept term. Three separate models for each species were built with  
302 this independent variable structure for three different dependent variables: (i)

303 carbon costs to acquire nitrogen ( $\text{gC gN}^{-1}$ ); (ii) whole plant nitrogen biomass  
304 (denominator of carbon cost to acquire nitrogen; gN); and (iii) belowground car-  
305 bon biomass (numerator of carbon cost to acquire nitrogen; gC). I constructed two  
306 additional models for *G. max* with the same model structure described above to  
307 investigate the effects of light availability and nitrogen fertilization on root nodule  
308 biomass (g) and the ratio of root nodule biomass to root biomass (unitless).

309 I used Shapiro–Wilk tests of normality to determine whether species spe-  
310 cific linear mixed-effects model residuals followed a normal distribution. Zero  
311 models satisfied residual normality assumptions when models were fit using un-  
312 transformed data (Shapiro–Wilk:  $p < 0.05$  in all cases). I attempted to satisfy  
313 residual normality assumptions by first fitting models using dependent variables  
314 that were natural-log transformed. If residual normality assumptions were still  
315 not met (Shapiro–Wilk:  $p < 0.05$ ), then models were fit using dependent variables  
316 that were square root transformed. All residual normality assumptions were satis-  
317 fied when models were fit with either a natural-log or square root transformation  
318 (Shapiro–Wilk:  $p > 0.05$  in all cases). Specifically, I natural-log transformed *G.*  
319 *hirsutum* carbon costs to acquire nitrogen and *G. hirsutum* whole-plant nitrogen  
320 biomass. I also square root transformed *G. max* carbon costs to acquire nitrogen,  
321 *G. max* whole-plant nitrogen biomass, root carbon biomass in both species, *G.*  
322 *max* root nodule biomass, and the *G. max* ratio of root nodule biomass to root  
323 biomass. I used the ‘lmer’ function in the ‘lme4’ R package (Bates et al. 2015) to  
324 fit each model and the ‘Anova’ function in the ‘car’ R package (Fox and Weisberg  
325 2019) to calculate Wald’s  $\chi^2$  to determine the significance ( $\alpha = 0.05$ ) of each fixed  
326 effect coefficient. Finally, I used the ‘emmeans’ R package (Lenth 2019) to conduct

327 post-hoc comparisons of our treatment combinations using Tukey's tests. Degrees  
328 of freedom for all Tukey's tests were approximated using the Kenward–Roger ap-  
329 proach (Kenward and Roger 1997). All analyses and plots were conducted in R  
330 version 4.0.1 (R Core Team 2021).

331 2.3 Results

332 2.3.1 *Carbon costs to acquire nitrogen*

333 Carbon costs to acquire nitrogen in *G. hirsutum* increased with increasing light  
334 availability ( $p<0.001$ ; Table 2.1; Fig. 2.1) and decreased with increasing nitrogen  
335 fertilization ( $p<0.001$ ; Table 2.1; Fig. 2.1). There was no interaction between  
336 light availability and nitrogen fertilization ( $p=0.486$ , Table 2.1; Fig. 2.1).

337 Carbon costs to acquire nitrogen in *G. max* also increased with increasing  
338 light availability ( $p<0.001$ , Table 2.1; Fig. 2.1) and decreased with increasing  
339 nitrogen fertilization ( $p<0.001$ ; Table 2.1; Fig. 2.1). There was no interaction  
340 between light availability and nitrogen fertilization ( $p=0.261$ , Table 2.1; Fig. 2.1).

**Table 2.1.** Analysis of variance results exploring species-specific effects of light availability, nitrogen fertilization, and their interactions on carbon costs to acquire nitrogen ( $N_{\text{cost}}$ ; gC gN $^{-1}$ ), whole plant nitrogen biomass ( $N_{\text{wp}}$ ; gN), and root carbon biomass ( $C_{\text{bg}}$ ; gC)

	$N_{\text{cost}}$			$N_{\text{wp}}$			$C_{\text{bg}}$			
	df	Coefficient	$\chi^2$	p	Coefficient	$\chi^2$	p	Coefficient	$\chi^2$	p
<i>G. hirsutum</i>										
Intercept		1.594	-	-	-3.232	-	-	0.432	-	-
Light (L)	1	-1.09E-02	56.494	<0.001	-6.41E-03	91.275	<0.001	-2.62E-03	169.608	<0.001
Nitrogen (N)	1	-1.34E-03	54.925	<0.001	1.83E-03	118.784	<0.001	1.15E-04	2.901	0.089
L*N	1	3.88E-06	0.485	0.486	-1.34E-05	10.721	0.001	-1.67E-06	3.140	0.076
<i>G. max</i>										
Intercept		1.877	-	-	0.239	-	-	0.438	-	-
Light (L)	1	-7.67E-03	174.156	<0.001	-6.72E-04	39.799	<0.001	-2.55E-03	194.548	<0.001
Nitrogen (N)	1	-2.35E-04	21.948	<0.001	1.55E-04	70.771	<0.001	2.52E-04	19.458	<0.001
L*N	1	-2.89E-06	1.262	0.261	-6.32E-07	1.435	0.231	-3.16E-06	10.803	0.001

341 \*Significance determined using Wald's  $\chi^2$  tests ( $p=0.05$ ).  $P$ -values less than 0.05 are in bold and  $p$ -values between  
 342 0.05 and 0.1 are italicized. Negative coefficients for light treatments indicate a positive effect of increasing light  
 343 availability on all response variables, as light availability is treated as percent shade cover in all linear mixed-effects  
 344 models.

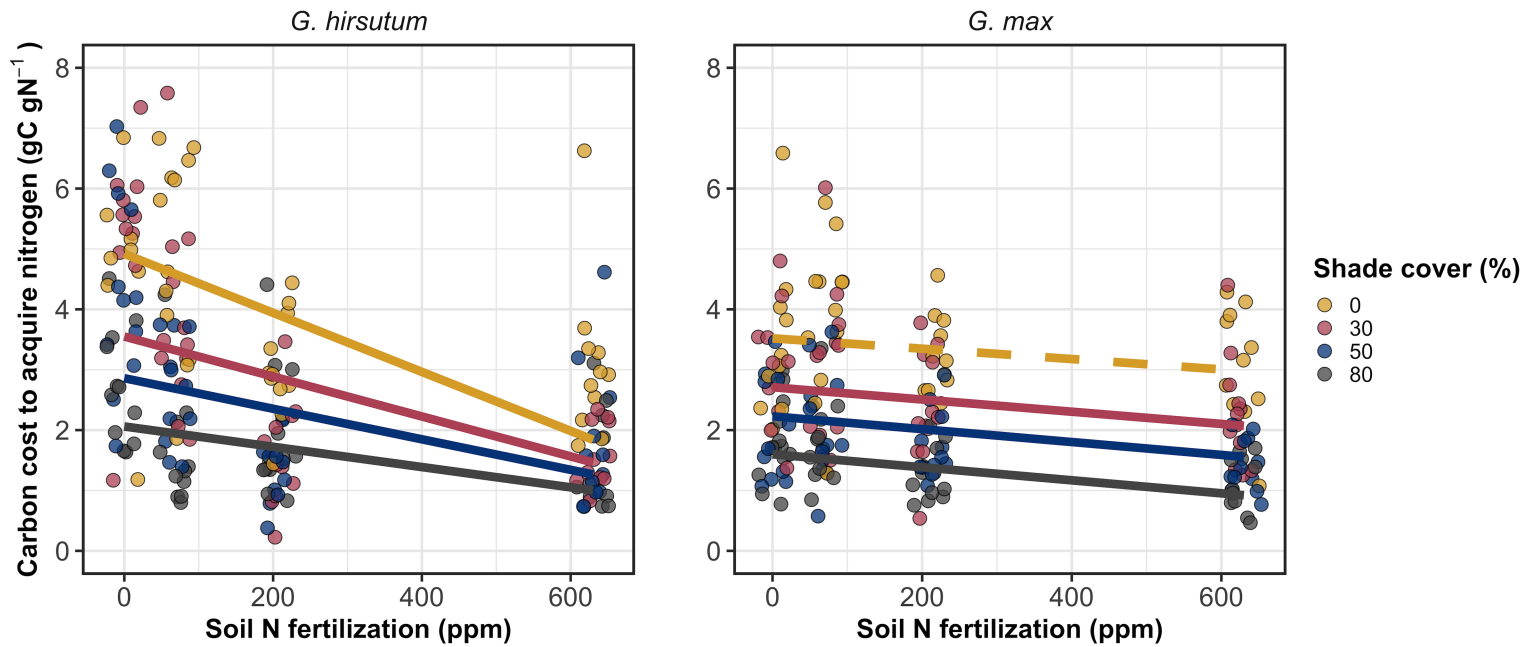


**Figure 2.1.** Relationships between soil nutrient fertilization and light availability on carbon costs to acquire nitrogen in *G. hirsutum* and *G. max*. Nitrogen fertilization treatments are represented on the x-axis. Shade cover treatments are represented through colored points and trendlines. Trendlines were created by back-transforming marginal mean slopes and intercepts from species-specific linear mixed-effects models. These values were calculated using the ‘emtrends’ and ‘emmeans’ functions in the ‘emmeans’ R package (Lenth, 2019). Yellow points and trendlines represent the 0% shade cover treatment, red points and trendlines represent the 30% shade cover treatment, blue points and trendlines represent the 50% shade cover treatment, and gray points and trendlines represent the 80% shade cover treatment. Solid trendlines indicate slopes that are significantly different from zero (Tukey:  $p < 0.05$ ), while dashed trendlines indicate slopes that are not statistically different from zero.

**345** 2.3.2 *Whole plant nitrogen biomass*

**346** Whole plant nitrogen biomass in *G. hirsutum* was driven by an interaction between  
**347** light availability and nitrogen fertilization ( $p=0.001$ ; Table 2.1; Fig. 2.2). This  
**348** interaction indicated a greater stimulation of whole-plant nitrogen biomass by  
**349** nitrogen fertilization as light levels increased (Table 2.1; Fig. 2.2).

**350** Whole plant nitrogen biomass in *G. max* increased with increasing light  
**351** availability ( $p<0.001$ ) and nitrogen fertilization ( $p<0.001$ ), with no interaction  
**352** between light availability and nitrogen fertilization ( $p=0.231$ ; Table 2.1; Fig. 2.2).

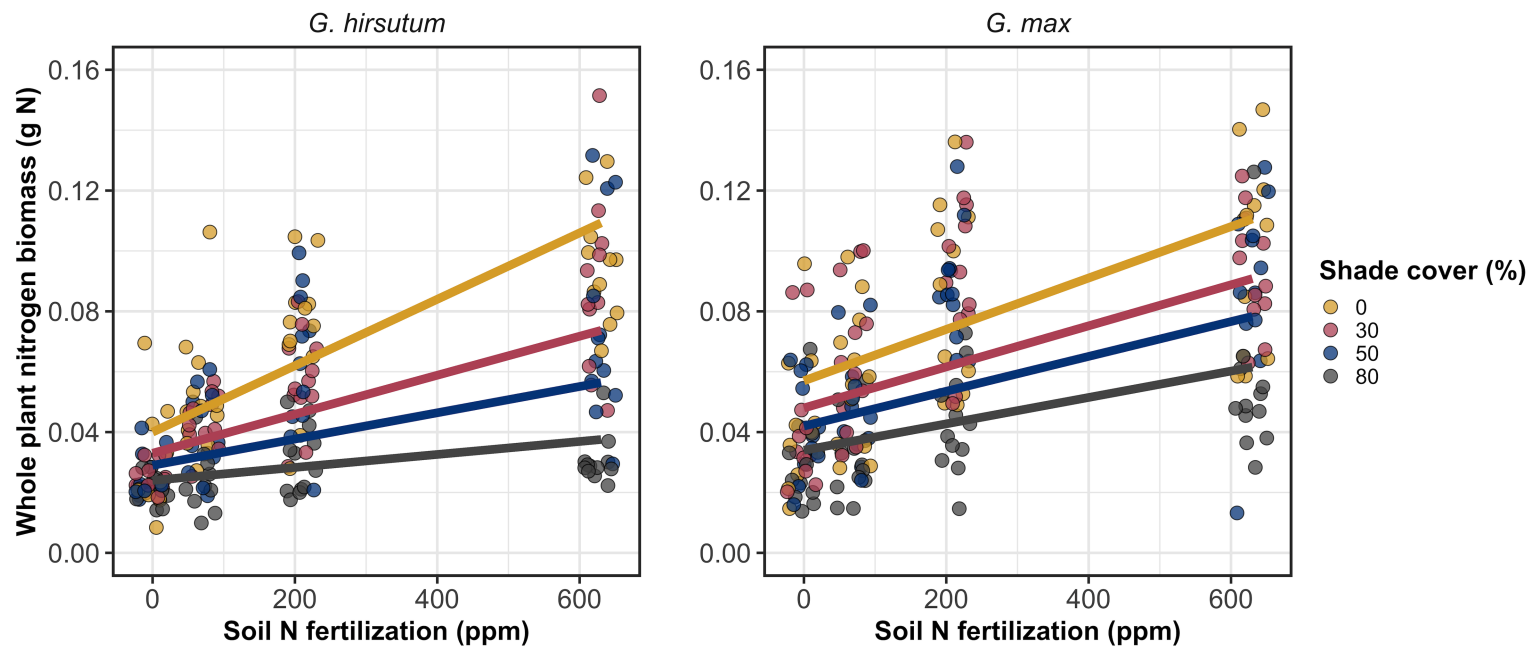


**Figure 2.2.** Relationships between soil nutrient fertilization and light availability on whole-plant nitrogen biomass in *G. hirsutum* and *G. max*. Whole-plant nitrogen biomass is the denominator of the carbon cost to acquire nitrogen calculation. Nitrogen fertilization treatments are represented on the x-axis. Shade cover treatments are represented through colored points and trendlines. Trendlines were created by back-transforming marginal mean slopes and intercepts from species-specific linear mixed-effects models. These values were calculated using the ‘emtrends’ and ‘emmeans’ functions in the ‘emmeans’ R package (Lenth 2019). Points are jittered for visibility. Colored points and trendlines are as explained in Fig. 2.1. Solid trendlines indicate slopes that are significantly different from zero (Tukey:  $p < 0.05$ ), while dashed trendlines indicate slopes that are not statistically different from zero.

**353** 2.3.3 *Root carbon biomass*

**354** Root carbon biomass in *G. hirsutum* significantly increased with increasing light  
**355** availability ( $p<0.001$ ; Table 2.1; Fig. 2.3) and marginally increased with nitrogen  
**356** fertilization ( $p=0.089$ ; Table 2.1; Fig. 2.3). There was also a marginal interaction  
**357** between light availability and nitrogen fertilization ( $p=0.076$ ; Table 2.1), driven by  
**358** an increase in the positive response of root carbon biomass to increasing nitrogen  
**359** fertilization as light availability increased (Table 2.3). This resulted in significantly  
**360** positive trends between root carbon biomass and nitrogen fertilization in the two  
**361** highest light treatments (Tukey:  $p<0.05$  in both cases; Table 2.3; Fig. 2.3) and no  
**362** effect of nitrogen fertilization in the two lowest light treatments (Tukey:  $p>0.05$   
**363** in both cases; Table 2.3; Fig. 2.3).

**364** There was an interaction between light availability and nitrogen fertiliza-  
**365** tion on root carbon biomass in *G. max* ( $p=0.001$ ; Table 2.1; Fig. 2.3). Post-hoc  
**366** analyses indicated that the positive effects of nitrogen fertilization on *G. max*  
**367** root carbon biomass increased with increasing light availability (Table 2.3; Fig.  
**368** 2.3). There were also positive individual effects of increasing nitrogen fertilization  
**369** ( $p<0.001$ ; Table 2.3) and light availability ( $p<0.001$ ; Table 2.3) on *G. max* root  
**370** carbon biomass (Table 2.1; Fig. 2.3).

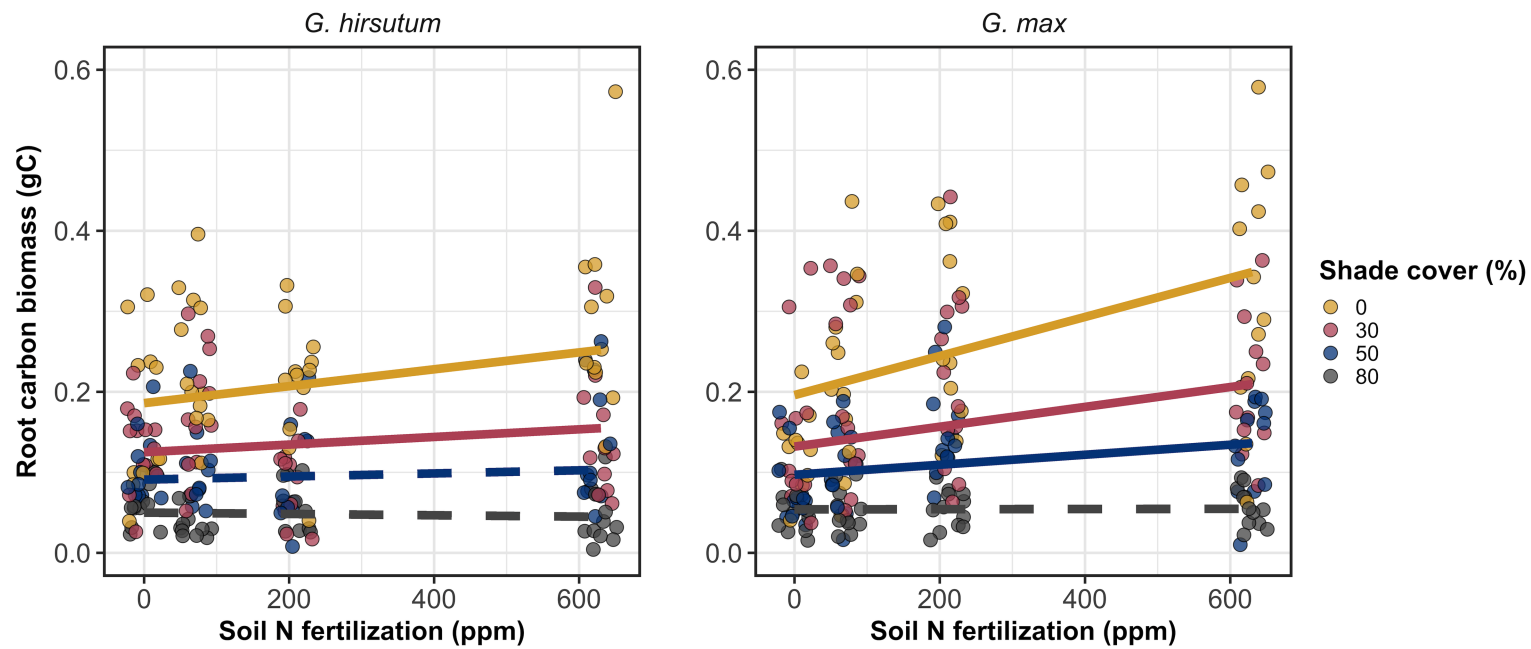


**Figure 2.3.** Relationships between soil nutrient fertilization and light availability on root carbon biomass in *G. hirsutum* and *G. max*. Root carbon biomass is the numerator of the carbon cost to acquire nitrogen calculation. Nitrogen fertilization treatments are represented on the x-axis. Colored points and trendlines are as explained in Fig. 2.1. Trendlines were created by back-transforming marginal mean slopes and intercepts from species-specific linear mixed-effects models. These values were calculated using the ‘emtrends’ and ‘emmeans’ functions in the ‘emmeans’ R package (Lenth 2019). Points are jittered for visibility. Colored points and trendlines are as explained in Fig. 2.1.

**371** 2.3.4 *Root nodule biomass*

**372** Root nodule biomass in *G. max* increased with increasing light availability ( $p <$   
**373** 0.001; Table 2.2; Fig. 2.4a) and decreased with increasing nitrogen fertilization  
**374** ( $p < 0.001$ ; Table 2.2; Fig. 2.4a). There was no interaction between nitrogen  
**375** fertilization and light availability ( $p = 0.133$ ; Table 2.2; Fig. 2.4a). The ratio of  
**376** root nodule biomass to root biomass did not change in response to light availability  
**377** ( $p = 0.481$ ; Table 2.2; Fig. 2.4b) but decreased with increasing nitrogen fertilization  
**378** ( $p < 0.001$ ; Table 2.2; Fig. 2.4b). There was no interaction between nitrogen  
**379** fertilization and light availability on the ratio of root nodule biomass to root  
**380** biomass ( $p = 0.621$ ; Table 2.2; Fig. 2.4b).

**Table 2.2.** Analysis of variance results exploring effects of light availability, nitrogen fertilization, and their interactions on *G. max* root nodule biomass (g) and the ratio of root nodule biomass to root biomass (g g<sup>-1</sup>)\*

	Nodule biomass			Nodule biomass: root biomass			<i>p</i>
	df	Coefficient	$\chi^2$	<i>p</i>	Coefficient	$\chi^2$	
(Intercept)		0.302	-	-	0.448	-	-
Light (L)	1	-1.81E-03	72.964	<b>&lt;0.001</b>	-8.76E-05	0.496	0.481
Nitrogen (N)	1	-2.83E-04	115.377	<b>&lt;0.001</b>	-5.09E-04	156.476	<b>&lt;0.001</b>
L*N	1	1.14E-06	2.226	0.133	-7.30E-07	0.244	0.621

381 \*Significance determined using Wald's  $\chi^2$  tests ( $\alpha=0.05$ ). *P*-values less than 0.05 are in bold. Negative coefficients for  
 382 light treatments indicate a positive effect of increasing light availability on all response variables, as light availability  
 383 is treated as percent shade cover in all linear mixed-effects models. Root nodule biomass and nodule biomass: root  
 384 biomass models were only constructed for *G. max* because *G. hirsutum* was not inoculated with *B. japonicum* and  
 385 is not capable of forming root nodules.

**Table 2.3.** Slopes of the regression line describing the relationship between each dependent variable and nitrogen fertilization at each light level\*

Shade cover	Carbon cost to acquire nitrogen	Whole plant nitrogen biomass	Belowground carbon biomass	Root nodule biomass	Nodule biomass: root biomass
<i>G. hirsutum</i>					
0%	<b>-1.34E-03<sup>a</sup></b>	<b>1.83E-03<sup>a</sup></b>	<b>1.15E-04<sup>b</sup></b>	-	-
30%	<b>-1.22E-03<sup>a</sup></b>	<b>1.43E-03<sup>a</sup></b>	<b>1.17E-04<sup>b</sup></b>	-	-
50%	<b>-1.14E-03<sup>a</sup></b>	<b>1.17E-03<sup>a</sup></b>	3.12E-05 <sup>b</sup>	-	-
80%	<b>-1.02E-03<sup>a</sup></b>	<b>7.66E-04<sup>a</sup></b>	-1.89E-06 <sup>b</sup>	-	-
<i>G. max</i>					
0%	-2.35E-04 <sup>b</sup>	<b>1.55E-05<sup>b</sup></b>	<b>2.51E-04<sup>b</sup></b>	<b>-2.83E-04<sup>b</sup></b>	<b>-5.09E-04<sup>b</sup></b>
30%	<b>-3.22E-04<sup>b</sup></b>	<b>1.35E-05<sup>b</sup></b>	<b>1.57E-04<sup>b</sup></b>	<b>-2.49E-04<sup>b</sup></b>	<b>-5.31E-04<sup>b</sup></b>
50%	<b>-3.80E-04<sup>b</sup></b>	<b>1.23E-05<sup>b</sup></b>	<b>9.37E-05<sup>b</sup></b>	<b>-2.26E-04<sup>b</sup></b>	<b>-5.45E-04<sup>b</sup></b>
80%	<b>-4.66E-04<sup>b</sup></b>	<b>1.04E-05<sup>b</sup></b>	-9.95E-07 <sup>b</sup>	<b>-1.92E-04<sup>b</sup></b>	<b>-5.67E-04<sup>b</sup></b>

**386** \* Slopes represent estimated marginal mean slopes from linear mixed-effects models described in the Methods. Slopes  
**387** were calculated using the ‘emmeans’ R package (Lenth 2019). Superscripts indicate slopes fit to natural-log (<sup>a</sup>) or  
**388** square root (<sup>b</sup>) transformed data. Slopes statistically different from zero (Tukey:  $p<0.05$ ) are indicated in bold.  
**389** Marginally significant slopes (Tukey:  $0.05< p<0.1$ ) are italicized.

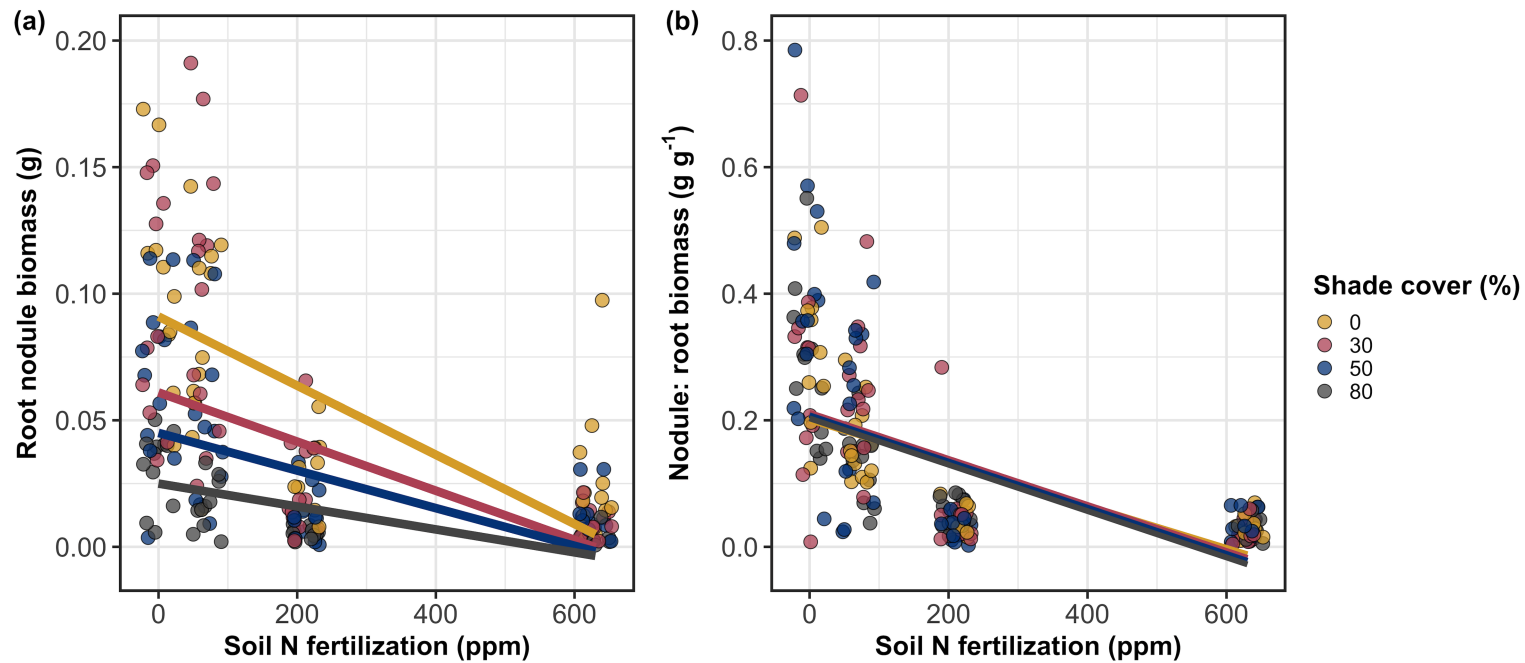


**Figure 2.4.** Effects of shade cover and nitrogen fertilization on root nodule biomass (a) and the ratio of root nodule biomass to root biomass (b) in *G. max*. Nitrogen fertilization treatments are represented on the x-axis. Shade cover treatments are represented through colored points and trendlines. Trendlines were created by back-transforming marginal mean slopes and intercepts from species-specific linear mixed-effects models. These values were calculated using the ‘emtrends’ and ‘emmeans’ functions in the ‘emmeans’ R package (Lenth 2019). Points are jittered for visibility. Yellow points and trendlines represent the 0% shade cover treatment, blue points and trendlines represent the 30% shade cover treatment, green points and trendlines represent the 50% shade cover treatment, and purple points and trendlines represent the 80% shade cover treatment. Solid trendlines indicate slopes that are significantly different from zero (Tukey:  $p < 0.05$ ), while dashed trendlines indicate slopes that are not statistically different from zero.

**390** 2.4 Discussion

**391** In this chapter, I determined the effects of light availability and soil nitrogen  
**392** fertilization on root mass carbon costs to acquire nitrogen in *G. hirsutum* and *G.*  
**393** *max*. In support of my hypotheses, I found that carbon costs to acquire nitrogen  
**394** generally increased with increasing light availability and decreased with increasing  
**395** soil nitrogen fertilization in both species. These findings suggest that carbon costs  
**396** to acquire nitrogen are determined by factors that influence plant nitrogen demand  
**397** and soil nitrogen availability. In contrast to my second hypothesis, root nodulation  
**398** data suggested that *G. max* and *G. hirsutum* achieved similar directional carbon  
**399** cost responses to nitrogen fertilization despite a likely shift in *G. max* allocation  
**400** from nodulation to root biomass along the nitrogen fertilization gradient.

**401** 2.4.1 *Carbon costs to acquire nitrogen increase with light availability and*  
**402** *decrease with fertilization*

**403** Both *G. max* and *G. hirsutum* experienced an increase in carbon costs to ac-  
**404** quire nitrogen due to increasing light availability. These patterns were driven by  
**405** a larger increase in root carbon biomass than whole-plant nitrogen biomass. In-  
**406** creases in root carbon biomass due to factors that increase plant nitrogen demand  
**407** are a commonly observed pattern, as carbon allocated belowground provides sub-  
**408** strate needed to produce and maintain structures that satisfy aboveground plant  
**409** nitrogen demand (Nadelhoffer and Raich 1992; Giardina et al. 2005; Raich et al.  
**410** 2014). Findings suggest that plants allocate relatively more carbon for acquiring  
**411** nitrogen when demand increases over short temporal scales, which may cause a  
**412** temporary state of diminishing return due to asynchrony between belowground

413 carbon and whole-plant nitrogen responses to plant nitrogen demand (Kulmatiski  
414 et al. 2017; Noyce et al. 2019). These responses might be attributed to a temporal  
415 lag associated with producing structures that enhance nitrogen acquisition. For  
416 example, fine roots (Matamala and Schlesinger 2000; Norby et al. 2004; Arndal  
417 et al. 2018) and root nodules (Parvin et al. 2020) take time to build and first  
418 require the construction of coarse roots. Thus, full nitrogen returns from these  
419 investments may not occur immediately (Kayler et al. 2010; Kayler et al. 2017),  
420 and may vary by species acquisition strategy. I speculate that increases in ni-  
421 trogen acquisition from a given carbon investment may occur beyond the 5-week  
422 scope of this experiment. A similar study conducted over a longer temporal scale  
423 would address this.

424 Increasing soil nitrogen fertilization generally decreased carbon costs to  
425 acquire nitrogen in both species. These patterns were driven by a larger increase  
426 in whole-plant nitrogen biomass than root carbon biomass. In *G. hirsutum*, re-  
427 ductions in carbon costs to acquire nitrogen may have been due to an increase in  
428 per-root nitrogen uptake, allowing individuals to maximize the amount of nitro-  
429 gen acquired from a belowground carbon investment. Interestingly, increased soil  
430 nitrogen fertilization increased whole-plant nitrogen biomass in *G. max* despite  
431 reductions in root nodule biomass that likely reduced the nitrogen-fixing capac-  
432 ity of *G. max* (Andersen et al. 2005; Muñoz et al. 2016). While reductions in  
433 root nodulation due to increased soil nitrogen availability are commonly observed  
434 (Gibson and Harper 1985; Fujikake et al. 2003), root nodulation responses were  
435 observed in tandem with increased root carbon biomass, implying that *G. max*  
436 shifted relative carbon allocation from nitrogen fixation to soil nitrogen acquisition

437 (Markham and Zekveld 2007; Dovrat et al. 2020). This was likely because there  
438 was a reduction in the carbon cost advantage of acquiring fixed nitrogen relative  
439 to soil nitrogen, and suggests that species capable of associating with symbiotic  
440 nitrogen-fixing bacteria shift their relative nitrogen acquisition pathway to opti-  
441 mize nitrogen uptake (Rastetter et al. 2001). Future studies should investigate  
442 these patterns with a larger quantity of phylogenetically related species, or differ-  
443 ent varieties of a single species that differ in their ability to form associations with  
444 symbiotic nitrogen-fixing bacteria to more directly test the impact of nitrogen  
445 fixation on the patterns observed in this study.

446 2.4.2 *Modeling implications*

447 Carbon costs to acquire nitrogen are subsumed [DWS: ?] in the general discussion  
448 of economic analogies to plant resource uptake (Bloom et al. 1985; Rastetter et al.  
449 2001; Vitousek et al. 2002; Phillips et al. 2013; Terrer et al. 2018; Henneron et al.  
450 2020). Despite this, terrestrial biosphere models rarely include costs of nitrogen  
451 acquisition to predict plant nitrogen uptake. There is currently one plant resource  
452 uptake model, FUN [DWS: is this an acronym? Why caps?], that quantitatively  
453 predicts carbon costs to acquire nitrogen within a framework for predicting plant  
454 nitrogen uptake for different nitrogen acquisition strategies (Fisher et al. 2010;  
455 Brzostek et al. 2014). Iterations of FUN are currently coupled to two terrestrial  
456 biosphere models: the Community Land Model 5.0 and the Joint UK Land En-  
457 vironment Simulator (Clark et al. 2011; Shi et al. 2016; Lawrence et al. 2019).  
458 Recent work suggests that coupling FUN to CLM 5.0 caused a large overpredic-  
459 tion of plant nitrogen uptake associated with nitrogen fixation (Davies-Barnard

460 et al. 2020) compared to other terrestrial biosphere model products. Thus, em-  
461 pirical data from manipulative experiments that explicitly quantify carbon costs  
462 to acquire nitrogen in species capable of associating with nitrogen-fixing bacteria  
463 across different environmental contexts is an important step toward identifying  
464 potential biases in models such as FUN.

465 These findings broadly [DWS: ? what would broad vs narrow support  
466 mean here?] support the FUN formulation of carbon costs to acquire nitrogen in  
467 response to soil nitrogen availability. FUN calculates carbon costs to acquire ni-  
468 trogen based on the sum of carbon costs to acquire nitrogen via nitrogen fixation,  
469 mycorrhizal active uptake, non-mycorrhizal active uptake, and retranslocation  
470 (Fisher et al. 2010; Brzostek et al. 2014). Carbon costs to acquire nitrogen via  
471 mycorrhizal or non-mycorrhizal active uptake pathways are derived as a function  
472 of nitrogen availability, root biomass, and two parameterized values based on ni-  
473 trogen acquisition strategy (Brzostek et al. 2014). Due to this, FUN simulates  
474 a net decrease in carbon costs to acquire nitrogen with increasing nitrogen avail-  
475 ability for mycorrhizal and non-mycorrhizal active uptake pathways, assuming  
476 constant root biomass. This was a pattern I observed in *G. hirsutum* regardless  
477 of light availability. In contrast, FUN would not simulate a net change in carbon  
478 costs to acquire nitrogen via nitrogen fixation due to nitrogen availability. This  
479 is because carbon costs to acquire nitrogen via nitrogen fixation are derived from  
480 a well established function of soil temperature, which is independent of soil ni-  
481 trogen availability (Houlton et al. 2008; Fisher et al. 2010). I observed a net  
482 reduction in carbon costs to acquire nitrogen in *G. max*, except when individu-  
483 als were grown under 0% shade cover. While a net reduction of carbon costs in

484 response to nitrogen fertilization runs counter to nitrogen fixation carbon costs  
485 simulated by FUN, these patterns were likely because *G. max* individuals switched  
486 their primary mode of nitrogen acquisition from symbiotic nitrogen fixation to a  
487 non-symbiotic active uptake pathway.

488 2.4.3 *Study limitations*

489 The metric used in this study to determine carbon costs to acquire nitrogen has  
490 several limitations. Most notably, this metric uses root carbon biomass as a  
491 proxy for estimating the amount of carbon spent on nitrogen acquisition. While  
492 [although?] it is true that most carbon allocated belowground has at least an  
493 indirect structural role in acquiring soil resources, it remains unclear whether this  
494 assumption holds true for species that acquire nitrogen via symbiotic nitrogen fix-  
495 ation. I also cannot quantify carbon lost through root exudates or root turnover,  
496 which may increase due to factors that increase plant nitrogen demand (Tingey  
497 et al. 2000; Phillips et al. 2011), and can increase the magnitude of available  
498 nitrogen from soil organic matter through priming effects on soil microbial com-  
499 munities (Uselman et al. 2000; Bengtson et al. 2012). It is also not clear whether  
500 these assumptions hold under all environmental conditions, such as those that  
501 shift belowground carbon allocation toward a different mode of nitrogen acqui-  
502 sition (Taylor and Menge 2018; Friel and Friesen 2019) or between species with  
503 different acquisition strategies. In this study, increasing soil nitrogen fertiliza-  
504 tion increased carbon investment to roots relative to carbon transferred to root  
505 nodules. By assuming that carbon allocated to root carbon was proportional to  
506 carbon allocated to root nodules across all treatment combinations, these observed

507 responses to soil nitrogen fertilization were likely to be overestimated in *G. max*.

508 I encourage future research to quantify these carbon fates independently.

509 [DWS: also you looked at two species out of hundreds of thousands of  
510 possible species! It is anecdotal]

511 Researchers conducting pot experiments must carefully choose pot volume  
512 to minimize the likelihood of growth limitations induced by pot volume (Poorter  
513 et al. 2012). Poorter et al. (2012) indicate that researchers are likely to avoid  
514 growth limitations associated with pot volume if measurements are collected when  
515 the plant biomass:pot volume ratio is less than  $1 \text{ g L}^{-1}$ . In this experiment, all  
516 treatment combinations in both species had biomass:pot volume ratios less than  
517  $1 \text{ g L}^{-1}$  except for *G. max* and *G. hirsutum* that were grown under 0% shade  
518 cover and had received 630 ppm N. Specifically, *G. max* and *G. hirsutum* had  
519 average respective biomass:pot volume ratios of  $1.24 \pm 0.07 \text{ g L}^{-1}$  and  $1.34 \pm 0.13$   
520  $\text{g L}^{-1}$ , when grown under 0% shade cover and received 630 ppm N (Table A2,  
521 A3; Fig. A1). If growth in this treatment combination was limited by pot vol-  
522 ume, then individuals may have had larger carbon costs to acquire nitrogen than  
523 would be expected if they were grown in larger pots. This pot volume induced  
524 growth limitation could cause a reduction in per-root nitrogen uptake associated  
525 with more densely packed roots, which could reduce the positive effect of nitro-  
526 gen fertilization on whole-plant nitrogen biomass relative to root carbon biomass  
527 (Poorter et al. 2012).

528 Growth limitation associated with pot volume [DWS: Can you write this  
529 directly? Eg: “small pots limited growth?” You litter your writing with these ver-  
530 bose and awkward sentences/] provides a possible explanation for the marginally

531 insignificant effect of increasing nitrogen fertilization on *G. max* carbon costs to  
532 acquire nitrogen when grown under 0% shade cover. This is because the regres-  
533 sion line describing the relationship between carbon costs to acquire nitrogen and  
534 nitrogen fertilization in *G. max* grown under 0% shade cover would have flattened  
535 if growth limitation had caused larger than expected carbon costs to acquire ni-  
536 trogen in the 0% shade cover, 630 ppm N treatment combination. This may have  
537 been exacerbated by the fact that *G. max* likely shifted relative carbon allocation  
538 from nitrogen fixation to soil nitrogen acquisition, which could have increased the  
539 negative effect of more densely packed roots on nitrogen uptake. These patterns  
540 could have also occurred in *G. hirsutum* grown under 0% shade cover; however,  
541 there was no change in the effect of nitrogen fertilization on *G. hirsutum* carbon  
542 costs to acquire nitrogen grown under 0% shade cover relative to other shade  
543 cover treatments. Regardless, the possibility of growth limitation due to pot vol-  
544 ume suggests that effects of increasing nitrogen fertilization on carbon costs to  
545 acquire nitrogen in both species grown under 0% shade cover could have been un-  
546 derestimated. Follow-up studies using a similar experimental design with a larger  
547 pot volume would be necessary in order to determine whether these patterns were  
548 impacted by pot volume-induced growth limitation.

#### 549 2.4.4 *Conclusions*

550 In conclusion, this chapter provides empirical evidence that carbon costs to ac-  
551 quire nitrogen are influenced by light availability and soil nitrogen fertilization  
552 in a species capable of acquiring nitrogen via symbiotic nitrogen fixation and a  
553 species not capable of forming such associations. We show that carbon costs to

554 acquire nitrogen generally increase with increasing light availability and decrease  
555 with increasing nitrogen fertilization. This chapter provides important empirical  
556 data needed to evaluate the formulation of carbon costs to acquire nitrogen in  
557 terrestrial biosphere models, particularly carbon costs to acquire nitrogen that  
558 are associated with symbiotic nitrogen fixation. Findings broadly support the  
559 general formulation of these carbon costs in the FUN biogeochemical model in  
560 response to shifts in nitrogen availability. However, there is a need for future  
561 studies to explicitly quantify carbon costs to acquire nitrogen under different en-  
562 vironmental contexts, over longer temporal scales, and using larger selections of  
563 phylogenetically related species. In addition, I suggest that future studies mini-  
564 mize the limitations associated with the metric used here by explicitly measuring  
565 belowground carbon fates independently.

566

## Chapter 3

567 Soil nitrogen availability modifies leaf nitrogen economies in mature  
568 temperate deciduous forests: a direct test of photosynthetic least-cost  
569 theory

570 3.1 Introduction

571 Photosynthesis represents the largest carbon flux between the atmosphere and  
572 land surface (IPCC 2021), and plays a central role in biogeochemical cycling at  
573 multiple spatial and temporal scales (Vitousek and Howarth 1991; LeBauer and  
574 Treseder 2008; Kaiser et al. 2015; Wieder et al. 2015). Therefore, carbon and  
575 energy fluxes simulated by terrestrial biosphere models are sensitive to the formu-  
576 lation of photosynthetic processes (Ziehn et al. 2011; Bonan et al. 2011; Booth  
577 et al. 2012; Smith et al. 2016; Smith et al. 2017) and must be represented using  
578 robust, empirically tested processes (Prentice et al. 2015; Wieder et al. 2019).  
579 Current formulations of photosynthesis vary across terrestrial biosphere models  
580 (Smith and Dukes 2013; Rogers et al. 2017), which causes variation in modeled  
581 ecosystem processes (Knorr 2000; Knorr and Heimann 2001; Bonan et al. 2011;  
582 Friedlingstein et al. 2014) and casts uncertainty on the ability of these models to  
583 accurately predict terrestrial ecosystem responses and feedbacks to global change  
584 (Zaehle et al. 2005; Schaefer et al. 2012; Davies-Barnard et al. 2020).

585 Terrestrial biosphere models commonly represent C<sub>3</sub> photosynthesis through  
586 variants of the Farquhar et al. (1980) biochemical model (Smith and Dukes 2013;  
587 Rogers 2014; Rogers et al. 2017). This well-tested photosynthesis model es-  
588 timates leaf-level carbon assimilation, or photosynthetic capacity, as a function  
589 of the maximum rate of Ribulose-1,5-bisphosphate carboxylase-oxygenase (Ru-

590 bisco) carboxylation ( $V_{cmax}$ ) and the maximum rate of Ribulose-1,5-bisphosphate  
591 (RuBP) regeneration ( $J_{max}$ ) (Farquhar et al. 1980). Many terrestrial biosphere  
592 models predict these model inputs based on plant functional group specific lin-  
593 ear relationships between leaf nutrient content and  $V_{cmax}$  (Smith and Dukes 2013;  
594 Rogers 2014; Rogers et al. 2017) under the tenet that a large fraction of leaf nutri-  
595 ents, and nitrogen in particular, are partitioned toward building and maintaining  
596 enzymes that support photosynthetic capacity, such as Rubisco (Brix 1971; Gul-  
597 mon and Chu 1981; Evans 1989; Kattge et al. 2009; Walker et al. 2014). Terres-  
598 trial biosphere models predict leaf nutrient content from soil nutrient availability  
599 based on the assumption that increasing soil nutrients generally increases leaf nu-  
600 trients (Firn et al. 2019; Li et al. 2020; Liang et al. 2020) which, in the case of  
601 nitrogen, generally corresponds with an increase in photosynthetic processes (Li  
602 et al. 2020; Liang et al. 2020).

603       Recent work calls the generality of relationships between soil nutrient avail-  
604 ability, leaf nutrient content, and photosynthetic capacity into question, suggest-  
605 ing instead that leaf nutrients and photosynthetic capacity are better predicted as  
606 an integrated product of aboveground climate, leaf traits, and soil nutrient avail-  
607 ability, rather than soil nutrient availability alone (Dong et al. 2017; Dong et al.  
608 2020; Dong et al. 2022; Firn et al. 2019; Smith et al. 2019; Peng et al. 2021).  
609 It has been reasoned that this result is because plants allocate added nutrients to  
610 growth and storage rather than alterations in leaf chemistry (Smith et al. 2019),  
611 perhaps as a result of nutrient limitation of primary productivity (LeBauer and  
612 Treseder 2008; Fay et al. 2015). Additionally, recent work suggests that relation-  
613 ships between leaf nutrient content and photosynthesis vary across environments,

614 and that the proportion of leaf nutrient content allocated to photosynthetic tis-  
615 sue varies over space and time with plant acclimation and adaptation responses  
616 to light availability, vapor pressure deficit, soil pH, soil nutrient availability, and  
617 environmental factors that influence leaf mass per area (Pons and Pearcy 1994;  
618 Niinemets and Tenhunen 1997; Evans and Poorter 2001; Hikosaka and Shigeno  
619 2009; Ghimire et al. 2017; Onoda et al. 2017; Luo et al. 2021). The use of linear  
620 relationships between leaf nutrient content and  $V_{cmax}$  to predict photosynthetic  
621 capacity, as commonly used in terrestrial biosphere models (Rogers 2014), is not  
622 capable of detecting such responses.

623 Photosynthetic least-cost theory provides an alternative framework for un-  
624 derstanding relationships between soil nutrient availability, leaf nutrient content,  
625 and photosynthetic capacity (Harrison et al. 2021). Leveraging a two-input mi-  
626 croeconomics approach (Wright et al. 2003), the theory posits that plants accli-  
627 mate to a given environment by optimizing leaf photosynthesis rates at the lowest  
628 summed cost of using nutrients and water (Prentice et al. 2014; Wang et al. 2017;  
629 Smith et al. 2019; Paillassa et al. 2020). Across resource availability gradients,  
630 the theory predicts that optimal photosynthetic rates can be achieved by trading  
631 less efficient use of a resource that is less costly to acquire (or more abundant)  
632 for more efficient use of a resource more costly to acquire (or less abundant). For  
633 example, an increase in soil nutrient availability should reduce the cost of acquir-  
634 ing and using nutrients (Bae et al. 2015; Eastman et al. 2021; Perkowski et al.  
635 2021), which could increase leaf nutrient investments in photosynthetic proteins to  
636 allow similar photosynthetic rates to be achieved with higher nutrient use (lower  
637 nutrient use efficiency) but lower water use (greater water use efficiency). The

638 theory suggests similar tradeoffs in response to increasing soil pH (Paillassa et al.  
639 2020), specifically, that increasing soil pH should reduce the cost of acquiring soil  
640 nutrients due to an increase in plant-available nutrient concentration (Paillassa  
641 et al. 2020; Dong et al. 2022). The theory is also capable of reconciling dynamic  
642 leaf nutrient-photosynthesis relationships at global scales (Luo et al. 2021).

643 Patterns expected from photosynthetic least-cost theory have recently re-  
644 ceived empirical support both in global environmental gradient (Smith et al.  
645 2019; Paillassa et al. 2020; Luo et al. 2021; Querejeta et al. 2022; Wester-  
646 band et al. 2023) and local manipulative invasion (Bialic-Murphy et al. 2021)  
647 studies. However, nutrient addition experiments that directly examine nutrient-  
648 water use tradeoffs expected from the theory are rare (but see Guerrieri et al.  
649 2011), and only global gradient studies testing the theory have considered soil pH  
650 in their analyses. As a result, there is a need to use nutrient addition and soil pH  
651 manipulation experiments to test mechanisms driving responses predicted by the  
652 theory.

653 In this study, I measured leaf responses to soil nitrogen availability in five  
654 deciduous tree species growing in the upper canopy of mature closed canopy tem-  
655 perate forests in the northeastern United States. Soil nitrogen availability and pH  
656 were manipulated through a nitrogen-by-pH field manipulation experiment with  
657 treatments applied since 2011, eight years prior to measurement. Two different soil  
658 nitrogen treatments were applied to increase nitrogen availability with opposing  
659 effects on soil pH. An additional nitrogen-free acidifying treatment was expected  
660 to decrease soil pH. I hypothesized that increased soil nitrogen availability would  
661 enable plants to increase nutrient uptake and create more photosynthetic enzymes

662 per leaf, allowing similar photosynthetic rates achieved with lower leaf C<sub>i</sub>:C<sub>a</sub> and  
663 increased leaf nitrogen content allocated to photosynthetic leaf tissue. I expected  
664 that this response would be driven by a reduction in the cost of acquiring nitrogen,  
665 which would cause trees to sacrifice efficient nitrogen use to enable more efficient  
666 use of other limiting resources (i.e., water). Finally, I hypothesized similar leaf  
667 responses to increasing soil pH.

668 3.2 Methods

669 3.2.1 *Study site description*

670 I conducted this study in summer 2019 at three stands located within a 20-km ra-  
671 dius of Ithaca, NY, USA (42.444 °N, 76.502 °W). All stands contain mature,  
672 closed-canopy forests dominated by deciduous tree species. Stands contained  
673 abundant sugar maple (*Acer saccharum* Marshall), American beech (*Fagus gran-*  
674 *difolia* Ehrh.), and white ash (*Fraxinus americana* L.), accounting for 43%, 15%,  
675 and 17% of the total aboveground biomass across the three stands, respectively,  
676 with less frequent red maple (*Acer rubrum* L.; 9% of total aboveground biomass)  
677 and red oak occurrences (*Quercus rubra* L.; 10% of total aboveground biomass).  
678 Soils at each site were broadly classified as a channery silt loam Inceptisols using  
679 the USDA NRCS Web Soil Survey data product (Soil Survey Staff 2022). Between  
680 2006 and 2020, study sites averaged 972 mm of precipitation per year and had an  
681 average temperature of 7.9 °C per a weather station located near the Cornell Uni-  
682 versity campus (42.449 °N, 76.449 °W) part of the NOAA NCEI Global Historical  
683 Climatology Network (Menne et al. 2012).

**684** 3.2.2 *Experimental design*

**685** Four 40 m x 40 m plots were set up at each site in 2009, each with an additional  
**686** 10 m buffer along plot perimeters (60 m x 60 m total). The plots were set up as a  
**687** nitrogen-by-pH field manipulation experiment, with one each of four treatments  
**688** at each site. Two nitrogen treatments were applied, both at  $50 \text{ kg N ha}^{-1} \text{ yr}^{-1}$ , as  
**689** either sodium nitrate ( $\text{NaNO}_3$ ) to raise soil pH, or ammonium sulfate ( $(\text{NH}_4)_2\text{SO}_4$ )  
**690** to acidify; an elemental sulfur treatment was selected to acidify without nitrogen,  
**691** applied at the same rate of S addition ( $57 \text{ kg S ha}^{-1} \text{ yr}^{-1}$ ); and control plots  
**692** received no additions. All amendments were added in pelletized form using hand-  
**693** held fertilizer spreaders to both the main plots and buffers. Amendments were  
**694** divided into three equal doses distributed across the growing season from 2011-  
**695** 2017 and added as a single dose from 2018 onward. During 2019, plots were  
**696** fertilized during the week of May 20.

**697** 3.2.3 *Leaf gas exchange and trait measurements*

**698** I sampled one leaf each from 6 to 10 individuals per plot between June 25 and July  
**699** 12, 2019 for gas exchange measurements (Table B1). Leaves were collected from  
**700** deciduous broadleaf trees represented across all sites and plots and were replicated  
**701** in efforts to mimic the species abundance of each plot at each site. I attempted  
**702** to collect leaves from the upper canopy to reduce differential shading effects on  
**703** leaf physiology. Leaves were accessed by pulling down small branches using an  
**704** arborist's slingshot and weighted beanbag attached to a throw line. Branches  
**705** were immediately recut under deionized water and remained submerged to reduce  
**706** stomatal closure and avoid xylem embolism, as done in Smith and Dukes (2018),

707 until gas exchange data were collected.

708 Randomly selected leaves with little to no visible external damage were  
709 attached to a Li-COR LI-6800 (Li-COR Bioscience, Lincoln, Nebraska, USA)  
710 portable photosynthesis machine to measure net photosynthesis ( $A_{\text{net}}$ ;  $\mu\text{mol m}^{-2}$   
711  $\text{s}^{-1}$ ), stomatal conductance ( $g_{\text{sw}}$ ;  $\text{mol m}^{-2} \text{s}^{-1}$ ), and intercellular  $\text{CO}_2$  concentra-  
712 tion ( $C_i$ ;  $\mu\text{mol mol}^{-1}$ ) at different reference  $\text{CO}_2$  concentrations ( $C_a$ ;  $\mu\text{mol mol}^{-1}$ )  
713 concentrations (i.e., an  $A_{\text{net}}/C_i$  curve) under saturating light conditions (2,000  
714  $\mu\text{mol m}^{-2} \text{s}^{-1}$ ). Reference  $\text{CO}_2$  concentrations followed the sequence: 400, 300,  
715 200, 100, 50, 400, 400, 600, 800, 1000, 1200, 1500, and 2000  $\mu\text{mol mol}^{-1} \text{CO}_2$ . Leaf  
716 temperatures were not controlled in the cuvette and ranged from 21.8 °C to 31.7  
717 °C (mean±SD: 27.2±2.2 °C). A linear and second order log-polynomial nonlinear  
718 regression suggested no effect of temperature on stomatal conductance measured  
719 at 400  $\mu\text{mol mol}^{-1} \text{CO}_2$  or net photosynthesis measured at 400  $\mu\text{mol mol}^{-1} \text{CO}_2$   
720 (Table B2, B3; Fig. B1). All  $A_{\text{net}}/C_i$  curves were generated within one hour of  
721 branch severance.

722 Leaf morphological and chemical traits were collected on the same leaf used  
723 to generate each  $A_{\text{net}}/C_i$  curve. Images of each leaf were taken using a flat-bed  
724 scanner to determine fresh leaf area using the ‘LeafArea’ R package (Katabuchi  
725 2015), which automates leaf area calculations using ImageJ software (Schneider  
726 et al. 2012). Each leaf was dried at 65°C for at least 48 hours, weighed, and  
727 ground using a Retsch MM200 ball mill grinder (Verder Scientific, Inc., Newtown,  
728 PA, USA) until homogenized. Leaf mass per unit leaf area ( $M_{\text{area}}$ ,  $\text{g m}^{-2}$ ) was  
729 calculated as the ratio of dry leaf biomass to fresh leaf area. Using a subsample  
730 of ground and homogenized leaf biomass, leaf nitrogen content ( $N_{\text{mass}}$ ;  $\text{gN g}^{-1}$ )

731 and leaf  $\delta^{13}\text{C}$  (‰, relative to Vienna Pee Dee Belemnite international reference  
 732 standard) were measured at the Cornell Stable Isotope Lab with an elemental  
 733 analyzer (NC 2500, CE Instruments, Wigan, UK) interfaced to an isotope ratio  
 734 mass spectrometer (Delta V Isotope Ratio Mass Spectrometer, ThermoFisher Sci-  
 735 entific, Waltham, MA, USA). Leaf nitrogen content per unit leaf area ( $N_{\text{area}}$ ; g N  
 736  $\text{m}^{-2}$ ) was calculated by multiplying  $N_{\text{mass}}$  by  $M_{\text{area}}$ .

737 I used leaf  $\delta^{13}\text{C}$  values to estimate  $\chi$  (unitless), which is an isotope-derived  
 738 estimate of the leaf  $C_i:C_a$  ratio. While intercellular and atmospheric  $\text{CO}_2$  concen-  
 739 trations were directly measured during each  $A_{\text{net}}/C_i$  curve, deriving  $\chi$  from  $\delta^{13}\text{C}$   
 740 provides a more integrative estimate of the leaf  $C_i:C_a$  over an individual leaf's  
 741 lifespan. I derived  $\chi$  following the approach of Farquhar et al. (1989) described  
 742 in Cernusak et al. (2013):

$$\chi = \frac{\Delta^{13}\text{C} - a}{b - a} \quad (3.1)$$

743 where  $\Delta^{13}\text{C}$  represents the relative difference between leaf  $\delta^{13}\text{C}$  (‰) and air  $\delta^{13}\text{C}$   
 744 (‰), and is calculated from the following equation:

$$\Delta^{13}\text{C} = \frac{\delta^{13}\text{C}_{\text{air}} - \delta^{13}\text{C}_{\text{leaf}}}{1 + \delta^{13}\text{C}_{\text{leaf}}} \quad (3.2)$$

745 where  $\delta^{13}\text{C}_{\text{air}}$  is assumed to be -8‰ (Keeling et al. 1979; Farquhar et al. 1989),  $a$   
 746 represents the fractionation between  $^{12}\text{C}$  and  $^{13}\text{C}$  due to diffusion in air, assumed  
 747 to be 4.4‰, and  $b$  represents the fractionation caused by Rubisco carboxylation,  
 748 assumed to be 27‰ (Farquhar et al. 1989).

**749** 3.2.4  $A_{net}/C_i$  curve-fitting and parameter estimation

**750** I fit  $A_{net}/C_i$  curves of each individual using the ‘fitaci’ function in the ‘plante-  
**751** cophys’ R package (Duursma 2015). This function estimates the maximum rate  
**752** of Rubisco carboxylation ( $V_{cmax}$ ;  $\mu\text{mol m}^{-2} \text{s}^{-1}$ ) and maximum rate of electron  
**753** transport for RuBP regeneration ( $J_{max}$ ;  $\mu\text{mol m}^{-2} \text{s}^{-1}$ ) based on the Farquhar,  
**754** von Caemmerer, and Berry biochemical model of C<sub>3</sub> photosynthesis (Farquhar  
**755** et al. 1980). For each curve fit, I included triose phosphate utilization (TPU)  
**756** limitation to avoid underestimating  $J_{max}$  (Gregory et al. 2021). Curves were  
**757** visually examined to confirm the likely presence of TPU limitation.

**758** I determined Michaelis-Menten coefficients for Rubisco affinity to CO<sub>2</sub> ( $K_c$ ;  
**759**  $\mu\text{mol mol}^{-1}$ ) and O<sub>2</sub> ( $K_o$ ;  $\mu\text{mol mol}^{-1}$ ), and the CO<sub>2</sub> compensation point ( $\Gamma^*$ ;  
**760**  $\mu\text{mol mol}^{-1}$ ) using leaf temperature and equations described in Medlyn et al.  
**761** (2002) and derived in Bernacchi et al. (2001). Specifically,  $K_c$  and  $K_o$  were  
**762** calculated as:

$$K_c = 404.9 * \exp^{\frac{79430(T_k - 298)}{298RT_k}} \quad (3.3)$$

**763** and

$$K_o = 278.4 * \exp^{\frac{36380(T_k - 298)}{298RT_k}} \quad (3.4)$$

**764** while  $\Gamma^*$  was calculated as:

$$\Gamma^* = 42.75 * \exp^{\frac{37830(T_k - 298)}{298RT_k}} \quad (3.5)$$

**765** In all three equations,  $T_k$  is the leaf temperature (in Kelvin) during each  $A_{\text{net}}/C_i$

**766** curve and R is the universal gas constant ( $8.314 \text{ J mol}^{-1} \text{ K}^{-1}$ ).

**767** I standardized  $V_{\text{cmax}}$  and  $J_{\text{max}}$  estimates to  $25^\circ\text{C}$  using a modified Arrhe-

**768** nius equation (Kattge and Knorr 2007):

$$k_{25} = \frac{k_{\text{obs}}}{e^{\frac{H_a(T_{\text{obs}} - T_{\text{ref}})}{T_{\text{ref}}RT_{\text{obs}}}} * \frac{1+e^{\frac{T_{\text{ref}}\Delta S - H_d}{T_{\text{obs}}}}}{1+e^{\frac{T_{\text{obs}}\Delta S - H_d}{T_{\text{obs}}}}}} \quad (3.6)$$

**769**  $k_{25}$  represents the standardized  $V_{\text{cmax}}$  or  $J_{\text{max}}$  rate at  $25^\circ\text{C}$ ,  $k_{\text{obs}}$  represents the

**770**  $V_{\text{cmax}}$  or  $J_{\text{max}}$  estimate at the average leaf temperature measured inside the cuvette

**771** during the  $A_{\text{net}}/C_i$  curve.  $H_a$  is the activation energy of  $V_{\text{cmax}}$  ( $71,513 \text{ J mol}^{-1}$ )

**772** Kattge and Knorr (2007) or  $J_{\text{max}}$  ( $49,884 \text{ J mol}^{-1}$ ) (Kattge and Knorr 2007).

**773**  $H_d$  represents the deactivation energy of both  $V_{\text{cmax}}$  and  $J_{\text{max}}$  ( $200,000 \text{ J mol}^{-1}$ )

**774** (Medlyn et al. 2002), and R represents the universal gas constant ( $8.314 \text{ J mol}^{-1}$

**775**  $\text{K}^{-1}$ ).  $T_{\text{ref}}$  represents the standardized temperature of  $298.15 \text{ K}$  ( $25^\circ\text{C}$ ) and  $T_{\text{obs}}$

**776** represents the mean leaf temperature (in K) during each  $A_{\text{net}}/C_i$  curve.  $\Delta S$  is an

**777** entropy term that (Kattge and Knorr 2007) derived as a linear relationship with

**778** average growing season temperature ( $T_g$ ;  $^\circ\text{C}$ ), where:

$$\Delta S_{v_{\text{cmax}}} = -1.07 T_g + 668.39 \quad (3.7)$$

**779** and

$$\Delta S_{j_{\text{max}}} = -0.75 T_g + 659.70 \quad (3.8)$$

**780** I estimated  $T_g$  in Equations 3.7 and 3.8 based on mean daily (24-hour) air tem-  
**781** perature of the 30 days leading up to the day of each sample collection using the  
**782** same weather station reported in the site description. I used  $V_{cmax25}$  and  $J_{max25}$   
**783** estimates to calculate the ratio of  $J_{max25}$  to  $V_{cmax25}$  ( $J_{max25}:V_{cmax25}$ ; unitless).

**784** 3.2.5 *Proportion of leaf nitrogen allocated to photosynthesis and structure*

**785** I used equations from Niinemets and Tenhunen (1997) to estimate the proportion  
**786** of leaf nitrogen content allocated to Rubisco and bioenergetics. The proportion of  
**787** leaf nitrogen allocated to Rubisco ( $\rho_{rubisco}$ ; gN gN $^{-1}$ ) was calculated as a function  
**788** of  $V_{cmax25}$  and  $N_{area}$ :

$$\rho_{rubisco} = \frac{V_{cmax25} N_r}{V_{cr} N_{area}} \quad (3.9)$$

**789** where  $N_r$  is the amount of nitrogen in Rubisco, set to 0.16 gN (gN in Rubisco) $^{-1}$   
**790** and  $V_{cr}$  is the maximum rate of RuBP carboxylation per unit Rubisco protein,  
**791** set to 20.5  $\mu$ mol CO $_2$  (g Rubisco) $^{-1}$ . The proportion of leaf nitrogen allocated to  
**792** bioenergetics ( $\rho_{bioe}$ ; gN gN $^{-1}$ ) was similarly calculated as a function of  $J_{max25}$  and  
**793**  $N_{area}$ :

$$\rho_{bioe} = \frac{J_{max25} N_b}{J_{mc} N_{area}} \quad (3.10)$$

**794** where  $N_b$  is the amount of nitrogen in cytochrome f, set to 0.12407 gN ( $\mu$ mol  
**795** cytochrome f) $^{-1}$  assuming a constant 1: 1: 1.2 cytochrome f: ferredoxin NADP  
**796** reductase: coupling factor molar ratio (Evans and Seemann 1989; Niinemets and  
**797** Tenhunen 1997), and  $J_{mc}$  is the capacity of electron transport per cytochrome f,

**798** set to 156  $\mu\text{mol}$  electron ( $\mu\text{mol}$  cytochrome f) $^{-1}\text{s}^{-1}$ .

**799** I estimated the proportion of leaf nitrogen content allocated to photosynthetic tissue ( $\rho_{\text{photo}}$ ;  $\text{gN gN}^{-1}$ ) as the sum of  $\rho_{\text{rubisco}}$  and  $\rho_{\text{bioe}}$ . This calculation  
**800** is an underestimate of the proportion of leaf nitrogen allocated to photosynthetic  
**801** tissue because it does not include nitrogen allocated to light harvesting proteins.  
**802** This leaf nitrogen pool was not included because I did not perform chlorophyll  
**803** extractions on focal leaves. However, the proportion of leaf nitrogen content al-  
**804** located to light harvesting proteins tends to be small relative to  $\rho_{\text{rubisco}}$  and  $\rho_{\text{bioe}}$ ,  
**805** and may scale with changes in  $\rho_{\text{rubisco}}$  and  $\rho_{\text{bioe}}$  (Niinemets and Tenhunen 1997).

**807** Finally, the proportion of leaf nitrogen content allocated to structural tissue  
**808** ( $\rho_{\text{structure}}$ ;  $\text{gN gN}^{-1}$ ) was estimated as:

$$\rho_{\text{structure}} = \frac{N_{\text{cw}}}{N_{\text{area}}} \quad (3.11)$$

**809** where  $N_{\text{cw}}$  is the leaf nitrogen content allocated to cell walls ( $\text{gN m}^{-2}$ ), calculated  
**810** as a function of  $M_{\text{area}}$  using an empirical equation from Onoda et al. (2017):

$$N_{\text{cw}} = 0.000355 * M_{\text{area}}^{1.39} \quad (3.12)$$

### **811** 3.2.6 *Tradeoffs between nitrogen and water use*

**812** Photosynthetic nitrogen use efficiency (PNUE;  $\mu\text{mol CO}_2 \text{ mol}^{-1} \text{ N s}^{-1}$ ) was cal-  
**813** culated by dividing  $A_{\text{net}}$  by  $N_{\text{area}}$ , first converting  $N_{\text{area}}$  to  $\text{mol N m}^{-2}$  using the  
**814** molar mass of nitrogen ( $14 \text{ g mol}^{-1}$ ). I used  $\chi$  as an indicator of water use effi-  
**815** ciency, which exploratory analyses suggest had similar responses to soil nitrogen

816 availability and pH as intrinsic water use efficiency measured from gas exchange  
817 ( $A_{\text{net}}/g_{\text{sw}}$ ). Tradeoffs between nitrogen and water use were determined by cal-  
818 culating the ratio of  $N_{\text{area}}$  to  $\chi$  ( $N_{\text{area}}:\chi$ ; gN m<sup>-2</sup>) and  $V_{\text{cmax25}}$  to  $\chi$  ( $V_{\text{cmax25}}:\chi$ ;  
819  $\mu\text{mol m}^{-2} \text{ s}^{-1}$ ). This approach is similar to tradeoff calculations in which nitrogen-  
820 water use tradeoffs are measured as the ratio of  $N_{\text{area}}$  or  $V_{\text{cmax25}}$  to  $g_{\text{sw}}$  (Paillassa  
821 et al. 2020; Bialic-Murphy et al. 2021). In this chapter, I quantify these rela-  
822 tionships using  $\chi$  in lieu of  $g_{\text{sw}}$  because  $g_{\text{sw}}$  rapidly changes with environmental  
823 conditions and therefore may have been altered by recent tree branch severance  
824 and/or placement in the cuvette.

825 3.2.7 *Soil nitrogen availability and pH*

826 To characterize soil nitrogen availability at the time of our leaf gas exchange  
827 measurements, I used mixed bed resin bags to quantify mobile ammonium-N and  
828 nitrate-N concentrations in each plot. Lycra mesh bags were filled with 5 g of  
829 Dowex® Marathon MR-3 hydrogen and hydroxide form resin (MilliporeSigma,  
830 Burlington, MA USA) and sealed with a zip tie. Each bag was activated by  
831 soaking in 0.5 M HCl for 20 minutes, then in 2 M NaCl until pH of the saline  
832 solution stabilized, as described in Allison et al. (2008). Five resin bags were  
833 inserted about 10 cm below the soil surface at each plot on June 25, 2019: one  
834 near each of the four plot corners and one near the plot center. All resin bags  
835 were collected 24 days later on July 19, 2019 and were frozen until extracted.

836 Prior to anion and cation extraction, each resin bag was rinsed with ul-  
837 trapure water (MilliQ IQ 7000; Millipore Sigma, Burlington, MA) to remove any  
838 surface soil residues. Anions and cations were extracted from surface-cleaned

839 resin bags by individually soaking and shaking each bag in 100 mL of a 0.1 M  
840 HCl/2.0 M NaCl matrix for one hour. Using a microplate reader (Biotek Synergy  
841 H1; Biotek Instruments, Winooski, VT USA), I quantified nitrate-N concentra-  
842 tions spectrophotometrically at 540 nm with the end product of a single reagent  
843 vanadium (III) chloride reaction (Doane and Horwáth 2003), and ammonium-N  
844 concentrations quantified at 650 nm with the end product of a modified phenol-  
845 hypochlorite reaction (Weatherburn 1967; Rhine et al. 1998). Both the single  
846 reagent vanadium (III) chloride and modified phenol-hypochlorite methodologies  
847 are well established for determining nitrate-N and ammonium-N concentrations  
848 in resin bag extracts (Arnone 1997; Allison et al. 2008). I used a series of nega-  
849 tive and positive controls throughout each well plate to verify the accuracy and  
850 precision of our measurements, assaying each resin bag extract and control in  
851 triplicate. Soil nitrogen availability was estimated as the sum of the nitrate-N  
852 and ammonium-N concentration in each resin bag, normalized per g of resin and  
853 duration in the field ( $\mu\text{g N g}^{-1}$  resin  $\text{d}^{-1}$ ), then subsequently averaged across all  
854 resin bags in a plot for a plot-level mean.

855 Soil pH was measured on 0-10 cm mineral soil samples collected prior to  
856 fertilization in 2019. Near each of the four plot corners, three 5.5 cm diameter soil  
857 cores were collected after first removing the forest floor where present. Each set  
858 of three cores was placed in a plastic bag, and later composited by hand mixing  
859 and sieved to 4mm. Soil pH was determined for a 1:2 soil:water slurry (10 g field-  
860 moist soil to 20 mL DI water) of each sample using an Accumet AB15 pH meter  
861 with flushable junction probe (Fisher Scientific; Hampton, NH, USA), and was  
862 estimated at the plot level as the mean soil pH within each plot.

**863** 3.2.8 *Statistical analyses*

**864** I built two separate series of linear mixed-effects models to explore effects of soil  
**865** nitrogen availability, soil pH, species, and leaf nitrogen content on leaf physiolog-  
**866** ical traits. In the first series of linear mixed-effects models, I explored the effect  
**867** of soil nitrogen availability, soil pH, and species on leaf nitrogen content, leaf  
**868** photosynthesis, stomatal conductance, and nitrogen-water use tradeoffs. Models  
**869** included plot-level soil nitrogen availability and plot-level soil pH as continuous  
**870** fixed effects, species as a categorical fixed effect, and site as a categorical ran-  
**871** dom intercept term. Interaction terms between fixed effects were not included  
**872** due to the small number of experimental plots. I built a series of separate mod-  
**873** els with this independent variable structure to quantify individual effects of soil  
**874** nitrogen availability, soil pH, and species on  $N_{\text{area}}$ ,  $M_{\text{area}}$ ,  $N_{\text{mass}}$ ,  $A_{\text{net}}$ ,  $V_{\text{cmax25}}$ ,  
**875**  $J_{\text{max25}}$ ,  $J_{\text{max25}}:V_{\text{cmax25}}$ ,  $\rho_{\text{rubisco}}$ ,  $\rho_{\text{bioenergetics}}$ ,  $\rho_{\text{photo}}$ ,  $\rho_{\text{structure}}$ ,  $\chi$ , PNUE,  $N_{\text{area}}:\chi$ , and  
**876**  $V_{\text{cmax25}}:\chi$ .

**877** A second series of linear mixed-effects models were built to investigate  
**878** relationships between leaf nitrogen content and photosynthetic parameters. Sta-  
**879** tistical models included  $N_{\text{area}}$  as a single continuous fixed effect with species and  
**880** site designated as individual random intercept terms. I used this independent  
**881** variable structure to quantify individual effects of leaf nitrogen content on  $A_{\text{net}}$ ,  
**882**  $V_{\text{cmax25}}$ ,  $J_{\text{max25}}$ ,  $J_{\text{max25}}:V_{\text{cmax25}}$ , and  $\chi$ .

**883** For all linear mixed-effects models, I used Shapiro-Wilk tests of normality  
**884** to determine whether linear mixed-effects models satisfied residual normality as-  
**885** sumptions. If residual normality assumptions were not met, then models were fit  
**886** using dependent variables that were natural log transformed. If residual normal-

887 ity assumptions were still not met (Shapiro-Wilk:  $p<0.05$ ), then models were fit  
888 using dependent variables that were square root transformed. All residual nor-  
889 mality assumptions for both sets of models that did not originally satisfy residual  
890 normality assumptions were met with either a natural log or square root data  
891 transformation (Shapiro-Wilk:  $p>0.05$  in all cases).

892 In the first series of models, models for  $N_{\text{area}}$ ,  $M_{\text{area}}$ ,  $N_{\text{mass}}$ ,  $V_{\text{cmax}25}$ ,  $J_{\text{max}25}$ ,  
893  $\chi$ ,  $N_{\text{area}}:\chi$ , and  $V_{\text{cmax}25}:\chi$ ,  $\rho_{\text{rubisco}}$ ,  $\rho_{\text{bioenergetics}}$ ,  $\rho_{\text{photo}}$ ,  $\rho_{\text{structure}}$  satisfied residual  
894 normality assumptions without data transformations (Shapiro-Wilk:  $p>0.05$  in  
895 all cases). The model for  $J_{\text{max}25}:V_{\text{cmax}25}$  satisfied residual normality assumptions  
896 with a natural log data transformation, while models for  $A_{\text{net}}$  and PNUE each  
897 satisfied residual normality assumptions with square root data transformations.  
898 In the second series of models, models for  $V_{\text{cmax}25}$ ,  $J_{\text{max}25}$ ,  $\chi$ , and  $V_{\text{cmax}25}:\chi$  satis-  
899 fied residual normality assumptions without data transformations (Shapiro-Wilk:  
900  $p>0.05$  in all cases). The model for  $J_{\text{max}25}:V_{\text{cmax}25}$  required a natural log data  
901 transformation and the model for  $A_{\text{net}}$  required a square root data transformation  
902 (Shapiro-Wilk:  $p>0.05$  in both cases).

903 In all models, I used the ‘lmer’ function in the ‘lme4’ R package (Bates  
904 et al. 2015) to fit each model and the ‘Anova’ function in the ‘car’ R package  
905 (Fox and Weisberg 2019) to calculate Type II Wald’s  $\chi^2$  and determine the signif-  
906 icance level ( $\alpha=0.05$ ) of each fixed effect coefficient. Finally, I used the ‘emmeans’  
907 R package (Lenth, 2019) to conduct post-hoc comparisons using Tukey’s tests,  
908 where degrees of freedom were approximated using the Kenward-Roger approach  
909 (Kenward and Roger 1997). All analyses and plots were conducted in R version  
910 4.1.1 (R Core Team 2021). All figure regression lines and associated 95% confi-

**911** dence interval error bars were plotted using predictions generated across the soil  
**912** nitrogen availability gradient using the ‘emmeans’ R package (Lenth 2019).

**913** 3.3 Results

**914** 3.3.1 *Leaf nitrogen content*

**915** Increasing soil nitrogen availability generally increased  $N_{\text{area}}$  (Table 3.1; Fig. 3.1a).  
**916** This pattern was driven by an increase in  $N_{\text{mass}}$  (Table 3.1; Fig. 3.1c) and a  
**917** marginal increase in  $M_{\text{area}}$  (Table 3.1; Fig. 3.1e) with increasing soil nitrogen  
**918** availability. There was no effect of soil pH on  $N_{\text{area}}$ ,  $N_{\text{mass}}$ , or  $M_{\text{area}}$  (Table 3.1);  
**919** however, I also observed strong differences in  $N_{\text{area}}$  (Fig. 3.1b),  $N_{\text{mass}}$  (Fig. 3.1d),  
**920** and  $M_{\text{area}}$  (Fig. 3.1e) between species (Table 3.1).

**Table 3.1.** Effects of soil nitrogen availability, soil pH, and species on leaf nitrogen content per unit leaf area ( $N_{\text{area}}$ ; gN m<sup>-2</sup>), leaf nitrogen content per unit leaf mass ( $N_{\text{mass}}$ ; gN g<sup>-1</sup>), and leaf mass per unit leaf area ( $M_{\text{area}}$ ; g m<sup>-2</sup>)\*

	$N_{\text{area}}$			$N_{\text{mass}}$			$M_{\text{area}}$			
	df	Coefficient	$\chi^2$	p	Coefficient	$\chi^2$	p	Coefficient	$\chi^2$	p
Intercept	-	9.03E-01	-	-	1.68E+00	-	-	4.60E+01	-	-
Soil N	1	1.68E-02	11.990	<b>0.001</b>	1.25E-02	6.902	<b>0.009</b>	4.87E-01	4.143	<b>0.042</b>
Soil pH	1	9.28E-02	0.836	0.361	8.08E-02	0.663	0.415	4.05E+00	0.653	0.419
Species	4	-	72.128	<b>&lt;0.001</b>	-	35.074	<b>&lt;0.001</b>	-	29.869	<b>&lt;0.001</b>

921 \*Significance determined using Type II Wald  $\chi^2$  tests ( $\alpha=0.05$ ). P-values<0.05 are in bold.

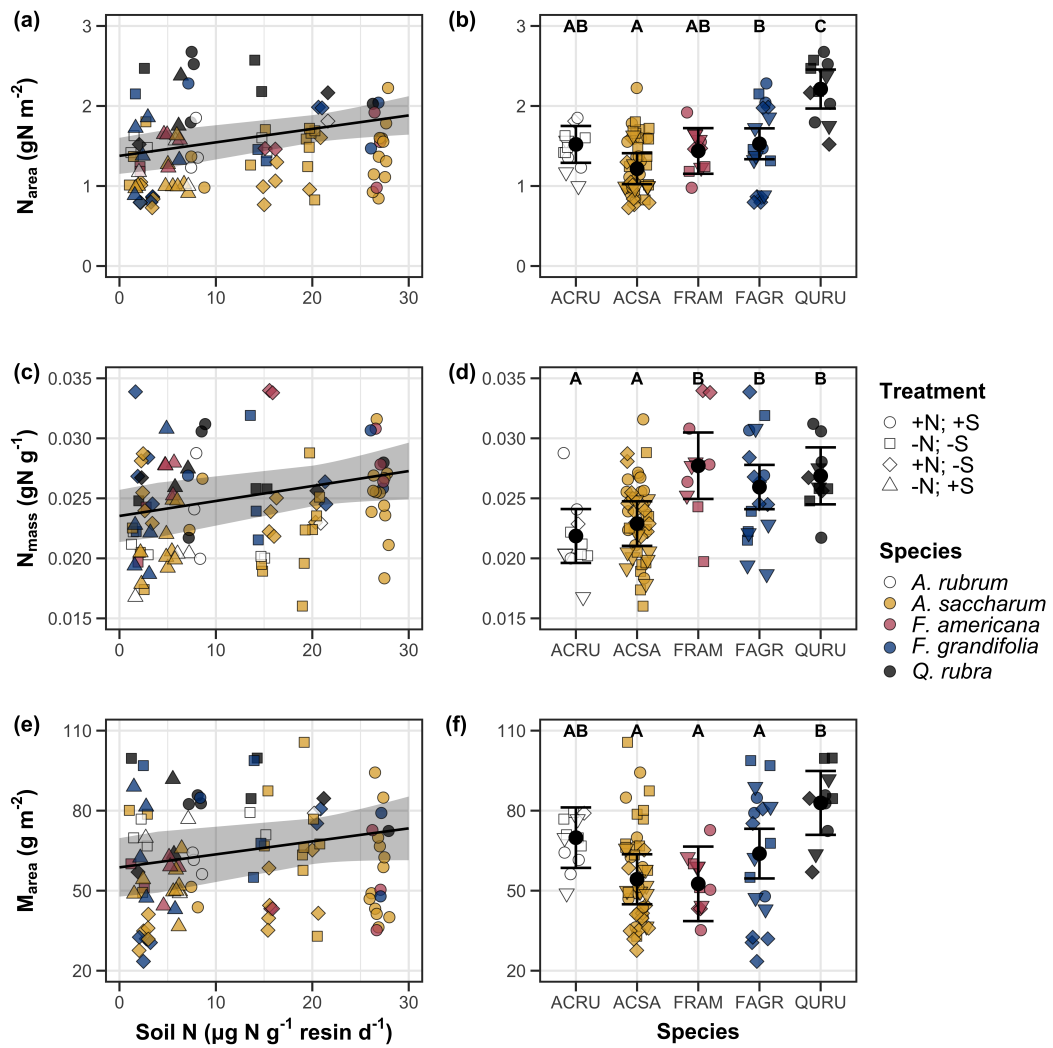


**Figure 3.1.** Effects of soil N availability and species on leaf nitrogen content per unit leaf area (a-b), leaf nitrogen content per unit leaf biomass (c-d), and leaf mass per unit leaf area (e-f). Soil nitrogen availability is represented on the x-axis in the left column of panels, while species is represented on the x-axis in the right column of panels. Tree species are represented as colored points and treatment plots are represented as shaped points, jittered for visibility. Species are abbreviated in the right column of panels through their assigned NRCS PLANTS Database symbol (USDA NRCS 2022), grouped along the x-axis per common mycorrhizal association, where the first three species commonly associate with arbuscular mycorrhizae (ACRU, ACSA, FAGR) and the second two species with ectomycorrhizae (FAGR, QURU). Trendlines are only included when the regression slope is statistically different from zero ( $p < 0.05$ ).

**922** 3.3.2 *Net photosynthesis and leaf biochemistry*

**923** Increasing soil nitrogen availability generally had no effect on  $A_{\text{net}}$ ,  $V_{\text{cmax25}}$ ,  $J_{\text{max25}}$ ,  
**924** or  $J_{\text{max25}}:V_{\text{cmax25}}$  (Table 3.2, Figs. 3.2a, 3.2d, 3.2g). I also observed strong species  
**925** effects on all measured leaf photosynthetic traits (Table 3.2; Figs. 3.2b, 3.2e, 3.2h).  
**926** Increasing soil pH had a marginal negative effect on  $A_{\text{net}}$ , but had no effect on  
**927**  $V_{\text{cmax25}}$ ,  $J_{\text{max25}}$ , or  $J_{\text{max25}}:V_{\text{cmax25}}$  (Table 3.2). There was a weak positive effect of  
**928** increasing  $N_{\text{area}}$  on  $A_{\text{net}}$  (Fig. 3.2c), but quite strong positive effects of increasing  
**929**  $N_{\text{area}}$  on  $V_{\text{cmax25}}$  and  $J_{\text{max25}}$  (Table 3.2; Fig. 3.2f and 3.2i).

**Table 3.2.** Effects of soil nitrogen availability, soil pH, species, and  $N_{\text{area}}$  on net photosynthesis ( $A_{\text{net}}$ ;  $\mu\text{mol m}^{-2} \text{s}^{-1}$ ), the maximum rate of Rubisco carboxylation ( $V_{\text{cmax25}}$ ;  $\mu\text{mol m}^{-2} \text{s}^{-1}$ ), the maximum rate of RuBP regeneration ( $J_{\text{max25}}$ ;  $\mu\text{mol m}^{-2} \text{s}^{-1}$ ), and the ratio of the maximum rate of RuBP regeneration to the maximum rate of Rubisco carboxylation ( $J_{\text{max25}}:V_{\text{cmax25}}$ ; unitless)\*

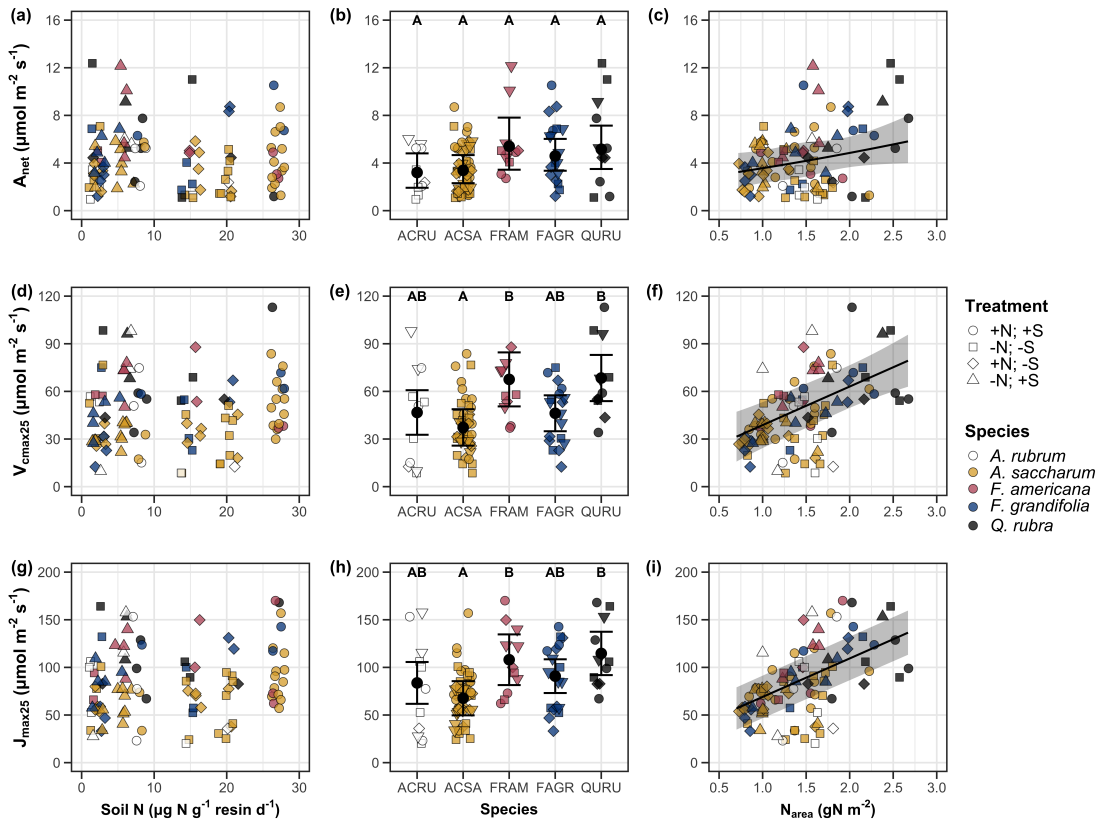
	$A_{\text{net}}$			$V_{\text{cmax25}}$			$J_{\text{max25}}$			
	df	Coefficient	$\chi^2$	p	Coefficient	$\chi^2$	p	Coefficient	$\chi^2$	p
(Intercept)	-	3.29E+00 <sup>b</sup>	-	-	6.38E+01	-	-	1.12E+02	-	-
Soil N	1	-1.23E-03 <sup>b</sup>	1.798	0.180	-3.84E-01	1.745	0.187	-6.70E-01	2.172	0.141
Soil pH	1	-3.09E-01 <sup>b</sup>	3.312	0.069	-4.91E+00	0.655	0.418	-8.18E+00	0.742	0.389
Species	4	-	11.838	<b>0.019</b>	-	31.748	<0.001	-	27.291	<0.001
$(N_{\text{area}} \text{ int.})$	-	6.59E-01 <sup>b</sup>	-	-	1.45E-01	-	-	2.86E+01	-	-
$N_{\text{area}}$	4	3.13E-01 <sup>b</sup>	4.790	<b>0.029</b>	2.43E+01	22.616	<0.001	4.04E+01	28.259	<0.001

	$J_{\text{max25}}:V_{\text{cmax25}}$			
	df	Coefficient	$\chi^2$	p
(Intercept)	-	6.59E-01 <sup>a</sup>	-	-
Soil N	1	7.04E-04 <sup>a</sup>	0.088	0.767
Soil pH	1	-7.84E-03 <sup>a</sup>	0.025	0.874
Species	4	-	12.745	<b>0.013</b>
$(N_{\text{area}} \text{ int.})$	-	6.69E-01 <sup>a</sup>	-	-
$N_{\text{area}}$	4	-4.69E-02 <sup>a</sup>	1.142	0.285

54

930 \*Significance determined using Type II Wald  $\chi^2$  tests ( $\alpha=0.05$ ). P-values less than 0.05 are in bold, while p-values  
 931 between 0.05 and 0.1 are italicized. Superscript letters indicate model coefficients fit to natural-log (<sup>a</sup>) or square-root  
 932 (<sup>b</sup>) transformed data. Relationships between  $N_{\text{area}}$  and each response variable were fit using the second series of  
 933 bivariate mixed-effects models, so model coefficients and results are independent of model coefficients and results  
 934 reported for relationships between soil nitrogen, soil pH, and species for each response variable.



**Figure 3.2.** Effects of soil nitrogen availability (left column of panels), species (middle column of panels), and leaf nitrogen content per unit leaf area (right column of panels) on net photosynthesis (a-c), maximum Rubisco carboxylation rate (d-f), and maximum RuBP regeneration rate (g-i). Soil nitrogen availability is represented on the x-axis in the left column of panels, species is represented on the x-axis in the middle column of panels, and leaf nitrogen content per unit leaf area is represented continuously on the x-axis in the right column of panels. Species abbreviations and position along the x-axis in the middle column of panels, colored points, shapes, and trendlines are as explained in Figure 3.1.

**935** 3.3.3 *Leaf nitrogen allocation*

**936** Neither soil nitrogen availability nor soil pH affected the proportion of leaf nitrogen  
**937** allocated to Rubisco or bioenergetics (Table 3.3; Fig. 3.3a, Fig. 3.3c). There was  
**938** also no effect of soil nitrogen availability or soil pH on the proportion of leaf  
**939** nitrogen allocated to photosynthesis (Table 3.3; Fig. 3.3f). I found no effect of  
**940** soil nitrogen availability or soil pH on the proportion of leaf nitrogen allocated to  
**941** structure (Table 3.3; Fig 3.3g). Species varied in the proportion of leaf nitrogen  
**942** allocated to Rubisco, photosynthesis, and structure (Fig 3.3b, Fig. 3.3f, Fig 3.3h),  
**943** with no detectable species effect on the proportion of leaf nitrogen allocated to  
**944** bioenergetics (Table 3.3, Fig. 3.3d).

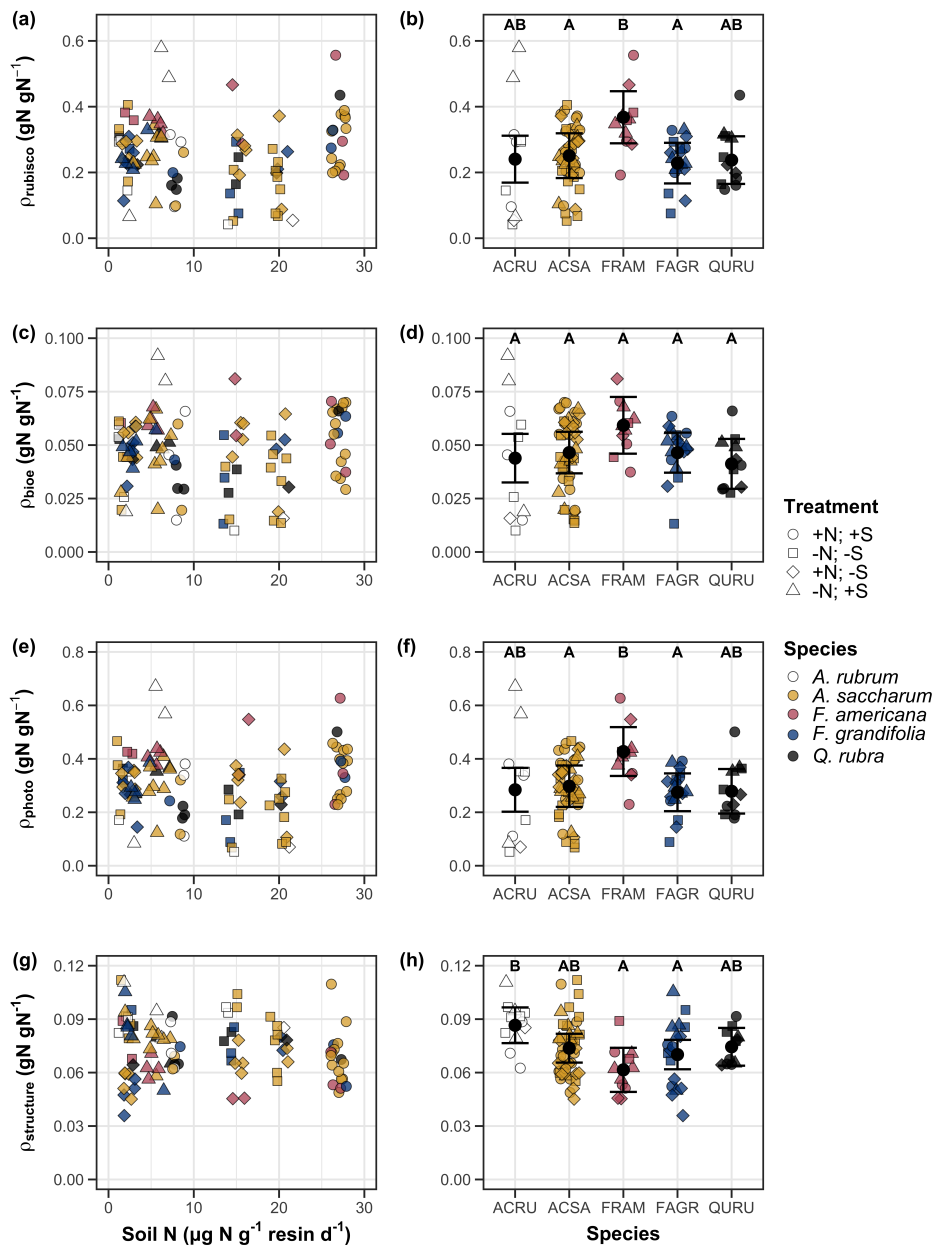
**Table 3.3.** Effects of soil nitrogen availability, soil pH, and species on the proportion of leaf nitrogen content allocated to photosynthesis ( $\rho_{\text{photo}}$ ; gN gN<sup>-1</sup>), Rubisco ( $\rho_{\text{rubisco}}$ ; gN gN<sup>-1</sup>), bioenergetics ( $\rho_{\text{bioe}}$ ; gN gN<sup>-1</sup>), and structure ( $\rho_{\text{structure}}$ ; gN gN<sup>-1</sup>)\*

	$\rho_{\text{photo}}$			$\rho_{\text{rubisco}}$			$\rho_{\text{bioe}}$			
	df	Coefficient	$\chi^2$	p	Coefficient	$\chi^2$	p	Coefficient	$\chi^2$	p
Intercept	-	4.93E-01	-	-	4.17E-01	-	-	7.64E-02	-	-
Soil N	1	-1.23E-03	0.521	0.470	-1.04E-03	0.501	0.479	-1.77E-04	0.557	0.455
Soil pH	1	-4.37E-02	1.581	0.209	-3.70E-02	1.511	0.219	-6.84E-03	1.941	0.164
Species	4	-	13.106	<b>0.011</b>	-	14.152	<b>0.007</b>	-	7.300	0.121

	$\rho_{\text{structure}}$			
	df	Coefficient	$\chi^2$	p
Intercept	-	9.77E-02	-	-
Soil N	1	-2.29E-04	1.165	0.280
Soil pH	1	-1.87E-03	0.179	0.672
Species	4	-	16.428	<b>0.002</b>

**945** \*Significance determined using Type II Wald  $\chi^2$  tests ( $\alpha=0.05$ ). P-values less than 0.05 are in bold.



**Figure 3.3.** Effects of soil nitrogen availability and species on the proportion of leaf nitrogen content allocated to Rubisco (a-b), bioenergetics (c-d), photosynthesis (e-f), and structure (g-h). Soil nitrogen availability is represented on the x-axis in the left column of panels and species are represented on the x-axis in the right column of panels. Species abbreviations and position along the x-axis in the middle column of panels, colored points, shapes, trendlines, error bars, and compact lettering are as explained in Figure 3.1.

**946** 3.3.4 *Tradeoffs between nitrogen and water use*

**947** Although soil nitrogen availability did not affect  $\chi$  (Table 3.4; Fig. 3.4a), increasing  
**948** soil nitrogen availability decreased PNUE (Table 3.4; Fig. 3.4d) and increased  
**949** the ratio of  $N_{\text{area}}:\chi$  (Table 3.4; Fig. 3.4f). Specifically, this response yielded a  
**950** 26% reduction in PNUE and 37% stimulation in  $N_{\text{area}}:\chi$  across the soil nitrogen  
**951** availability gradient. There was no apparent effect of soil nitrogen availability on  
**952**  $V_{\text{cmax25}}:\chi$  (Table 3.4; Fig. 3.4h). Increasing soil pH had a weak marginal nega-  
**953** tive effect on PNUE, but did not influence  $\chi$ ,  $N_{\text{area}}:\chi$ , or  $V_{\text{cmax25}}:\chi$  (Table 3.4). I  
**954** observed differences in  $\chi$  (Fig. 3.4b), PNUE (Fig. 3.4e),  $N_{\text{area}}:\chi$  (Fig. 3.4g), and  
**955**  $V_{\text{cmax25}}:\chi$  (Fig. 3.4i) between species (Table 3.4). Finally, increasing  $N_{\text{area}}$  had a  
**956** strong negative effect on  $\chi$  (Table 3.4; Fig. 3.4c) and a strong positive effect on  
**957**  $V_{\text{cmax25}}:\chi$  (Table 3.4; Fig. 3.4j).

**Table 3.4.** Effects of soil nitrogen availability, soil pH, species, and  $N_{\text{area}}$  on  $\chi$  (unitless), photosynthetic nitrogen use efficiency (PNUE;  $\mu\text{mol CO}_2 \text{ mol}^{-1} \text{ N s}^{-1}$ ), leaf nitrogen content per unit  $\chi$  ( $N_{\text{area}}:\chi$ ;  $\text{gN m}^{-2}$ ), and maximum Rubisco carboxylation rate per unit  $\chi$  ( $V_{\text{cmax25}}:\chi$ ;  $\mu\text{mol m}^{-2} \text{ s}^{-1}$ )<sup>\*</sup>

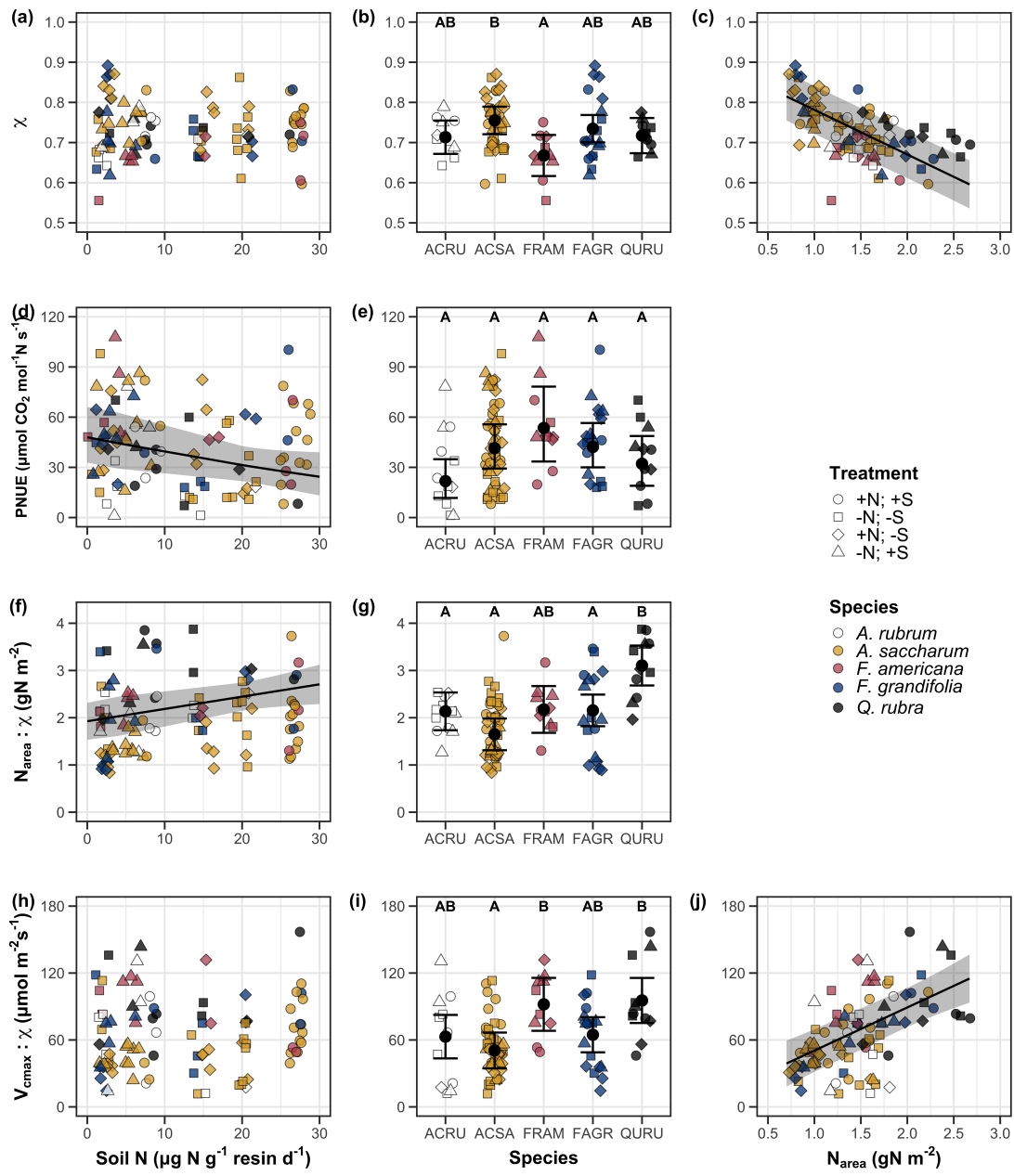
	df	$\chi$		PNUE				$N_{\text{area}}:\chi$		
		Coefficient	$\chi^2$	p	Coefficient	$\chi^2$	p	Coefficient	$\chi^2$	p
(Intercept)	-	8.12E-01	-	-	9.57E+00 <sup>b</sup>	-	-	9.19E-01	-	-
Soil N	1	-1.14E-03	1.698	0.193	-6.63E-02 <sup>b</sup>	6.396	<b>0.011</b>	2.60E-02	9.533	<b>0.002</b>
Soil pH	1	-1.91E-02	1.087	0.297	-9.25E-01 <sup>b</sup>	2.843	<i>0.092</i>	2.03E-01	1.321	0.250
Species	4	-	18.843	<b>0.001</b>	-	13.454	<b>0.009</b>	-	52.983	<b>&lt;0.001</b>
( $N_{\text{area}}$ int.)	-	8.93E-01	-	-	-	-	-	-	-	-
$N_{\text{area}}$	1	-1.11E-01	80.606	<b>&lt;0.001</b>	-	-	-	-	-	-

	df	$V_{\text{cmax25}}:\chi$		
		Coefficient	$\chi^2$	p
(Intercept)	-	7.20E+01	-	-
Soil N	1	3.99E-01	0.963	0.326
Soil pH	1	-3.12E+00	0.138	0.711
Species	4	-	31.450	<b>&lt;0.001</b>
( $N_{\text{area}}$ int.)	-	1.18E+01	-	-
$N_{\text{area}}$	4	3.87E+01	32.797	<b>&lt;0.001</b>

60

958 \*Significance determined using Type II Wald  $\chi^2$  tests ( $\alpha = 0.05$ ).  $P$ -values less than 0.05 are in bold, while  $p$ -values  
 959 between 0.05 and 0.1 are italicized. Superscript letters indicate model coefficients fit to natural-log (<sup>a</sup>) or square-root  
 960 (<sup>b</sup>) transformed data. Relationships between  $N_{\text{area}}$  and each response variable were fit using the second series of  
 961 bivariate mixed-effects models, so model coefficients and results are independent of model coefficients and results  
 962 reported for relationships between soil nitrogen, soil pH, and species for each response variable.



**Figure 3.4.** Effects of soil nitrogen availability and species on the proportion of leaf nitrogen content allocated to Rubisco (a-b), bioenergetics (c-d), photosynthesis (Rubisco + bioenergetics; e-f), and structure (g-h). Soil nitrogen availability is represented on the x-axis in the left column of panels and species are represented on the x-axis in the right column of panels. Species abbreviations and position along the x-axis in the middle column of panels, colored points, shapes, trendlines, error bars, and compact lettering are as explained in Figure 3.1.

**963** 3.4 Discussion

**964** Photosynthetic least-cost theory provides an explanation for understanding rela-  
**965** tionships between soil nutrient availability, leaf nutrient allocation, and photosyn-  
**966** thetic capacity. The theory suggests that plants acclimate to a given environment  
**967** by optimizing leaf photosynthesis rates at the lowest summed cost of using nu-  
**968** trients and water (Prentice et al. 2014; Wang et al. 2017; Smith et al. 2019;  
**969** Paillassa et al. 2020). The theory predicts that an increase in soil nutrient avail-  
**970** ability should allow similar photosynthesis rates to be achieved with increased leaf  
**971** nutrient content and photosynthetic capacity (i.e.,  $V_{cmax25}$  and  $J_{max25}$ ) at lower  
**972** leaf  $C_i:C_a$  ( $\chi$ ), resulting in an increase in water use efficiency, decrease in nutri-  
**973** ent use efficiency, and increase in both leaf nutrient content and photosynthetic  
**974** capacity per unit  $\chi$ . The theory predicts similar leaf responses to increasing soil  
**975** pH under acidic conditions, presumably due to generally faster nutrient cycle dy-  
**976** namics and consequent reductions in the cost of acquiring nutrients relative to  
**977** water with increasing soil pH (Wang et al. 2017; Paillassa et al. 2020; Dong et al.  
**978** 2020).

**979** Supporting the theory, increasing soil nitrogen availability was associated  
**980** with increased leaf nitrogen content, a pattern that reduced photosynthetic nitro-  
**981** gen use efficiency and increased leaf nitrogen content per unit  $\chi$ . Increasing soil  
**982** nitrogen coincided with slight, but non-significant decreases in  $\chi$  and increases  
**983** in  $V_{cmax25}$  and  $J_{max25}$  ( $p<0.2$ , Table 3.2). The positive trend between soil ni-  
**984** trogen availability and photosynthetic capacity was supported by the concurrent  
**985** strong increase in leaf nitrogen content with increasing soil nitrogen availability,  
**986** which resulted in no change in the proportion of leaf nitrogen content allocated to

987 photosynthesis across the soil nitrogen availability gradient. Additionally, leaf ni-  
988 trogen content exhibited a strong negative correlation with  $\chi$ , indicative of strong  
989 nitrogen-water use tradeoffs at the leaf level. Responses tended to vary more due  
990 to soil nitrogen availability than soil pH. Overall, these findings are consistent  
991 with the nutrient-water use tradeoffs predicted from theory.

992 3.4.1 *Soil nitrogen availability modifies tradeoffs between nitrogen and water use*  
993 In support of expected least-cost outcomes and past environmental gradient stud-  
994 ies (Dong et al. 2017; Paillassa et al. 2020), increasing soil nitrogen availability  
995 was associated with increased leaf nitrogen content. Soil nitrogen availability had  
996 smaller impacts on measures of net photosynthesis and  $\chi$ , which led to reductions  
997 in PNUE and increases in leaf nitrogen content per unit  $\chi$ , as expected from the-  
998 ory. Photosynthetic least-cost theory suggests that reductions in PNUE should  
999 be driven by an increase in the proportion of leaf nitrogen allocated to photosyn-  
1000 thetic tissue, a pattern that should allow plants to achieve optimal photosynthetic  
1001 rates with greater photosynthetic capacity to make better use of available light.  
1002 Contrasting theory predictions, I found no effect of soil nitrogen availability on  
1003 photosynthetic capacity. However, photosynthetic capacity did tend to increase  
1004 with increasing soil nitrogen availability ( $p<0.20$ ; Table 3.2) resulting in no effect  
1005 of soil nitrogen availability on the relative fraction of leaf nitrogen allocated to  
1006 photosynthesis, Rubisco, or bioenergetics. These lines of evidence support the  
1007 idea that trees use additional nitrogen to support increased leaf nitrogen alloca-  
1008 tion toward photosynthetic tissue and enhance photosynthetic capacity (Wright  
1009 et al. 2003).

1010        Soil nitrogen availability had a stronger effect on leaf nitrogen than photo-  
1011        synthetic capacity. This pattern suggests that additional plant nitrogen up-  
1012        take due to increased soil nitrogen availability was also being used to support  
1013        non-photosynthetic nitrogen pools, possibly to structural tissue or stress-induced  
1014        amino acid and polyamine synthesis (Minocha et al. 2000; Onoda et al. 2004;  
1015        Bubier et al. 2011). While I found no change in the proportion of leaf nitrogen  
1016        allocated to leaf structural tissue, the overall stimulation in leaf nitrogen content  
1017        with increasing soil nitrogen availability suggests an increase in the net amount of  
1018        nitrogen invested in leaf structural tissue along the nitrogen availability gradient.  
1019        Importantly, leaf nitrogen allocated to structure was calculated using an empiri-  
1020        cal relationship between  $M_{\text{area}}$  and the amount of leaf nitrogen allocated to cell  
1021        walls (Onoda et al. 2017). As the generality of relationships between  $M_{\text{area}}$  and  
1022        the amount of leaf nitrogen allocated to cell walls has been called into question  
1023        (Harrison et al. 2009), future work should consider explicitly measuring nitrogen  
1024        allocation to cell wall tissue and stress-induced amino acid synthesis to confirm  
1025        these patterns.

1026        In opposition to patterns expected from least-cost theory, increasing soil  
1027        nitrogen availability had no apparent effect on  $\chi$ . Interestingly, despite the null  
1028        effect of soil nitrogen availability on  $\chi$ , I observed a strong negative effect of  
1029        increasing  $N_{\text{area}}$  on  $\chi$ , consistent with the nitrogen-water use tradeoffs expected  
1030        from theory. The null response of  $\chi$  to increasing soil nitrogen availability may  
1031        have been due to a lack of water limitation in the system, given that the area  
1032        received approximately 20% more precipitation (1167 mm) during the 12-month  
1033        period leading up to our measurement period than normally expected (972 mm).

**1034** However, droughts can and do occur in temperate forests of the northeastern  
**1035** United States (Sweet et al. 2017), so the observed increase in leaf nitrogen content  
**1036** with increasing soil nitrogen availability could be a strategy that allows trees to  
**1037** hedge bets against drier than normal growing seasons (Onoda et al. 2004; Onoda  
**1038** et al. 2017; Hallik et al. 2009). As was suggested in Paillassa et al. (2020),  
**1039** and more recently by Querejeta et al. (2022), negative effects of soil nitrogen  
**1040** availability on  $\chi$  may increase with increasing aridity. This strategy would be  
**1041** especially advantageous if it allows individuals growing in arid regions to maintain  
**1042** carbon assimilation rates with reduced water loss. Future work should attempt to  
**1043** quantify interactive roles of climate and soil nitrogen availability on nitrogen-water  
**1044** use tradeoffs, which could be done using coordinated and multifactor nutrient  
**1045** (Borer et al. 2014) and water (Knapp et al. 2017) manipulation experiments  
**1046** across broad climatic gradients.

**1047** 3.4.2 *Soil pH did not modify tradeoffs between nitrogen and water usage*  
**1048** While the primary purpose of this study was to examine the role of soil nitrogen  
**1049** availability on nitrogen-water use tradeoffs, this experiment manipulated both  
**1050** soil nitrogen and pH, thus providing an opportunity to isolate the these variables  
**1051** [DWS: example edit]. Previous correlational studies along environmental gradi-  
**1052** ents have identified soil pH as a particularly important factor that can modify  
**1053** tradeoffs between nutrient and water use (Smith et al. 2019; Paillassa et al. 2020;  
**1054** Westerband et al. 2023) and the proportion of leaf nitrogen allocated to photosyn-  
**1055** thesis (Luo et al. 2021). Such studies implied that these patterns may be driven  
**1056** by reductions in the cost of acquiring nutrients relative to water with increasing

1057 pH, which may be exacerbated in acidic soils.

1058 Consistent with theory (Wright et al. 2003; Prentice et al. 2014), results  
1059 indicate that increasing soil pH was negatively associated with PNUE. However,  
1060 there was no effect of soil pH on leaf nitrogen content,  $\chi$ , or leaf nitrogen content  
1061 per unit  $\chi$ , most likely because the experimental nitrogen additions increased soil  
1062 nitrogen supply while both increasing (sodium nitrate) and decreasing (ammo-  
1063 nium sulfate) soil pH. These results suggest that soil pH did not play a major  
1064 role in modifying expected photosynthetic least-cost theory patterns, contrasting  
1065 findings from Paillassa et al. (2020) and other gradient studies that note positive  
1066 effects of increasing soil pH on leaf nitrogen content, Rubisco carboxylation, and  
1067  $\chi$  (Viet et al. 2013; Cornwell et al. 2018; Luo et al. 2021). Instead, null responses  
1068 to soil pH show that leaf photosynthetic parameters depend more on soil nitrogen  
1069 availability than pH per se, and that inferences from gradient studies might be  
1070 confounding covariation between nitrogen availability and soil acidity.

1071 3.4.3 *Species identity explains a large amount of variation in leaf and whole*  
1072 *plant traits*

1073 Species [species identity?] generally explained a larger amount of variation in  
1074 measured leaf traits than soil nitrogen availability or soil pH. Interspecific vari-  
1075 ation is an important factor to consider when deducing mechanisms that drive  
1076 photosynthetic least-cost theory, particularly for species that form distinct myc-  
1077 orrhizal associations or have different photosynthetic pathways, growth forms, or  
1078 leaf habit (Espelta et al. 2005; Adams et al. 2016; Bialic-Murphy et al. 2021;  
1079 Scott and Smith 2022). The need to consider species may also be important when

**1080** comparing nutrient-water use tradeoffs in early and late successional species, or in  
**1081** species with different resource economic strategies (Abrams and Mostoller 1995;  
**1082** Ellsworth and Reich 1996; Wright et al. 2004; Reich 2014; Onoda et al. 2017;  
**1083** Ziegler et al. 2020).

**1084** [DWS: implications for chapter 2?]

**1085** A strength of the study design and sampling effort is that it controls for  
**1086** many species differences that should modify nitrogen-water use tradeoffs expected  
**1087** from theory. All tree species measured in this study shared the leaf habit of de-  
**1088** ciduous broadleaves, were growing in forests of similar successional stage, but  
**1089** differed in mycorrhizal association and consequent resource economic strategies.  
**1090** As stands tended to be dominated by trees that associate with arbuscular myc-  
**1091** orrhizae (*Fraxinus* and both *Acer* species made up roughly 70% of total above-  
**1092** ground biomass across stands), ecosystem biogeochemical cycle dynamics may be  
**1093** more closely aligned to the inorganic nutrient economy proposed in Phillips et al.  
**1094** (2013), which may promote stronger nitrogen-water use tradeoffs in tree species  
**1095** that associate with arbuscular mycorrhizae. This result was not observed here,  
**1096** as photosynthetic properties varied as much within as across the two mycorrhizal  
**1097** associations represented.

**1098** 3.4.4 *Implications for photosynthetic least-cost theory model development*

**1099** In the field, soil nutrient availability is heterogeneous across time and space (Ta-  
**1100** ble B4). Unaccounted within-plot heterogeneity may have contributed to the low  
**1101** amount of variation explained by soil nitrogen availability in statistical models,  
**1102** as resin bags are a coarse surrogate for soil nitrogen availability. Despite this, I

1103 still observed evidence for nutrient-water use tradeoffs, suggesting that observed  
1104 responses reported here may be an underestimate toward the net effect of soil ni-  
1105 trogen availability on these tradeoffs. While I urge caution in the interpretation of  
1106 these results, they do provide a promising baseline for future studies investigating  
1107 patterns expected from photosynthetic least-cost theory at finer spatiotemporal  
1108 resolutions.

1109 The general stronger relationship between leaf nitrogen content and photo-  
1110 synthetic parameters versus between leaf nitrogen content and soil nitrogen avail-  
1111 ability suggests that leaf nitrogen content is more directly tied to photosynthesis  
1112 than soil nitrogen availability. While this could be due to the high spatiotemporal  
1113 heterogeneity of soil nitrogen availability, principles from photosynthetic least-  
1114 cost theory suggest that leaf nitrogen content is the downstream product of leaf  
1115 nutrient demand to build and maintain photosynthetic machinery, which is set by  
1116 aboveground environmental conditions such as light availability, CO<sub>2</sub>, tempera-  
1117 ture, or vapor pressure deficit (Smith et al. 2019; Paillassa et al. 2020; Peng et al.  
1118 2021; Westerband et al. 2023). The stronger relationship between leaf nitrogen  
1119 and photosynthetic parameters, paired with the strong negative relationship be-  
1120 tween leaf nitrogen and  $\chi$ , could indicate a relatively stronger effect of climate on  
1121 leaf nitrogen-photosynthesis relationships than soil resource availability. However,  
1122 the short distance between plots and across sites limited my ability to test this  
1123 mechanism.

1124 Variation in soil pH affected least cost responses less than variations in soil  
1125 nitrogen availability, in part because experimental treatments directly increased  
1126 soil nitrogen and affected soil pH in opposite directions. While soil pH has been

1127 shown to drive nitrogen-water tradeoffs in global gradient analyses (Viet et al.  
1128 2013; Paillassa et al. 2020), these responses may be due to covariations between  
1129 soil pH and nutrient cycling rather than a role of pH per se. The direct manipula-  
1130 tions of soil pH and soil nitrogen availability in this study partly disentangle these  
1131 factors and show that variation in nitrogen availability matters more for least-cost  
1132 tradeoffs than pH alone.

1133 3.4.5 *Conclusions*

1134 Increasing soil nitrogen availability generally increased leaf nitrogen content (both  
1135 area- and mass-based), but did not significantly influence  $\chi$ . This shift in leaf ni-  
1136 trogen led to a reduction in PNUE, and an increase in leaf nitrogen per unit  
1137  $\chi$  with increasing soil nitrogen availability. Despite null effects of soil nitrogen  
1138 availability on  $\chi$ , I observed a strong negative relationship between leaf nitrogen  
1139 content and  $\chi$ . These results provide empirical support for the nutrient-water use  
1140 tradeoffs expected from photosynthetic least-cost theory in response to increas-  
1141 ing soil nutrient availability, but suggest that all tenets of the theory may not  
1142 hold in every environment. These results experimentally test previous work sug-  
1143 gesting that leaf nitrogen-water economies vary across gradients of soil nutrient  
1144 availability and pH, and show that variations in nutrient availability matter more  
1145 for determining variation in leaf photosynthetic traits than soil pH.

1146

## Chapter 4

1147 The relative cost of resource use for photosynthesis drives variance in  
1148 leaf nitrogen content across a climate and soil resource availability  
1149 gradient

1150 4.1 Introduction

1151 Terrestrial biosphere models, which comprise the land surface component of Earth  
1152 system models, are sensitive to the formulation of photosynthetic processes (Knorr  
1153 and Heimann 2001; Ziehn et al. 2011; Booth et al. 2012; Walker et al. 2021).  
1154 This is because photosynthesis is the largest carbon flux between the atmosphere  
1155 and terrestrial biosphere (IPCC 2021), and is constrained by ecosystem carbon  
1156 and nutrient cycles (Hungate et al. 2003; LeBauer and Treseder 2008; Fay et al.  
1157 2015). Many terrestrial biosphere models formulate photosynthesis by parame-  
1158 terizing photosynthetic capacity within plant functional groups through empiri-  
1159 cal linear relationships between area-based leaf nitrogen content ( $N_{\text{area}}$ ) and the  
1160 maximum carboxylation rate of Ribulose-1,5-bisphosphate carboxylase/oxygenase  
1161 ( $V_{\text{cmax}}$ ) (Kattge et al. 2009; Rogers 2014; Rogers et al. 2017). Models are also  
1162 beginning to include connected carbon-nitrogen cycles (Wieder et al. 2015; Shi  
1163 et al. 2016; Davies-Barnard et al. 2020; Braghieri et al. 2022), which allows leaf  
1164 photosynthesis to be predicted directly through changes in  $N_{\text{area}}$  and indirectly  
1165 through changes in soil nitrogen availability (e.g., LPJ-GUESS, CLM5.0) (Smith  
1166 et al. 2014; Lawrence et al. 2019). Despite recent model developments, open  
1167 questions remain regarding the generality of ecological relationships between soil  
1168 nitrogen availability, leaf nitrogen content, and leaf photosynthesis across edaphic  
1169 and climatic gradients.

1170 Empirical support for positive relationships between soil nitrogen availabil-  
1171 ity and  $N_{\text{area}}$  is abundant (Firn et al. 2019; Liang et al. 2020), and is a result  
1172 often attributed to the high nitrogen cost of building and maintaining Rubisco  
1173 (Evans 1989; Evans and Seemann 1989; Onoda et al. 2004; Walker et al. 2014;  
1174 Onoda et al. 2017; Dong et al. 2020). Such patterns imply that positive relation-  
1175 ships between soil nitrogen availability and  $N_{\text{area}}$  should increase leaf photosyn-  
1176 thesis and photosynthetic capacity by increasing the maximum rate of Rubisco  
1177 carboxylation through increased investments to Rubisco construction and mainte-  
1178 nance. This integrated  $N_{\text{area}}$ -photosynthesis response to soil nitrogen availability  
1179 has been observed both in manipulative experiments and across environmental  
1180 gradients (Field and Mooney 1986; Evans 1989; Walker et al. 2014; Li et al.  
1181 2020), and is thought to be driven by ecosystem nitrogen limitation, which lim-  
1182 its primary productivity globally (LeBauer and Treseder 2008; Fay et al. 2015).  
1183 However, this response is not consistently observed, as recent studies note variable  
1184  $N_{\text{area}}$ -photosynthesis relationships across edaphic and climatic gradients (Liang  
1185 et al. 2020; Luo et al. 2021) and that aboveground growing conditions (e.g., light  
1186 availability, temperature, vapor pressure deficit) or species identity traits (e.g.,  
1187 photosynthetic pathway, nitrogen acquisition strategy) may be more important  
1188 for explaining variance in  $N_{\text{area}}$  and photosynthetic capacity across environmental  
1189 gradients (Adams et al. 2016; Dong et al. 2017; Smith et al. 2019; Dong et al.  
1190 2020; Peng et al. 2021; Dong et al. 2022; Westerband et al. 2023).

1191 One hypothesized mechanism to explain variance in  $N_{\text{area}}$  across environ-  
1192 mental gradients has been proposed via photosynthetic least-cost theory (Wright  
1193 et al. 2003; Prentice et al. 2014; Paillassa et al. 2020; Harrison et al. 2021).

**1194** The theory predicts that plants acclimate to environments by optimizing photo-  
**1195** synthetic assimilation rates at the lowest summed cost of nitrogen and water use  
**1196** (Wright et al. 2003; Prentice et al. 2014). In a given environment, the theory  
**1197** suggests that nitrogen and water use can be substituted for each other to maintain  
**1198** the lowest summed cost of resource use, such that optimal photosynthetic rates  
**1199** are achieved with less efficient use of the more abundant and less costly resource  
**1200** to acquire in exchange for more efficient use of the less abundant and more costly  
**1201** resource to acquire.

**1202** Photosynthetic least-cost theory predicts that, all else equal, an increase in  
**1203** soil nitrogen availability should decrease the cost of acquiring and using nitrogen  
**1204** relative to water (a ratio referred to herein as  $\beta$ ), resulting in optimal photosyn-  
**1205** thetic rates achieved with greater  $N_{\text{area}}$  at lower stomatal conductance and lower  
**1206** leaf  $C_i:C_a$  (Wright et al. 2003; Prentice et al. 2014; Paillassa et al. 2020). Alter-  
**1207** natively, an increase in soil moisture should reduce costs of water acquisition and  
**1208** use, increasing  $\beta$  (Lavergne et al. 2020), stomatal conductance, and leaf  $C_i:C_a$ , re-  
**1209** sulting in optimal photosynthetic rates achieved with decreased  $N_{\text{area}}$ . The theory  
**1210** also predicts variability in stomatal conductance and  $N_{\text{area}}$  in response to climatic  
**1211** factors, suggesting that the optimal response to increased vapor pressure deficit  
**1212** should be a reduction in stomatal conductance and leaf  $C_i:C_a$  that is counter-  
**1213** balanced by an increase in  $N_{\text{area}}$  to support the greater photosynthetic capacity  
**1214** needed to maintain high assimilation at lower conductance (Grossiord et al. 2020;  
**1215** Dong et al. 2020; López et al. 2021; Westerband et al. 2023).

**1216** Leaf nitrogen allocation responses to changing climates or soil resource  
**1217** availability may also depend on their mode of nutrient acquisition or photo-

1218 synthetic pathway. For example, species that form associations with symbiotic  
1219 nitrogen-fixing bacteria (referred as “N-fixing species” from this point forward)  
1220 should, in theory, have access to less finite nitrogen supply than species not capa-  
1221 ble of forming such associations (referred as “non-fixing species” from this point  
1222 forward), which may result in lower  $\beta$  values in N-fixing species than non-fixing  
1223 species. This result was previously shown in a greenhouse experiment, where a  
1224 leguminous species generally had lower costs of nitrogen acquisition compared to a  
1225 non-leguminous species, although these differences were generally stronger under  
1226 increased nitrogen limitation (Perkowski et al. 2021). Lower  $\beta$  values could be an  
1227 explanation for why N-fixing species commonly have greater leaf nitrogen content  
1228 than non-fixing species (Adams et al. 2016; Dong et al. 2017).

1229         Similarly, leaf nitrogen allocation patterns across environmental gradients  
1230 may be dependent on photosynthetic pathway. Lower leaf  $C_i:C_a$  values in C<sub>4</sub>  
1231 species suggests that C<sub>4</sub> species should have lower  $\beta$  values than C<sub>3</sub> species (Scott  
1232 and Smith 2022), a pattern that could be the result of increased costs associated  
1233 with water acquisition and use or reduced costs of nitrogen acquisition and use  
1234 relative to C<sub>3</sub> species. Theory predicts that this response in C<sub>4</sub> species will cause  
1235 C<sub>4</sub> species to have higher leaf nitrogen content on average compared to C<sub>3</sub> species,  
1236 though ample evidence exists documenting general lower leaf nitrogen content in  
1237 C<sub>4</sub> species (Schmitt and Edwards 1981; Sage and Pearcy 1987; Ghannoum et al.  
1238 2011). No study to date has directly quantified  $\beta$  in C<sub>4</sub> species aside from the  
1239 initial parameterization of  $\beta$  in an optimality model for C<sub>4</sub> species (Scott and  
1240 Smith 2022) using a global dataset of leaf  $\delta^{13}\text{C}$  values (Cornwell et al. 2018).

1241         While photosynthetic least-cost theory provides a unified framework for

1242 understanding integrated effects of climate and soil resource availability on  $N_{\text{area}}$ ,  
1243 empirical tests of the theory are sparse. Previous work shows that increasing  
1244 soil nitrogen availability decreases costs of acquiring nutrients (Bae et al. 2015;  
1245 Perkowski et al. 2021; Lu et al. 2022), which can induce predictable nutrient-  
1246 water use tradeoffs expected from the theory across broad environmental gradients  
1247 (Paillassa et al. 2020; Querejeta et al. 2022; Westerband et al. 2023) and in  
1248 manipulation experiments (Balic-Murphy et al. 2021). Additionally, increasing  
1249 vapor pressure deficit has been shown to have a positive effect on  $N_{\text{area}}$ , which is  
1250 commonly associated with reduced leaf  $C_i:C_a$  (Dong et al. 2017; Dong et al. 2020;  
1251 Firn et al. 2019; López et al. 2021).

1252 Despite evidence for patterns expected from photosynthetic least-cost the-  
1253 ory, studies have been restricted to exploring these patterns in C<sub>3</sub> species and,  
1254 while variance in  $N_{\text{area}}$  across environmental gradients has been shown to be driven  
1255 by strong negative relationships with leaf  $C_i:C_a$  (Dong et al. 2017; Paillassa et al.  
1256 2020; Westerband et al. 2023), no study has explicitly investigated effects of soil  
1257 resource availability or species identity on  $N_{\text{area}}$  using  $\beta$  as a direct predictor of  
1258 leaf  $C_i:C_a$ . Furthermore, as  $N_{\text{area}}$  can be broken down into structural (leaf mass  
1259 per area;  $M_{\text{area}}$ ; g m<sup>-2</sup>) and metabolic (mass-based leaf nitrogen content;  $N_{\text{mass}}$ ;  
1260 gN g<sup>-1</sup>) components (Dong et al. 2017), no study has investigated which compo-  
1261 nent of  $N_{\text{area}}$  drives the hypothesized response of  $N_{\text{area}}$  to leaf  $C_i:C_a$ , which limits  
1262 our ability to assess whether changes in  $N_{\text{area}}$  across environmental gradients are  
1263 driven by changes in leaf morphology (i.e.  $M_{\text{area}}$ ), leaf stoichiometry (i.e.  $N_{\text{mass}}$ ),  
1264 or both.

1265 In this study, I measured  $N_{\text{area}}$ ,  $N_{\text{mass}}$ ,  $M_{\text{area}}$ , leaf  $\delta^{13}\text{C}$ -derived estimates

1266 of leaf  $C_i:C_a$ , and leaf  $\delta^{13}\text{C}$ -derived estimates of  $\beta$  in 504 individuals spanning  
1267 52 species scattered across 24 grassland sites in Texas, USA. The state of Texas  
1268 contains a diverse climatic gradient, indicated by 2006-2020 mean annual precipi-  
1269 tation totals ranging from 204 to 1803 mm and 2006-2020 mean annual tempera-  
1270 ture ranging from  $11.8^\circ$  to  $24.6^\circ\text{C}$  within state boundaries (Fig. 4.1). Variability  
1271 in soil nitrogen availability and soil moisture was expected across sites, owing to  
1272 differences in soil texture and aboveground climate that would drive differential  
1273 rates of water retention and nitrogen transformations to plant-available nitrogen  
1274 substrate. I leveraged the expected climatic and soil resource variability across  
1275 sites to test the following hypotheses:

- 1276 1. Soil nitrogen availability will decrease  $\beta$  through a reduction in costs of  
1277 nitrogen acquisition and use, while soil moisture will increase  $\beta$  through a  
1278 reduction in costs of water acquisition and use. Following previous results, I  
1279 expected that N-fixing species would have lower  $\beta$  values and that  $C_4$  species  
1280 would have lower  $\beta$  values.
- 1281 2. Leaf  $C_i:C_a$  will be positively related to  $\beta$ , a pattern that will result in a  
1282 negative indirect effect of increasing soil nitrogen availability on leaf  $C_i:C_a$ ,  
1283 a positive indirect effect of increasing soil moisture on leaf  $C_i:C_a$ , and lower  
1284 leaf  $C_i:C_a$  in both N-fixing species and  $C_4$  species. I expected that leaf  
1285  $C_i:C_a$  would be negatively related to vapor pressure deficit, as increasing  
1286 atmospheric dryness would cause plants to close stomata to minimize water  
1287 loss.
- 1288 3.  $N_{\text{area}}$  will be negatively related to leaf  $C_i:C_a$ . This response will result in an  
1289 indirect positive and negative effect of increasing soil nitrogen availability

1290 and soil moisture, respectively, on  $N_{\text{area}}$ , and larger  $N_{\text{area}}$  values in N-fixing  
1291 species. While theory predicts that lower  $\beta$  values in C<sub>4</sub> species should  
1292 yield larger  $N_{\text{area}}$  in C<sub>4</sub> species, I expected that C<sub>4</sub> species would have lower  
1293  $N_{\text{area}}$  than C<sub>3</sub> species due to greater nitrogen use efficiency in C<sub>4</sub> species.  
1294 Additionally, I expected vapor pressure deficit to increase  $N_{\text{area}}$ , a pattern  
1295 that would be directly mediated through the reduction in leaf  $C_i:C_a$  with  
1296 increasing vapor pressure deficit.

1297 4.2 Methods

1298 4.2.1 *Site descriptions and sampling methodology*

1299 Leaf and soil samples were collected from 24 open canopy grassland sites scattered  
1300 across central and eastern Texas in summer 2020 and summer 2021 (Fig. 4.1).  
1301 Twelve sites were visited between June and July 2020 and 14 sites (11 unique from  
1302 2020) were visited between May and June 2021 (Table 4.1). Sites were chosen to  
1303 maximize precipitation and edaphic variability across sites (Table 4.1). No site  
1304 with personally communicated or anecdotal evidence of grazing or disturbance  
1305 (e.g., mowing, feral hog activity, etc.) was used. Leaf material was collected  
1306 from three individuals each of the five most abundant species at random locations  
1307 at each site, only selecting species that were broadly classified as graminoid or  
1308 forb/herb growth habits per the USDA PLANTS database (USDA NRCS 2022).  
1309 All collected leaves were fully expanded with no visible herbivory or other external  
1310 damage and also free from shading by nearby shrubs or trees. Five soil samples  
1311 were collected from 0-15 cm below the soil surface at each site near the leaf  
1312 collection sample locations. Soil samples were mixed together by hand to create

**1313** one composite soil sample per site.

**1314** 4.2.2 *Leaf trait measurements*

**1315** Images of each leaf were taken immediately following each site visit using a flat-

**1316** bed scanner. Fresh leaf area was determined from each image using the ‘LeafArea’

**1317** R package (Katabuchi 2015), which automates leaf area calculations using ImageJ

**1318** software (Schneider et al. 2012). Each leaf was dried at 65°C for at least 48 hours

**1319** to a constant mass, weighed, and manually ground in a mortar and pestle until

**1320** homogenized. Leaf mass per area ( $M_{\text{area}}$ ; g m<sup>-2</sup>) was calculated as the ratio of

**1321** dry leaf biomass to fresh leaf area. Subsamples of dried and homogenized leaf

**1322** tissue were used to measure leaf nitrogen content ( $N_{\text{mass}}$ ; gN g<sup>-1</sup>) through ele-

**1323** mental combustion analysis (Costech-4010, Costech Instruments, Valencia, CA).

**1324** Leaf nitrogen content per unit leaf area ( $N_{\text{area}}$ ; gN m<sup>-2</sup>) was calculated as the

**1325** product of  $N_{\text{mass}}$  and  $M_{\text{area}}$ .

**1326** Subsamples of dried and homogenized leaf tissue were sent to the University

**1327** of California-Davis Stable Isotope Facility to determine leaf  $\delta^{13}\text{C}$ . Leaf  $\delta^{13}\text{C}$  values

**1328** were determined using an elemental analyzer (PDZ Europa ANCA-GSL; Sercon

**1329** Ltd., Chestshire, UK) interfaced to an isotope ratio mass spectrometer (PDZ

**1330** Europa 20-20 Isotope Ratio Mass Spectrometer, Sercon Ltd., Chestshire, UK).

**1331** I used leaf  $\delta^{13}\text{C}$  values (‰; relative to Vienna Pee Dee Belemnite international

**1332** reference standard) to estimate the ratio of intercellular ( $C_i$ ) to extracellular ( $C_a$ )

**1333** CO<sub>2</sub> ratio (leaf  $C_i:C_a$ ; unitless) following the approach of Farquhar et al. (1989)

**1334** described in Cernusak et al. (2013). Specifically, I derived leaf  $C_i:C_a$  as:

$$C_i : C_a = \frac{\Delta^{13}C - a}{b - a} \quad (4.1)$$

**1335** where  $\Delta^{13}C$  represents the relative difference between leaf  $\delta^{13}\text{C}$  ( $\text{\textperthousand}$ ) and air  $\delta^{13}\text{C}$

**1336** ( $\text{\textperthousand}$ ), calculated as:

$$\Delta^{13}C = \frac{\delta^{13}C_{air} - \delta^{13}C_{leaf}}{1 + \delta^{13}C_{leaf}} \quad (4.2)$$

**1337**  $\delta^{13}\text{C}_{air}$ , which is commonly assumed to be  $-8\text{\textperthousand}$  (Keeling et al. 1979; Farquhar

**1338** et al. 1989), was calculated as a function of calendar year  $t$  using an empirical

**1339** equation derived in Feng (1999):

$$\delta^{13}C_{air} = -6.429 - 0.006e^{0.0217(t-1740)} \quad (4.3)$$

**1340** Using this equation,  $\delta^{13}\text{C}_{air}$  values were set to  $-9.04\text{\textperthousand}$  and  $-9.09\text{\textperthousand}$  for 2020 and

**1341** 2021, respectively. The parameter  $a$  represents the fractionation between  $^{12}\text{C}$

**1342** and  $^{13}\text{C}$  due to diffusion in air, assumed to be  $4.4\text{\textperthousand}$ , while  $b$  represents the

**1343** fractionation caused by Rubisco carboxylation, assumed to be  $27\text{\textperthousand}$  (Farquhar

**1344** et al. 1989). For  $\text{C}_4$  species,  $b$  in Eqn. 4.1 was set to  $6.3\text{\textperthousand}$ , and was derived from:

$$b = c + (d \cdot \phi) \quad (4.4)$$

**1345** Where  $c$  was set to  $-5.7\text{\textperthousand}$  and  $d$  was set to  $30\text{\textperthousand}$  (Farquhar et al. 1989).  $\phi$ , which

**1346** is the bundle sheath leakiness term, was set to 0.4. All leaf  $C_i:C_a$  values less than

**1347** 0.1 and greater than 0.95 were assumed to be incorrect and removed from the

**1348** analysis.

**1349** I derived the unit cost of resource use ( $\beta$ ) using leaf  $C_i:C_a$  and site climate  
**1350** data using equations first described in Prentice et al. (2014) and simplified in  
**1351** Lavergne et al. (2020):

$$\beta = 1.6\eta^*VPD \frac{\chi - (\frac{\Gamma^*}{C_a})^2}{(1 - \chi)^2(K_m + \Gamma^*)} \quad (4.5)$$

**1352** where  $\eta^*$  is the viscosity of water relative to 25°C, calculated using elevation and  
**1353** mean air temperature of the seven days leading up to each site visit following equa-  
**1354** tions in Huber et al. (2009). VPD (Pa) was set to the mean vapor pressure deficit  
**1355** of the seven days leading up to each site visit,  $C_a$  represents atmospheric CO<sub>2</sub>  
**1356** concentration, arbitrarily set to 420  $\mu\text{mol mol}^{-1}$  CO<sub>2</sub>.  $K_m$  (Pa) is the Michaelis-  
**1357** Menten coefficient for Rubisco affinity to CO<sub>2</sub> and O<sub>2</sub>, calculated as:

$$K_m = K_c \cdot \left(1 + \frac{O_i}{K_o}\right) \quad (4.6)$$

**1358** where  $K_c$  (Pa) and  $K_o$  (Pa) are the Michaelis-Menten coefficients for Rubisco  
**1359** affinity to CO<sub>2</sub> and O<sub>2</sub>, respectively, and  $O_i$  is the intercellular O<sub>2</sub> concentration.  
**1360**  $\Gamma^*$  (Pa) is the CO<sub>2</sub> compensation point in the absence of dark respiration.  $K_c$ ,  $K_o$ ,  
**1361** and  $\Gamma^*$  were determined using equations described in Medlyn et al. (2002) and  
**1362** derived in Bernacchi et al. (2001), invoking an elevation correction for atmospheric  
**1363** pressure as explained in Stocker et al. (2020).

**Table 4.1.** Site locality information, sampling year, 2006-2020 mean annual precipitation (MAP; mm), mean annual temperature (MAT; °C), and water holding capacity (WHC; mm)\*

Site	Latitude	Longitude	Sampling year	MAP	MAT	WHC
Edwards_2019_17	29.95	-100.36	2020	563.5	19.0	224.7
Uvalde_2020_02	29.59	-100.09	2020, 2021	648.5	19.5	224.7
Menard_2020_01	30.91	-99.59	2020	641.9	18.3	220.2
Kerr_2020_03	30.06	-99.34	2021	672.4	18.3	237.5
Bandera_2020_03	29.85	-99.30	2021	789.4	18.8	235.1
Sansaba_2020_01	31.29	-98.62	2020	733.0	18.8	234.3
Comal_2020_21	29.79	-98.43	2020	878.5	19.9	220.7
Blanco_2019_16	29.99	-98.43	2020	833.0	19.2	222.2
Bexar_2019_13	29.24	-98.43	2020	759.3	21.5	206.0
Burnet_2020_14	30.84	-98.34	2021	763.3	19.5	217.8
Comal_2020_19	30.01	-98.32	2021	845.0	19.3	220.4
Hays_2020_54	29.96	-98.17	2021	861.3	20.0	225.6
Burnet_2020_12	30.82	-98.06	2021	815.1	19.4	245.3
Williamson_2019_09	30.71	-97.86	2020	867.7	19.7	270.2
Williamson_2019_10	30.54	-97.77	2020	819.5	19.9	239.8
Bell_2021_08	31.06	-97.55	2021	937.3	19.6	232.3
Fayette_2021_12	29.86	-97.21	2021	985.7	20.4	165.6
Fayette_2019_04	30.09	-96.78	2020	1017.4	20.6	226.9
Fayette_2020_09	29.86	-96.71	2021	1002.7	20.8	187.6
Washington_2020_08	30.28	-96.41	2021	1077.4	20.4	203.9
Austin_2020_03	29.78	-96.24	2021	1108.7	20.6	253.0
Brazos_2020_16	30.93	-96.23	2021	1078.0	20.1	202.2
Brazos_2020_18	30.52	-96.21	2020, 2021	1099.4	20.4	233.5
Harris_2020_03	29.88	-95.31	2020, 2021	1492.0	21.6	265.6

**1364** \* Rows are arranged by longitude to visualize precipitation variability across sites

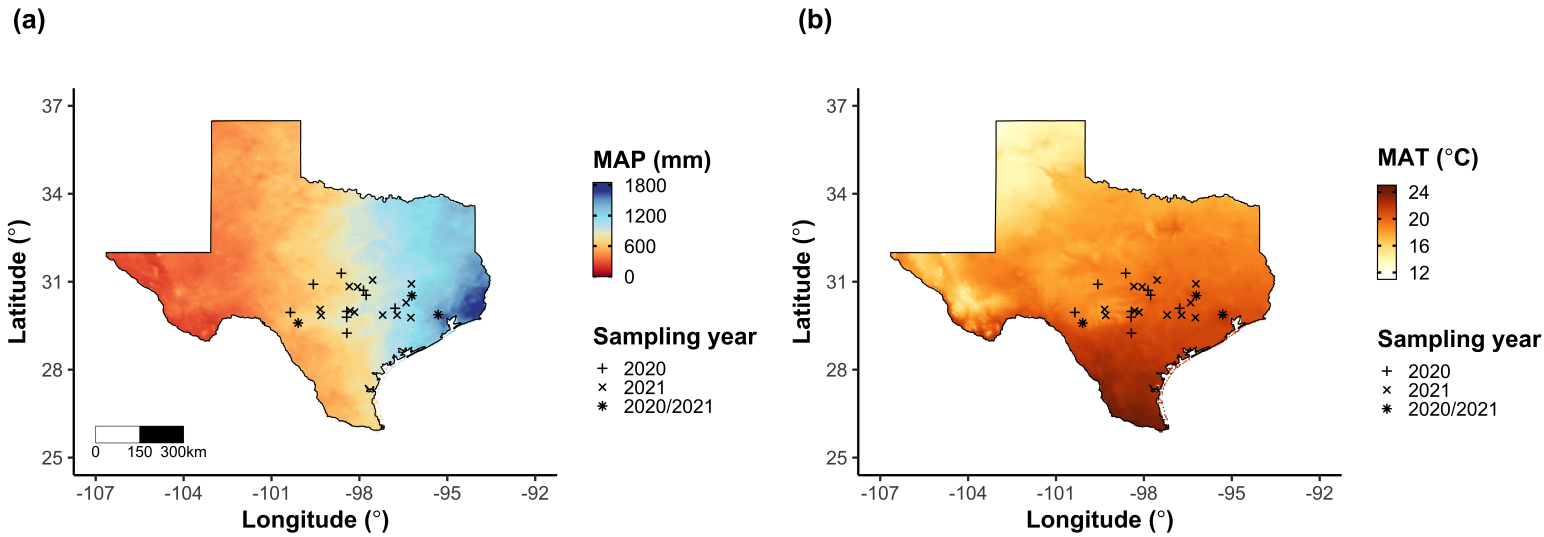


**Figure 4.1.** Site locations along 2006-2020 mean annual precipitation (a) and mean annual temperature (b) gradients in Texas, USA. Precipitation and temperature data were plotted using PRISM data at a 4-km grid resolution and are masked to include only grid cells that occur within the Texas state boundary of the United States. In both panels, addition signs refer to sites visited in 2020, multiplication signs to sites visited in 2021, and asterisks to sites visited in 2020 and 2021. The scale bar in (a) also applies to (b).

**1365** 4.2.3 *Site climate data*

**1366** I used the Parameter elevation Regressions on Independent Slopes Model (PRISM)  
**1367** (Daly et al. 2008) climate product to access gridded daily temperature and precip-  
**1368** itation data for the coterminous United States at a 4-km grid resolution between  
**1369** January 1, 2006 and July 31, 2021 (PRISM Climate Group, Oregon State Uni-  
**1370** versity, <https://prism.oregonstate.edu>, data created 4 Feb 2014, accessed 24  
**1371** Mar 2022). Mean daily air temperature, mean daily vapor pressure deficit, and  
**1372** total daily precipitation data were extracted from the grid cell that contained the  
**1373** latitude and longitude of each property using the ‘extract’ function in the ‘terra’  
**1374** R package (Hijmans 2022). PRISM data were used in lieu of local weather sta-  
**1375** tion data because several rural sites did not have a local weather station present  
**1376** within a 20-km radius of the site. Daily site climate data were used to estimate  
**1377** mean annual precipitation and mean annual temperature for each site between  
**1378** 2006 and 2020 (Table 4.1). I calculated total precipitation and mean daily vapor  
**1379** pressure deficit for the prior 1, 2, 3, 4, 5, 6, 7, 8, 9, 10, 15, 20, 25, 30, 60, and 90  
**1380** days leading up to each site visit. Temperature was not included in any analy-  
**1381** sis due to the close range in mean annual temperature between sites (mean±SD:  
**1382**  $19.8 \pm 0.9^\circ\text{C}$ ; Table 4.1).

**1383** 4.2.4 *Site edaphic characteristics*

**1384** Composted soil samples were sent to the Texas A&M Soil, Water and Forage  
**1385** Laboratory to quantify soil nitrate concentration ( $\text{NO}_3\text{-N}$ ; ppm). Soil  $\text{NO}_3\text{-N}$   
**1386** was determined by extracting composite soil samples in 1 M KCl, measuring  
**1387** absorbance values of extracts at 520 nm using the end product of a  $\text{NO}_3\text{-N}$  to

**1388** NO<sub>2</sub>-N cadmium reduction reaction (Kachurina et al. 2000; Keeney and Nelson  
**1389** 1983). Soil texture data from 0-15 cm below the soil surface were accessed using  
**1390** the SoilGrids2.0 data product (Poggio et al. 2021) through the ‘fetchSoilGrids’  
**1391** function in the ‘soilDB’ R package (Beaudette et al. 2022). I used SoilGrids2.0  
**1392** to access soil texture data in lieu of analyses using the composite soil sample due  
**1393** to a lack of soil material from some sites after sending samples for soil NO<sub>3</sub>-N.

**1394** Soil moisture was not measured in the field, but was estimated using the  
**1395** ‘Simple Process-Led Algorithms for Simulating Habitats’ model (SPLASH) (Davis  
**1396** et al. 2017). This model, derived from the STASH model (Cramer and Prentice  
**1397** 1988), spins up a bucket model using Priestley-Taylor equations (Priestley and  
**1398** Taylor 1972) to calculate daily soil moisture ( $W_n$ ; mm) as a function of the previous  
**1399** day’s soil moisture ( $W_{n-1}$ ; mm), daily precipitation ( $P_n$ ; mm), condensation ( $C_n$ ;  
**1400** mm), actual evapotranspiration ( $E_n^a$ ; mm), and runoff (RO; mm):

$$W_n = W_{n-1} + P_n + C_n - E_n^a - RO \quad (4.7)$$

**1401** Models were spun up by equilibrating the previous day’s soil moisture using succes-  
**1402** sive model iterations with daily mean air temperature, daily precipitation total,  
**1403** the number of daily sunlight hours, and latitude as model inputs (Davis et al.  
**1404** 2017). Daily sunlight hours were estimated for each day at each site using the  
**1405** ‘getSunlightTimes’ function in the ‘suncalc’ R package, which estimated sunrise  
**1406** and sunset times of each property using date and site coordinates (Thieurmel and  
**1407** Elmarhraoui 2019). Water holding capacity (mm), or bucket size, was estimated  
**1408** as a function of soil texture using pedotransfer equations explained in Saxton and

1409 Rawls (2006), as done in Stocker et al. (2020) and Bloomfield et al. (2023). A  
1410 summary of these equations is included in Appendix C.1.

1411 Daily soil moisture outputs from the SPLASH model for each site were  
1412 used to calculate mean daily soil moisture for the prior 1, 2, 3, 4, 5, 6, 7, 8, 9,  
1413 10, 15, 20, 25, 30, 60, and 90 days leading up to each site visit. Mean daily  
1414 soil moisture values were then expressed as a fraction of water holding capacity  
1415 to normalize across sites with different bucket depths, as done in Stocker et al.  
1416 (2018). Site water holding capacity values are referenced in Table 4.1.

1417 4.2.5 *Plant functional group assignments*

1418 Plant functional group was assigned to each species and used as the primary de-  
1419 scriptor of species identity. Specifically, plant functional groups were assigned  
1420 based on photosynthetic pathway ( $C_3$ ,  $C_4$ ) and ability to form associations with  
1421 symbiotic nitrogen-fixing bacteria (N-fixer, non-fixer). The ability to form asso-  
1422 ciations with symbiotic nitrogen-fixing bacteria was assigned based on whether  
1423 species were in the *Fabaceae* family, and photosynthetic pathway of each species  
1424 was determined from past literature and confirmed through leaf  $\delta^{13}C$  values. I  
1425 chose these plant functional groups based on *a priori* hypotheses regarding the  
1426 functional role of nitrogen fixation and photosynthetic pathway on the sensitivity  
1427 of plant nitrogen uptake and leaf nitrogen allocation to soil nitrogen availability  
1428 and aboveground growing conditions. These plant functional group classifications  
1429 resulted in three distinct plant functional groups within our dataset:  $C_3$  N-fixers  
1430 (n=53),  $C_3$  non-fixers (n=334), and  $C_4$  non-fixers (n=117).

**1431** 4.2.6 *Data analysis*

**1432** All analyses and plotting were conducted in R version 4.1.1 (R Core Team 2021).

**1433** I constructed a series of separate linear mixed-effects models to investigate en-

**1434** vironmental drivers of  $\beta$ , leaf  $C_i:C_a$ ,  $N_{\text{area}}$ ,  $N_{\text{mass}}$ , and  $M_{\text{area}}$ , followed by a path

**1435** analysis using a piecewise structural equation model to investigate direct and

**1436** indirect effects of climate and soil resource availability on  $N_{\text{area}}$ .

**1437** To explore environmental drivers of  $\beta$ , I built a linear mixed-effects model

**1438** that included soil moisture, soil nitrogen availability, and plant functional group

**1439** as fixed effect coefficients. Species were designated as a random intercept term.

**1440** Interaction coefficients between all possible combinations of the three fixed effect

**1441** coefficients were also included.  $\beta$  was natural log transformed to linearize data.

**1442** I used an information-theoretic model selection approach to determine whether

**1443** 90-, 60-, 30-, 20-, 15-, 10-, 9-, 8-, 7-, 6-, 5-, 4-, 3-, 2-, or 1-day mean daily soil

**1444** moisture conferred the best model fit for  $\beta$ . To do this, I constructed 16 separate

**1445** linear mixed-effects models where log-transformed  $\beta$  was included as the response

**1446** variable and each soil moisture time step was separately included as a single

**1447** continuous fixed effect. Species were included as a random intercept term for all

**1448** models. I used corrected Akaike Information Criterion (AICc) to select the soil

**1449** moisture timescale that conferred the best model fit, indicated by the model with

**1450** the lowest AICc score (Table C3; Fig. C1).

**1451** To explore environmental drivers of leaf  $C_i:C_a$ , I constructed a second lin-

**1452** ear mixed effects model that included vapor pressure deficit, soil moisture, soil

**1453** nitrogen availability, and plant functional group as fixed effect coefficients. Two-

**1454** way interactions between plant functional group and vapor pressure deficit, soil

1455 nitrogen availability, or soil moisture were included as additional fixed effect coef-  
1456 ficients, in addition to a three-way interaction between soil moisture, soil nitrogen  
1457 availability, and plant functional group. Species were included as a random inter-  
1458 cept term. I used an information-theoretic model selection approach to determine  
1459 whether 90-, 60-, 30-, 20-, 15-, 10-, 9-, 8-, 7-, 6-, 5-, 4-, 3-, 2-, or 1-day mean daily  
1460 vapor pressure deficit conferred the best model fit for leaf  $C_i:C_a$  using the same  
1461 approach explained above for the soil moisture effect on  $\beta$ . The soil moisture  
1462 timescale was set to the same timescale that conferred the best fit for  $\beta$ .

1463 To explore environmental drivers of  $N_{\text{area}}$ ,  $N_{\text{mass}}$ , and  $M_{\text{area}}$ , I constructed  
1464 a linear mixed effects model for each trait, including leaf  $C_i:C_a$ , soil nitrogen  
1465 availability, soil moisture, and plant functional group as fixed effect coefficients  
1466 for each model. Two-way interactions between plant functional group and  $\beta$ , leaf  
1467  $C_i:C_a$ , soil nitrogen availability, or soil moisture were included as additional fixed  
1468 effect coefficients, in addition to a three-way interaction between soil nitrogen  
1469 availability, soil moisture, and plant functional group. Species were included as a  
1470 random intercept term, with the soil moisture timescale set to the same timescale  
1471 that conferred the best fit for  $\beta$ .

1472 In all linear mixed-effects models explained above, including those to select  
1473 relevant timescales, I used the ‘lmer’ function in the ‘lme4’ R package (Bates et al.  
1474 2015) to fit each model and the ‘Anova’ function in the ‘car’ R package (Fox and  
1475 Weisberg 2019) to calculate Type II Wald’s  $\chi^2$  and determine the significance  
1476 level ( $\alpha=0.05$ ) of each fixed effect coefficient. I used the ‘emmeans’ R package  
1477 (Lenth 2019) to conduct post-hoc comparisons using Tukey’s tests, where degrees  
1478 of freedom were approximated using the Kenward-Roger approach (Kenward and

1479 Roger 1997). Trendlines and error ribbons for all plots were drawn using a series  
1480 of ‘emmeans’ outputs across the range in plotted x-axis values.

1481 Finally, I conducted a path analysis using a piecewise structural equation  
1482 model to examine direct and indirect pathways that determined variance in  $N_{\text{area}}$ .  
1483 Six separate linear mixed effects models were loaded into the piecewise structural  
1484 equation model. Models were constructed per *a priori* hypotheses following pat-  
1485 terns expected from photosynthetic least-cost theory. The first model regressed  
1486  $N_{\text{area}}$  against  $N_{\text{mass}}$  and  $M_{\text{area}}$ . The second model regressed  $M_{\text{area}}$  against leaf  
1487  $C_i:C_a$  and soil nitrogen availability. The third model regressed  $N_{\text{mass}}$  against  
1488 leaf  $C_i:C_a$  and  $M_{\text{area}}$  (Dong et al. 2017; Dong et al. 2020). The fourth model re-  
1489 gressed leaf  $C_i:C_a$  against  $\beta$  and vapor pressure deficit. The fifth model regressed  $\beta$   
1490 against soil nitrogen availability, soil moisture, ability to associate with symbiotic  
1491 nitrogen-fixing bacteria, and photosynthetic pathway. The sixth model regressed  
1492 soil nitrogen availability against soil moisture. All models included the relevant  
1493 timescale selected in the individual linear mixed effect models explained above.  
1494 Models included species as a random intercept term, were built using the ‘lme’  
1495 function in the ‘nlme’ R package (Pinheiro and Bates 2022), and subsequently  
1496 loaded into the piecewise structural equation model using the ‘psem’ function in  
1497 the ‘piecewiseSEM’ R package (Lefcheck 2016).

**1498** 4.3 Results

**1499** 4.3.1 *Cost to acquire nitrogen relative to water*

**1500** Model selection indicated that 90-day mean soil moisture conferred the best model

**1501** fit for  $\beta$  (AICc=1387.54; Table C3; Fig. C1).

**1502** Increasing soil nitrogen availability generally decreased  $\beta$  ( $p<0.001$ ; Table

**1503** 4.2; Fig. 4.2a), a pattern driven by a negative effect of increasing soil nitrogen on  $\beta$

**1504** in C<sub>3</sub> non-fixers (Tukey:  $p=0.005$ ) and C<sub>3</sub> N-fixers (Tukey:  $p=0.035$ ) despite a null

**1505** effect of increasing soil nitrogen on  $\beta$  in C<sub>4</sub> non-fixers (Tukey:  $p=0.856$ ). There

**1506** was no effect of soil moisture on  $\beta$  ( $p=0.872$ ; Table 4.2; Fig. 4.2b). A functional

**1507** group effect ( $p<0.001$ ; Table 4.2) indicated that C<sub>4</sub> non-fixers generally had lower

**1508**  $\beta$  values than both C<sub>3</sub> N-fixers and C<sub>3</sub> non-fixers (Tukey:  $p<0.001$  in both cases),

**1509** while  $\beta$  values in C<sub>3</sub> N-fixers did not differ from C<sub>3</sub> non-fixers (Tukey:  $p=0.854$ ).

**Table 4.2.** Effects of soil moisture, soil nitrogen availability, and plant functional group on  $\beta$  (unitless)\*

	df	Coefficient	$\chi^2$	p
Intercept	-	3.39E+00	-	-
Soil moisture (SM <sub>90</sub> )	1	-1.96E-01	0.026	0.872
Soil N (N)	1	-1.42E-02	12.031	<b>&lt;0.001</b>
PFT	2	-	199.617	<b>&lt;0.001</b>
SM <sub>90</sub> *N	1	-3.02E-03	1.000	0.317
SM <sub>90</sub> *PFT	2	-	0.623	0.732
N*PFT	2	-	5.271	0.072
SM <sub>90</sub> *N*PFT	2	-	5.271	0.182

**1510** \*Significance determined using Type II Wald  $\chi^2$  tests ( $\alpha=0.05$ ). P-values<0.05  
**1511** are in bold. Model coefficients are expressed on the natural-log scale and are only  
**1512** included for continuous fixed effects. Key: df=degrees of freedom;  $\chi^2$ =Wald Type  
**1513** II chi-square test statistic

**1514** [DWS: exponential notation not used correctly in these tables. Looks

**1515** copied from a graphing calculator output]

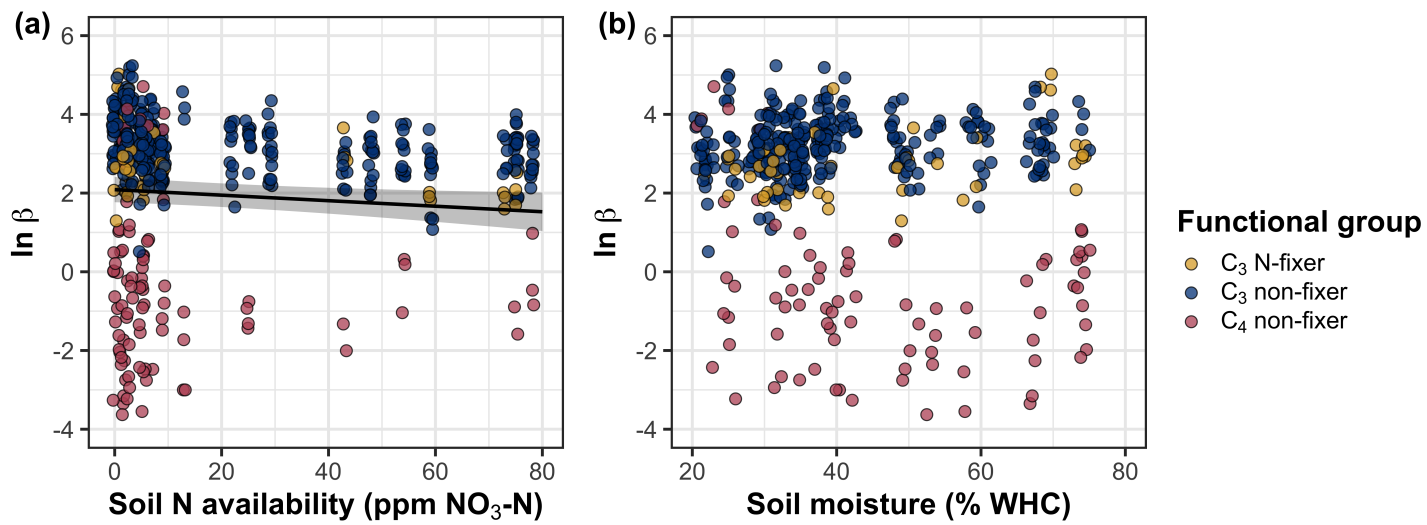


**Figure 4.2.** Effects of soil nitrogen availability (a) and soil moisture (b) on the cost of acquiring and using nitrogen ( $\beta$ ; unitless). Soil nitrogen availability is represented on the x-axis in (a), soil moisture is represented on the x-axis in (b) as a percent of site water holding capacity, and natural-log transformed  $\beta$  is represented on the y-axis for both panels. Yellow points represent C<sub>3</sub> N-fixers, blue points represent C<sub>3</sub> non-fixers, and red points represent C<sub>4</sub> non-fixers. Throughout, points are jittered for visibility. A black solid trendline is drawn to denote bivariate relationships where the slope is different from zero ( $p<0.05$ ), with error ribbons representing the upper and lower 95% confidence intervals.

**1516** 4.3.2 *Leaf C<sub>i</sub>:C<sub>a</sub>*

**1517** Model selection indicated that 4-day mean vapor pressure deficit was the timescale

**1518** that conferred the best model fit for leaf  $C_i:C_a$  (AICc=-755.81; Table C3; Fig. C1).

**1519** Model results revealed that increasing vapor pressure deficit generally de-

**1520** creased leaf  $C_i:C_a$  ( $p<0.001$ ; Table 4.3; Fig. 4.3a). There was no effect of soil mois-

**1521** ture ( $p=0.549$ ; Table 4.3; Fig. 4.3b) or soil nitrogen availability ( $p=0.549$ ; Table

**1522** 4.3; Fig. 4.3c) on leaf  $C_i:C_a$ . A strong plant functional group effect ( $p<0.001$ ; Ta-

**1523** ble 4.3) indicated that C<sub>4</sub> non-fixers had lower leaf  $C_i:C_a$  than C<sub>3</sub> N-fixers and C<sub>3</sub>

**1524** non-fixers (Tukey:  $p<0.001$  in both cases), with no difference between C<sub>3</sub> N-fixers

**1525** and C<sub>3</sub> non-fixers (Tukey:  $p=0.866$ ).

**Table 4.3.** Effects of soil moisture, soil nitrogen availability, and plant functional group on leaf  $C_i:C_a$  (unitless)\*

	df	Coefficient	$\chi^2$	<i>p</i>
Intercept	-	1.32E+00	-	-
Vapor pressure deficit ( $VPD_4$ )	1	-4.53E-01	10.987	<b>&lt;0.001</b>
Soil moisture ( $SM_{90}$ )	1	-1.71E-01	0.039	0.843
Soil N (N)	1	-1.71E-03	0.043	0.549
PFT	2	-	205.274	<b>&lt;0.001</b>
$SM_{90}^*N$	1	7.29E-03	2.266	0.132
$VPD_4^*PFT$	2	-	0.887	0.642
$SM_{90}^*PFT$	2	-	0.814	0.666
$N^*PFT$	2	-	4.158	0.125
$SM_{90}^*N^*PFT$	2	-	3.465	0.177

**1526** \*Significance determined using Type II Wald  $\chi^2$  tests ( $\alpha=0.05$ ). *P*-values less  
**1527** than 0.05 are in bold and *p*-values where  $0.05 < p < 0.1$  are italicized. Leaf  $C_i:C_a$   
**1528** was not transformed prior to model fitting, so model coefficients are reported  
**1529** on the response scale. Model coefficients are only included for continuous fixed  
**1530** effects. Key: df=degrees of freedom;  $\chi^2$ =Wald Type II chi-square test statistic

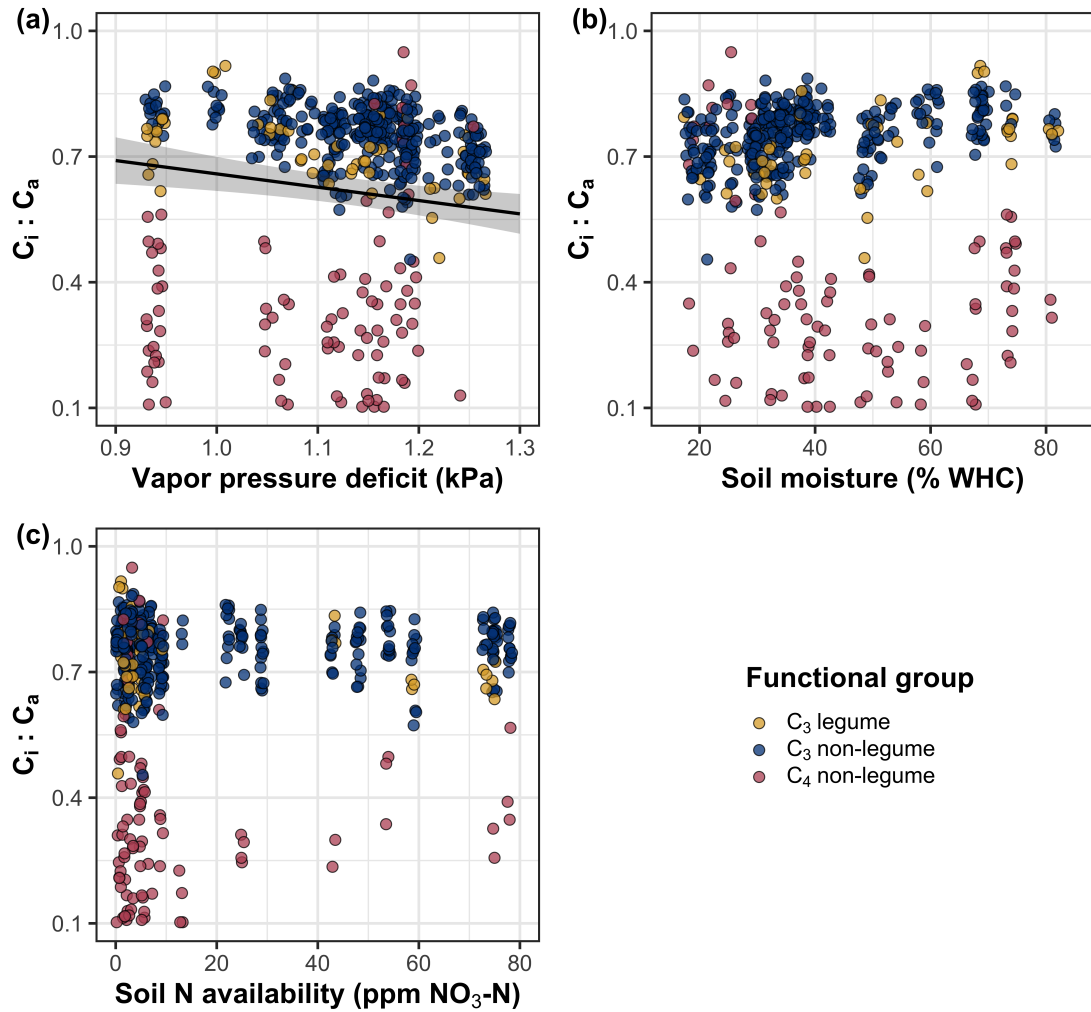


**Figure 4.3.** Effects of 4-day mean vapor pressure deficit (a), 90-day soil moisture (per water holding capacity; b), and soil nitrogen availability (c) on leaf  $C_i:C_a$ . Shading and trendlines are as explained in Figure 4.2. Points are jittered for visibility. Variably colored trendlines are only included if there is an interaction between the x-axis and plant functional group, where solid trendlines indicate slopes that are different from zero ( $p < 0.05$ ) and dashed trendlines indicate slopes that are not different from zero ( $p > 0.05$ ). Error ribbons represent the upper and lower 95% confidence intervals of each fitted trendline.

**1531** 4.3.3 *Leaf nitrogen content*

**1532** An interaction between leaf  $C_i:C_a$  and plant functional group ( $p<0.001$ ; Table  
**1533** 4.4) revealed that the negative effect of increasing leaf  $C_i:C_a$  on  $N_{area}$  ( $p<0.001$ ;  
**1534** Table 4.4) was driven by a negative effect of increasing leaf  $C_i:C_a$  on  $N_{area}$  in  
**1535**  $C_3$  non-fixers and  $C_3$  N-fixers (Tukey:  $p<0.001$  in both cases), but not  $C_4$  non-  
**1536** fixers (Tukey:  $p=0.786$ ; Fig. 4.4a). A marginal interaction between soil nitrogen  
**1537** availability and plant functional group ( $p=0.057$ ; Table 4.4) indicated that the  
**1538** positive effect of increasing soil nitrogen ( $p=0.007$ ; Table 4.4) was only apparent  
**1539** in  $C_3$  N-fixers (Tukey:  $p<0.001$ ; Table 4.4; Fig. 4.4d), but not  $C_3$  non-fixers  
**1540** (Tukey:  $p=0.329$ ) or  $C_4$  non-fixers (Tukey:  $p=0.682$ ). Increasing soil moisture  
**1541** increased  $N_{area}$  ( $p=0.011$ , Table 4.4). A plant functional group effect ( $p<0.001$ ;  
**1542** Table 4.4) indicated that  $C_4$  non-fixers had lower  $N_{area}$  compared to  $C_3$  N-fixers  
**1543** and  $C_3$  non-fixers (Tukey:  $p<0.001$  in both cases), while  $C_3$  N-fixers had lower  
**1544**  $N_{area}$  compared to  $C_3$  non-fixers (Tukey:  $p=0.024$ ).

**1545** Leaf  $C_i:C_a$  had no effect on  $N_{mass}$  ( $p=0.455$ ; Table 4.4; Fig. 4.4b). Increas-  
**1546** ing soil nitrogen availability and soil moisture each had a positive effect on  $N_{mass}$   
**1547** ( $p<0.001$  in both cases; Table 4.4; Fig. 4.4h). A plant functional group effect  
**1548** ( $p<0.001$ ; Table 4.4) indicated that  $C_4$  non-fixers had lower  $N_{mass}$  compared to  
**1549**  $C_3$  N-fixers and  $C_3$  non-fixers (Tukey:  $p=0.001$  in both cases), while  $N_{mass}$  did  
**1550** not differ between  $C_3$  N-fixers and  $C_3$  non-fixers (Tukey:  $p=0.323$ ).

**1551** Variance in  $M_{area}$  was driven by a three-way interaction between soil nitro-  
**1552** gen availability, soil moisture, and plant functional group ( $p=0.018$ ; Table 4.4).  
**1553** This interaction indicated that increasing soil moisture increased the positive effect  
**1554** of increasing soil nitrogen availability on  $M_{area}$  in  $C_3$  N-fixers (Tukey:  $p=0.028$ )

1555 but did not modify the negative effect of increasing soil nitrogen availability on  
1556  $M_{\text{area}}$  in C<sub>4</sub> non-fixers (Tukey:  $p=0.806$ ) or C<sub>3</sub> non-fixers (Tukey:  $p=0.998$ ). There  
1557 was otherwise no effect of soil moisture on  $M_{\text{area}}$  ( $p=0.436$ ; Table 4.4). An inter-  
1558 action between leaf  $C_i:C_a$  and plant functional group ( $p<0.001$ ; Table 4.4; Fig.  
1559 4.4c) indicated that the negative effect of increasing leaf  $C_i:C_a$  on  $M_{\text{area}}$  ( $p<0.001$ ;  
1560 Table 4.4) was driven by a negative effect of increasing leaf  $C_i:C_a$  on  $M_{\text{area}}$  in  
1561 C<sub>3</sub> N-fixers (Tukey:  $p<0.001$ ) and C<sub>3</sub> non-fixers(Tukey:  $p=0.003$ ), but not C<sub>4</sub>  
1562 non-fixers (Tukey:  $p=0.257$ ; Fig. 4.4c).

**Table 4.4.** Effects of soil moisture, soil nitrogen availability, plant functional group, and leaf  $C_i:C_a$  on leaf nitrogen content per unit leaf area ( $N_{\text{area}}$ ; gN m<sup>-2</sup>), leaf nitrogen content per unit leaf biomass ( $N_{\text{mass}}$ ; gN g<sup>-1</sup>), and leaf biomass per unit leaf area ( $M_{\text{area}}$ ; g m<sup>-2</sup>)

		$N_{\text{area}}$			$N_{\text{mass}}$			$M_{\text{area}}$		
	df	Coefficient	$\chi^2$	p	Coefficient	$\chi^2$	p	Coefficient	$\chi^2$	p
(Intercept)	-	2.41E+00	-	-	7.72E-02	-	-	6.91E+00	-	-
$C_i:C_a$	1	-2.32E+00	6.841	<b>0.009</b>	7.91E-01	0.558	0.455	-3.13E+00	15.913	<0.001
Soil N (N)	1	1.26E-02	7.072	<b>0.011</b>	1.21E-02	87.457	<0.001	-2.66E-02	41.791	<0.001
Soil moisture (SM <sub>90</sub> )	1	5.60E-01	6.493	<b>0.011</b>	7.94E-01	10.889	<0.001	-2.54E-01	0.605	0.437
PFT	1	-	49.273	<0.001	-	21.786	<0.001	-	6.673	<b>0.036</b>
SM <sub>90</sub> *N	1	5.45E-02	0.482	0.488	-2.18E-02	2.606	0.106	8.16E-02	0.791	0.374
$C_i:C_a$ *PFT	1	-	24.380	<0.001	-	5.367	0.068	-	30.073	<0.001
N*PFT	1	-	5.713	0.057	-	1.286	0.526	-	19.405	<0.001
SM <sub>90</sub> *PFT	1	-	3.487	0.175	-	0.889	0.641	-	2.998	0.223
SM <sub>90</sub> *N*PFT	1	-	3.523	0.172	-	0.161	0.923	-	7.996	<b>0.018</b>

97

**1563** \*Significance determined using Type II Wald  $\chi^2$  tests ( $\alpha=0.05$ ). P-values less than 0.05 are in bold and p-values where  $0.05 < p < 0.1$  are italicized. Coefficients are reported on the natural-log scale for all traits and are only included for continuous fixed effects. Key: df=degrees of freedom;  $\chi^2$ =Wald Type II chi-square test statistic

**1564**

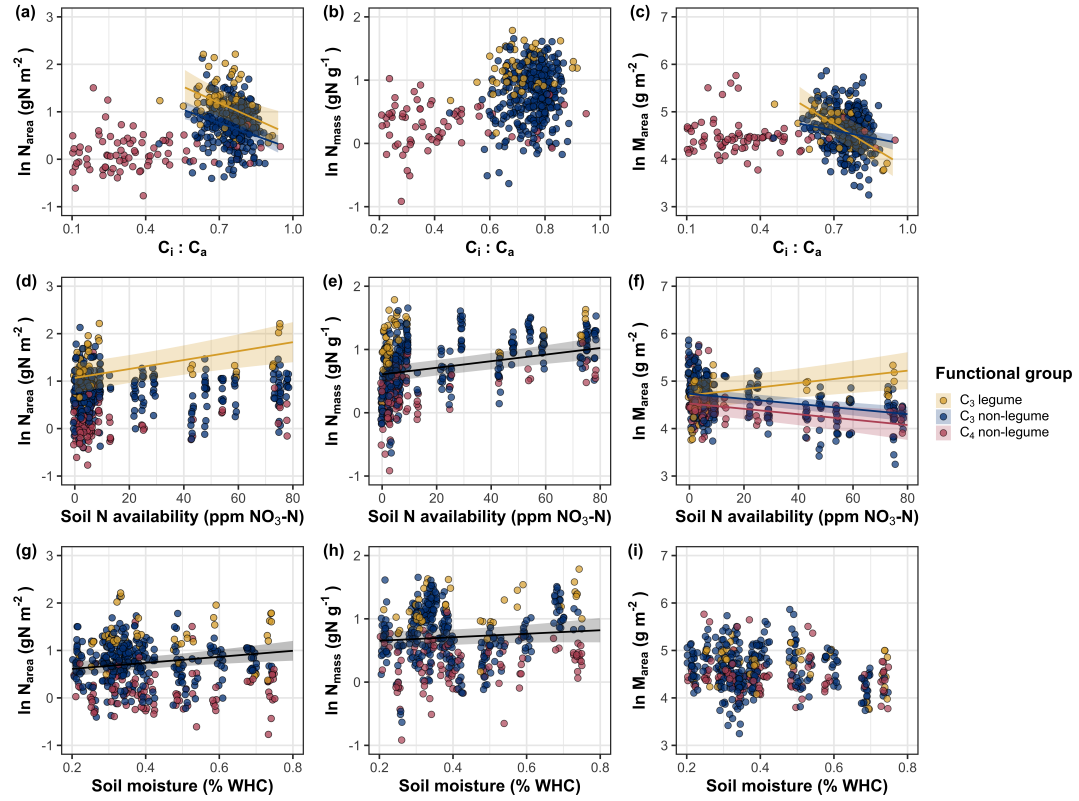


**Figure 4.4.** Effects of leaf  $C_i:C_a$  (a-c), soil nitrogen availability (d-f), and soil moisture (g-i) on leaf nitrogen content per unit leaf area (a, d, g), leaf nitrogen content per unit leaf biomass (b, e, h), and leaf mass per area (c, f, i). Yellow points and trendlines indicate C<sub>3</sub> N-fixers, blue points and trendlines indicate C<sub>3</sub> non-fixers, and red points and trendlines indicate C<sub>4</sub> non-fixers. Points are jittered for visibility. Variably colored trendlines are only included if there is an interaction between plant functional group and the x-axis. Black solid trendlines denote bivariate slopes that are different from zero ( $p < 0.05$ ) where there is no apparent interaction between plant functional group and the x-axis.

**1566** 4.3.4 *Structural equation model*

**1567** The piecewise structural equation model explained 89%, 55%, 56%, 82%, and  
**1568** 38% of variance in  $N_{\text{area}}$ ,  $N_{\text{mass}}$ ,  $M_{\text{area}}$ , leaf  $C_i:C_a$ , and  $\beta$ , respectively (Table  
**1569** 4.5; Fig. 4.5). Increasing  $N_{\text{mass}}$  and  $M_{\text{area}}$  were each positively related to  $N_{\text{area}}$   
**1570** ( $p<0.001$  in both cases; Table 4.5; Fig. 4.5).  $N_{\text{mass}}$  increased with increasing  
**1571** soil nitrogen availability ( $p<0.001$ ; Table 4.5) and leaf  $C_i:C_a$  ( $p=0.040$ ; Table  
**1572** 4.5), and was generally larger in N-fixing species ( $p<0.001$ ; Table 4.5), but was  
**1573** negatively related to increasing  $M_{\text{area}}$  ( $p<0.001$ ; Table 4.5).  $M_{\text{area}}$  decreased with  
**1574** increasing leaf  $C_i:C_a$  and soil nitrogen availability ( $p<0.001$  in both cases; Table  
**1575** 4.5). Leaf  $C_i:C_a$  declined with increasing vapor pressure deficit, but was positively  
**1576** related to  $\beta$  ( $p<0.001$  in both cases; Table 4.5).  $\beta$  decreased with increasing soil  
**1577** nitrogen availability and was higher in C<sub>3</sub> species ( $p<0.001$  in both cases; Table  
**1578** 4.5), but did not change with soil moisture ( $p=0.895$ ; Table 4.5) or with ability  
**1579** to acquire nitrogen via symbiotic nitrogen fixation ( $p=0.519$ ; Table 4.5). Finally,  
**1580** soil nitrogen availability was positively associated with increasing soil moisture  
**1581** ( $p=0.003$ ; Table 4.5; Fig. 4.5).

**Table 4.5.** Structural equation model results investigating direct effects of climatic and soil resource availability on leaf nitrogen content ( $N_{\text{area}}$ ; g m<sup>-2</sup>)\*

Predictor	Coefficient	<i>p</i>
$N_{\text{area}}$ ( $R^2_c=0.89$ )		
$M_{\text{area}}$	0.714	<b>&lt;0.001</b>
$N_{\text{mass}}$	0.778	<b>&lt;0.001</b>
$N_{\text{mass}}$ ( $R^2_c=0.55$ )		
Leaf $C_i:C_a$	0.113	<b>0.040</b>
$M_{\text{area}}$	-0.201	<b>&lt;0.001</b>
Soil N	0.246	<b>&lt;0.001</b>
N-fixing ability	0.326	<b>&lt;0.001</b>
$M_{\text{area}}$ ( $R^2_c=0.56$ )		
Leaf $C_i:C_a$	-0.224	<b>&lt;0.001</b>
Soil N	-0.199	<b>&lt;0.001</b>
Leaf $C_i:C_a$ ( $R^2_c=0.82$ )		
$\beta$	0.308	<b>&lt;0.001</b>
$VPD_4$	-0.111	<b>&lt;0.001</b>
$\beta$ ( $R^2_c=0.38$ )		
Soil N	-0.207	<b>&lt;0.001</b>
$SM_{90}$	-0.006	0.895
Photo. pathway	0.446	<b>&lt;0.001</b>
N-fixing ability	-0.059	0.519
Soil N ( $R^2_c=0.35$ )		
$SM_{90}$	-0.148	<b>0.003</b>

**1582** \*Coefficients are standardized across the structural equation model. *P*-values less  
**1583** than 0.05 are noted in bold. Positive coefficients for photosynthetic pathway  
**1584** indicate generally larger values in C<sub>3</sub> species, while positive coefficients for N-  
**1585** fixing ability indicate generally larger values in N-fixing species. Key: df=degrees  
**1586** of freedom;  $\chi^2$ =Wald Type II chi-square test statistic;  $R^2_c$ =conditional R<sup>2</sup> value;  
**1587**  $N_{\text{mass}}$ =leaf nitrogen content per unit leaf biomass (gN g<sup>-1</sup>);  $M_{\text{area}}$ =leaf mass per  
**1588** unit leaf biomass (g m<sup>-2</sup>);  $\beta$ =cost of acquiring nitrogen relative to water (unitless);  
**1589**  $VPD_4$ =4-day mean vapor pressure deficit (kPa);  $SM_{90}$ =90-day mean soil moisture  
**1590** (mm)

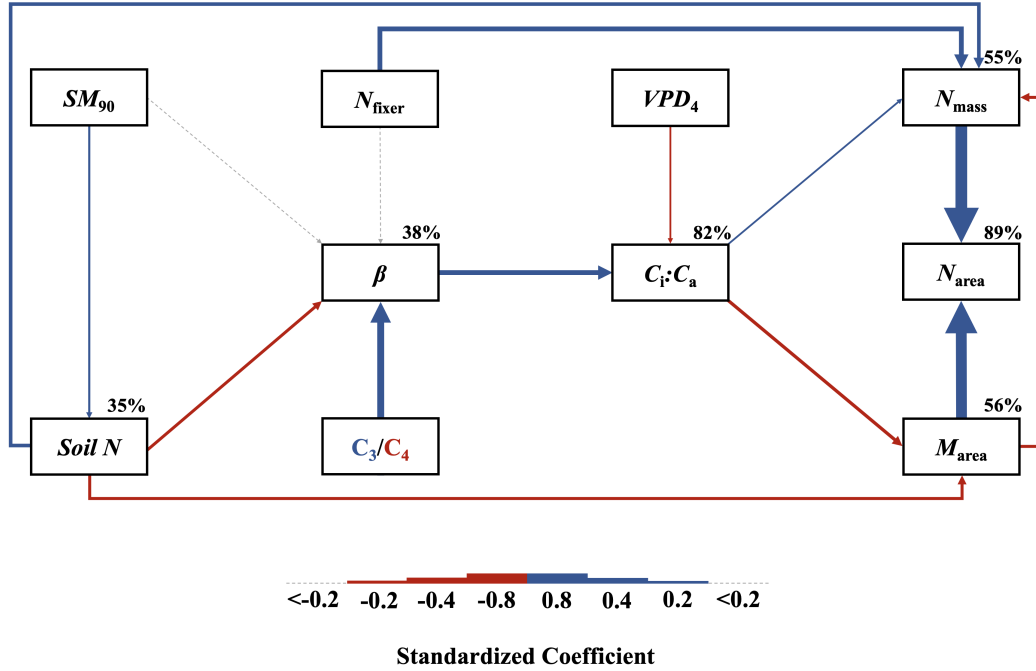


**Figure 4.5.** Structural equation model results exploring drivers of  $N_{\text{area}}$ . Boxes indicate measured edaphic factors, climatic factors, and leaf traits. Solid arrows indicate bivariate relationships where  $p < 0.05$ , while dashed arrows indicate relationships where  $p > 0.05$ . Positive model coefficients are indicated through blue arrows, negative model coefficients are indicated through red arrows, and insignificant coefficients are indicated through gray dashed arrows. Arrow thickness scales with the standardized model coefficient of each bivariate relationship. A positive coefficient for photosynthetic pathway indicates larger values in  $C_3$  species, while a positive coefficient for  $N_{\text{fixer}}$  indicates larger values in N-fixing species. Standardized model coefficients and associated  $p$ -values are reported in Table 4.5, with conditional  $R^2$  values for each response variable reported on the top right of each box.

**1591** 4.4 Discussion

**1592** In this study, direct and indirect effects of edaphic and climatic characteristics on  
**1593**  $N_{\text{area}}$  and components of  $N_{\text{area}}$  ( $N_{\text{mass}}$  and  $M_{\text{area}}$ ) were quantified in 504 individuals  
**1594** spanning across a soil resource availability and climate gradient in Texas, USA.  
**1595** Consistent patterns emerged in support of those expected from photosynthetic  
**1596** least-cost theory, a result driven by a strong direct negative relationship between  
**1597** leaf  $C_i:C_a$  and  $N_{\text{area}}$  mediated through changes in  $M_{\text{area}}$ . In further support of  
**1598** patterns expected from theory, increasing soil nitrogen availability had a nega-  
**1599** tive effect on  $\beta$ , resulting in an indirect stimulation in  $N_{\text{area}}$  mediated through  
**1600** a positive relationship between  $\beta$  and  $C_i:C_a$ . Increasing vapor pressure deficit  
**1601** also indirectly increased  $N_{\text{area}}$  through a direct negative effect of increasing vapor  
**1602** pressure deficit on leaf  $C_i:C_a$ , following hypotheses and patterns expected from  
**1603** theory. Interestingly, a positive association between soil moisture and  $N_{\text{area}}$  was  
**1604** driven by covariance between soil moisture and soil nitrogen availability and was  
**1605** not associated with a direct effect of soil moisture on  $\beta$ . Overall, results provide  
**1606** strong and consistent support for patterns expected from photosynthetic least-cost  
**1607** theory, showing that both soil resource availability and climate drive variance in  
**1608**  $N_{\text{area}}$  through changes in leaf  $C_i:C_a$ .

**1609** 4.4.1 *Negative effects of leaf  $C_i:C_a$  on  $N_{\text{area}}$  are driven by reductions in  $M_{\text{area}}$ ,*  
**1610** *not  $N_{\text{mass}}$*

**1611** The negative response of  $N_{\text{area}}$  to increasing leaf  $C_i:C_a$  is consistent with pre-  
**1612** vious environmental gradient (Dong et al. 2017; Querejeta et al. 2022) and  
**1613** manipulation experiments (3.4c), showing strong support for the nitrogen-water

**1614** use tradeoffs expected from photosynthetic least cost theory (Wright et al. 2003;  
**1615** Prentice et al. 2014). Negative effects of increasing leaf  $C_i:C_a$  on  $N_{area}$  were driven  
**1616** by negative effect of increasing leaf  $C_i:C_a$  on  $M_{area}$  coupled with a weak positive  
**1617** effect of increasing leaf  $C_i:C_a$  on  $N_{mass}$ , suggesting that changes in  $N_{area}$  across  
**1618** the environmental gradient were driven more strongly by changes in leaf morphol-  
**1619** ogy than leaf chemistry. Interestingly, the negative relationship between  $M_{area}$   
**1620** and  $N_{mass}$  suggested that stimulations in  $N_{mass}$  were often associated with larger,  
**1621** thinner leaves (i.e., lower  $M_{area}$ ). These results are consistent with patterns re-  
**1622** ported from previous studies indicating that variance in  $N_{area}$  is driven by changes  
**1623** in  $M_{area}$  across environmental gradients, and that part of this response is due to  
**1624** negative covariance between  $M_{area}$  and  $N_{mass}$  (Dong et al. 2017; Dong et al. 2020).  
**1625** Negative covariance between  $M_{area}$  and  $N_{mass}$  could be a response associated with  
**1626** tradeoffs between leaf longevity and leaf productivity (Wright et al. 2004; Dong  
**1627** et al. 2017; Dong et al. 2022; Querejeta et al. 2022; Wang et al. 2023).

**1628** The negative relationship between leaf  $C_i:C_a$  and  $M_{area}$  could be indicative  
**1629** of tradeoffs between leaf longevity and leaf productivity. Tradeoffs between leaf  
**1630** longevity and leaf productivity are commonly observed and are included in a  
**1631** continuum of coordinated leaf traits that position individuals along a fast- or  
**1632** slow-growing leaf economics spectrum (Wright et al. 2003; Onoda et al. 2004;  
**1633** Reich 2014; Onoda et al. 2017; Wang et al. 2023). Negative relationships between  
**1634** leaf  $C_i:C_a$  and  $M_{area}$  indicate that increased stomatal conductance and reduced  
**1635** water use efficiency were associated with thinner, larger leaves (i.e., lower  $M_{area}$ ).  
**1636** Combined with the negative covariance between  $M_{area}$  and  $N_{mass}$  mentioned above,  
**1637** these responses may have allowed individuals to maximize light interception and

**1638** productivity by exploiting high light environments at the expense of increased  
**1639** water loss and decreased water-use efficiency. This strategy may be especially  
**1640** advantageous for fast-growing species in open canopy systems. In this study, C<sub>3</sub>  
**1641** N-fixers and C<sub>3</sub> non-fixers dominated the dataset (77% of total sampling effort),  
**1642** of which 23% (17% of total sampling effort) were classified as annual species with  
**1643** short growing seasons. We observed no effect of leaf  $C_i:C_a$  on  $N_{\text{area}}$  or  $M_{\text{area}}$  in C<sub>4</sub>  
**1644** non-fixers, which made up 23% of the sampling effort and were generally classified  
**1645** as warm season graminoid species with slower growth rates and longer growing  
**1646** seasons. These patterns indicate that stronger tradeoffs between nitrogen and  
**1647** water use may be more apparent in fast-growing species with high demand for  
**1648** building and maintaining productive leaf tissues.

**1649** 4.4.2 *Soil nitrogen availability increases  $N_{\text{area}}$  through changes in  $\beta$*   
**1650** The structural equation model indicated multiple pathways where increasing soil  
**1651** nitrogen availability increased  $N_{\text{area}}$ . First,  $N_{\text{area}}$  increased with increasing soil  
**1652** nitrogen availability due to larger positive direct effects of increasing soil nitrogen  
**1653** availability on  $N_{\text{mass}}$  than the corresponding negative direct effect of increasing  
**1654** soil nitrogen availability on  $M_{\text{area}}$ . These patterns corroborate those observed in  
**1655** the individual linear mixed effect models and previous work. Second, soil nitrogen  
**1656** availability increased  $N_{\text{area}}$  indirectly through reductions in  $\beta$ , which increased leaf  
**1657**  $C_i:C_a$  and stimulated  $N_{\text{area}}$  through a stronger negative effect of increasing leaf  
**1658**  $C_i:C_a$  on  $M_{\text{area}}$  than corresponding positive effect of increasing leaf  $C_i:C_a$  on  $N_{\text{mass}}$ .  
**1659** Reductions in  $\beta$  with increasing soil nitrogen availability were likely driven by re-  
**1660** ductions in the cost of acquiring and using nitrogen, following patterns observed

1661 in previous experiments (Bae et al. 2015; Eastman et al. 2021; Perkowski et al.  
1662 2021; Lu et al. 2022). These pathways indicate that soil nitrogen availability can  
1663 have direct positive effects on  $N_{\text{area}}$  by increasing leaf nitrogen concentration, fol-  
1664 lowing previous work (Firn et al. 2019; Liang et al. 2020), or can alternatively have  
1665 indirect positive effects on  $N_{\text{area}}$  through changes in leaf morphology associated  
1666 with a reduction in the cost of acquiring nitrogen, following patterns expected  
1667 from photosynthetic least-cost theory. Results reported here indicate that pho-  
1668 tosynthetic least-cost frameworks are capable of detecting predictable variance in  
1669  $N_{\text{area}}$  and tradeoffs between nitrogen and water use across soil nitrogen availability  
1670 gradients.

1671 4.4.3 *Soil moisture increases  $N_{\text{area}}$  by facilitating increases in soil nitrogen  
1672 availability*

1673 Increasing soil moisture had a positive effect on  $N_{\text{area}}$ , though this response was  
1674 associated with a null effect of soil moisture on  $\beta$ . These results contrast patterns  
1675 expected from theory, where increasing soil moisture is expected to indirectly  
1676 decrease  $N_{\text{area}}$  through an increase in  $\beta$  due to a reduction in costs associated  
1677 with water acquisition and use (Wright et al. 2003; Prentice et al. 2014; Lavergne  
1678 et al. 2020). Interestingly, structural equation model results revealed a strong  
1679 positive association between soil moisture and soil nitrogen availability, indicating  
1680 an indirect positive effect of increasing soil moisture on  $N_{\text{area}}$  mediated by the  
1681 negative effect of increasing soil nitrogen availability on  $\beta$ . In Texan grasslands,  
1682 productivity and nutrient uptake are often co-limited by precipitation and nutrient  
1683 availability (Yahdjian et al. 2011; Wang et al. 2017). Thus, increases in soil  
1684 moisture may have facilitated more favorable and productive environments for  
1685 soil microbial communities (Reichman et al. 1966; Stark and Firestone 1995;

1686 Paul et al. 2003), or alternatively greater nitrogen mobility in soil solution. As  
1687 discussed above, the positive indirect response of  $N_{\text{area}}$  to increasing soil nitrogen  
1688 availability as mediated through reductions in  $\beta$  follow patterns expected from  
1689 theory.

1690 4.4.4 *Indirect effects of climate on  $N_{\text{area}}$  are mediated through changes in leaf*  
1691  $C_i:C_a$  *and  $\beta$*

1692 In support of hypotheses and patterns expected from theory, increasing vapor  
1693 pressure deficit indirectly increased  $N_{\text{area}}$ , mediated through the negative effect  
1694 of increasing vapor pressure deficit on leaf  $C_i:C_a$ . These responses are consistent  
1695 with previous work noting strong reductions in stomatal conductance with increas-  
1696 ing vapor pressure deficit (Oren et al. 1999; Novick et al. 2016; Sulman et al.  
1697 2016; Grossiord et al. 2020; López et al. 2021), a response that allows plants  
1698 to minimize water loss as a result of high atmospheric water demand. Results  
1699 also support findings from previous experiments across environmental gradients,  
1700 where increasing vapor pressure deficit generally increases  $N_{\text{area}}$  at lower stomatal  
1701 conductance across environmental gradients (Dong et al. 2017; Dong et al. 2022;  
1702 Paillassa et al. 2020; Westerband et al. 2023). The increase in  $N_{\text{area}}$  with increas-  
1703 ing vapor pressure deficit could allow plants to maximize photosynthetic capacity  
1704 under reduced stomatal conductance (Dong et al. 2022), though this pattern con-  
1705 trasts previous work suggesting that long-term increases in vapor pressure deficit  
1706 are associated with increased plant mortality, reduced net primary productivity,  
1707 and perhaps reductions in net photosynthesis rates over time due to prolonged  
1708 stomatal closure (Eamus et al. 2013; Yuan et al. 2019; Grossiord et al. 2020).  
1709 Importantly, such negative effects of increasing vapor pressure deficit often occur  
1710 along much broader timescales compared to the timescale used here. Responses

1711 observed here suggest that variance in  $N_{\text{area}}$  across environmental gradients is  
1712 a deterministic acclimation response to changing aboveground climate, allowing  
1713 plants to satisfy demand to build and maintain photosynthetic enzymes and op-  
1714 timize photosynthetic processes by maximizing resource use efficiency (Paillassa  
1715 et al. 2020; Peng et al. 2021; Dong et al. 2022; Westerband et al. 2023).

1716 4.4.5 *Species identity traits modify effects of the environment on  $\beta$ , leaf  $C_i:C_a$ ,*  
1717 *and  $N_{\text{area}}$*

1718 N-fixing species had greater  $N_{\text{area}}$  values on average compared to non-fixing species,  
1719 a pattern driven by a stronger stimulation in  $N_{\text{mass}}$  in N-fixing species coupled with  
1720 no change in  $M_{\text{area}}$  between species with different N-fixation ability. There was  
1721 no evidence to suggest that N-fixing species had different  $\beta$  or leaf  $C_i:C_a$  values  
1722 compared to non-fixing species across the environmental gradient. These results  
1723 follow patterns from previous environmental gradient experiments that investi-  
1724 gate variance in leaf nitrogen allocation in N-fixing species (Adams et al. 2016;  
1725 Dong et al. 2017; Dong et al. 2020), and that increases in  $N_{\text{mass}}$  and  $N_{\text{area}}$  in  
1726 N-fixing species are not necessarily correlated to increases in water use efficiency  
1727 or reductions in leaf  $C_i:C_a$  (Adams et al. 2016). While results are consistent with  
1728 results from previous environmental gradient experiments, they do not support  
1729 hypotheses presented here or patterns expected from theory, which predicts that  
1730 stimulations in  $N_{\text{area}}$  by N-fixing species should be driven by a reduction in  $\beta$   
1731 relative to non-fixing species, and that this response should decrease stomatal  
1732 conductance and leaf  $C_i:C_a$ .

1733 C<sub>4</sub> species had reduced  $\beta$ , leaf  $C_i:C_a$ , and  $N_{\text{area}}$  than C<sub>3</sub> species. Reduced  
1734  $\beta$  and leaf  $C_i:C_a$  values in C<sub>4</sub> species follow hypotheses listed above, a pattern

1735 that could be the result of either reduced costs of nitrogen acquisition and use,  
1736 increased costs of water acquisition and use, or both (Wright et al. 2003; Prentice  
1737 et al. 2014). Results also indicate that  $\beta$  in C<sub>4</sub> non-fixers was unresponsive to  
1738 changes in soil nitrogen availability despite an apparent negative effect of increas-  
1739 ing soil nitrogen availability on  $\beta$  in C<sub>3</sub> N-fixers and C<sub>3</sub> non-fixers. Combined  
1740 with a general null response of  $\beta$  to soil moisture regardless of plant functional  
1741 group, these patterns imply that reduced  $\beta$  values in C<sub>4</sub> species may be the re-  
1742 sult of lower costs of nitrogen acquisition and use relative to C<sub>3</sub> species. While  
1743 lower  $\beta$  values in C<sub>4</sub> species provides a possible explanation for why C<sub>4</sub> species  
1744 often have lower leaf  $C_i:C_a$  and greater water use efficiency, theory predicts that  
1745 this response should cause C<sub>4</sub> species to have greater  $N_{area}$  values compared to  
1746 C<sub>3</sub> species, though C<sub>4</sub> species commonly exhibit lower  $N_{area}$  and higher nitrogen  
1747 use efficiency than C<sub>3</sub> species (Schmitt and Edwards 1981; Sage and Pearcy 1987;  
1748 Ghannoum et al. 2011). We speculate that lowered costs of nitrogen acquisition  
1749 and use in C<sub>4</sub> species could be driven by more efficient Rubisco carboxylation effi-  
1750 ciency in C<sub>4</sub> species associated with CO<sub>2</sub> concentrating mechanisms that eliminate  
1751 photorespiration (Ghannoum et al. 2011), which could reduce or eliminate the  
1752 need to sacrifice inefficient nitrogen use for efficient water use to achieve optimal  
1753 photosynthesis rates.

1754 4.4.6 *Next steps for optimality model development*

1755 Optimality models for both C<sub>3</sub> and C<sub>4</sub> species have been developed using principles  
1756 from photosynthetic least-cost theory (Prentice et al. 2014; Wang et al. 2017;  
1757 Smith et al. 2019; Stocker et al. 2020; Scott and Smith 2022). In both C<sub>3</sub> and C<sub>4</sub>  
1758 model variants,  $\beta$  values are held constant using global datasets of leaf  $\delta^{13}\text{C}$  (Wang

1759 et al. 2017; Cornwell et al. 2018). Specifically, the C<sub>3</sub> optimality model initially  
1760 assumed a constant  $\beta$  value of 240 (Wang et al. 2017), later corrected to 146  
1761 (Stocker et al. 2020), while the C<sub>4</sub> optimality model assumes a constant  $\beta$  value of  
1762 166 (Scott and Smith 2022). These results, which build on findings from Paillassa  
1763 et al. (2020) and Lavergne et al. (2020), demonstrate high variability in calculated  
1764  $\beta$  values across the environmental gradient. Specifically,  $\beta$  values in C<sub>3</sub> species  
1765 ranged from 1.7 to 188.0 (mean: 30.2; median: 23.1; standard deviation: 25.4),  
1766 while ranged from 0.1 to 110.6 in C<sub>4</sub> species (mean: 7.2; median: 0.7; standard  
1767 deviation: 18.6). Mean  $\beta$  values in both C<sub>3</sub> and C<sub>4</sub> species were consistently lower  
1768 than values currently implemented in optimality models, though this was likely  
1769 the result of increased water limitation across sites relative to global averages.  
1770 Regardless, the high degree of  $\beta$  variability across this environmental gradient,  
1771 together with findings from Lavergne et al. (2020) and Paillassa et al. (2020),  
1772 suggests that the use of constant  $\beta$  values may contribute to erroneous errors when  
1773 conducting optimality model simulations. Results from this experiment build  
1774 on suggestions from Wang et al. (2017), suggesting that future photosynthetic  
1775 least-cost optimality model developments should consider adopting frameworks  
1776 for dynamically calculating  $\beta$ .

1777 4.4.7 *Conclusions*

1778 To summarize, variability in  $N_{\text{area}}$  across an environmental gradient in Texan  
1779 grasslands was driven by indirect effects of climate and soil resource availability  
1780 mediated by changes in  $\beta$  and leaf  $C_i:C_a$ . Results from this experiment provide  
1781 strong and consistent support for patterns expected from photosynthetic least-

**1782** cost theory, demonstrating that negative relationships between  $C_i:C_a$  and  $N_{\text{area}}$   
**1783** unify expected effects of climatic and edaphic characteristics on  $N_{\text{area}}$  across en-  
**1784** vironmental gradients. Results reported here also demonstrate a need to consider  
**1785** the dynamic nature of the relative cost of nitrogen versus water uptake ( $\beta$ ) across  
**1786** environmental gradients in optimality models that leverage principles of photo-  
**1787** synthetic least-cost theory.

1788

## Chapter 5

1789     Optimal resource investment to photosynthetic capacity maximizes  
1790       nutrient allocation to whole plant growth under elevated CO<sub>2</sub>

1791     5.1   Introduction

1792     Terrestrial ecosystems are regulated by complex carbon and nitrogen cycles. As  
1793     a result, terrestrial biosphere models, which are beginning to include coupled  
1794     carbon and nitrogen cycles (Shi et al. 2016; Davies-Barnard et al. 2020; Braghieri  
1795     et al. 2022), must accurately represent these cycles under different environmental  
1796     scenarios to reliably simulate carbon and nitrogen atmosphere-biosphere fluxes  
1797     (Hungate et al. 2003; Prentice et al. 2015). While the inclusion of coupled carbon  
1798     and nitrogen cycles tends to reduce model uncertainty (Arora et al. 2020), large  
1799     uncertainty in role of soil nitrogen availability and nitrogen acquisition strategy  
1800     on leaf and whole plant acclimation responses to CO<sub>2</sub> remains (Smith and Dukes  
1801     2013; Terrer et al. 2018; Smith and Keenan 2020). This source of uncertainty  
1802     likely contributes to the widespread divergence in future carbon and nitrogen flux  
1803     simulations across terrestrial biosphere models (Friedlingstein et al. 2014; Zaehle  
1804     et al. 2014; Meyerholt et al. 2020).

1805           Plants grown under elevated CO<sub>2</sub> generally have less leaf nitrogen content  
1806     than those grown under ambient CO<sub>2</sub>, a response that often corresponds with  
1807     reductions in photosynthetic capacity and stomatal conductance at the leaf-level  
1808     and biomass stimulation over time at the whole plant level (Curtis 1996; Drake  
1809     et al. 1997; Ainsworth et al. 2002; Makino 2003; Morgan et al. 2004; Ainsworth  
1810     and Long 2005; Ainsworth and Rogers 2007; Smith and Dukes 2013; Poorter et al.  
1811     2022). As net primary productivity is generally limited by nitrogen availability

1812 (Vitousek and Howarth 1991; LeBauer and Treseder 2008; Fay et al. 2015), and  
1813 soil nitrogen availability is often positively correlated with leaf nitrogen content  
1814 and photosynthetic capacity (Field and Mooney 1986; Evans and Seemann 1989;  
1815 Evans 1989; Walker et al. 2014; Firn et al. 2019; Liang et al. 2020), some  
1816 have hypothesized that leaf and whole plant acclimation responses to CO<sub>2</sub> are  
1817 constrained by soil nitrogen availability.

1818 The progressive nitrogen limitation hypothesis predicts that elevated CO<sub>2</sub>  
1819 will increase plant nitrogen demand, which will increase plant nitrogen uptake and  
1820 progressively deplete soil nitrogen if soil nitrogen supply does not exceed plant  
1821 nitrogen demand (Luo et al. 2004). The hypothesis predicts that this response  
1822 should result in strong acute stimulations in whole plant growth and primary  
1823 productivity that diminish over time as nitrogen becomes more limiting. Assuming  
1824 a positive relationship between soil nitrogen availability, leaf nitrogen content, and  
1825 photosynthetic capacity, this hypothesis also implies that progressive reductions in  
1826 soil nitrogen availability should be the mechanism that drives the downregulation  
1827 of leaf nitrogen content and photosynthetic capacity under elevated CO<sub>2</sub>. This  
1828 hypothesis has received some support from free air CO<sub>2</sub> enrichment experiments  
1829 (Reich et al. 2006; Norby et al. 2010), although is not consistently observed across  
1830 experiments (Finzi et al. 2006; Moore et al. 2006; Liang et al. 2016).

1831 While possible that progressive nitrogen limitation may determine leaf and  
1832 whole plant acclimation responses to CO<sub>2</sub>, growing evidence indicates that leaf ni-  
1833 trogen and photosynthetic capacity are more strongly determined through above-  
1834 ground growing conditions than by soil resource availability (Dong et al. 2017;  
1835 Dong et al. 2020; Dong et al. 2022; Smith et al. 2019; Smith and Keenan 2020;

1836 Paillassa et al. 2020; Peng et al. 2021; Querejeta et al. 2022; Westerband et al.  
1837 2023), and satellite-derived chlorophyll fluorescence data indicate that increasing  
1838 atmospheric CO<sub>2</sub> may decrease leaf and canopy demand for nitrogen (Dong et al.  
1839 2022). Together, results from these studies suggest that the downregulation in  
1840 leaf nitrogen content and photosynthetic capacity due to increasing CO<sub>2</sub> may not  
1841 be as tightly linked to progressive nitrogen limitation as previously hypothesized.

1842 A unification of optimal coordination and least-cost theories predicts that  
1843 leaves acclimate to elevated CO<sub>2</sub> by downregulating nitrogen allocation to Ribulose-  
1844 1,5-bisphosphate (RuBP) carboxylase/oxygenase (Rubisco) to optimize resource  
1845 use efficiencies at the leaf level, which allows for greater resource allocation to  
1846 whole plant growth (Drake et al. 1997; Wright et al. 2003; Prentice et al. 2014;  
1847 Smith et al. 2019). The theory predicts that the downregulation in nitrogen  
1848 allocation to Rubisco results in a stronger downregulation in the maximum rate  
1849 of Rubisco carboxylation ( $V_{cmax}$ ) than the maximum rate of RuBP regeneration  
1850 ( $J_{max}$ ), which maximizes photosynthetic efficiency by allowing net photosynthesis  
1851 rates to be equally co-limited by Rubisco carboxylation and RuBP regeneration  
1852 (Chen et al. 1993; Maire et al. 2012). This acclimation response allows plants to  
1853 make more efficient use of available light while avoiding overinvestment in Rubisco,  
1854 which has high nitrogen and energetic costs of building and maintaining (Evans  
1855 1989; Evans and Clarke 2019). Instead, additional acquired resources not needed  
1856 to optimize leaf photosynthesis are allocated to the maintenance of structures that  
1857 support whole plant growth (e.g., total leaf area, whole plant biomass, etc.) or  
1858 to allocation processes not related to leaf photosynthesis or growth, such as plant  
1859 defense mechanisms. Regardless, optimized resource allocation at the leaf level

**1860** should allow for greater resource allocation to whole plant growth. The theory  
**1861** indicates that leaf acclimation responses to CO<sub>2</sub> should be independent of changes  
**1862** in soil nitrogen availability. While this leaf acclimation response maximizes nitro-  
**1863** gen allocation to structures that support whole plant growth, the theory suggests  
**1864** that the positive effect of elevated CO<sub>2</sub> on whole plant growth may be further  
**1865** stimulated by soil nitrogen availability through reductions in the cost of acquiring  
**1866** nitrogen (Bae et al. 2015; Perkowski et al. 2021; Lu et al. 2022).

**1867** Plants acquire nitrogen by allocating photosynthetically derived carbon be-  
**1868** lowground in exchange for nitrogen through different nitrogen acquisition strate-  
**1869** gies. These nitrogen acquisition strategies can include direct uptake pathways  
**1870** such as mass flow or diffusion (Barber 1962), symbioses with mycorrhizal fungi or  
**1871** symbiotic nitrogen-fixing bacteria (Vance and Heichel 1991; Marschner and Dell  
**1872** 1994; Smith and Read 2008; Udvardi and Poole 2013), or through the release  
**1873** of root exudates that prime free-living soil microbial communities (Phillips et al.  
**1874** 2011; Wen et al. 2022). Plants cannot acquire nitrogen without first allocating  
**1875** carbon belowground, which implies an inherent carbon cost to the plant for acquir-  
**1876** ing nitrogen regardless of nitrogen acquisition strategy. Carbon costs to acquire  
**1877** nitrogen often vary in species with different nitrogen acquisition strategies and  
**1878** are dependent on external environmental factors such as atmospheric CO<sub>2</sub>, light  
**1879** availability, and soil nitrogen availability (Brzostek et al. 2014; Terrer et al. 2016;  
**1880** Terrer et al. 2018; Allen et al. 2020; Perkowski et al. 2021; Lu et al. 2022). These  
**1881** patterns suggest that acquisition strategy may at least partially determine the net  
**1882** effect of soil nitrogen availability on leaf and whole plant acclimation responses to  
**1883** elevated CO<sub>2</sub>.

1884        A recent meta-analysis using data across 20 grassland and forest CO<sub>2</sub> en-  
1885 richment experiments suggested that species which acquire nitrogen from sym-  
1886 biotic nitrogen-fixing bacteria had reduced costs of nitrogen acquisition under  
1887 elevated CO<sub>2</sub> (Terrer et al. 2018). Though these analyses only included data  
1888 from two experimental sites, findings from this meta-analysis indicated that re-  
1889 ductions in costs of nitrogen acquisition in species that form associations with  
1890 symbiotic nitrogen-fixing bacteria under elevated CO<sub>2</sub> may drive stronger stim-  
1891 ulations in whole plant growth and downregulations in  $V_{cmax}$  than species that  
1892 associate with arbuscular mycorrhizal fungi (Smith and Keenan 2020), which gen-  
1893 erally have greater costs of nitrogen acquisition under elevated CO<sub>2</sub> (Terrer et al.  
1894 2018). However, plant investments in symbiotic nitrogen fixation generally de-  
1895 cline with increasing nitrogen availability (Dovrat et al. 2018; Perkowski et al.  
1896 2021), a response that has been previously inferred to be the result of a shift in  
1897 the dominant mode of nitrogen acquisition to direct uptake pathways as costs of  
1898 direct uptake decrease with increasing soil nitrogen availability (Rastetter et al.  
1899 2001; Perkowski et al. 2021). Thus, effects of symbiotic nitrogen fixation on plant  
1900 acclimation responses to CO<sub>2</sub> should decline with increasing soil nitrogen avail-  
1901 ability, although manipulative experiments that directly test these patterns are  
1902 rare.

1903        Here, I conducted a 7-week growth chamber experiment using *Glycine max*  
1904 L. (Merr.) to examine the effects of soil nitrogen fertilization and inoculation with  
1905 symbiotic nitrogen-fixing bacteria on leaf and whole plant acclimation responses  
1906 to elevated CO<sub>2</sub>. Following patterns expected from theory, I hypothesized that in-  
1907 dividual leaves should acclimate to elevated CO<sub>2</sub> by more strongly downregulating

1908  $V_{cmax}$  relative to  $J_{max}$ , allowing leaf photosynthesis to approach optimal coordi-  
1909 nation. I expected this response to correspond with a stronger downregulation in  
1910 leaf nitrogen content than  $V_{cmax}$  and  $J_{max}$ , which would increase the fraction of  
1911 leaf nitrogen content allocated to photosynthesis and photosynthetic nitrogen use  
1912 efficiency. At the whole-plant level, I hypothesized that plants would acclimate  
1913 to elevated CO<sub>2</sub> by stimulating whole plant growth and productivity, a response  
1914 that would be driven by a strong positive response of total leaf area and above-  
1915 ground biomass to elevated CO<sub>2</sub>. I predicted that leaf acclimation responses to  
1916 elevated CO<sub>2</sub> would be independent of soil nitrogen fertilization and inoculation  
1917 with symbiotic nitrogen-fixing bacteria; however, I expected that increasing soil  
1918 nitrogen fertilization would increase the positive effect of elevated CO<sub>2</sub> on mea-  
1919 sures of whole plant growth due to a stronger reduction in the cost of acquiring  
1920 nitrogen under elevated CO<sub>2</sub> with increasing fertilization. I also expected stronger  
1921 stimulations in whole plant growth due to inoculation, but that this effect would  
1922 only be apparent under low fertilization due to a reduction in root nodulation  
1923 with increasing fertilization.

1924 5.2 Methods

1925 5.2.1 *Seed treatments and experimental design*

1926 *Glycine max* L. (Merr) seeds were planted in 144 6-liter surface sterilized pots (NS-  
1927 600, Nursery Supplies, Orange, CA, USA) containing a steam-sterilized 70:30 v:v  
1928 mix of Sphagnum peat moss (Premier Horticulture, Quakertown, PA, USA) to  
1929 sand (Pavestone, subsidiary of Quikrete Companies, Atlanta, GA, USA). Before  
1930 planting, all *G. max* seeds were surface sterilized in 2% sodium hypochlorite for 3

1931 minutes, followed by three separate 3-minute washes with ultrapure water (MilliQ  
1932 7000; MilliporeSigma, Burlington, MA USA). A subset of surface sterilized seeds  
1933 were inoculated with *Bradyrhizobium japonicum* (Verdesian N-Dure<sup>TM</sup> Soybean,  
1934 Cary, NC, USA) in a slurry following manufacturer recommendations (3.12 g  
1935 inoculant and 241 g deionized water per 1 kg seed).

1936 Seventy-two pots were randomly planted with surface-sterilized seeds inoc-  
1937 ulated with *B. japonicum*, while the remaining 72 pots were planted with surface-  
1938 sterilized uninoculated seeds. Thirty-six pots within each inoculation treatment  
1939 were randomly placed in one of two atmospheric CO<sub>2</sub> treatments (ambient and  
1940 1000  $\mu\text{mol mol}^{-1}$  CO<sub>2</sub>). Pots within each unique inoculation-by-CO<sub>2</sub> treatment  
1941 combination randomly received one of nine soil nitrogen fertilization treatments  
1942 equivalent to 0, 35, 70, 105, 140, 210, 280, 350, or 630 ppm N. Nitrogen fertil-  
1943 ization treatments were created using a modified Hoagland solution (Hoagland  
1944 and Arnon 1950) designed to keep concentrations of other macronutrients and  
1945 micronutrients equivalent across treatments (Table D1). Pots received the same  
1946 fertilization treatment throughout the entire duration experiment, which were ap-  
1947 plied twice per week in 150 mL doses as topical agents to the soil surface. This  
1948 experimental design yielded a fully factorial experiment with four replicates per  
1949 unique fertilization-by-inoculation-by-CO<sub>2</sub> combination.

1950 5.2.2 *Growth chamber conditions*

1951 Upon experiment initiation, pots were randomly placed in one of six Percival  
1952 LED-41L2 growth chambers (Percival Scientific Inc., Perry, IA, USA) over two  
1953 experimental iterations due to chamber space limitation. Two iterations were

1954 conducted such that one iteration included all elevated CO<sub>2</sub> pots and the second  
1955 iteration included all ambient CO<sub>2</sub> pots. Mean ( $\pm$  SD) CO<sub>2</sub> concentrations across  
1956 chambers throughout the experiment were  $439 \pm 5 \mu\text{mol mol}^{-1}$  CO<sub>2</sub> for the ambient  
1957 CO<sub>2</sub> treatment and  $989 \pm 4 \mu\text{mol mol}^{-1}$  CO<sub>2</sub> for the elevated CO<sub>2</sub> treatment.

1958 Daytime growing conditions were simulated using a 16-hour photoperiod,  
1959 with incoming light radiation set to chamber maximum (mean  $\pm$  SD:  $1240 \pm 32$   
1960  $\mu\text{mol m}^{-2} \text{s}^{-1}$  across chambers), air temperature set to 25°C, and relative humid-  
1961 ity set to 50%. The remaining 8 hours simulated nighttime growing conditions,  
1962 with incoming light radiation set to 0  $\mu\text{mol m}^{-2} \text{s}^{-1}$ , chamber temperature set  
1963 to 17°C, and relative humidity set to 50%. Transitions between daytime and  
1964 nighttime growing conditions were simulated by ramping incoming light radiation  
1965 in 45-minute increments and temperature in 90-minute increments over a 3-hour  
1966 period (Table D2).

1967 Including the two, 3-hour ramping periods, pots grew under average ( $\pm$  SD)  
1968 daytime light intensity of  $1049 \pm 27 \mu\text{mol m}^{-2} \text{s}^{-1}$ . In the elevated CO<sub>2</sub> iteration,  
1969 pots grew under  $24.0 \pm 0.2^\circ\text{C}$  during the day,  $16.4 \pm 0.8^\circ\text{C}$  during the night, and  
1970 51.6  $\pm 0.4\%$  relative humidity. In the ambient CO<sub>2</sub> iteration, pots grew under  
1971  $23.9 \pm 0.2^\circ\text{C}$  during the day,  $16.0 \pm 1.4^\circ\text{C}$  during the night, and 50.3  $\pm 0.2\%$  relative  
1972 humidity. I accounted for any climatic differences across the six chambers by  
1973 shuffling the same group of pots daily throughout the growth chambers. This  
1974 process was done by iteratively moving the group of pots on the top rack of a  
1975 chamber to the bottom rack of the same chamber, while simultaneously moving  
1976 the group of pots on the bottom rack of a chamber to the top rack of the adjacent  
1977 chamber. I moved pots within and across chambers every day throughout the

**1978** course of each experiment iteration.

**1979** 5.2.3 *Leaf gas exchange measurements*

**1980** Gas exchange measurements were collected for all individuals on the seventh week  
**1981** of development. All gas exchange measurements were collected on the center leaf  
**1982** of the most recent fully expanded trifoliate leaf set. Specifically, I measured net  
**1983** photosynthesis ( $A_{\text{net}}$ ;  $\mu\text{mol m}^{-2} \text{s}^{-1}$ ), stomatal conductance ( $g_{\text{sw}}$ ;  $\text{mol m}^{-2} \text{s}^{-1}$ ),  
**1984** and intercellular  $\text{CO}_2$  ( $C_i$ ;  $\mu\text{mol mol}^{-1}$ ) concentrations across a range of atmo-  
**1985** spheric  $\text{CO}_2$  concentrations (i.e., an  $A_{\text{net}}/C_i$  curve) using the Dynamic Assimila-  
**1986** tion Technique™. The Dynamic Assimilation Technique™ has been shown to  
**1987** correspond well with traditional steady-state  $\text{CO}_2$  response curves in *G. max*  
**1988** (Saathoff and Welles 2021).  $A_{\text{net}}/C_i$  curves were generated along a reference  $\text{CO}_2$   
**1989** ramp down from  $420 \mu\text{mol mol}^{-1} \text{CO}_2$  to  $20 \mu\text{mol mol}^{-1} \text{CO}_2$ , followed by a ramp  
**1990** up from  $420 \mu\text{mol mol}^{-1} \text{CO}_2$  to  $1620 \mu\text{mol mol}^{-1} \text{CO}_2$  after a 90-second wait  
**1991** period at  $420 \mu\text{mol mol}^{-1} \text{CO}_2$ . The ramp rate for each curve was set to  $200$   
**1992**  $\mu\text{mol mol}^{-1} \text{min}^{-1}$ , logging every five seconds, which generated 96 data points per  
**1993** response curve. All  $A_{\text{net}}/C_i$  curves were generated after  $A_{\text{net}}$  and  $g_{\text{sw}}$  stabilized  
**1994** in a LI-6800 cuvette set to a  $500 \text{ mol s}^{-1}$ , 10,000 rpm mixing fan speed, 1.5 kPa  
**1995** vapor pressure deficit,  $25^\circ\text{C}$  leaf temperature,  $2000 \mu\text{mol m}^{-2} \text{s}^{-1}$  incoming light  
**1996** radiation, and initial reference  $\text{CO}_2$  set to  $420 \mu\text{mol mol}^{-1}$ .

**1997** With the same focal leaf used to generate  $A_{\text{net}}/C_i$  curves, I measured dark  
**1998** respiration ( $R_{d25}$ ;  $\mu\text{mol m}^{-2} \text{s}^{-1}$ ) following at least a 30-minute period of darkness.  
**1999** Measurements were collected on a 5-second log interval for 60 seconds after stabi-  
**2000** lizing in a LI-6800 cuvette set to a  $500 \text{ mol s}^{-1}$ , 10,000 rpm mixing fan speed, 1.5

**2001** kPa vapor pressure deficit, 25°C leaf temperature, and 420  $\mu\text{mol mol}^{-1}$  reference  
**2002** CO<sub>2</sub> concentration (for both CO<sub>2</sub> concentrations), with incoming light radiation  
**2003** set to 0  $\mu\text{mol m}^{-2} \text{s}^{-1}$ . A single dark respiration value was determined for each  
**2004** focal leaf by calculating the mean dark respiration value (i.e. the absolute value  
**2005** of  $A_{\text{net}}$  during the logging period) across the logging interval.

**2006** 5.2.4 *Leaf trait measurements*

**2007** The focal leaf used to generate  $A_{\text{net}}/C_i$  curves and dark respiration was harvested  
**2008** immediately following gas exchange measurements. Images of each focal leaf were  
**2009** curated using a flat-bed scanner to determine wet leaf area using the ‘LeafArea’ R  
**2010** package (Katabuchi 2015), which automates leaf area calculations using ImageJ  
**2011** software (Schneider et al. 2012). Each leaf was dried at 65°C for at least 48  
**2012** hours, and subsequently weighed and ground until homogenized. Leaf mass per  
**2013** area ( $M_{\text{area}}$ ; g m<sup>-2</sup>) was calculated as the ratio of dry leaf biomass to fresh leaf  
**2014** area. Using subsamples of ground and homogenized leaf tissue, I measured leaf  
**2015** nitrogen content ( $N_{\text{mass}}$ ; gN g<sup>-1</sup>) through elemental combustion analysis (Costech-  
**2016** 4010, Costech, Inc., Valencia, CA, USA). Leaf nitrogen content per unit leaf area  
**2017** ( $N_{\text{area}}$ ; gN m<sup>-2</sup>) was calculated by multiplying  $N_{\text{mass}}$  and  $M_{\text{area}}$ . Subsamples of  
**2018** ground and homogenized leaf tissue were also sent to the UC-Davis Stable Isotope  
**2019** Facility to quantify leaf  $\delta^{15}\text{N}$ , later used to estimate the fraction of leaf nitrogen  
**2020** derived from the atmosphere.

**2021** I extracted chlorophyll content from a second leaf in the same trifoliolate  
**2022** leaf set as the focal leaf used to generate  $A_{\text{net}}/C_i$  curves. Prior to chlorophyll  
**2023** extraction, I used a cork borer to punch between 3 and 5 0.6 cm<sup>2</sup> disks from the

**2024** leaf. Separate images of each punched leaf and set of leaf disks were curated using  
**2025** a flat-bed scanner to determine wet leaf area, again quantified using the ‘LeafArea’  
**2026** R package (Katabuchi 2015). The punched leaf was dried and weighed after at  
**2027** least 65°C in the drying oven to determine  $M_{\text{area}}$  of the chlorophyll leaf.

**2028** Leaf disks were shuttled into a test tube containing 10mL dimethyl sulfoxide, vortexed, and incubated at 65°C for 120 minutes (Barnes et al. 1992). Incubated test tubes were vortexed again before loaded in 150  $\mu\text{L}$  triplicate aliquots to a 96-well plate. Dimethyl sulfoxide was also loaded in a 150  $\mu\text{L}$  triplicate aliquot as a blank. Absorbance measurements at 649.1 nm ( $A_{649.1}$ ) and 665.1 nm ( $A_{665.1}$ ) were read in each well using a plate reader (Bioteck Synergy H1; Bioteck Instruments, Winooski, VT USA) (Wellburn 1994), with triplicates subsequently averaged and corrected by the mean of the blank absorbance value. Blank-corrected absorbance values were used to estimate  $Chl_a$  ( $\mu\text{g mL}^{-1}$ ) and  $Chl_b$  ( $\mu\text{g mL}^{-1}$ ) following equations from Wellburn (1994):

$$Chl_a = 12.47A_{665.1} - 3.62A_{649.1} \quad (5.1)$$

**2038** and

$$Chl_b = 25.06A_{665.1} - 6.50A_{649.1} \quad (5.2)$$

**2039**  $Chl_a$  and  $Chl_b$  were converted to mmol  $\text{mL}^{-1}$  using the molar mass of chlorophyll a  
**2040** (893.51 g  $\text{mol}^{-1}$ ) and the molar mass of chlorophyll b (907.47 g  $\text{mol}^{-1}$ ), then added  
**2041** together to calculate total chlorophyll content in the dimethyl sulfoxide extractant  
**2042** (mmol  $\text{mL}^{-1}$ ). Total chlorophyll content was multiplied by the volume of the  
**2043** dimethyl sulfoxide extractant (10 mL) and converted to area-based chlorophyll

2044 content by dividing by the total area of the leaf disks ( $Chl_{area}$ ; mmol m<sup>-2</sup>). Mass-  
2045 based chlorophyll content ( $Chl_{mass}$ ; mmol g<sup>-1</sup>) was calculated by dividing  $Chl_{area}$   
2046 by the leaf mass per area of the punched leaf.

2047 5.2.5 *A/C<sub>i</sub> curve fitting and parameter estimation*

2048 I fit  $A_{net}/C_i$  curves of each individual using the ‘fitaci’ function in the ‘plante-  
2049 cophys’ R package (Duursma 2015). This function estimates the maximum rate  
2050 of Rubisco carboxylation ( $V_{cmax}$ ;  $\mu\text{mol m}^{-2} \text{s}^{-1}$ ) and maximum rate of electron  
2051 transport for RuBP regeneration ( $J_{max}$ ;  $\mu\text{mol m}^{-2} \text{s}^{-1}$ ) based on the Farquhar  
2052 biochemical model of C<sub>3</sub> photosynthesis (Farquhar et al. 1980). Triose phosphate  
2053 utilization (TPU) limitation was included in all curve fits, and all curve fits in-  
2054 cluded measured dark respiration values. As  $A_{net}/C_i$  curves were generated using  
2055 a common leaf temperature, curves were fit using Michaelis-Menten coefficients  
2056 for Rubisco affinity to CO<sub>2</sub> ( $K_c$ ;  $\mu\text{mol mol}^{-1}$ ) and O<sub>2</sub> ( $K_o$ ;  $\mu\text{mol mol}^{-1}$ ), and the  
2057 CO<sub>2</sub> compensation point ( $\Gamma^*$ ;  $\mu\text{mol mol}^{-1}$ ) reported in Bernacchi et al. (2001).  
2058 Specifically,  $K_c$  was set to 404.9  $\mu\text{mol mol}^{-1}$ ,  $K_o$  was set to 278.4  $\mu\text{mol mol}^{-1}$ ,  
2059 and  $\Gamma^*$  was set to 42.75  $\mu\text{mol mol}^{-1}$ . All curve fits were visually examined for  
2060 goodness-of-fit. The use of a common leaf temperature across curves and dark  
2061 respiration measurements eliminated the need to temperature standardize rate  
2062 estimates. For clarity, I reference  $V_{cmax}$ ,  $J_{max}$ , and  $R_d$  estimates throughout the  
2063 rest of the chapter as  $V_{cmax25}$ ,  $J_{max25}$ , and  $R_{d25}$ .

**2064** 5.2.6 *Stomatal limitation*

**2065** I quantified the extent by which stomatal conductance limited photosynthesis ( $l$ ;

**2066** unitless) following equations originally described in Farquhar and Sharkey (1982).

**2067** Stomatal limitation was calculated as:

$$l = 1 - \frac{A_{net}}{A_{mod}} \quad (5.3)$$

**2068** where  $A_{mod}$  represents the photosynthetic rate where  $C_i = C_a$ .  $A_{mod}$  was calculated

**2069** as:

$$A_{mod} = V_{cmax25} - \frac{420 - \Gamma^*}{420 + K_m} - R_{d25} \quad (5.4)$$

**2070**  $K_m$  is the Michaelis-Menten coefficient for Rubisco-limited photosynthesis, calcu-

**2071** lated as:

$$K_m = K_c \cdot \left(1 + \frac{O_i}{K_o}\right) \quad (5.5)$$

**2072** where  $O_i$  refers to leaf intercellular  $O_2$  concentrations, set to  $210 \mu\text{mol mol}^{-1}$ .

**2073** 5.2.7 *Proportion of leaf nitrogen allocated to photosynthesis and structure*

**2074** I used equations from Niinemets and Tenhunen (1997) to estimate the proportion

**2075** of leaf nitrogen content allocated to Rubisco, bioenergetics, and light harvesting

**2076** proteins. The proportion of leaf nitrogen allocated to Rubisco ( $\rho_{rubisco}$ ;  $\text{gN g}^{-1}$ )

**2077** was calculated as a function of  $V_{cmax25}$  and  $N_{area}$ :

$$\rho_{rubisco} = \frac{V_{cmax25} N_r}{V_{cr} N_{area}} \quad (5.6)$$

**2078** where  $N_r$  is the amount of nitrogen in Rubisco, set to 0.16 gN (gN in Rubisco) $^{-1}$   
**2079** and  $V_{cr}$  is the maximum rate of RuBP carboxylation per unit Rubisco protein,  
**2080** set to 20.5  $\mu\text{mol CO}_2$  (g Rubisco) $^{-1}$ . The proportion of leaf nitrogen allocated to  
**2081** bioenergetics ( $\rho_{bioe}$ ; gN gN $^{-1}$ ) was similarly calculated as a function of  $J_{max25}$  and  
**2082**  $N_{area}$ :

$$\rho_{bioe} = \frac{J_{max25} N_b}{J_{mc} N_{area}} \quad (5.7)$$

**2083** where  $N_b$  is the amount of nitrogen in cytochrome f, set to 0.12407 gN ( $\mu\text{mol}$   
**2084** cytochrome f) $^{-1}$  assuming a constant 1: 1: 1.2 cytochrome f: ferredoxin NADP  
**2085** reductase: coupling factor molar ratio (Evans and Seemann 1989; Niinemets and  
**2086** Tenhunen 1997), and  $J_{mc}$  is the capacity of electron transport per cytochrome f,  
**2087** set to 156  $\mu\text{mol electron}$  ( $\mu\text{mol cytochrome f}$ ) $^{-1}\text{s}^{-1}$ .

**2088** The proportion of leaf nitrogen allocated to light harvesting proteins ( $\rho_{light}$ ;  
**2089** gN gN $^{-1}$ ) was calculated as a function of  $Chl_{mass}$  and  $N_{mass}$ :

$$\rho_{light} = \frac{Chl_{mass}}{N_{mass} c_b} \quad (5.8)$$

**2090** where  $c_b$  is the stoichiometry of the light-harvesting chlorophyll complexes of  
**2091** photosystem II, set to 2.75 mmol chlorophyll (gN in chlorophyll) $^{-1}$ . I used the  
**2092**  $N_{mass}$  value of the focal leaf used to generate  $A_{net}/C_i$  curves instead of the leaf  
**2093** used to extract chlorophyll content, as the two leaves are from the same trifoliolate  
**2094** leaf set and are highly correlated (Figure D1).

**2095** The proportion of leaf nitrogen content allocated to photosynthetic tissue  
**2096** ( $\rho_{photo}$ ; gN gN $^{-1}$ ) was estimated as the sum of  $\rho_{rubisco}$ ,  $\rho_{bioe}$ , and  $\rho_{light}$ . Finally,  
**2097** the proportion of leaf nitrogen content allocated to structural tissue ( $\rho_{structure}$ ; gN

2098  $\text{gN}^{-1}$ ) was estimated as:

$$\rho_{structure} = \frac{N_{cw}}{N_{area}} \quad (5.9)$$

2099 where  $N_{cw}$  is the leaf nitrogen content allocated to cell walls ( $\text{gN m}^{-2}$ ), calculated

2100 as a function of  $M_{area}$  using an empirical equation from Onoda et al. (2017):

$$N_{cw} = 0.000355 * M_{area}^{1.39} \quad (5.10)$$

2101 5.2.8 *Whole plant traits*

2102 Seven weeks after experiment initiation and immediately following gas exchange

2103 measurements, I harvested all experimental individuals and separated biomass of

2104 each experimental individual into major organ types (leaves, stems, roots, and

2105 nodules when present). Fresh leaf area of all harvested leaves was measured using

2106 an LI-3100C (Li-COR Biosciences, Lincoln, Nebraska, USA). Total fresh leaf area

2107 ( $\text{cm}^2$ ) was calculated as the sum of all leaf areas, including the focal leaf used to

2108 collect gas exchange data and the focal leaf used to extract chlorophyll content. All

2109 harvested material was dried in an oven set to  $65^\circ\text{C}$  for at least 48 hours, weighed,

2110 and ground to homogeneity. Leaves and nodules were manually ground with a

2111 mortar and pestle, while stems and roots were ground using a Wiley mill (E3300

2112 Mini Mill; Eberbach Corp., MI, USA). Total dry biomass (g) was calculated as

2113 the sum of dry leaf (including focal leaf for both the  $A_{net}/C_i$  curve and leaf used

2114 to extract chlorophyll content), stem, root, and root nodule biomass. I quantified

2115 carbon and nitrogen content of each respective organ type through elemental

2116 combustion (Costech-4010, Costech, Inc., Valencia, CA, USA) using subsamples

2117 of ground and homogenized organ tissue.

2118 Following the approach explained in the first experimental chapter, I calcu-  
 2119 lated structural carbon costs to acquire nitrogen as the ratio of total belowground  
 2120 carbon biomass to whole plant nitrogen biomass ( $N_{\text{cost}}$ ; gC gN<sup>-1</sup>). Belowground  
 2121 carbon biomass ( $C_{\text{bg}}$ ; gC) was calculated as the sum of root carbon biomass  
 2122 and root nodule carbon biomass. Root carbon biomass and root nodule carbon  
 2123 biomass was calculated as the product of the organ biomass and the respective  
 2124 organ carbon content. Whole plant nitrogen biomass ( $N_{\text{wp}}$ ; gN) was similarly  
 2125 calculated as the sum of total leaf, stem, root, and root nodule nitrogen biomass,  
 2126 including the focal leaf used for  $A_{\text{net}}/C_i$  curve and chlorophyll extractions. Leaf,  
 2127 stem, root, and root nodule nitrogen biomass was calculated as the product of  
 2128 the organ biomass and the respective organ nitrogen content. This calculation  
 2129 only quantifies plant structural carbon costs to acquire nitrogen and does not  
 2130 include any additional costs of nitrogen acquisition associated with respiration,  
 2131 root exudation, or root turnover. An explicit explanation of the limitations for  
 2132 interpreting this calculation can be found in Perkowski et al. (2021) and Terrer  
 2133 et al. (2018).

2134 Finally, plant investments in nitrogen fixation were calculated as the ratio  
 2135 of root nodule biomass to root biomass, where increasing values indicate an in-  
 2136 crease in plant investments to nitrogen fixation (Dovrat et al. 2018; Dovrat et al.  
 2137 2020; Perkowski et al. 2021). I also calculated the percent of leaf nitrogen ac-  
 2138 quired from the atmosphere (% $N_{\text{dfa}}$ ; %) using leaf  $\delta^{15}\text{N}$  and the following equation  
 2139 from Andrews et al. (2011):

$$\%N_{\text{dfa}} = \frac{\delta^{15}N_{\text{reference}} - \delta^{15}N_{\text{sample}}}{\delta^{15}N_{\text{reference}} - B} \quad (5.11)$$

2140 where  $\delta^{15}\text{N}_{\text{reference}}$  refers to a reference plant that exclusively acquires nitrogen via  
2141 direct uptake,  $\delta^{15}\text{N}_{\text{sample}}$  refers to an individual's leaf  $\delta^{15}\text{N}$ , and B refers to individuals  
2142 that are entirely reliant on nitrogen fixation. Within each unique nitrogen  
2143 fertilization treatment-by-CO<sub>2</sub> treatment combination, I calculated the mean leaf  
2144  $\delta^{15}\text{N}$  for individuals growing in the non-inoculated treatment for  $\delta^{15}\text{N}_{\text{reference}}$ . Any  
2145 individuals with visual confirmation of root nodule formation were omitted from  
2146 the calculation of  $\delta^{15}\text{N}_{\text{reference}}$ . Following recommendations from Andrews et al.  
2147 (2011) I calculated B within each CO<sub>2</sub> treatment using the mean leaf  $\delta^{15}\text{N}$  of  
2148 inoculated individuals that received 0 ppm N. I did not calculate B within each  
2149 unique soil nitrogen-by-CO<sub>2</sub> treatment combination, as previous studies suggest  
2150 decreased reliance on nitrogen fixation with increasing soil nitrogen availability  
2151 (Perkowski et al. 2021).

2152 5.2.9 *Statistical analyses*

2153 Uninoculated pots that had substantial root nodule formation (nodule biomass:  
2154 root biomass values greater than 0.05 g g<sup>-1</sup>) were removed from all analyses, as  
2155 pots were assumed to have been colonized by symbiotic nitrogen-fixing bacteria  
2156 from outside sources. This decision resulted in the removal of sixteen pots from  
2157 analyses: two pots in the elevated CO<sub>2</sub> treatment that received 35 ppm N, three  
2158 pots in the elevated CO<sub>2</sub> treatment that received 70 ppm N, one pot in the elevated  
2159 CO<sub>2</sub> treatment that received 210 ppm N, two pots in the elevated CO<sub>2</sub> treatment  
2160 that received 280 ppm N, two pots in the ambient CO<sub>2</sub> treatment that received  
2161 0 ppm N, three pots in the ambient CO<sub>2</sub> treatment that received 70 ppm N, two  
2162 pots in the ambient CO<sub>2</sub> treatment that received 105 ppm N, and one pot in the

**2163** ambient CO<sub>2</sub> treatment that received 280 ppm N.

**2164** I built a series of linear mixed effects models to investigate the impacts of  
**2165** CO<sub>2</sub> concentration, soil nitrogen fertilization, and inoculation with *B. japonicum*  
**2166** on *G. max* gas exchange, tradeoffs between nitrogen and water use, whole plant  
**2167** growth, and investment in nitrogen fixation. All models included CO<sub>2</sub> treatment  
**2168** as a categorical fixed effect, inoculation treatment as a categorical fixed effect,  
**2169** soil nitrogen fertilization as a continuous fixed effect, with interaction terms be-  
**2170** tween all three fixed effects. All models also accounted for climatic difference  
**2171** between chambers across experiment iterations by including a random intercept  
**2172** term that nested starting chamber rack by CO<sub>2</sub> treatment. Models with this  
**2173** independent variable structure were created for each of the following dependent  
**2174** variables:  $N_{\text{area}}$ ,  $M_{\text{area}}$ ,  $N_{\text{mass}}$ ,  $Chl_{\text{area}}$ ,  $V_{\text{cmax25}}$ ,  $J_{\text{max25}}$ ,  $J_{\text{max25}}:V_{\text{cmax25}}$ ,  $R_{\text{d25}}$ ,  $g_{\text{sw}}$ ,  
**2175** stomatal limitation,  $\rho_{\text{rubisco}}$ ,  $\rho_{\text{bioe}}$ ,  $\rho_{\text{light}}$ ,  $\rho_{\text{photo}}$ ,  $\rho_{\text{structure}}$ , total biomass, total leaf  
**2176** area,  $N_{\text{cost}}$ ,  $C_{\text{bg}}$ ,  $N_{\text{wp}}$ , nodule biomass, the ratio of nodule biomass to root biomass,  
**2177** and % $N_{\text{dfa}}$ .

**2178** I used Shapiro-Wilk tests of normality to determine whether linear mixed  
**2179** effects models satisfied residual normality assumptions. If residual normality as-  
**2180** sumptions were not met (Shapiro-Wilk:  $p < 0.05$ ), then models were fit using de-  
**2181** pendent variables that were natural log transformed. If residual normality as-  
**2182** sumptions were still not met (Shapiro-Wilk:  $p < 0.05$ ), then models were fit using  
**2183** dependent variables that were square root transformed. All residual normality  
**2184** assumptions that did not originally satisfy residual normality assumptions were  
**2185** met with either a natural log or square root data transformation (Shapiro-Wilk:  
**2186**  $p > 0.05$  in all cases). Specifically, models for  $N_{\text{area}}$ ,  $N_{\text{mass}}$ ,  $Chl_{\text{area}}$ ,  $V_{\text{cmax25}}$ ,  $J_{\text{max25}}$ ,

2187  $J_{\max25}$ :  $V_{\text{cmax}25}$ ,  $R_{d25}$ ,  $g_{sw}$ , stomatal limitation,  $\rho_{\text{rubisco}}$ ,  $\rho_{\text{bioe}}$ ,  $\rho_{\text{light}}$ ,  $\rho_{\text{photo}}$ , total leaf  
2188 area,  $N_{\text{cost}}$  satisfied residual normality assumptions without data transformation.  
2189 Models for  $M_{\text{area}}$ ,  $\rho_{\text{structure}}$ ,  $C_{bg}$ , and total biomass satisfied residual normality as-  
2190 sumptions with a natural log data transformation, while models for  $N_{wp}$ , nodule  
2191 biomass, nodule biomass: root biomass, and  $\%N_{dfa}$  satisfied residual normality  
2192 assumptions with a square root data transformation.

2193 In all statistical models, I used the ‘lmer’ function in the ‘lme4’ R package  
2194 (Bates et al. 2015) to fit each model and the ‘Anova’ function in the ‘car’ R  
2195 package (Fox and Weisberg 2019) to calculate Type II Wald’s  $\chi^2$  and determine  
2196 the significance ( $\alpha=0.05$ ) of each fixed effect coefficient. I used the ‘emmeans’  
2197 R package (Lenth 2019) to conduct post-hoc comparisons using Tukey’s tests,  
2198 where degrees of freedom were approximated using the Kenward-Roger approach  
2199 (Kenward and Roger 1997). All analyses and plots were conducted in R version  
2200 4.2.0 (R Core Team 2021).

## 2201 5.3 Results

### 2202 5.3.1 Leaf nitrogen and chlorophyll content

2203 Elevated CO<sub>2</sub> reduced  $N_{\text{area}}$ ,  $N_{\text{mass}}$ , and  $Chl_{\text{area}}$  by 29%, 50%, and 31%, respec-  
2204 tively, and stimulated  $M_{\text{area}}$  by 44% ( $p<0.001$  in all cases; Table 5.1). An inter-  
2205 action between fertilization and CO<sub>2</sub> (CO<sub>2</sub>-by-fertilization interaction:  $p_{N_{\text{area}}}=$   
2206 0.017,  $p_{N_{\text{mass}}}<0.001$ ,  $p_{Chl_{\text{area}}}=0.083$ ; Table 5.1) indicated that the positive effect  
2207 of increasing fertilization on  $N_{\text{area}}$ ,  $N_{\text{mass}}$ , and  $Chl_{\text{area}}$  ( $p<0.001$  in all cases; Table  
2208 5.1) was stronger under ambient CO<sub>2</sub> (Tukey <sub>$N_{\text{area}}$</sub> :  $p=0.026$ ; Tukey <sub>$N_{\text{mass}}$</sub> :  $p<0.001$ ;  
2209 Tukey <sub>$Chl_{\text{area}}$</sub> :  $p=0.065$ ; Table 5.1; Figs. 5.1a, 5.1b, 5.1d). An interaction between

2210 fertilization and CO<sub>2</sub> on  $M_{\text{area}}$  (CO<sub>2</sub>-by-fertilization interaction:  $p=0.006$ ; Ta-  
2211 ble 5.1) indicated that the positive effect of increasing fertilization on  $M_{\text{area}}$  was  
2212 stronger under elevated CO<sub>2</sub> (Tukey:  $p=0.009$ ; Fig. 5.1c). Overall, interactions  
2213 between fertilization and CO<sub>2</sub> resulted in stronger reductions in  $N_{\text{area}}$ ,  $N_{\text{mass}}$ , and  
2214  $Chl_{\text{area}}$ , and a stronger stimulation in  $M_{\text{area}}$  under elevated CO<sub>2</sub> with increasing  
2215 fertilization.

2216 An interaction between inoculation and CO<sub>2</sub> on  $N_{\text{area}}$  (CO<sub>2</sub>-by-inoculation  
2217 interaction:  $p=0.030$ ; Table 5.1) indicated that the positive effect of inoculation  
2218 on  $N_{\text{area}}$  ( $p<0.001$ ; Table 5.1) was stronger under elevated CO<sub>2</sub> (45% increase;  
2219 Tukey:  $p<0.001$ ) than under ambient CO<sub>2</sub> (18% increase; Tukey:  $p<0.001$ ), a  
2220 result that increased the reduction in  $N_{\text{area}}$  in inoculated pots under elevated  
2221 CO<sub>2</sub>. Inoculation treatment did not modify the downregulation in  $N_{\text{mass}}$  (CO<sub>2</sub>-  
2222 by-inoculation interaction:  $p=0.148$ ; Table 5.1) and  $Chl_{\text{area}}$  ( $p = 0.147$ ; Table  
2223 5.1) or the stimulation in  $M_{\text{area}}$  ( $p=0.866$ ; Table 5.1) under elevated CO<sub>2</sub>. How-  
2224 ever, interactions between fertilization and inoculation on  $N_{\text{area}}$ ,  $N_{\text{mass}}$ ,  $M_{\text{area}}$ ,  
2225 and  $Chl_{\text{area}}$  (fertilization-by-inoculation interaction:  $p_{N_{\text{area}}}<0.001$ ,  $p_{N_{\text{mass}}}=0.001$ ,  
2226  $p_{M_{\text{area}}}=0.025$ ,  $p_{Chl_{\text{area}}}=0.083$ ; Table 5.1) indicated that the positive effect of in-  
2227 creasing fertilization on each trait was stronger in uninoculated pots (Tukey <sub>$N_{\text{area}}$</sub> :  
2228  $p<0.001$ ; Tukey <sub>$N_{\text{mass}}$</sub> :  $p=0.001$ ; Tukey <sub>$M_{\text{area}}$</sub> :  $p=0.031$ ; Tukey <sub>$Chl_{\text{area}}$</sub> :  $p<0.001$ ;  
2229 Figs. 5.1a-d).

**Table 5.1.** Effects of soil nitrogen fertilization, inoculation, and CO<sub>2</sub> treatments on leaf nitrogen content per unit leaf area ( $N_{\text{area}}$ ; gN m<sup>-2</sup>), leaf nitrogen content per unit leaf mass ( $N_{\text{mass}}$ , gN g<sup>-1</sup>), leaf mass per unit leaf area ( $M_{\text{area}}$ ; g m<sup>-2</sup>), and chlorophyll content per unit leaf area ( $Chl_{\text{area}}$ ; mmol m<sup>-2</sup>)<sup>\*</sup>

	$N_{\text{area}}$			$N_{\text{mass}}$			$M_{\text{area}}^a$			
	df	Coefficient	$\chi^2$	p	Coefficient	$\chi^2$	p	Coefficient	$\chi^2$	p
(Intercept)	-	1.10E+00	-	-	3.05E-02	-	-	3.64E+00	-	-
CO <sub>2</sub>	1	-5.67E-01	155.908	<0.001	-1.80E-02	272.362	<0.001	3.04E-01	151.319	<0.001
Inoculation (I)	1	6.21E-01	86.029	<0.001	7.54E-03	15.576	<0.001	1.81E-01	19.158	<0.001
Fertilization (N)	1	3.06E-03	316.408	<0.001	5.78E-05	106.659	<0.001	3.10E-04	21.440	<0.001
CO <sub>2</sub> *I	1	2.63E-01	4.729	0.030	3.96E-03	2.025	0.155	-3.37E-02	0.029	0.866
CO <sub>2</sub> *N	1	-3.68E-04	5.723	0.017	-2.85E-05	22.542	<0.001	2.80E-04	7.619	0.006
I*N	1	-1.36E-03	43.381	<0.001	-2.00E-05	11.137	0.001	-3.36E-04	5.022	0.025
CO <sub>2</sub> *I*N	1	-3.23E-04	0.489	0.484	-2.59E-06	0.041	0.839	1.15E-04	0.208	0.649
Chl <sub>area</sub>										
	df	Coefficient	$\chi^2$	p						
(Intercept)	-	2.13E-02	-	-						
CO <sub>2</sub>	1	-1.33E-02	69.233	<0.001						
Inoculation (I)	1	1.24E-01	136.341	<0.001						
Fertilization (N)	1	3.35E-04	163.111	<0.001						
CO <sub>2</sub> *I	1	-3.18E-02	2.102	0.147						
CO <sub>2</sub> *N	1	-8.79E-05	2.999	0.083						
I*N	1	-2.65E-04	75.769	<0.001						
CO <sub>2</sub> *I*N	1	7.68E-05	2.144	0.147						

2230 \*Significance determined using Type II Wald  $\chi^2$  tests ( $\alpha=0.05$ ). P-values less than 0.05 are in bold, while p-values  
 2231 between 0.05 and 0.1 are italicized. A superscript “a” is included after trait labels to indicate if models were fit with  
 2232 natural log transformed response variables. Key: df=degrees of freedom,  $\chi^2$ =Wald Type II chi-square test statistic.

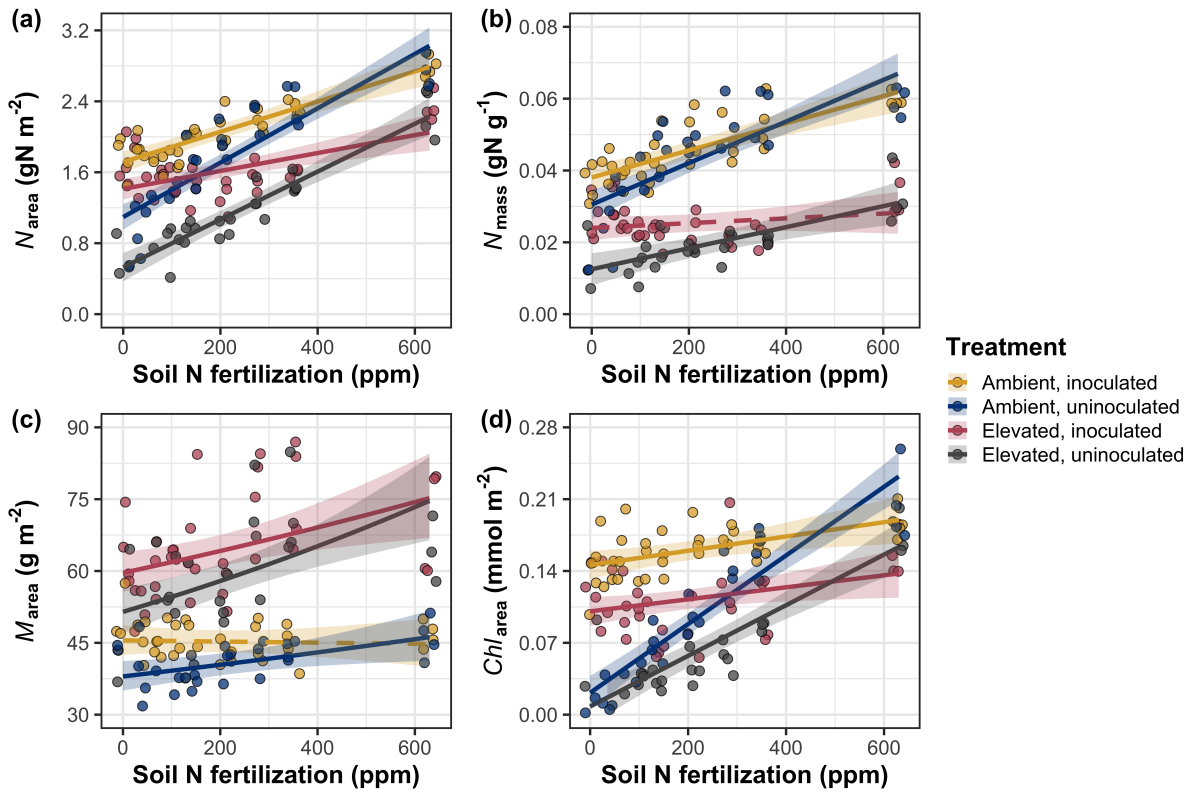


**Figure 5.1.** Effects of  $\text{CO}_2$ , fertilization, and inoculation on leaf nitrogen per unit leaf area (a), leaf nitrogen content (b), leaf mass per unit leaf area (c), and chlorophyll content per unit leaf area (d). Soil nitrogen fertilization is represented on the x-axis in all panels. Yellow points and trendlines indicate inoculated individuals grown under ambient  $\text{CO}_2$ , blue points and trendlines indicate uninoculated individuals grown under ambient  $\text{CO}_2$ , red points and trendlines indicate inoculated individuals grown under elevated  $\text{CO}_2$ , and grey points indicate uninoculated individuals grown under elevated  $\text{CO}_2$ . Solid trendlines indicate regression slopes that are different from zero ( $p < 0.05$ ), while dashed trendlines indicate slopes that are not distinguishable from zero ( $p > 0.05$ ).

**2233** 5.3.2 *Leaf biochemistry and stomatal conductance*

**2234** Elevated CO<sub>2</sub> resulted in plants with 16% lower  $V_{cmax25}$  ( $p<0.001$ ; Table 5.2) and  
**2235** 10% lower  $J_{max25}$  ( $p=0.014$ ; Table 5.2) compared to those grown under ambient  
**2236** CO<sub>2</sub>. However, CO<sub>2</sub> concentration did not influence  $R_{d25}$  ( $p=0.613$ ; Table 5.2;  
**2237** Fig. 5.2d). A relatively stronger downregulation in  $V_{cmax25}$  than  $J_{max25}$  resulted  
**2238** in an 8% stimulation in  $J_{max25}:V_{cmax25}$  under elevated CO<sub>2</sub> ( $p<0.001$ ; Table 5.2).  
**2239** The downregulatory effect of CO<sub>2</sub> on  $V_{cmax25}$  and  $J_{max25}$  was not modified across  
**2240** the fertilization gradient (CO<sub>2</sub>-by-fertilization interaction:  $p=0.185$  and  $p=0.389$   
**2241** for  $V_{cmax25}$  and  $J_{max25}$ , respectively; Table 5.2; Figs. 5.2a, 5.2b) or between in-  
**2242** oculation treatments (CO<sub>2</sub>-by-inoculation interaction:  $p=0.799$  and  $p=0.714$  for  
**2243**  $V_{cmax25}$  and  $J_{max25}$ , respectively; Table 5.2). However, a strong interaction between  
**2244** fertilization and inoculation (fertilization-by-inoculation interaction:  $p\leq0.001$  in  
**2245** all cases; Table 5.2) indicated that the positive effect of increasing fertilization  
**2246** on  $V_{cmax25}$  ( $p<0.001$ ; Table 5.2),  $J_{max25}$  ( $p<0.001$ ; Table 5.2), and  $R_{d25}$  ( $p=0.015$ ;  
**2247** Table 5.2) was only observed in uninoculated pots (Tukey:  $p\leq0.001$  in all cases;  
**2248** Figs. 5.2a, 5.2b). A stronger positive effect of increasing fertilization on  $V_{cmax25}$   
**2249** than  $J_{max25}$  resulted in a reduction in  $J_{max25}:V_{cmax25}$  with increasing fertilization  
**2250** ( $p<0.001$ ; Table 5.2), though this pattern was only observed in uninoculated pots  
**2251** (fertilization-by-inoculation interaction:  $p=0.002$ ; Table 5.2; Fig. 5.2c).  
  
**2252** Elevated CO<sub>2</sub> reduced stomatal conductance by 20% ( $p<0.001$ ; Table 5.2;  
**2253** Fig. 5.2e), but this downregulation did not influence stomatal limitation of pho-  
**2254** tosynthesis ( $p=0.355$ ; Table 5.2; Fig. 5.2f). As with  $V_{cmax25}$  and  $J_{max25}$ , the down-  
**2255** regulation of stomatal conductance due to elevated CO<sub>2</sub> was not modified across  
**2256** the fertilization gradient (CO<sub>2</sub>-by-fertilization interaction:  $p=0.141$ ; Table 5.2) or

**2257** between inoculation treatments ( $\text{CO}_2$ -by-inoculation interaction:  $p=0.179$ ; Table  
**2258** 5.2). Fertilization also did not modify the null effect of  $\text{CO}_2$  on stomatal limitation  
**2259** ( $\text{CO}_2$ -by-fertilization interaction:  $p=0.554$ ; Table 5.2), although an interaction  
**2260** between  $\text{CO}_2$  and inoculation ( $\text{CO}_2$ -by-inoculation interaction:  $p=0.043$ ; Table  
**2261** 5.2) indicated that inoculation increased stomatal limitation under ambient  $\text{CO}_2$   
**2262** (Tukey:  $p=0.021$ ), but not under elevated  $\text{CO}_2$  (Tukey:  $p>0.999$ ). An interaction  
**2263** between inoculation and fertilization on stomatal conductance (fertilization-by-  
**2264** inoculation interaction:  $p<0.001$ ; Table 5.2) indicated that increasing fertilization  
**2265** increased stomatal conductance in uninoculated pots (Tukey:  $p=0.003$ ) but de-  
**2266** creased stomatal conductance in inoculated pots (Tukey:  $p=0.021$ ). The similar  
**2267** in magnitude, but opposite direction, trend in the effect of increasing fertiliza-  
**2268** tion on stomatal conductance between inoculation treatments likely drove a null  
**2269** response of stomatal conductance to increasing fertilization ( $p=0.642$ ; Table 5.2).

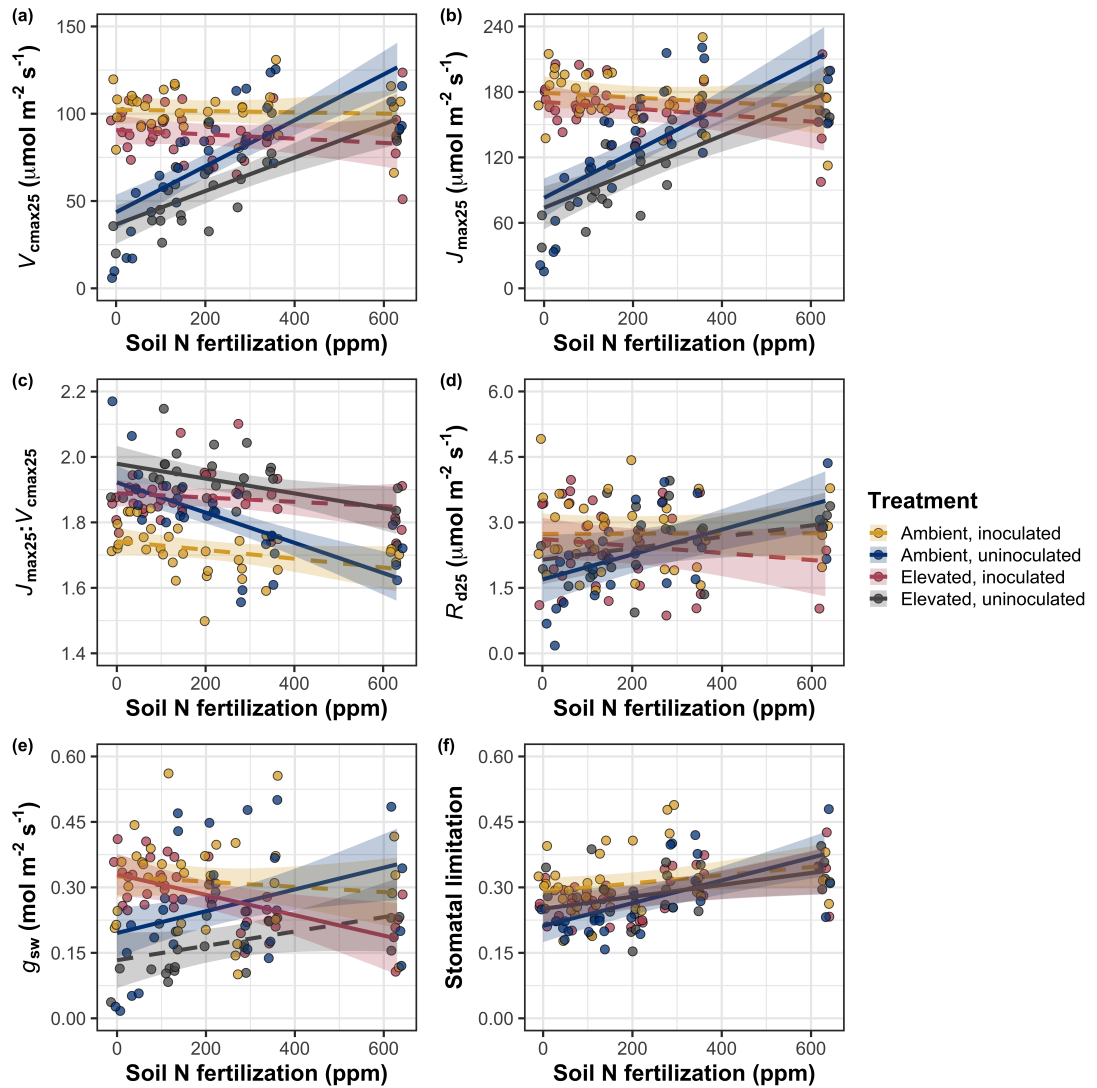
**Table 5.2.** Effects of soil nitrogen fertilization, inoculation, and CO<sub>2</sub> on the maximum rate of Rubisco carboxylation ( $V_{\text{cmax}25}$ ;  $\mu\text{mol m}^{-2} \text{s}^{-1}$ ), the maximum rate of RuBP regeneration ( $J_{\text{max}25}$ ;  $\mu\text{mol m}^{-2} \text{s}^{-1}$ ), dark respiration ( $R_{\text{d}25}$ ;  $\mu\text{mol m}^{-2} \text{s}^{-1}$ ), the ratio of the maximum rate of RuBP regeneration to the maximum rate of Rubisco carboxylation ( $J_{\text{max}25}:V_{\text{cmax}25}$ ; unitless), stomatal conductance ( $g_{\text{sw}}$ ;  $\text{mol m}^{-2} \text{s}^{-1}$ ), and stomatal limitation (unitless)\*

	$V_{\text{cmax}25}$			$J_{\text{max}25}$			$R_{\text{d}25}$			
	df	Coefficient	$\chi^2$	p	Coefficient	$\chi^2$	p	Coefficient	$\chi^2$	p
(Intercept)	-	4.36E+01	-	-	8.30E+01	-	-	1.69E+00	-	-
CO <sub>2</sub>	1	-7.05E+00	18.039	<0.001	-9.11E+00	6.042	0.014	4.53E-01	0.256	0.613
Inoculation (I)	1	5.87E+01	98.579	<0.001	9.62E+01	85.064	<0.001	1.04E+00	3.094	0.079
Fertilization (N)	1	1.32E-01	37.053	<0.001	2.09E-01	25.356	<0.001	2.86E-03	5.965	0.015
CO <sub>2</sub> *I	1	-4.65E+00	0.065	0.799	7.84E-01	0.667	0.414	-5.71E-01	2.563	0.109
CO <sub>2</sub> *N	1	-3.58E-02	1.758	0.185	-4.33E-02	0.742	0.389	-1.55E-03	2.675	0.102
I*N	1	-1.35E-01	60.394	<0.001	-2.30E-01	57.410	<0.001	-2.84E-03	12.083	0.001
CO <sub>2</sub> *I*N	1	2.73E-02	0.748	0.387	3.46E-02	0.377	0.539	7.21E-04	0.244	0.622

	$J_{\text{max}25}:V_{\text{cmax}25}$			$g_{\text{sw}}$			Stomatal limitation			
	df	Coefficient	$\chi^2$	p	Coefficient	$\chi^2$	p	Coefficient	$\chi^2$	p
(Intercept)	-	1.92E+00	-	-	1.95E-01	-	-	2.12E-01	-	-
CO <sub>2</sub>	1	5.71E-02	92.010	<0.001	-6.23E-02	9.718	0.002	3.91E-02	0.856	0.355
Inoculation (I)	1	-1.79E-01	27.768	<0.001	1.30E-01	22.351	<0.001	7.87E-02	4.582	0.032
Fertilization (N)	1	-4.61E-04	28.147	<0.001	2.50E-04	0.066	0.797	2.60E-04	32.218	<0.001
CO <sub>2</sub> *I	1	8.94E-02	2.916	0.088	6.69E-02	1.810	0.179	-7.84E-02	4.093	0.043
CO <sub>2</sub> *N	1	2.35E-04	3.210	0.073	-8.50E-05	2.165	0.141	-1.24E-04	0.350	0.554
I*N	1	3.27E-04	9.607	0.002	-3.09E-04	14.696	<0.001	-1.67E-04	2.547	0.110
CO <sub>2</sub> *I*N	1	-1.66E-04	1.102	0.294	-8.89E-05	0.234	0.629	1.67E-04	2.231	0.135

2270 \*Significance determined using Type II Wald  $\chi^2$  tests ( $\alpha=0.05$ ). P-values less than 0.05 are in bold, while p-values  
 2271 between 0.05 and 0.1 are italicized. Key: df=degrees of freedom;  $\chi^2$ =Wald Type II chi-square test statistic.



**Figure 5.2.** Effects of CO<sub>2</sub>, fertilization, and inoculation on maximum rate of Rubisco carboxylation (a), the maximum rate of RuBP regeneration (b), and the ratio of the maximum rate of RuBP regeneration to the maximum rate of Rubisco carboxylation leaf mass per unit leaf area (c), dark respiration (d), stomatal conductance (e), and stomatal limitation (f). Soil nitrogen fertilization is represented on the x-axis in all panels. Colored points and trendlines are as explained in Figure 5.1.

**2272** 5.3.3 *Leaf nitrogen allocation*

**2273** A relatively stronger downregulation in  $N_{\text{area}}$  than  $V_{\text{cmax}25}$  and  $J_{\text{max}25}$  resulted in  
**2274** an 20% and 29% respective stimulation in  $\rho_{\text{rubisco}}$  and  $\rho_{\text{bioe}}$  under elevated CO<sub>2</sub>  
**2275** ( $p<0.001$  in both cases; Table 5.3). There was no effect of CO<sub>2</sub> on  $\rho_{\text{light}}$  ( $p=0.700$ ;  
**2276** Table 5.3), but the stimulation in  $\rho_{\text{rubisco}}$  and  $\rho_{\text{bioe}}$  resulted in a 21% stimulation  
**2277** of  $\rho_{\text{photo}}$  under elevated CO<sub>2</sub> ( $p<0.001$ ; Table 5.3; Fig. 5.3a). The stimulation  
**2278** of  $\rho_{\text{rubisco}}$ ,  $\rho_{\text{bioe}}$ , and  $\rho_{\text{photo}}$  under elevated CO<sub>2</sub> was not modified across the fer-  
**2279** tilization gradient (CO<sub>2</sub>-by-fertilization interaction:  $p_{\text{rubisco}}=0.269$ ,  $p_{\text{bioe}}=0.298$ ,  
**2280**  $p_{\text{photo}}=0.281$ ; Table 5.3). A marginal interaction between inoculation and CO<sub>2</sub> on  
**2281**  $\rho_{\text{rubisco}}$  and  $\rho_{\text{photo}}$  (CO<sub>2</sub>-by-inoculation interaction:  $p_{\text{rubisco}}=0.057$ ,  $p_{\text{photo}}=0.055$ ;  
**2282** Table 5.3) indicated that the positive effect of inoculation on  $\rho_{\text{rubisco}}$  and  $\rho_{\text{photo}}$   
**2283** ( $p<0.001$  in both cases; Table 5.3) was only apparent under ambient CO<sub>2</sub> (Tukey:  
**2284**  $p<0.001$  in both cases). Inoculation did not modify the stimulation of  $\rho_{\text{bioe}}$  un-  
**2285** der elevated CO<sub>2</sub> (CO<sub>2</sub>-by-inoculation interaction:  $p=0.122$ ; Table 5.3) or the  
**2286** null effect of CO<sub>2</sub> on  $\rho_{\text{bioe}}$  (CO<sub>2</sub>-by-inoculation interaction:  $p=0.298$ ; Table 5.3).  
**2287** An interaction between fertilization and inoculation on  $\rho_{\text{rubisco}}$ ,  $\rho_{\text{bioe}}$ , and  $\rho_{\text{photo}}$   
**2288** (fertilization-by-inoculation interaction:  $p<0.001$  in all cases; Table 5.3) indicated  
**2289** that the negative effect of increasing fertilization on each trait ( $p<0.001$  in all  
**2290** cases; Table 5.3) was only observed in inoculated pots (Tukey:  $p<0.001$  in all  
**2291** cases). An additional interaction between fertilization and inoculation on  $\rho_{\text{light}}$   
**2292** (fertilization-by-inoculation interaction:  $p<0.001$ ; Table 5.3) indicated a negative  
**2293** effect of increasing fertilization on  $\rho_{\text{light}}$  in inoculated pots (Tukey:  $p=0.041$ ), but  
**2294** a positive effect of increasing fertilization in uninoculated pots (Tukey:  $p<0.001$ ).  
**2295** The stimulation in  $M_{\text{area}}$  under elevated CO<sub>2</sub> resulted in an 133% stimu-

2296 lation of  $\rho_{\text{structure}}$  ( $p<0.001$ ; Table 5.3; Fig 5.3b). An interaction between fertil-  
2297 ization and CO<sub>2</sub> (CO<sub>2</sub>-by-fertilization interaction:  $p=0.039$ ; Table 5.3) indicated  
2298 that the negative effect of increasing fertilization ( $p<0.001$ ; Table 5.3) on  $\rho_{\text{structure}}$   
2299 was marginally stronger under ambient CO<sub>2</sub> (Tukey:  $p=0.055$ ). A marginal inter-  
2300 action between inoculation and CO<sub>2</sub> (CO<sub>2</sub>-by-inoculation interaction:  $p=0.057$ ;  
2301 Table 5.3) indicated that the positive effect of inoculation on  $\rho_{\text{structure}}$  ( $p<0.001$ ;  
2302 Table 5.3) was only observed under elevated CO<sub>2</sub> (Tukey:  $p<0.001$ ), with no ap-  
2303 parent inoculation effect observed under ambient CO<sub>2</sub> (Tukey:  $p=0.513$ ). Finally,  
2304 an interaction between fertilization and inoculation (fertilization-by-inoculation  
2305 interaction:  $p<0.001$ ; Table 5.3) indicated that, while increasing fertilization in-  
2306 creased  $\rho_{\text{structure}}$  ( $p<0.001$ ; Table 5.3), this response was stronger in uninoculated  
2307 pots (Tukey:  $p=0.001$ ; Fig. 5.3b).

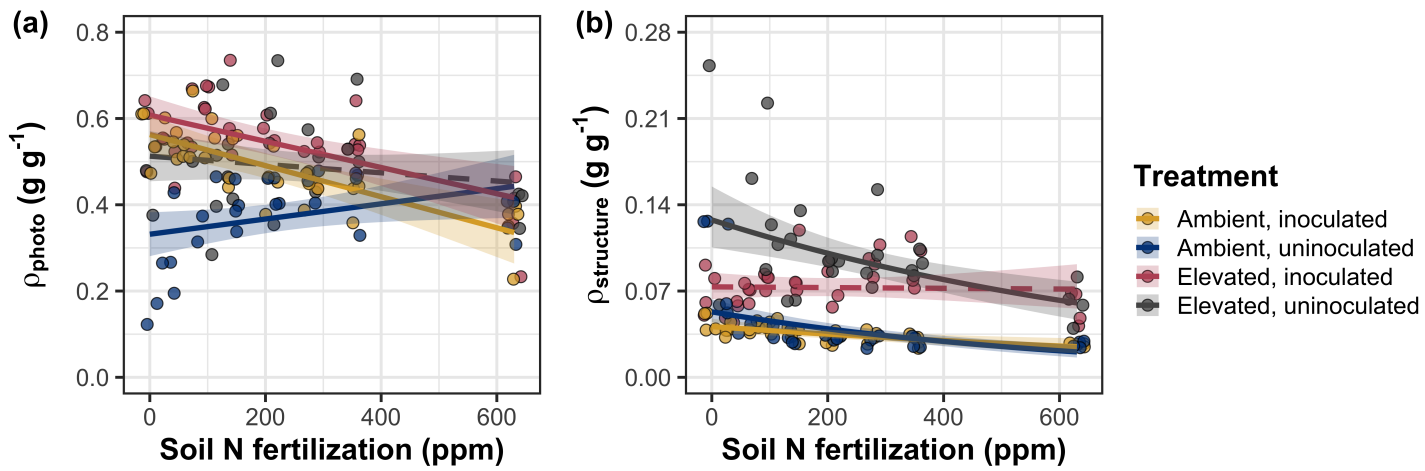
**Table 5.3.** Effects of soil nitrogen fertilization, inoculation, and CO<sub>2</sub> on the fraction of leaf nitrogen allocated to Rubisco ( $\rho_{\text{rubisco}}$ ; gN gN<sup>-1</sup>), bioenergetics ( $\rho_{\text{bioe}}$ ; gN gN<sup>-1</sup>), light harvesting proteins ( $\rho_{\text{light}}$ ; gN gN<sup>-1</sup>), photosynthesis ( $\rho_{\text{photo}}$ ; gN gN<sup>-1</sup>), and structure ( $\rho_{\text{structure}}$ ; gN gN<sup>-1</sup>)\*

	$\rho_{\text{rubisco}}$			$\rho_{\text{bioe}}$			$\rho_{\text{light}}$			
	df	Coefficient	$\chi^2$	p	Coefficient	$\chi^2$	p	Coefficient	$\chi^2$	p
(Intercept)	-	2.70E-01	-	-	5.26E-02	-	-	8.48E-03	-	-
CO <sub>2</sub>	1	1.42E-01	23.510	<0.001	3.00E-02	53.899	<0.001	2.03E-03	0.149	0.700
Inoculation (I)	1	1.83E-01	23.475	<0.001	2.80E-02	13.860	<0.001	2.04E-02	147.234	<0.001
Fertilization (N)	1	1.35E-04	16.609	<0.001	1.22E-05	26.827	<0.001	3.22E-05	19.378	<0.001
CO <sub>2</sub> *I	1	-1.07E-01	3.629	0.057	-1.67E-02	2.390	0.122	-5.33E-03	0.684	0.408
CO <sub>2</sub> *N	1	-2.16E-04	1.223	0.269	-3.59E-05	1.085	0.298	-7.01E-06	0.351	0.553
I*N	1	-4.26E-04	20.045	<0.001	-6.87E-05	15.458	<0.001	-4.37E-05	64.042	<0.001
CO <sub>2</sub> *I*N	1	2.50E-04	3.327	0.068	4.08E-05	2.651	0.103	1.74E-05	3.735	0.053

	$\rho_{\text{photo}}$			$\rho_{\text{structure}}^a$			
	df	Coefficient	$\chi^2$	p	Coefficient	$\chi^2$	p
(Intercept)	-	3.32E-01	-	-	-2.93E+00	-	-
CO <sub>2</sub>	1	1.81E-01	27.651	<0.001	8.77E-01	229.571	<0.001
Inoculation (I)	1	2.31E-01	26.238	<0.001	-2.55E-01	13.872	<0.001
Fertilization (N)	1	1.76E-04	15.899	<0.001	-1.51E-03	38.128	<0.001
CO <sub>2</sub> *I	1	-1.36E-01	3.671	0.055	-2.99E-01	3.622	0.057
CO <sub>2</sub> *N	1	-2.72E-04	1.163	0.281	3.14E-04	4.266	0.039
I*N	1	-5.37E-04	21.355	<0.001	7.00E-04	11.025	0.001
CO <sub>2</sub> *I*N	1	3.29E-04	4.009	0.045	4.52E-04	0.669	0.413

2308 \*Significance determined using Type II Wald  $\chi^2$  tests ( $\alpha=0.05$ ). P-values less than 0.05 are in bold, while p-values  
 2309 between 0.05 and 0.1 are italicized. A superscript “a” is included after trait labels to indicate if models were fit with  
 2310 natural log transformed response variable. Key: df=degrees of freedom;  $\chi^2$ =Wald Type II chi-square test statistic.



**Figure 5.3.** Effects of  $\text{CO}_2$ , fertilization, and inoculation on the relative fraction of leaf nitrogen allocated to photosynthesis (a) and the fraction of leaf nitrogen allocated to structure (b). Soil nitrogen fertilization is represented on the x-axis in both panels. Colored points and trendlines are as explained in Figure 5.1.

**2311** 5.3.4 *Whole plant traits*

**2312** Total leaf area and total biomass were 51% and 102% greater under elevated CO<sub>2</sub>,  
**2313** respectively ( $p<0.001$  in both cases; Table 5.4). The stimulation in total leaf area  
**2314** and total biomass under elevated CO<sub>2</sub> was enhanced by increasing fertilization  
**2315** (CO<sub>2</sub>-by-fertilization interaction:  $p<0.001$  in both cases; Table 5.4; Figs. 5.4a,  
**2316** 5.4b) but was not modified across inoculation treatments (CO<sub>2</sub>-by-inoculation  
**2317** interaction:  $p_{total\_leaf\_area}=0.151$ ,  $p_{total\_biomass}=0.472$ ; Table 5.4). The positive  
**2318** effect of increasing fertilization on total leaf area and total biomass was modified by  
**2319** inoculation treatment (fertilization-by-inoculation interaction:  $p<0.001$  in both  
**2320** cases; Table 5.4), indicating a stronger positive effect of increasing fertilization in  
**2321** uninoculated pots (Tukey:  $p_{total\_leaf\_area}=0.002$ ,  $p_{total\_biomass}=0.001$ , Figs. 5.4a,  
**2322** 5.4b).

**2323** A 62% stimulation in  $N_{cost}$  under elevated CO<sub>2</sub> was modified through a  
**2324** strong three-way interaction between CO<sub>2</sub>, fertilization, and inoculation (CO<sub>2</sub>-  
**2325** by-inoculation-by-fertilization interaction:  $p<0.001$ ; Table 5.4; Fig. 5.4). This  
**2326** interaction revealed a general negative effect of increasing fertilization on  $N_{cost}$   
**2327** ( $p<0.001$ ; Table 5.4) that was observed in all treatment combinations (Tukey:  
**2328**  $p<0.001$  in all cases) except for inoculated pots grown under elevated CO<sub>2</sub> (Tukey:  
**2329**  $p=0.779$ ; Fig. 5.4c). This response also resulted in stronger negative effects of in-  
**2330** creasing fertilization on  $N_{cost}$  in uninoculated pots grown under elevated CO<sub>2</sub> than  
**2331** uninoculated pots grown under ambient CO<sub>2</sub> (Tukey:  $p=0.001$ ) and inoculated  
**2332** pots grown under either ambient CO<sub>2</sub> (Tukey:  $p<0.001$ ) or elevated CO<sub>2</sub> (Tukey:  
**2333**  $p<0.001$ ), while uninoculated pots grown under ambient CO<sub>2</sub> had stronger nega-  
**2334** tive effects of increasing fertilization on  $N_{cost}$  than inoculated pots grown under

**2335** elevated CO<sub>2</sub> (Tukey:  $p=0.002$ ), but not inoculated pots grown under ambient  
**2336** CO<sub>2</sub> (Tukey:  $p=0.216$ ; Fig. 5.4). The reduction in  $N_{\text{cost}}$  with increasing fertiliza-  
**2337** tion and in uninoculated pots were driven by a stronger positive effect of increasing  
**2338** fertilization on  $N_{\text{wp}}$  (denominator of  $N_{\text{cost}}$ ) than  $C_{\text{bg}}$  (numerator of  $N_{\text{cost}}$ ), while  
**2339** the stimulation in  $N_{\text{cost}}$  under elevated CO<sub>2</sub> was driven by a stronger positive  
**2340** effect of elevated CO<sub>2</sub> on  $C_{\text{bg}}$  than  $N_{\text{wp}}$  (Table 5.4).

**Table 5.4.** Effects of CO<sub>2</sub>, fertilization, and inoculation on total leaf area (cm<sup>2</sup>), whole plant biomass (g), carbon costs to acquire nitrogen ( $N_{\text{cost}}$ ; gC gN<sup>-1</sup>), belowground carbon biomass ( $C_{\text{bg}}$ ; gC), and whole plant nitrogen biomass ( $N_{\text{wp}}$ ; gN)<sup>\*</sup>

Total leaf area				Total biomass <sup>b</sup>				$N_{\text{cost}}$				
	df	Coefficient	$\chi^2$		df	Coefficient	$\chi^2$		df	Coefficient	$\chi^2$	p
(Intercept)	-	8.78E+01	-	-		9.96E-01	-	-		8.67E+00	-	-
CO <sub>2</sub>	1	3.36E+01	69.291	<0.001		5.07E-01	131.477	<0.001		8.75E+00	88.189	<0.001
Inoculation (I)	1	1.88E+02	35.715	<0.001		7.96E-01	34.264	<0.001		-1.68E+00	136.343	<0.001
Fertilization (N)	1	9.35E-01	274.199	<0.001		3.14E-03	269.046	<0.001		-8.50E-03	80.501	<0.001
CO <sub>2</sub> *I	1	6.44E+01	2.064	0.151		-7.69E-02	0.518	0.472		-8.38E+00	85.237	<0.001
CO <sub>2</sub> *N	1	5.05E-01	18.655	<0.001		1.61E-03	16.877	<0.001		-9.17E-03	1.050	0.306
I*N	1	-3.84E-01	10.804	<b>0.001</b>		-1.45E-03	15.779	<0.001		4.20E-03	46.489	<0.001
CO <sub>2</sub> *I*N	1	-2.97E-03	<0.001	0.990		-1.14E-04	0.023	0.880		1.32E-02	18.125	<0.001
$C_{\text{bg}}^{\text{a}}$				$N_{\text{wp}}^{\text{b}}$								
	df	Coefficient	$\chi^2$	p		Coefficient	$\chi^2$	p		Coefficient	$\chi^2$	p
(Intercept)	-	-1.70E+00	-	-		1.24E-01	-	-		-	-	-
CO <sub>2</sub>	1	9.21E-01	84.134	<0.001		-3.41E-03	23.890	<0.001		-	-	-
Inoculation (I)	1	1.18E+00	41.030	<0.001		1.68E-01	134.460	<0.001		-	-	-
N fertilization (N)	1	3.38E-03	152.248	<0.001		6.69E-04	529.021	<0.001		-	-	-
CO <sub>2</sub> * I	1	-6.18E-01	8.965	<b>0.003</b>		3.68E-02	1.190	0.275		-	-	-
CO <sub>2</sub> * N	1	-3.66E-05	1.188	0.276		1.58E-04	5.915	<b>0.015</b>		-	-	-
I * N	1	-2.22E-03	22.648	<0.001		-3.20E-04	55.562	<0.001		-	-	-
CO <sub>2</sub> * I * N	1	8.09E-04	1.109	0.292		-7.54E-05	0.620	0.431		-	-	-

2341 \*Significance determined using Type II Wald  $\chi^2$  tests ( $\alpha=0.05$ ). P-values less than 0.05 are in bold. Superscripts  
 2342 included after trait labels indicate if models were fit with natural log (<sup>a</sup>) or square root (<sup>b</sup>) transformed response  
 2343 variables. Key: df=degrees of freedom;  $\chi^2$ =Wald Type II chi-square test statistic.

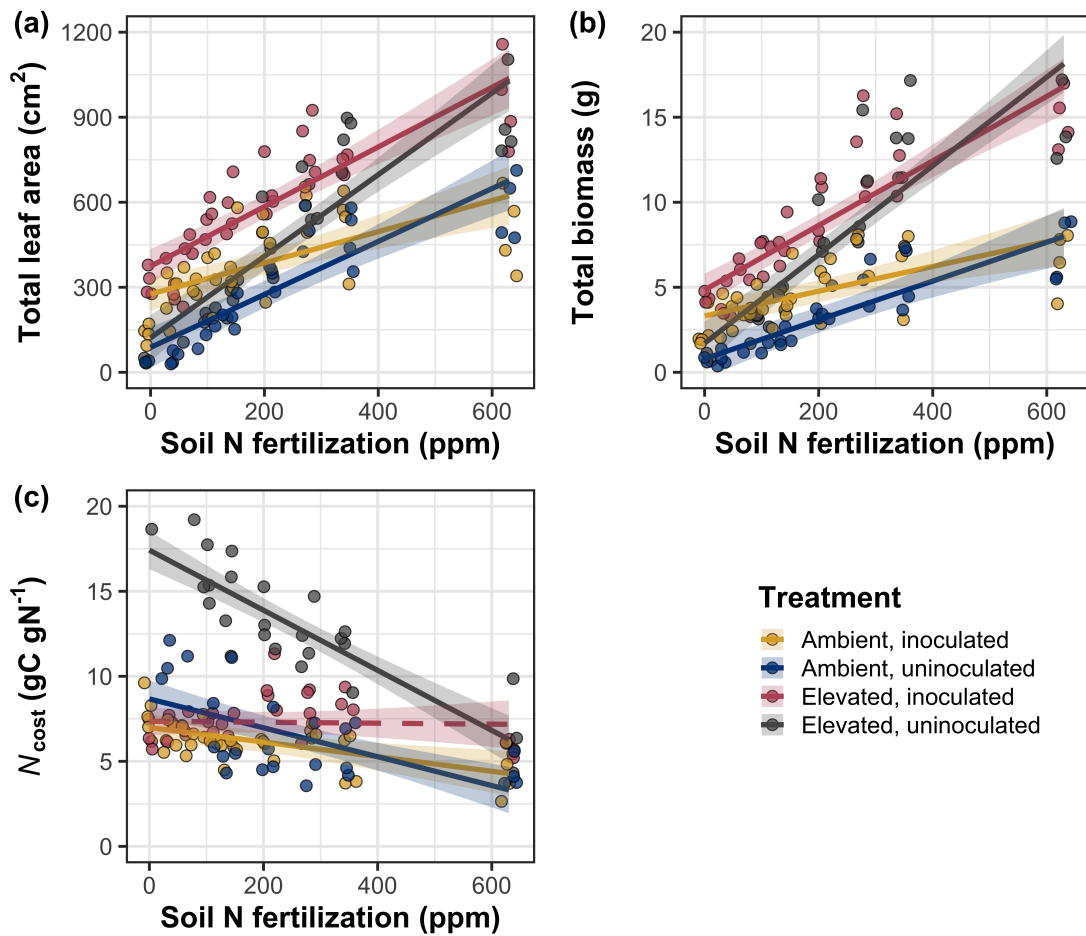


**Figure 5.4.** Effects of  $\text{CO}_2$ , fertilization, and inoculation on total leaf area (a), total biomass (b), and structural carbon costs to acquire nitrogen (c). Soil nitrogen fertilization is represented on the x-axis in all panels. Colored points and trendlines are as explained in Figure 5.1.

**2344** 5.3.5 *Nitrogen fixation*

**2345** Nodule biomass was stimulated by 30% under elevated CO<sub>2</sub> ( $p<0.001$ ; Table 5.5),  
**2346** a pattern that was modified across the fertilization gradient (CO<sub>2</sub>-by-fertilization  
**2347** interaction:  $p=0.479$ ; Table 5.5), but not between inoculation treatments (CO<sub>2</sub>-  
**2348** by-inoculation interaction:  $p=0.404$ ; Table 5.5). Specifically, the negative effect  
**2349** of increasing fertilization on nodule biomass ( $p<0.001$ ; Table 5.5) was stronger  
**2350** under elevated CO<sub>2</sub> (Tukey:  $p<0.001$ ; Fig. 5.5a). An interaction between fertil-  
**2351** ization and inoculation (fertilization-by-inoculation interaction:  $p<0.001$ ; Table  
**2352** 5.5) indicated a stronger negative effect of increasing fertilization in inoculated  
**2353** pots (Tukey:  $p<0.001$ ; Fig. 5.5a).

**2354** There was no effect of CO<sub>2</sub> on nodule: root biomass ( $p=0.767$ ; Table 5.5),  
**2355** although an interaction between CO<sub>2</sub> and inoculation (CO<sub>2</sub>-by-inoculation in-  
**2356** teraction:  $p<0.001$ ; Table 5.5) indicated that the positive effect of inoculation  
**2357** on nodule: root biomass ( $p<0.001$ ; Table 5.5) was stronger under ambient CO<sub>2</sub>  
**2358** (3129% increase; Tukey:  $p<0.001$ ) than elevated CO<sub>2</sub> (379% increase; Tukey:  
**2359**  $p<0.001$ ; Fig. 5.5b). The null effect of CO<sub>2</sub> on nodule: root biomass was consis-  
**2360** tently observed across the fertilization gradient (CO<sub>2</sub>-by-fertilization interaction:  
**2361**  $p=0.183$ ; Table 5.5; Fig. 5.5b). An interaction between fertilization and inocula-  
**2362** tion (fertilization-by-inoculation interaction:  $p<0.001$ ; Table 5.5) indicated that  
**2363** the negative effect of increasing fertilization on nodule: root biomass ( $p<0.001$ ;  
**2364** Table 5.5) was stronger in inoculated pots (Tukey:  $p<0.001$ ; Fig. 5.5b).

**2365** There was no effect of CO<sub>2</sub> on %N<sub>dfa</sub> ( $p=0.472$ ; Table 5.5), a pattern  
**2366** that was not modified by inoculation (CO<sub>2</sub>-by-inoculation interaction:  $p=0.156$ ;  
**2367** Table 5.5) or fertilization (CO<sub>2</sub>-by-fertilization interaction:  $p=0.099$ ; Table 5.5).

- 2368** An interaction between fertilization and inoculation (fertilization-by-inoculation  
**2369** interaction:  $p<0.001$ ; Table 5.5) indicated that the negative effect of increasing  
**2370** fertilization on  $\%N_{dfa}$  ( $p<0.001$ ; Table 5.5) was only observed in inoculated pots  
**2371** (Tukey:  $p<0.001$ ; Fig. 5.5c).

**Table 5.5.** Effects of CO<sub>2</sub>, fertilization, and inoculation on root nodule biomass (g), plant investments in symbiotic nitrogen fixation (unitless), and percent nitrogen fixed from the atmosphere (%N<sub>dfa</sub>; unitless)\*

	Root nodule biomass <sup>b</sup>			Root nodule: root biomass <sup>b</sup>			%N <sub>dfa</sub> <sup>b</sup>			
	df	Coefficient	$\chi^2$	p	Coefficient	$\chi^2$	p	Coefficient	$\chi^2$	p
(Intercept)	-	9.41E-03	-	-	1.33E-02	-	-	7.48E-01	-	-
CO <sub>2</sub>	1	1.20E-01	19.258	<b>&lt;0.001</b>	9.94E-02	0.087	0.768	-1.00E-01	0.518	0.472
Inoculation (I)	1	5.74E-01	755.020	<b>&lt;0.001</b>	5.40E-01	903.691	<b>&lt;0.001</b>	9.01E+00	955.570	<b>&lt;0.001</b>
Fertilization (N)	1	7.71E-06	84.376	<b>&lt;0.001</b>	-5.99E-06	258.099	<b>&lt;0.001</b>	3.64E-04	292.938	<b>&lt;0.001</b>
CO <sub>2</sub> *I	1	-4.68E-02	0.950	0.330	-1.38E-01	20.614	<b>&lt;0.001</b>	-1.44E-01	2.010	0.156
CO <sub>2</sub> *N	1	-1.59E-04	2.106	0.147	-1.73E-04	1.773	0.183	-6.21E-05	2.716	0.099
I*N	1	-5.82E-04	44.622	<b>&lt;0.001</b>	-7.45E-04	133.918	<b>&lt;0.001</b>	-1.58E-02	231.290	<b>&lt;0.001</b>
CO <sub>2</sub> *I*N	1	7.26E-05	0.196	0.658	1.76E-04	2.359	0.125	2.77E-03	2.119	0.145

2372 \*Significance determined using Type II Wald  $\chi^2$  tests ( $\alpha=0.05$ ). P-values less than 0.05 are in bold, while p-values  
 2373 between 0.05 and 0.1 are italicized. Superscript letters indicate model coefficients fit to square-root (<sup>b</sup>) transformed  
 2374 data. Key: df=degrees of freedom;  $\chi^2$ =Wald Type II chi-square test statistic.

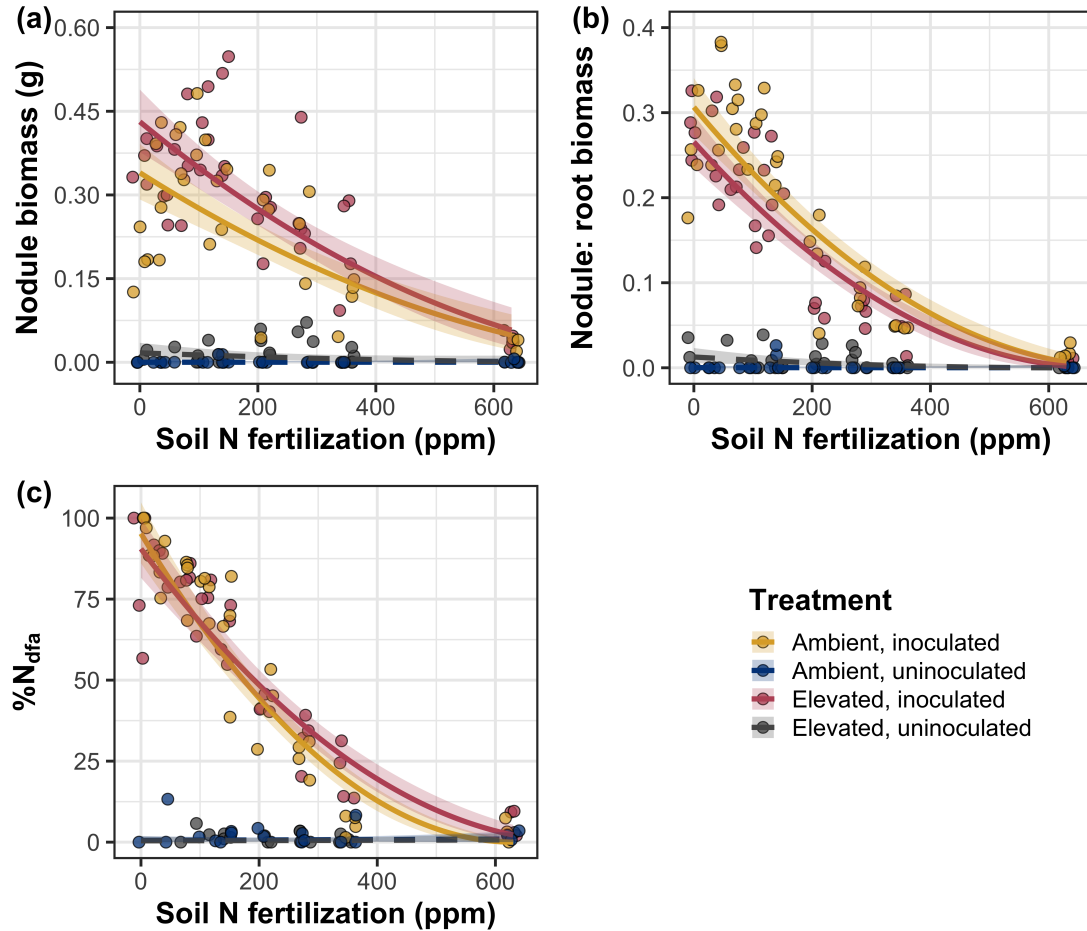


**Figure 5.5.** Effects of CO<sub>2</sub>, fertilization, and inoculation on nodule biomass (a), nodule biomass: root biomass (b), and percent nitrogen fixed from the atmosphere (c). Soil nitrogen fertilization is represented on the x-axis. Colored points and trendlines are as explained in Figure 5.1. Curvilinear trendlines occur as a result of back-transforming models where response variables received either a natural log or square root transformation prior to fitting.

**2375** 5.4 Discussion

**2376** In this study, I determined leaf and whole plant acclimation responses of 7-week *G.*  
**2377** *max* seedlings grown under two CO<sub>2</sub> concentrations, two inoculation treatments,  
**2378** and nine soil nitrogen fertilization treatments in a full-factorial growth chamber  
**2379** experiment. In support of hypotheses and patterns expected from theory, elevated  
**2380** CO<sub>2</sub> reduced  $N_{\text{area}}$ ,  $V_{\text{cmax25}}$ , and  $J_{\text{max25}}$ . The relatively stronger downregulation in  
**2381**  $V_{\text{cmax25}}$  than  $J_{\text{max25}}$  under elevated CO<sub>2</sub> resulted in a stimulation in  $J_{\text{max25}}:V_{\text{cmax25}}$   
**2382** under elevated CO<sub>2</sub>. The downregulation of  $V_{\text{cmax25}}$  and  $J_{\text{max25}}$  under elevated  
**2383** CO<sub>2</sub> was similar across fertilization and inoculation treatments, indicating that  
**2384** the CO<sub>2</sub> responses were not associated with nitrogen limitation. Interestingly,  
**2385** results indicate that elevated CO<sub>2</sub> increased the fraction of leaf nitrogen allocated  
**2386** to photosynthesis and structure, leading to a stimulation in nitrogen use efficiency  
**2387** under elevated CO<sub>2</sub> despite the apparent downregulation in  $N_{\text{area}}$ ,  $V_{\text{cmax25}}$ , and  
**2388**  $J_{\text{max25}}$ .

**2389** The downregulation in leaf photosynthetic processes under elevated CO<sub>2</sub>  
**2390** corresponded with a strong stimulation in total leaf area and total biomass. Strong  
**2391** stimulations in whole plant growth due to elevated CO<sub>2</sub> were generally enhanced  
**2392** with increasing fertilization and were negatively related to structural carbon costs  
**2393** to acquire nitrogen. Inoculation generally did not modify whole plant responses  
**2394** to elevated CO<sub>2</sub> across the fertilization gradient, likely due to a strong reduc-  
**2395** tion in root nodulation with increasing fertilization. However, strong positive  
**2396** effects of inoculation on whole plant growth were observed under low fertilization,  
**2397** consistent with hypotheses. Overall, observed leaf and whole plant acclimation  
**2398** responses to CO<sub>2</sub> support hypotheses and patterns expected from photosynthetic

2399 least-cost theory, showing that leaf acclimation responses to CO<sub>2</sub> were decoupled  
2400 from soil nitrogen availability and ability to acquire nitrogen via symbiotic nitro-  
2401 gen fixation. Instead, leaf and whole plant acclimation responses to CO<sub>2</sub> were  
2402 driven by optimal resource investment to photosynthetic capacity, where optimal  
2403 resource investment at the leaf level maximized nitrogen allocation to structures  
2404 that support whole plant growth.

2405 5.4.1 *Soil nitrogen fertilization has divergent effects on leaf and whole plant*  
2406 *acclimation responses to CO<sub>2</sub>*

2407 Elevated CO<sub>2</sub> reduced  $N_{\text{area}}$ ,  $V_{\text{cmax25}}$ ,  $J_{\text{max25}}$ , and stomatal conductance by 29%,  
2408 16%, 10%, and 20%, respectively. The larger downregulation of  $V_{\text{cmax25}}$  than  
2409  $J_{\text{max25}}$  led to an 8% stimulation in  $J_{\text{max25}}:V_{\text{cmax25}}$ , while the larger downregulation  
2410 of  $N_{\text{area}}$  than  $V_{\text{cmax25}}$  resulted in a 21% stimulation in the fraction of leaf nitro-  
2411 gen allocated to photosynthesis under elevated CO<sub>2</sub>. These acclimation responses  
2412 are directionally consistent with previous studies that have investigated or re-  
2413 viewed leaf acclimation responses to CO<sub>2</sub> (Drake et al. 1997; Makino et al. 1997;  
2414 Ainsworth et al. 2002; Ainsworth and Long 2005; Ainsworth and Rogers 2007;  
2415 Smith and Dukes 2013; Smith and Keenan 2020; Poorter et al. 2022), and fol-  
2416 low patterns expected from photosynthetic least-cost theory (Wright et al. 2003;  
2417 Prentice et al. 2014; Smith et al. 2019; Smith and Keenan 2020). Together, the  
2418 stimulation in  $J_{\text{max25}}:V_{\text{cmax25}}$  and the fraction of leaf nitrogen allocated to pho-  
2419 tosynthesis under elevated CO<sub>2</sub> provide strong support for the idea that leaves  
2420 were downregulating  $V_{\text{cmax25}}$  in response to elevated CO<sub>2</sub> in order to optimally co-  
2421 ordinate photosynthesis such that net photosynthesis rates approached becoming

**2422** equally co-limited by Rubisco carboxylation and RuBP regeneration (Chen et al.  
**2423** 1993; Maire et al. 2012) while optimizing resource use efficiency.

**2424** Increasing fertilization and inoculation induced strong positive effects on  
**2425**  $N_{\text{area}}$ ,  $V_{\text{cmax25}}$ ,  $J_{\text{max25}}$ . The general positive response of  $N_{\text{area}}$  to increasing fertiliza-  
**2426** tion and in inoculated pots was enhanced under ambient CO<sub>2</sub>, which, paired with  
**2427** the general downregulation of  $N_{\text{area}}$  under elevated CO<sub>2</sub>, resulted in a stronger  
**2428** downregulation of  $N_{\text{area}}$  under elevated CO<sub>2</sub> with increasing fertilization and in  
**2429** inoculated pots. These patterns suggest that  $N_{\text{area}}$  responses to CO<sub>2</sub> were at least  
**2430** partially dependent on soil nitrogen fertilization and nitrogen acquisition strat-  
**2431** egy. However, the general stimulation in the fraction of leaf nitrogen allocated to  
**2432** Rubisco, bioenergetics, or photosynthesis under elevated CO<sub>2</sub> was not modified  
**2433** across the fertilization gradient and was only marginally enhanced in inoculated  
**2434** pots. These patterns suggest that the increased downregulation of  $N_{\text{area}}$  under  
**2435** elevated CO<sub>2</sub> with increasing fertilization was not necessarily associated with a  
**2436** change in relative investment to photosynthetic tissue, providing another line of  
**2437** evidence suggesting that leaf acclimation responses to CO<sub>2</sub> are decoupled from  
**2438** changes in soil nitrogen availability.

**2439** Leaf acclimation responses to elevated CO<sub>2</sub> corresponded with a 62% and  
**2440** 100% stimulation in total leaf area and total biomass, respectively. The stimula-  
**2441** tion in total leaf area and total biomass under elevated CO<sub>2</sub> corresponded with  
**2442** generally larger structural carbon costs to acquire nitrogen, a pattern driven by  
**2443** a stimulation in belowground carbon biomass and reduction in whole plant ni-  
**2444** trogen biomass. This result suggests that elevated CO<sub>2</sub> reduces plant nitrogen  
**2445** uptake efficiency, which does not explain why plants grown under elevated CO<sub>2</sub>

2446 generally had higher biomass and total leaf area, unless growth stimulations un-  
2447 der elevated CO<sub>2</sub> were driven by reductions in per-tissue nitrogen demand (Dong  
2448 et al. 2022). Interestingly, strong negative effects of increasing fertilization on  
2449 structural carbon costs to acquire nitrogen, which were generally similar between  
2450 CO<sub>2</sub> concentrations, were driven by stronger increases in whole plant nitrogen  
2451 biomass than belowground carbon biomass. This response allowed plants to in-  
2452 crease nitrogen uptake efficiency with increasing fertilization, which could be the  
2453 mechanism that drove the enhanced growth stimulation under elevated CO<sub>2</sub> with  
2454 increasing fertilization.

2455 Interestingly, results indicate that the stimulation in total leaf area and  
2456 whole plant growth under elevated CO<sub>2</sub> was not modified by inoculation despite  
2457 an apparent general negative effect of inoculation on  $N_{cost}$ . This response could  
2458 have been due to strong negative effect of increasing fertilization on nodulation,  
2459 which may have caused the strong increase in the positive effect of elevated CO<sub>2</sub> on  
2460 whole plant growth with increasing fertilization to mask any increase in the posi-  
2461 tive effect of elevated CO<sub>2</sub> on whole plant growth due to inoculation. Reductions  
2462 in nodulation with increasing fertilization are commonly observed patterns that  
2463 have been inferred to be a response that allows species optimize nitrogen uptake  
2464 efficiency as costs to acquire nitrogen via direct uptake become more similar (Gib-  
2465 son and Harper 1985; Rastetter et al. 2001). In this study, pairwise comparisons  
2466 indicated strong positive effects of inoculation on total leaf area and total biomass  
2467 (158% increase in total leaf area, 119% increase in total biomass) under elevated  
2468 CO<sub>2</sub> at 0 ppm N ( $p < 0.05$  in both cases), but no observable inoculation effect on  
2469 total leaf area or total biomass under elevated CO<sub>2</sub> at 350 ppm N or 630 ppm N

2470 ( $p>0.05$  in both cases). While these responses did not generally differ from those  
2471 observed under ambient CO<sub>2</sub>, they do confirm the hypothesis that positive effects  
2472 of inoculation on whole plant growth responses to elevated CO<sub>2</sub> would decrease  
2473 with increasing fertilization.

2474 Combined, results reported here suggest that soil nitrogen availability plays  
2475 divergent roles in shaping leaf and whole plant acclimation responses to CO<sub>2</sub>. Leaf  
2476 acclimation responses were generally decoupled from fertilization, while whole  
2477 plant acclimation responses relied heavily on an increase in nitrogen uptake ef-  
2478 ficiency and consequent reduction in costs of acquiring nitrogen associated with  
2479 increasing fertilization. Whole plant responses to CO<sub>2</sub> indicated that fertilization  
2480 may play a more important role in determining whole plant acclimation responses  
2481 to CO<sub>2</sub> than nitrogen acquisition strategy, although any inoculation effect was  
2482 likely masked by the strong reduction in root nodulation with increasing fertil-  
2483 ization. These results suggest that plants acclimate to CO<sub>2</sub> in nitrogen-limited  
2484 systems by minimizing the number of optimally coordinated leaves, and that  
2485 downregulations in leaf nitrogen content under elevated CO<sub>2</sub> are not driven by  
2486 changes in soil nitrogen availability as has been previously implied.

2487 5.4.2 *Implications for future model development*

2488 Many terrestrial biosphere models predict photosynthetic capacity through plant  
2489 functional group-specific linear regressions between  $N_{\text{area}}$  and  $V_{\text{cmax}}$  (Rogers 2014;  
2490 Rogers et al. 2017), which assumes that leaf nitrogen-photosynthesis relation-  
2491 ships are constant across growing environments. These results build on previ-  
2492 ous work suggesting that leaf nitrogen-photosynthesis relationships dynamically  
2493 change across growing environments (Luo et al. 2021; Dong et al. 2022), showing

2494 that CO<sub>2</sub> concentration increases the fraction of leaf nitrogen content allocated to  
2495 photosynthesis independent of fertilization or acquisition strategy. Additionally,  
2496 increasing fertilization strongly decreased the fraction of leaf nitrogen allocated  
2497 to photosynthesis, a response that was largely determined by acquisition strategy.  
2498 Specifically, reductions in the fraction of leaf nitrogen allocated to photosynthesis  
2499 with increasing fertilization were only observed in inoculated pots that had less  
2500 finite access to nitrogen, suggesting that constant leaf nitrogen-photosynthesis  
2501 relationships may only be apparent in environments where nitrogen is limiting.  
2502 Terrestrial biosphere models that parameterize photosynthetic capacity through  
2503 linear relationships between  $N_{\text{area}}$  and  $V_{\text{cmax}}$  (Rogers 2014; Rogers et al. 2017) may  
2504 therefore be overestimating photosynthetic capacity in systems where nitrogen is  
2505 not as limiting. Such models are also not capable of detecting stimulations in the  
2506 fraction of leaf nitrogen allocated to photosynthesis with increasing CO<sub>2</sub> concen-  
2507 tration. The inability of models to predict these responses likely contributes to the  
2508 widespread divergence of model simulations under future environmental scenarios  
2509 (Friedlingstein et al. 2014; Davies-Barnard et al. 2020), and should therefore be  
2510 a target for resolving in future generations of terrestrial biosphere models.

2511 These results demonstrate that optimal resource investment to photosyn-  
2512 thetic capacity defines leaf acclimation responses to elevated CO<sub>2</sub>, and that these  
2513 responses were independent of fertilization or inoculation treatment. Current  
2514 model approaches for simulating photosynthetic responses to CO<sub>2</sub> generally invoke  
2515 patterns expected from progressive nitrogen limitation, where the downregulation  
2516 in  $N_{\text{area}}$ , and therefore photosynthetic capacity, due to elevated CO<sub>2</sub> is formu-  
2517 lated as a function of progressive reductions in soil nitrogen availability. Results

2518 reported here contradict this formulation, suggesting that the leaf acclimation re-  
2519 sponse is driven by optimal resource investment to photosynthetic capacity and  
2520 is independent of soil resource supply. Optimality models that leverage prin-  
2521 ciples from optimal coordination and photosynthetic least-cost theories (Wang  
2522 et al. 2017; Stocker et al. 2020; Scott and Smith 2022) are capable of capturing  
2523 such acclimation responses to CO<sub>2</sub> (Smith and Keenan 2020), suggesting that the  
2524 implementation of these models may improve the simulation of photosynthetic  
2525 processes in terrestrial biosphere models under increasing CO<sub>2</sub> concentrations.

2526 5.4.3 *Study limitations and future directions*

2527 There are two study limitations that must be addressed to contextualize patterns  
2528 observed in this study. First, restricting the volume of belowground substrate  
2529 via a potted experiment does not adequately replicate belowground environments  
2530 of natural systems, and therefore may modify effects of soil resource availability  
2531 and inoculation on plant nitrogen uptake. This limitation may be particularly  
2532 relevant if pot size limits whole plant growth (Poorter et al. 2012). I attempted  
2533 to minimize the extent of pot size limitation experienced in the first experimen-  
2534 tal chapter while accounting for the expected stimulation in whole plant growth  
2535 under elevated CO<sub>2</sub> by using 6-liter pots. Despite attempts to minimize growth  
2536 limitation imposed by pot volume, fertilization and CO<sub>2</sub> treatments increased the  
2537 biomass: pot volume ratio such that all treatment combinations to exceed 1 g L<sup>-1</sup>  
2538 biomass: pot volume under high fertilization (Table D3; Fig. D2). The 1 g L<sup>-1</sup>  
2539 biomass: pot volume recommendation from Poorter et al. (2012) was designated  
2540 to avoid growth limitation imposed by pot volume. However, if pot size limita-

2541 tion indeed limited whole plant growth, then structural carbon costs to acquire  
2542 nitrogen, belowground carbon biomass, whole plant nitrogen biomass, and whole  
2543 plant biomass should each exhibit strong saturation points with increasing fertil-  
2544 ization, which was not observed here. Importantly, leaf acclimation responses to  
2545 CO<sub>2</sub> observed in this study are consistent with findings reported in (Smith and  
2546 Keenan 2020), who used data from field manipulation experiments that did not  
2547 have any belowground space limitation.

2548 Second, this study evaluated leaf and whole plant responses to CO<sub>2</sub> in 7-  
2549 week seedlings. Given the long-term scale of the progressive nitrogen limitation  
2550 hypothesis, patterns observed here should be validated in longer-term nitrogen  
2551 manipulation experiments. Previous work in free air CO<sub>2</sub> enrichment experiments  
2552 show some support for patterns expected from the progressive nitrogen limitation  
2553 hypothesis (Reich et al. 2006; Norby et al. 2010), although results are not consis-  
2554 tent across experimental sites (Finzi et al. 2006; Moore et al. 2006; Liang et al.  
2555 2016). I found some support for patterns expected by the progressive nitrogen  
2556 limitation hypothesis, namely the increase in plant nitrogen uptake under elevated  
2557 CO<sub>2</sub> (Luo et al. 2004), though leaf acclimation responses to CO<sub>2</sub> were strongly  
2558 indicative of optimal resource investment to photosynthetic capacity as expected  
2559 from photosynthetic least-cost theory (Prentice et al. 2014; Smith et al. 2019;  
2560 Smith and Keenan 2020).

#### 2561 5.4.4 *Conclusions*

2562 This study provides strong evidence suggesting that leaf acclimation responses  
2563 to elevated CO<sub>2</sub> did not vary with soil nitrogen fertilization or ability to acquire  
2564 nitrogen through symbiotic nitrogen fixation. However, whole plant acclimation

**2565** responses to CO<sub>2</sub> were dependent on fertilization, where increasing fertilization  
**2566** increased the positive effect of whole plant growth under elevated CO<sub>2</sub>. Results  
**2567** also indicate that fertilization played a relatively more important role in modify-  
**2568** ing whole plant responses to CO<sub>2</sub> than inoculation with symbiotic nitrogen-fixing  
**2569** bacteria, perhaps due to a reduction in nodulation across the fertilization gra-  
**2570** dient. These patterns strongly support the hypothesis that leaf and whole plant  
**2571** acclimation responses are driven by optimal resource investment to photosynthetic  
**2572** capacity, and that leaf acclimation responses to CO<sub>2</sub> were not modified by changes  
**2573** in soil nitrogen availability. These results build on previous work suggesting that  
**2574** constant leaf nitrogen-photosynthesis relationships are dynamic and change across  
**2575** growing environments, calling the current formulation of photosynthetic processes  
**2576** used in many terrestrial biosphere models into question.

2577

## Chapter 6

2578

### Conclusions

2579 The experiments included in this dissertation test mechanisms that drive patterns  
2580 expected from photosynthetic least-cost theory across various edaphic and climatic  
2581 gradients. Specifically, I investigate environmental drivers of carbon costs to ac-  
2582 quire nitrogen, tradeoffs between nitrogen and water use, and plant acclimation  
2583 responses to CO<sub>2</sub>. These experiments provide important empirical data needed to  
2584 test assumptions made in optimality models that leverage photosynthetic least-  
2585 cost frameworks, and are among the first manipulative experiments to show sup-  
2586 port for patterns expected from theory. Below, I summarize main findings of each  
2587 chapter, synthesize common patterns observed across experiments, and conclude  
2588 with a few study ideas that I think will help refine our understanding of plant  
2589 nutrient acquisition and allocation responses to environmental change leveraging  
2590 patterns predicted by photosynthetic least-cost theory.

2591 In the first experimental chapter, I quantified carbon costs to acquire ni-  
2592 trogen in a species capable of forming associations with symbiotic nitrogen-fixing  
2593 bacteria (*Glycine max*) and a species not capable of forming such associations  
2594 (*Gossypium hirsutum*) grown under four soil nitrogen fertilization treatments and  
2595 four light availability treatments in a full factorial greenhouse experiment. Sup-  
2596 porting hypotheses, increasing light availability increased carbon costs to acquire  
2597 nitrogen in both species due to a larger increase in belowground carbon biomass  
2598 than whole plant nitrogen biomass. In further support of hypotheses, increasing  
2599 fertilization decreased carbon costs to acquire nitrogen due to a larger increase in

2600 whole plant nitrogen biomass than belowground carbon biomass. Root nodulation  
2601 data indicated that *G. max* shifted relative carbon allocation from nitrogen fixa-  
2602 tion to direct uptake with increasing fertilization, which may explain the reduced  
2603 responsiveness of *G. max* carbon costs to acquire nitrogen across the fertilization  
2604 gradient.

2605 Despite evidence that reductions in the response of *G. max* carbon costs  
2606 to acquire nitrogen to increasing fertilization may have been driven by shifts away  
2607 from nitrogen fixation with increasing fertilization, I urge caution in assigning  
2608 causality to the differential response of carbon costs to acquire nitrogen between  
2609 species. This is because *G. max* and *G. hirsutum* are not phylogenetically related  
2610 and have different life histories. Differences in life history between the two species  
2611 limit my ability to assess whether reductions in the negative effect of increasing  
2612 fertilization on carbon costs to acquire nitrogen in *G. max* were driven by shifts  
2613 to direct uptake with increasing fertilization. However, these patterns were later  
2614 confirmed in the fourth experimental chapter, where similar weaker negative ef-  
2615 fects of increasing fertilization on carbon costs to acquire nitrogen were observed  
2616 in *G. max* that were inoculated with symbiotic nitrogen-fixing bacteria compared  
2617 to *G. max* that were left uninoculated across a similar soil nitrogen fertilization  
2618 gradient.

2619 In the second experimental chapter, I assessed whether changes in soil  
2620 nitrogen availability or soil pH drove changes in nitrogen-water use tradeoffs pre-  
2621 dicted by photosynthetic least-cost theory. I measured leaf traits of mature upper  
2622 canopy deciduous trees growing in a nine-year nitrogen-by-sulfur field manipula-  
2623 tion experiment, where experimental sulfur additions were added with intent to

2624 acidify plots. Following patterns expected from the theory, increasing soil nitrogen  
2625 availability was associated with increased leaf nitrogen content, but not net photo-  
2626 tosynthesis, resulting in an increase in photosynthetic nitrogen use efficiency. In  
2627 further support of theory, increasing soil nitrogen availability exhibited slight, but  
2628 nonsignificant, decreases in leaf  $C_i:C_a$  and increases in measures of photosynthetic  
2629 capacity. Perhaps the strongest evidence for the theory was a strong negative  
2630 relationship between leaf nitrogen content and leaf  $C_i:C_a$ , of which increased with  
2631 increasing soil nitrogen availability through a stronger increase in leaf nitrogen  
2632 content than leaf  $C_i:C_a$ .

2633 I found no effect of soil pH on nitrogen-water use tradeoffs aside from a  
2634 marginal reduction in net photosynthesis rates that marginally reduced photosyn-  
2635 thetic nitrogen use efficiency with increasing soil pH. Directionally, reductions in  
2636 photosynthetic nitrogen use efficiency with increasing soil pH were expected per  
2637 theory; however, this response was driven by no change in leaf nitrogen content  
2638 and a reduction in net photosynthesis. Theory predicts that these tradeoffs should  
2639 be driven by no change in net photosynthesis and an increase in leaf nitrogen con-  
2640 tent. The general null leaf response to changing soil pH may have been due to  
2641 experimental treatments directly increased soil nitrogen availability and affected  
2642 soil pH in opposite patterns, suggesting that soil nitrogen availability may be more  
2643 important in dictating nitrogen-water use tradeoffs than soil pH per se.

2644 In the third experimental chapter, I quantified variance in leaf nitrogen  
2645 content across a precipitation and soil resource availability gradient in Texan  
2646 grasslands. Specifically, I measured area-based leaf nitrogen content, components  
2647 of area-based leaf nitrogen content (leaf mass per unit leaf area, leaf nitrogen per

**2648** unit dry biomass), leaf  $C_i:C_a$ , and the unit cost of acquiring nitrogen relative to  
**2649** water in 520 individuals comprising 57 species. I found that variance in area-  
**2650** based leaf nitrogen content was positively associated with increasing soil nitrogen  
**2651** availability, soil moisture, vapor pressure deficit, and was negatively related to  
**2652** increasing leaf  $C_i:C_a$ . Following patterns expected from theory, a path analysis  
**2653** revealed that the positive soil nitrogen-leaf nitrogen relationship was driven by a  
**2654** positive relationship between soil nitrogen availability and the unit cost of acquir-  
**2655** ing and using nitrogen relative to water, a positive relationship between the unit  
**2656** cost of acquiring and using nitrogen relative to water, and negative relationship  
**2657** between leaf  $C_i:C_a$  and leaf mass per unit leaf area. Interestingly, there was no  
**2658** effect of  $C_i:C_a$  on leaf nitrogen content per unit dry biomass, indicating that vari-  
**2659** ance in area-based leaf nitrogen content across the environmental gradient was  
**2660** driven by a change in leaf morphology and not leaf chemistry.

**2661** In the fourth experimental chapter, I quantified leaf and whole plant accli-  
**2662** mation responses in *G. max* grown under two atmospheric CO<sub>2</sub> levels, with and  
**2663** without inoculation with *Bradyrhizobium japonicum*, and across nine nitrogen fer-  
**2664** tilization treatments in a full factorial growth chamber experiment. I found strong  
**2665** evidence that leaf nitrogen content,  $V_{cmax}$ , and  $J_{max}$  were each downregulated un-  
**2666** der elevated CO<sub>2</sub>. A stronger downregulation in  $V_{cmax}$  than  $J_{max}$  and stronger  
**2667** downregulation in leaf nitrogen content than  $V_{cmax}$  or  $J_{max}$  provided strong sup-  
**2668** port suggesting that leaves were acclimating to elevated CO<sub>2</sub> by optimizing leaf  
**2669** photosynthetic resource use efficiency to achieve optimal coordination. In striking  
**2670** support of my hypotheses, I find strong evidence suggesting that leaf acclimation  
**2671** responses to elevated CO<sub>2</sub> were decoupled from soil nitrogen fertilization and in-

**2672** oculation treatment, despite apparent strong increases in leaf nitrogen content,  
**2673**  $V_{\text{cmax}}$ , and  $J_{\text{max}}$  with increasing fertilization and in inoculated pots. These find-  
**2674** ings contrast the current formulation of photosynthetic processes in terrestrial  
**2675** biosphere models, where many models simulate downregulations in leaf nitrogen  
**2676** content under elevated CO<sub>2</sub> as a function of progressive nitrogen limitation.

**2677** There are currently two iterations of optimality models that employ the  
**2678** use of patterns expected from photosynthetic least-cost theory, one for C<sub>3</sub> species  
**2679** (Wang et al. 2017; Smith et al. 2019; Stocker et al. 2020) and one more recently  
**2680** developed for C<sub>4</sub> species (Scott and Smith 2022). In both model variants, costs  
**2681** to acquire and use nitrogen relative to water are held constant using a global  
**2682** dataset of δ<sup>13</sup>C (Cornwell et al. 2018). Throughout experiments, I show strong  
**2683** evidence suggesting that costs to acquire and use nitrogen are dynamic and vary  
**2684** predictably across environmental gradients, and that changes in these costs scale  
**2685** to alter leaf nitrogen-water use tradeoffs and acclimation responses to changing  
**2686** environments in ways predicted through photosynthetic least-cost theory. Thus,  
**2687** while optimality model simulations show good agreement with measured data  
**2688** (Smith et al. 2019; Stocker et al. 2020), such models may not be capturing an  
**2689** important source of variability in leaf nitrogen-water use tradeoffs by holding costs  
**2690** of resource use constant across environmental gradients.

**2691** First principles of photosynthetic least-cost theory suggest that, in a given  
**2692** environment, plants optimize photosynthesis rates by sacrificing inefficient use of  
**2693** a relatively more abundant (and less costly to acquire) resource for more efficient  
**2694** use of a relatively less abundant (and more costly to acquire) resource. Through-  
**2695** out experimental chapters, I show strong support for these patterns across ex-

2696 periments, where increasing soil nitrogen fertilization generally decreased the cost  
2697 of acquiring nitrogen relative to water, a pattern that scaled to influence leaf  
2698 nitrogen-water use tradeoffs. I did not find evidence to suggest that soil moisture  
2699 influenced nitrogen-water use tradeoffs, though this was due to strong covariation  
2700 between soil moisture and soil nitrogen availability. Overall, findings across exper-  
2701 iments provide empirical validation of photosynthetic least-cost theory needed to  
2702 further develop optimality models and eventually implement such models in ter-  
2703 restrial biosphere model products. Many terrestrial biosphere model products do  
2704 not include robust frameworks for simulating acclimation responses to changing  
2705 environmental conditions, and empirical findings shown here provide some support  
2706 that optimality models that leverage photosynthetic least-cost theory predictions  
2707 may improve the ability of terrestrial biosphere models to accurately simulate  
2708 photosynthetic processes.

2709       Many terrestrial biosphere models predict photosynthetic capacity through  
2710 plant functional group-specific linear regressions between area-based leaf nitrogen  
2711 content and  $V_{cmax}$  (Rogers 2014; Rogers et al. 2017), which assumes that leaf  
2712 nitrogen-photosynthesis relationships are constant across growing environments.  
2713 I found constant leaf nitrogen-photosynthesis relationships with increasing soil ni-  
2714 trogen availability in the nitrogen-by-sulfur field manipulation experiment. How-  
2715 ever, results from the CO<sub>2</sub>-by-nitrogen-by-inoculation manipulation experiment  
2716 indicated that leaf nitrogen-photosynthesis responses to soil nitrogen availability  
2717 were dependent on whether nitrogen was limiting. Further investigation regard-  
2718 ing the effect of soil nitrogen availability in modifying leaf nitrogen-photosynthesis  
2719 relationships is warranted to better understand the generality of leaf nitrogen pho-

**2720** tosynthesis relationships across environmental gradients. However, findings from  
**2721** these experiments suggest that representing photosynthetic processes through pos-  
**2722** itive relationships between soil nitrogen availability, leaf nitrogen, and photosyn-  
**2723** thetic capacity are likely contributing to erroneous errors in model simulations and  
**2724** may explain the high degree of divergence in simulated processes across terrestrial  
**2725** biosphere models (Friedlingstein et al. 2014; Davies-Barnard et al. 2020).

**2726** The experiments included in this dissertation have provided a strong foun-  
**2727** dation for me to continue growing as a plant physiological ecologist. I envision  
**2728** five primary avenues for future research that build on the work presented here,  
**2729** which are briefly summarized below:

- 2730** 1. Manipulative and environmental gradient experiments included here were  
**2731** designed to provide empirical data needed to test photosynthetic least-cost  
**2732** theory assumptions. While these results show promising patterns for pat-  
**2733** terns expected from photosynthetic least-cost theory, they do not necessarily  
**2734** address whether these patterns follow those simulated by optimality models  
**2735** that leverage photosynthetic least-cost principles. Thus, a clear future di-  
**2736** rection of these experiments would be to conduct model-data comparisons  
**2737** using data collected here (or similar experiments) to compare against opti-  
**2738** mality model simulations.
  
- 2739** 2. Experiments included here explicitly quantify effects of symbiotic nitrogen  
**2740** fixation on carbon costs to acquire nitrogen, nitrogen-water use tradeoffs,  
**2741** and leaf nitrogen-photosynthesis relationships. However, carbon costs to ac-  
**2742** quire nitrogen also vary in species that associate with different mycorrhizal  
**2743** types (Brzostek et al. 2014; Terrer et al. 2018), and dominant mycorrhizal

2744 type in an ecosystem has been shown to determine net biogeochemical cycle  
2745 dynamics in deciduous forests of the northeastern United States (Phillips  
2746 et al. 2013). Thus, future work should consider conducting similar experi-  
2747 ments while manipulating mycorrhizal association to better understand how  
2748 microbial symbioses modify leaf and whole plant acclimation responses to  
2749 changing environments.

2750 3. Recent work indicates a high degree of variance in symbiotic nitrogen fixa-  
2751 tion rates across terrestrial biosphere models (Meyerholt et al. 2016; Davies-  
2752 Barnard et al. 2020), perhaps due to nitrogen fixation rates that are im-  
2753 plemented across terrestrial biosphere models as a function of temperature  
2754 (Houlton et al. 2008). While energetic costs of nitrogen fixation are de-  
2755 pendent on temperature, I show that structural carbon costs to acquire  
2756 nitrogen via symbiotic nitrogen fixation are driven by factors that influence  
2757 demand to acquire nitrogen (i.e. CO<sub>2</sub>, light) and are modified by soil ni-  
2758 trogen supply. The light-by-nitrogen greenhouse experiment was published  
2759 in *Journal of Experimental Botany*, and a reviewer encouraged future work  
2760 to include a model-data comparison comparing structural carbon costs to  
2761 acquire nitrogen measured in the experiment to carbon costs to acquire ni-  
2762 trogen simulated by the FUN biogeochemical model (Fisher et al. 2010;  
2763 Brzostek et al. 2014; Allen et al. 2020). Conveniently, FUN calculates car-  
2764 bon costs to acquire nitrogen following the same calculation used in the first  
2765 and fourth experimental chapter. Conducting such a model-data comparison  
2766 would be a useful step toward identifying biases in the FUN biogeochemi-  
2767 cal model, which is currently coupled to several terrestrial biosphere models

2768 (Clark et al. 2011; Shi et al. 2016; Lawrence et al. 2019; Davies-Barnard  
2769 et al. 2020).

2770 4. Carbon costs to acquire nitrogen relative to water were quantified at the  
2771 leaf level as a function of  $\delta^{13}\text{C}$  and vapor pressure deficit, while structural  
2772 carbon costs to acquire nitrogen were quantified at the whole plant level  
2773 as the ratio of belowground carbon allocation per unit whole plant nitro-  
2774 gen biomass. As increasing soil nitrogen availability decreases both leaf and  
2775 whole plant estimates of costs to acquire and use nitrogen, one might expect  
2776 leaf and whole plant carbon cost to acquire nitrogen estimates to covary. Fu-  
2777 ture work should consider investigating if leaf and whole plant estimates of  
2778 carbon costs to acquire nitrogen covary and evaluate whether environmental  
2779 conditions (or species acquisition strategy) modifies any of this possible co-  
2780 variance. Strong covariance between leaf and whole plant costs of nitrogen  
2781 acquisition could be a possible avenue to implement frameworks for allowing  
2782 costs of nitrogen acquisition to vary in optimality models, as the FUN model  
2783 calculates carbon costs of nitrogen acquisition at the whole plant level.

2784 5. While experiments included here target effects of soil nitrogen availability  
2785 on carbon costs to acquire nitrogen and associated leaf nitrogen-water use  
2786 tradeoffs, photosynthetic least-cost theory predicts that plants acclimate  
2787 their photosynthetic processes by minimizing the summed cost of nutrient  
2788 (not just nitrogen) and water use. Therefore, the theory would predict  
2789 similar leaf acclimation responses across soil phosphorus or other nutrient  
2790 availability gradients. Recent iterations of the FUN biogeochemical cycle  
2791 includes a framework for determining the carbon and nitrogen cost of ac-

**2792** quiring and using phosphorus, which similarly varies in species with different  
**2793** nutrient acquisition strategies (Allen et al. 2020). The implementation of  
**2794** this model in a terrestrial biosphere model (E3SM) was also recently shown  
**2795** to improve model performance of ecosystem nutrient limitation (Braghieri  
**2796** et al. 2022). As nitrogen and phosphorus commonly co-limit leaf photo-  
**2797** synthesis and primary productivity, extending experiments reported here to  
**2798** investigate carbon and nitrogen costs of phosphorus use, and whether these  
**2799** patterns scale to leaf nutrient-water use tradeoffs would be a useful next  
**2800** step in understanding extensions and limitations of photosynthetic least-  
**2801** cost theory.

**2802** The experiments included in this dissertation and the proposed experiments sum-  
**2803** marized above provide a snapshot view of the things that I have learned through-  
**2804** out my time as a graduate student. I am excited to continue learning and growing  
**2805** as a plant ecophysiologicalist, ecologist, and scientist, and look forward to continuing  
**2806** along my journey of investigating nutrient acquisition and allocation responses to  
**2807** global change.

**2808**

**References**

- 2809** Abrams, M. D. and S. A. Mostoller (1995). Gas exchange, leaf structure and  
**2810** nitrogen in contrasting successional tree species growing in open and under-  
**2811** story sites during a drought. *Tree Physiology* 15(6), 361–370.
- 2812** Adams, M. A., T. L. Turnbull, J. I. Sprent, and N. Buchmann (2016). Legumes  
**2813** are different: Leaf nitrogen, photosynthesis, and water use efficiency. *Pro-  
**2814** ceedings of the National Academy of Sciences of the United States of Amer-  
**2815** ica* 113(15), 4098–4103.
- 2816** Ainsworth, E. A., P. A. Davey, C. J. Bernacchi, O. C. Dermody, E. A. Heaton,  
**2817** D. J. Moore, P. B. Morgan, S. L. Naidu, H. S. Y. Ra, X. G. Zhu, P. S. Curtis,  
**2818** and S. P. Long (2002). A meta-analysis of elevated [CO<sub>2</sub>] effects on soybean  
**2819** (*Glycine max*) physiology, growth and yield. *Global Change Biology* 8(8),  
**2820** 695–709.
- 2821** Ainsworth, E. A. and S. P. Long (2005). What have we learned from 15 years of  
**2822** free-air CO<sub>2</sub> enrichment (FACE)? A meta-analytic review of the responses  
**2823** of photosynthesis, canopy properties and plant production to rising CO<sub>2</sub>.  
**2824** *New Phytologist* 165(2), 351–372.
- 2825** Ainsworth, E. A. and A. Rogers (2007). The response of photosynthesis and  
**2826** stomatal conductance to rising [CO<sub>2</sub>]: mechanisms and environmental in-  
**2827** teractions. *Plant, Cell and Environment* 30(3), 258–270.
- 2828** Allen, K., J. B. Fisher, R. P. Phillips, J. S. Powers, and E. R. Brzostek (2020).  
**2829** Modeling the carbon cost of plant nitrogen and phosphorus uptake across  
**2830** temperate and tropical forests. *Frontiers in Forests and Global Change* 3,

- 2831 1–12.
- 2832 Allison, S. D., C. I. Czimczik, and K. K. Treseder (2008). Microbial activity  
2833 and soil respiration under nitrogen addition in Alaskan boreal forest. *Global  
2834 Change Biology* 14(5), 1156–1168.
- 2835 Andersen, M. K., H. Hauggaard-Nielsen, P. Ambus, and E. S. Jensen (2005).  
2836 Biomass production, symbiotic nitrogen fixation and inorganic N use in dual  
2837 and tri-component annual intercrops. *Plant and Soil* 266(1-2), 273–287.
- 2838 Andrews, M., E. K. James, J. I. Sprent, R. M. Boddey, E. Gross, and F. B. dos  
2839 Reis (2011). Nitrogen fixation in legumes and actinorhizal plants in natural  
2840 ecosystems: Values obtained using  $^{15}\text{N}$  natural abundance. *Plant Ecology  
2841 and Diversity* 4(2-3), 117–130.
- 2842 Arndal, M. F., A. Tolver, K. S. Larsen, C. Beier, and I. K. Schmidt (2018). Fine  
2843 root growth and vertical distribution in response to elevated CO<sub>2</sub>, warming  
2844 and drought in a mixed heathland–grassland. *Ecosystems* 21(1), 15–30.
- 2845 Arnone, J. A. (1997). Indices of plant N availability in an alpine grassland under  
2846 elevated atmospheric CO<sub>2</sub>. *Plant and Soil* 190(1), 61–66.
- 2847 Arora, V. K., A. Katavouta, R. G. Williams, C. D. Jones, V. Brovkin,  
2848 P. Friedlingstein, J. Schwinger, L. Bopp, O. Boucher, P. Cadule, M. A.  
2849 Chamberlain, J. R. Christian, C. Delire, R. A. Fisher, T. Hajima, T. Ilyina,  
2850 E. Joetzjer, M. Kawamiya, C. D. Koven, J. P. Krasting, R. M. Law, D. M.  
2851 Lawrence, A. Lenton, K. Lindsay, J. Pongratz, T. Raddatz, R. Séférian,  
2852 K. Tachiiri, J. F. Tjiputra, A. Wiltshire, T. Wu, and T. Ziehn (2020).  
2853 Carbon-concentration and carbon-climate feedbacks in CMIP6 models and  
2854 their comparison to CMIP5 models. *Biogeosciences* 17(16), 4173–4222.

- 2855 Bae, K., T. J. Fahey, R. D. Yanai, and M. Fisk (2015). Soil nitrogen availability affects belowground carbon allocation and soil respiration in northern  
2856 hardwood forests of New Hampshire. *Ecosystems* 18(7), 1179–1191.
- 2857
- 2858 Barber, S. A. (1962). A diffusion and mass-flow concept of soil nutrient availability. *Soil Science* 93(1), 39–49.
- 2859
- 2860 Barnes, J. D., L. Balaguer, E. Manrique, S. Elvira, and A. W. Davison (1992).  
2861 A reappraisal of the use of DMSO for the extraction and determination  
2862 of chlorophylls a and b in lichens and higher plants. *Environmental and  
2863 Experimental Botany* 32(2), 85–100.
- 2864 Bates, D., M. Mächler, B. Bolker, and S. Walker (2015). Fitting linear mixed-  
2865 effects models using lme4. *Journal of Statistical Software* 67(1), 1–48.
- 2866 Beaudette, D., J. Skovlin, S. Roeker, and A. Brown (2022). soilDB: Soil  
2867 Database Interface.
- 2868 Bengtson, P., J. Barker, and S. J. Grayston (2012). Evidence of a strong cou-  
2869 pling between root exudation, C and N availability, and stimulated SOM  
2870 decomposition caused by rhizosphere priming effects. *Ecology and Evolu-  
2871 tion* 2(8), 1843–1852.
- 2872 Bernacchi, C. J., E. L. Singsaas, C. Pimentel, A. R. Portis, and S. P. Long  
2873 (2001). Improved temperature response functions for models of Rubisco-  
2874 limited photosynthesis. *Plant, Cell and Environment* 24(2), 253–259.
- 2875 Bialic-Murphy, L., N. G. Smith, P. Voothuluru, R. M. McElderry, M. D.  
2876 Roche, S. T. Cassidy, S. N. Kivlin, and S. Kalisz (2021). Invasion-induced  
2877 root–fungal disruptions alter plant water and nitrogen economies. *Ecology*

- 2878 *Letters* 24(6), 1145–1156.
- 2879 Bloom, A. J., F. S. Chapin, and H. A. Mooney (1985). Resource limitation  
2880 in plants - an economic analogy. *Annual Review of Ecology and Systemat-*  
2881 *ics* 16(1), 363–392.
- 2882 Bloomfield, K. J., B. D. Stocker, T. F. Keenan, and I. C. Prentice (2023).  
2883 Environmental controls on the light use efficiency of terrestrial gross primary  
2884 production. *Global Change Biology* 29(4), 0–2.
- 2885 Bonan, G. B., M. D. Hartman, W. J. Parton, and W. R. Wieder (2013). Eval-  
2886 uating litter decomposition in earth system models with long-term litter  
2887 bag experiments: an example using the Community Land Model version 4  
2888 (CLM4). *Global Change Biology* 19(3), 957–974.
- 2889 Bonan, G. B., P. J. Lawrence, K. W. Oleson, S. Levis, M. Jung, M. Reich-  
2890 stein, D. M. Lawrence, and S. C. Swenson (2011). Improving canopy pro-  
2891 cesses in the Community Land Model version 4 (CLM4) using global flux  
2892 fields empirically inferred from FLUXNET data. *Journal of Geophysical Re-*  
2893 *search* 116(G2), G02014.
- 2894 Booth, B. B. B., C. D. Jones, M. Collins, I. J. Totterdell, P. M. Cox, S. Sitch,  
2895 C. Huntingford, R. A. Betts, G. R. Harris, and J. Lloyd (2012). High sen-  
2896 sitivity of future global warming to land carbon cycle processes. *Environ-*  
2897 *mental Research Letters* 7(2), 024002.
- 2898 Borer, E. T., W. S. Harpole, P. B. Adler, E. M. Lind, J. L. Orrock, E. W.  
2899 Seabloom, and M. D. Smith (2014). Finding generality in ecology: A model  
2900 for globally distributed experiments. *Methods in Ecology and Evolution* 5(1),  
2901 65–73.

- 2902 Braghieri, R. K., J. B. Fisher, K. Allen, E. Brzostek, M. Shi, X. Yang, D. M.  
2903 Ricciuto, R. A. Fisher, Q. Zhu, and R. P. Phillips (2022). Modeling global  
2904 carbon costs of plant nitrogen and phosphorus acquisition. *Journal of Ad-*  
2905 *vances in Modeling Earth Systems* 14(8), 1–23.
- 2906 Brix, H. (1971). Effects of nitrogen fertilization on photosynthesis and respi-  
2907 ration in Douglas-fir. *Forest Science* 17(4), 407–414.
- 2908 Brzostek, E. R., J. B. Fisher, and R. P. Phillips (2014). Modeling the carbon  
2909 cost of plant nitrogen acquisition: Mycorrhizal trade-offs and multipath  
2910 resistance uptake improve predictions of retranslocation. *Journal of Geo-*  
2911 *physical Research: Biogeosciences* 119, 1684–1697.
- 2912 Bubier, J. L., R. Smith, S. Juutinen, T. R. Moore, R. Minocha, S. Long, and  
2913 S. Minocha (2011). Effects of nutrient addition on leaf chemistry, morphol-  
2914 ogy, and photosynthetic capacity of three bog shrubs. *Oecologia* 167(2),  
2915 355–368.
- 2916 Cernusak, L. A., N. Ubierna, K. Winter, J. A. M. Holtum, J. D. Marshall, and  
2917 G. D. Farquhar (2013). Environmental and physiological determinants of  
2918 carbon isotope discrimination in terrestrial plants. *New Phytologist* 200(4),  
2919 950–965.
- 2920 Chen, J.-L., J. F. Reynolds, P. C. Harley, and J. D. Tenhunen (1993). Coor-  
2921 dination theory of leaf nitrogen distribution in a canopy. *Oecologia* 93(1),  
2922 63–69.
- 2923 Clark, D. B., L. M. Mercado, S. Sitch, C. D. Jones, N. Gedney, M. J. Best,  
2924 M. Pryor, G. G. Rooney, R. L. H. Essery, E. Blyth, O. Boucher, R. J.  
2925 Harding, C. Huntingford, and P. M. Cox (2011). The Joint UK Land Envi-

- 2926 ronment Simulator (JULES), model description. Part 2: Carbon fluxes and  
2927 vegetation dynamics. *Geoscientific Model Development* 4(3), 701–722.
- 2928 Cornwell, W. K., J. H. C. Cornelissen, K. Amatangelo, E. Dorrepaal, V. T.  
2929 Eviner, O. Godoy, S. E. Hobbie, B. Hoorens, H. Kurokawa, N. Pérez-  
2930 Harguindeguy, H. M. Quested, L. S. Santiago, D. A. Wardle, I. J. Wright,  
2931 R. Aerts, S. D. Allison, P. van Bodegom, V. Brovkin, A. Chatain, T. V.  
2932 Callaghan, S. Díaz, E. Garnier, D. E. Gurvich, E. Kazakou, J. A. Klein,  
2933 J. Read, P. B. Reich, N. A. Soudzilovskaia, M. V. Vaieretti, and M. Westoby  
2934 (2008). Plant species traits are the predominant control on litter decompo-  
2935 sition rates within biomes worldwide. *Ecology Letters* 11(10), 1065–1071.
- 2936 Cornwell, W. K., I. J. Wright, J. Turner, V. Maire, M. M. Barbour, L. A.  
2937 Cernusak, T. E. Dawson, D. S. Ellsworth, G. D. Farquhar, H. Griffiths,  
2938 C. Keitel, A. Knohl, P. B. Reich, D. G. Williams, R. Bhaskar, J. H. C. Cor-  
2939 nelissen, A. Richards, S. Schmidt, F. Valladares, C. Körner, E.-D. Schulze,  
2940 N. Buchmann, and L. S. Santiago (2018). Climate and soils together regulate  
2941 photosynthetic carbon isotope discrimination within C<sub>3</sub> plants worldwide.  
2942 *Global Ecology and Biogeography* 27(9), 1056–1067.
- 2943 Cramer, W. and I. C. Prentice (1988). Simulation of regional soil moisture  
2944 deficits on a European scale. *Norsk Geografisk Tidsskrift - Norwegian Jour-*  
2945 *nal of Geography* 42(2-3), 149–151.
- 2946 Curtis, P. S. (1996). A meta-analysis of leaf gas exchange and nitrogen in trees  
2947 grown under elevated carbon dioxide. *Plant, Cell and Environment* 19(2),  
2948 127–137.
- 2949 Daly, C., M. Halbleib, J. I. Smith, W. P. Gibson, M. K. Doggett, G. H. Taylor,

- 2950** J. Curtis, and P. P. Pasteris (2008). Physiographically sensitive mapping  
**2951** of climatological temperature and precipitation across the conterminous  
**2952** United States. *International Journal of Climatology* 28(15), 2031–2064.
- 2953** Davies-Barnard, T., J. Meyerholt, S. Zaehle, P. Friedlingstein, V. Brovkin,  
**2954** Y. Fan, R. A. Fisher, C. D. Jones, H. Lee, D. Peano, B. Smith, D. Wårlind,  
**2955** and A. J. Wiltshire (2020). Nitrogen cycling in CMIP6 land surface models:  
**2956** progress and limitations. *Biogeosciences* 17(20), 5129–5148.
- 2957** Davis, T. W., I. C. Prentice, B. D. Stocker, R. T. Thomas, R. J. Whitley,  
**2958** H. Wang, B. J. Evans, A. V. Gallego-Sala, M. T. Sykes, and W. Cramer  
**2959** (2017). Simple process-led algorithms for simulating habitats (SPLASH  
**2960** v.1.0): robust indices of radiation, evapotranspiration and plant-available  
**2961** moisture. *Geoscientific Model Development* 10, 689–708.
- 2962** Delaire, M., E. Frak, M. Sigogne, B. Adam, F. Beaujard, and X. Le Roux  
**2963** (2005). Sudden increase in atmospheric CO<sub>2</sub> concentration reveals strong  
**2964** coupling between shoot carbon uptake and root nutrient uptake in young  
**2965** walnut trees. *Tree Physiology* 25(2), 229–235.
- 2966** Doane, T. A. and W. R. Horwáth (2003). Spectrophotometric determination of  
**2967** nitrate with a single reagent. *Analytical Letters* 36(12), 2713–2722.
- 2968** Dong, N., I. C. Prentice, B. J. Evans, S. Caddy-Retalic, A. J. Lowe, and I. J.  
**2969** Wright (2017). Leaf nitrogen from first principles: field evidence for adaptive  
**2970** variation with climate. *Biogeosciences* 14(2), 481–495.
- 2971** Dong, N., I. C. Prentice, I. J. Wright, B. J. Evans, H. F. Togashi, S. Caddy-  
**2972** Retalic, F. A. McInerney, B. Sparrow, E. Leitch, and A. J. Lowe (2020).  
**2973** Components of leaf-trait variation along environmental gradients. *New Phy-*

- 2974** *tologist* 228(1), 82–94.
- 2975** Dong, N., I. C. Prentice, I. J. Wright, H. Wang, O. K. Atkin, K. J. Bloomfield,
- 2976** T. F. Domingues, S. M. Gleason, V. Maire, Y. Onoda, H. Poorter, and N. G.
- 2977** Smith (2022). Leaf nitrogen from the perspective of optimal plant function.
- 2978** *Journal of Ecology* 110(11), 2585–2602.
- 2979** Dong, N., I. J. Wright, J. M. Chen, X. Luo, H. Wang, T. F. Keenan, N. G.
- 2980** Smith, and I. C. Prentice (2022). Rising CO<sub>2</sub> and warming reduce global
- 2981** canopy demand for nitrogen. *New Phytologist* 235(5), 1692–1700.
- 2982** Dovrat, G., H. Bakhshian, T. Masci, and E. Sheffer (2020). The nitrogen eco-
- 2983** nomic spectrum of legume stoichiometry and fixation strategy. *New Phytol-*
- 2984** *ogist* 227(2), 365–375.
- 2985** Dovrat, G., T. Masci, H. Bakhshian, E. Mayzlish Gati, S. Golan, and E. Shef-
- 2986** fer (2018). Drought-adapted plants dramatically downregulate dinitrogen
- 2987** fixation: Evidences from Mediterranean legume shrubs. *Journal of Ecol-*
- 2988** *ogy* 106(4), 1534–1544.
- 2989** Drake, B. G., M. A. Gonzàlez-Meler, and S. P. Long (1997). More efficient
- 2990** plants: a consequence of rising atmospheric CO<sub>2</sub>? *Annual Review of Plant*
- 2991** *Biology* 48, 609–639.
- 2992** Duursma, R. A. (2015). Plantecophys - An R package for analyzing and mod-
- 2993** elling leaf gas exchange data. *PLOS ONE* 10(11), e0143346.
- 2994** Eamus, D., N. Boulain, J. Cleverly, and D. D. Breshears (2013). Global change-
- 2995** type drought-induced tree mortality: Vapor pressure deficit is more impor-
- 2996** tant than temperature per se in causing decline in tree health. *Ecology and*

- 2997** *Evolution* 3(8), 2711–2729.
- 2998** Eastman, B. A., M. B. Adams, E. R. Brzostek, M. B. Burnham, J. E. Carrara,
- 2999** C. Kelly, B. E. McNeil, C. A. Walter, and W. T. Peterjohn (2021). Altered
- 3000** plant carbon partitioning enhanced forest ecosystem carbon storage after 25
- 3001** years of nitrogen additions. *New Phytologist* 230(4), 1435–1448.
- 3002** Ellsworth, D. S. and P. B. Reich (1996). Photosynthesis and leaf nitrogen in five
- 3003** Amazonian tree species during early secondary succession. *Ecology* 77(2),
- 3004** 581–594.
- 3005** Espelta, J. M., P. Cortés, M. Mangirón, and J. Retana (2005). Differences
- 3006** in biomass partitioning, leaf nitrogen content, and water use efficiency  $\delta^{13}$
- 3007** result in similar performance of seedlings of two Mediterranean oaks with
- 3008** contrasting leaf habit. *Ecoscience* 12(4), 447–454.
- 3009** Evans, J. R. (1989). Photosynthesis and nitrogen relationships in leaves of C<sub>3</sub>
- 3010** plants. *Oecologia* 78(1), 9–19.
- 3011** Evans, J. R. and V. C. Clarke (2019). The nitrogen cost of photosynthesis.
- 3012** *Journal of Experimental Botany* 70(1), 7–15.
- 3013** Evans, J. R. and H. Poorter (2001). Photosynthetic acclimation of plants to
- 3014** growth irradiance: the relative importance of specific leaf area and nitrogen
- 3015** partitioning in maximizing carbon gain. *Plant, Cell and Environment* 24(8),
- 3016** 755–767.
- 3017** Evans, J. R. and J. R. Seemann (1989). The allocation of protein nitrogen in
- 3018** the photosynthetic apparatus: costs, consequences, and control. *Photosyn-*
- 3019** *thesis* 8, 183–205.

- 3020** Exbrayat, J.-F., A. A. Bloom, P. Falloon, A. Ito, T. L. Smallman, and  
**3021** M. Williams (2018). Reliability ensemble averaging of 21<sup>st</sup> century projec-  
**3022** tions of terrestrial net primary productivity reduces global and regional  
**3023** uncertainties. *Earth System Dynamics* 9(1), 153–165.
- 3024** Farquhar, G. D., J. R. Ehleringer, and K. T. Hubick (1989). Carbon isotope  
**3025** discrimination and photosynthesis. *Annual Review of Plant Physiology and*  
**3026** *Plant Molecular Biology* 40(1), 503–537.
- 3027** Farquhar, G. D. and T. D. Sharkey (1982). Stomatal conductance and photo-  
**3028** synthesis. *Annual Review of Plant Physiology* 33(1), 317–345.
- 3029** Farquhar, G. D., S. von Caemmerer, and J. A. Berry (1980). A biochemical  
**3030** model of photosynthetic CO<sub>2</sub> assimilation in leaves of C<sub>3</sub> species.  
**3031** *Planta* 149(1), 78–90.
- 3032** Fay, P. A., S. M. Prober, W. S. Harpole, J. M. H. Knops, J. D. Bakker, E. T.  
**3033** Borer, E. M. Lind, A. S. MacDougall, E. W. Seabloom, P. D. Wragg, P. B.  
**3034** Adler, D. M. Blumenthal, Y. M. Buckley, C. Chu, E. E. Cleland, S. L.  
**3035** Collins, K. F. Davies, G. Du, X. Feng, J. Firn, D. S. Gruner, N. Hagenah,  
**3036** Y. Hautier, R. W. Heckman, V. L. Jin, K. P. Kirkman, J. A. Klein, L. M.  
**3037** Ladwig, Q. Li, R. L. McCulley, B. A. Melbourne, C. E. Mitchell, J. L. Moore,  
**3038** J. W. Morgan, A. C. Risch, M. Schütz, C. J. Stevens, D. A. Wedin, and  
**3039** L. H. Yang (2015). Grassland productivity limited by multiple nutrients.  
**3040** *Nature Plants* 1(7), 15080.
- 3041** Feng, X. (1999). Trends in intrinsic water-use efficiency of natural trees for the  
**3042** past 100-200 years: A response to atmospheric CO<sub>2</sub> concentration. *Geochim-  
ica et Cosmochimica Acta* 63(13-14), 1891–1903.

- 3044** Field, C. B. and H. A. Mooney (1986). The photosynthesis-nitrogen relationship  
**3045** in wild plants. In T. J. Givnish (Ed.), *On the Economy of Plant Form and*  
**3046** *Function*, pp. 25–55. Cambridge: Cambridge University Press.
- 3047** Finzi, A. C., D. J. P. Moore, E. H. DeLucia, J. Lichter, K. S. Hofmockel, R. B.  
**3048** Jackson, H. S. Kim, R. Matamala, H. R. McCarthy, R. Oren, J. S. Pippen,  
**3049** and W. H. Schlesinger (2006). Progressive nitrogen limitation of ecosystem  
**3050** processes under elevated CO<sub>2</sub> in a warm-temperate forest. *Ecology* 87(1),  
**3051** 15–25.
- 3052** Firn, J., J. M. McGree, E. Harvey, H. Flores Moreno, M. Schutz, Y. M. Buckley,  
**3053** E. T. Borer, E. W. Seabloom, K. J. La Pierre, A. M. MacDougall, S. M.  
**3054** Prober, C. J. Stevens, L. L. Sullivan, E. Porter, E. Ladouceur, C. Allen,  
**3055** K. H. Moromizato, J. W. Morgan, W. S. Harpole, Y. Hautier, N. Eisen-  
**3056** hauer, J. P. Wright, P. B. Adler, C. A. Arnillas, J. D. Bakker, L. Biederman,  
**3057** A. A. D. Broadbent, C. S. Brown, M. N. Bugalho, M. C. Caldeira, E. E. Cle-  
**3058** land, A. Ebeling, P. A. Fay, N. Hagenah, A. R. Kleinhesselink, R. Mitchell,  
**3059** J. L. Moore, C. Nogueira, P. L. Peri, C. Roscher, M. D. Smith, P. D. Wragg,  
**3060** and A. C. Risch (2019). Leaf nutrients, not specific leaf area, are consistent  
**3061** indicators of elevated nutrient inputs. *Nature Ecology and Evolution* 3(3),  
**3062** 400–406.
- 3063** Fisher, J. B., S. Sitch, Y. Malhi, R. A. Fisher, C. Huntingford, and S.-Y. Tan  
**3064** (2010). Carbon cost of plant nitrogen acquisition: A mechanistic, globally  
**3065** applicable model of plant nitrogen uptake, retranslocation, and fixation.  
**3066** *Global Biogeochemical Cycles* 24(1), 1–17.
- 3067** Fox, J. and S. Weisberg (2019). *An R companion to applied regression* (Third

- 3068** edit ed.). Thousand Oaks, California: Sage.
- 3069** Franklin, O., R. E. McMurtrie, C. M. Iversen, K. Y. Crous, A. C. Finzi, D. Tis-
- 3070** sue, D. S. Ellsworth, R. Oren, and R. J. Norby (2009). Forest fine-root
- 3071** production and nitrogen use under elevated CO<sub>2</sub>: contrasting responses
- 3072** in evergreen and deciduous trees explained by a common principle. *Global*
- 3073** *Change Biology* 15(1), 132–144.
- 3074** Friedlingstein, P., M. Meinshausen, V. K. Arora, C. D. Jones, A. Anav, S. K.
- 3075** Liddicoat, and R. Knutti (2014). Uncertainties in CMIP5 climate projections
- 3076** due to carbon cycle feedbacks. *Journal of Climate* 27(2), 511–526.
- 3077** Friel, C. A. and M. L. Friesen (2019). Legumes modulate allocation to rhizobial
- 3078** nitrogen fixation in response to factorial light and nitrogen manipulation.
- 3079** *Frontiers in Plant Science* 10, 1316.
- 3080** Fujikake, H., A. Yamazaki, N. Ohtake, K. Sueoshi, S. Matsuhashi, T. Ito,
- 3081** C. Mizuniwa, T. Kume, S. Hoshimoto, N.-S. Ishioka, S. Watanabe, A. Osa,
- 3082** T. Sekine, H. Uchida, A. Tsuji, and T. Ohyama (2003). Quick and reversible
- 3083** inhibition of soybean root nodule growth by nitrate involves a decrease in
- 3084** sucrose supply to nodules. *Journal of Experimental Botany* 54(386), 1379–
- 3085** 1388.
- 3086** Ghannoum, O., J. R. Evans, and S. von Caemmerer (2011). Nitrogen and water
- 3087** use efficiency of C<sub>4</sub> plants. In A. S. Raghavendra and R. F. Sage (Eds.), *C<sub>4</sub>*
- 3088** *Photosynthesis and Related CO<sub>2</sub> Concentrating Mechanisms*, Chapter 8, pp.
- 3089** 129–146. Springer.
- 3090** Ghimire, B., W. J. Riley, C. D. Koven, J. Kattge, A. Rogers, P. B. Reich, and
- 3091** I. J. Wright (2017). A global trait-based approach to estimate leaf nitro-

- 3092 gen functional allocation from observations:. *Ecological Applications* 27(5),  
3093 1421–1434.
- 3094 Giardina, C. P., M. D. Coleman, J. E. Hancock, J. S. King, E. A. Lilleskov,  
3095 W. M. Loya, K. S. Pregitzer, M. G. Ryan, and C. C. Trettin (2005). The  
3096 response of belowground carbon allocation in forests to global change. In  
3097 D. Binkley and O. Manyailo (Eds.), *Tree Species Effects on Soils: Implica-*  
3098 *tions for Global Change* (Volume 55 ed.), Chapter Chapter 7, pp. 119–154.  
3099 Berlin/Heidelberg: Springer-Verlag.
- 3100 Gibson, A. H. and J. E. Harper (1985). Nitrate effect on nodulation of soybean  
3101 by *Bradyrhizobium japonicum*. *Crop Science* 25(3), 497–501.
- 3102 Gill, A. L. and A. C. Finzi (2016). Belowground carbon flux links biogeochemical  
3103 cycles and resource-use efficiency at the global scale. *Ecology Letters* 19(12),  
3104 1419–1428.
- 3105 Goll, D. S., V. Brovkin, B. R. Parida, C. H. Reick, J. Kattge, P. B. Reich, P. M.  
3106 van Bodegom, and Ü. Niinemets (2012). Nutrient limitation reduces land  
3107 carbon uptake in simulations with a model of combined carbon, nitrogen  
3108 and phosphorus cycling. *Biogeosciences Discussions* 9(3), 3173–3232.
- 3109 Gregory, L. M., A. M. McClain, D. M. Kramer, J. D. Pardo, K. E. Smith, O. L.  
3110 Tessmer, B. J. Walker, L. G. Ziccardi, and T. D. Sharkey (2021, oct). The  
3111 triose phosphate utilization limitation of photosynthetic rate: Out of global  
3112 models but important for leaf models. *Plant, Cell and Environment* 44(10),  
3113 3223–3226.
- 3114 Grossiord, C., T. N. Buckley, L. A. Cernusak, K. A. Novick, B. Poulter, R. T. W.  
3115 Siegwolf, J. S. Sperry, and N. G. McDowell (2020). Plant responses to rising

- 3116** vapor pressure deficit. *New Phytologist* 226(6), 1550–1566.
- 3117** Gulmon, S. L. and C. C. Chu (1981). The effects of light and nitrogen on photo-
- 3118** synthesis, leaf characteristics, and dry matter allocation in the chaparral
- 3119** shrub, *Diplacus aurantiacus*. *Oecologia* 49(2), 207–212.
- 3120** Gutschick, V. P. (1981). Evolved strategies in nitrogen acquisition by plants.
- 3121** *The American Naturalist* 118(5), 607–637.
- 3122** Hallik, L., Ü. Niinemets, and I. J. Wright (2009). Are species shade and drought
- 3123** tolerance reflected in leaf-level structural and functional differentiation in
- 3124** Northern Hemisphere temperate woody flora? *New Phytologist* 184(1), 257–
- 3125** 274.
- 3126** Harrison, M. T., E. J. Edwards, G. D. Farquhar, A. B. Nicotra, and J. R.
- 3127** Evans (2009). Nitrogen in cell walls of sclerophyllous leaves accounts for
- 3128** little of the variation in photosynthetic nitrogen-use efficiency. *Plant, Cell*
- 3129** and *Environment* 32(3), 259–270.
- 3130** Harrison, S. P., W. Cramer, O. Franklin, I. C. Prentice, H. Wang,
- 3131** Å. Brännström, H. de Boer, U. Dieckmann, J. Joshi, T. F. Keenan,
- 3132** A. Lavergne, S. Manzoni, G. Mengoli, C. Morfopoulos, J. Peñuelas,
- 3133** S. Pietsch, K. T. Rebel, Y. Ryu, N. G. Smith, B. D. Stocker, and I. J.
- 3134** Wright (2021). Eco-evolutionary optimality as a means to improve vegetation
- 3135** and land-surface models. *New Phytologist* 231(6), 2125–2141.
- 3136** Henneron, L., P. Kardol, D. A. Wardle, C. Cros, and S. Fontaine (2020). Rhizo-
- 3137** sphere control of soil nitrogen cycling: a key component of plant economic
- 3138** strategies. *New Phytologist* 228(4), 1269–1282.

- 3139** Hijmans, R. J. (2022). *terra: Spatial Data Analysis*.
- 3140** Hikosaka, K. and A. Shigeno (2009). The role of Rubisco and cell walls in the  
**3141** interspecific variation in photosynthetic capacity. *Oecologia* 160(3), 443–  
**3142** 451.
- 3143** Hoagland, D. R. and D. I. Arnon (1950). The water culture method for growing  
**3144** plants without soil. *California Agricultural Experiment Station: 347* 347(2),  
**3145** 1–32.
- 3146** Hobbie, E. A. (2006). Carbon allocation to ectomycorrhizal fungi correlates  
**3147** with belowground allocation in culture studies. *Ecology* 87(3), 563–569.
- 3148** Hobbie, E. A. and J. E. Hobbie (2008). Natural abundance of  $^{15}\text{N}$  in nitrogen-  
**3149** limited forests and tundra can estimate nitrogen cycling through mycorrhizal  
**3150** fungi: a review. *Ecosystems* 11(5), 815–830.
- 3151** Hoek, T. A., K. Axelrod, T. Biancalani, E. A. Yurtsev, J. Liu, and J. Gore  
**3152** (2016). Resource availability modulates the cooperative and competitive na-  
**3153** nature of a microbial cross-feeding mutualism. *PLOS Biology* 14(8), e1002540.
- 3154** Höglberg, M. N., M. J. I. Briones, S. G. Keel, D. B. Metcalfe, C. Campbell, A. J.  
**3155** Midwood, B. Thornton, V. Hurry, S. Linder, T. Näsholm, and P. Höglberg  
**3156** (2010). Quantification of effects of season and nitrogen supply on tree below-  
**3157** ground carbon transfer to ectomycorrhizal fungi and other soil organisms in  
**3158** a boreal pine forest. *New Phytologist* 187(2), 485–493.
- 3159** Höglberg, P., M. N. Höglberg, S. G. Göttlicher, N. R. Betson, S. G. Keel, D. B.  
**3160** Metcalfe, C. Campbell, A. Schindlbacher, V. Hurry, T. Lundmark, S. Linder,  
**3161** and T. Näsholm (2008). High temporal resolution tracing of photosynthate

- 3162** carbon from the tree canopy to forest soil microorganisms. *New Phytologist* 177(1), 220–228.
- 3164** Houlton, B. Z., Y.-P. Wang, P. M. Vitousek, and C. B. Field (2008). A unifying framework for dinitrogen fixation in the terrestrial biosphere. *Nature* 454(7202), 327–330.
- 3167** Huber, M. L., R. A. Perkins, A. Laesecke, D. G. Friend, J. V. Sengers, M. J. Assael, I. N. Metaxa, E. Vogel, R. Mareš, and K. Miyagawa (2009). New international formulation for the viscosity of H<sub>2</sub>O. *Journal of Physical and Chemical Reference Data* 38(2), 101–125.
- 3171** Hungate, B. A., J. S. Dukes, M. R. Shaw, Y. Luo, and C. B. Field (2003). Nitrogen and climate change. *Science* 302(5650), 1512–1513.
- 3173** IPCC (2021). *Climate Change 2021: The Physical Science Basis. Contribution of Working Group I to the Sixth Assessment Report of the Intergovernmental Panel on Climate Change*, Volume In Press. Cambridge, United Kingdom and New York, NY, USA: Cambridge University Press.
- 3177** Johnson, N. C., J. H. Graham, and F. A. Smith (1997). Functioning of mycorrhizal associations along the mutualism-parasitism continuum. *New Phytologist* 135(4), 575–585.
- 3180** Kachurina, O. M., H. Zhang, W. R. Raun, and E. G. Krenzer (2000). Simultaneous determination of soil aluminum, ammonium- and nitrate- nitrogen using 1 M potassium chloride. *Communications in Soil Science and Plant Analysis* 31(7-8), 893–903.
- 3184** Kaiser, C., M. R. Kilburn, P. L. Clode, L. Fuchslueger, M. Koranda, J. B. Cliff,

- 3185 Z. M. Solaiman, and D. V. Murphy (2015). Exploring the transfer of recent  
3186 plant photosynthates to soil microbes: mycorrhizal pathway vs direct root  
3187 exudation. *New Phytologist* 205(4), 1537–1551.
- 3188 Katabuchi, M. (2015). LeafArea: An R package for rapid digital analysis of leaf  
3189 area. *Ecological Research* 30(6), 1073–1077.
- 3190 Kattge, J. and W. Knorr (2007). Temperature acclimation in a biochemical  
3191 model of photosynthesis: a reanalysis of data from 36 species. *Plant, Cell  
3192 and Environment* 30(9), 1176–1190.
- 3193 Kattge, J., W. Knorr, T. Raddatz, and C. Wirth (2009). Quantifying photosyn-  
3194 thetic capacity and its relationship to leaf nitrogen content for global-scale  
3195 terrestrial biosphere models. *Global Change Biology* 15(4), 976–991.
- 3196 Kayler, Z., A. Gessler, and N. Buchmann (2010). What is the speed of link  
3197 between aboveground and belowground processes? *New Phytologist* 187(4),  
3198 885–888.
- 3199 Kayler, Z., C. Keitel, K. Jansen, and A. Gessler (2017). Experimental evidence  
3200 of two mechanisms coupling leaf-level C assimilation to rhizosphere CO<sub>2</sub>  
3201 release. *Environmental and Experimental Botany* 135, 21–26.
- 3202 Keeling, C. D., W. G. Mook, and P. P. Tans (1979, jan). Recent trends in the  
3203 <sup>13</sup>C:<sup>12</sup>C ratio of atmospheric carbon dioxide. *Nature* 277(5692), 121–123.
- 3204 Keeney, D. R. and D. W. Nelson (1983). Nitrogen—Inorganic Forms. In A. L.  
3205 Page (Ed.), *Methods of Soil Analysis* (2nd ed.), Chapter 33, pp. 643–698.  
3206 Madison, WI, USA: ASA and SSSA.
- 3207 Kenward, M. G. and J. H. Roger (1997). Small sample inference for fixed effects

- 3208** from restricted maximum likelihood. *Biometrics* 53(3), 983.
- 3209** Knapp, A. K., M. L. Avolio, C. Beier, C. J. W. Carroll, S. L. Collins, J. S.
- 3210** Dukes, L. H. Fraser, R. J. Griffin-Nolan, D. L. Hoover, A. Jentsch, M. E.
- 3211** Loik, R. P. Phillips, A. K. Post, O. E. Sala, I. J. Slette, L. Yahdjian, and
- 3212** M. D. Smith (2017). Pushing precipitation to the extremes in distributed
- 3213** experiments: recommendations for simulating wet and dry years. *Global*
- 3214** *Change Biology* 23(5), 1774–1782.
- 3215** Knorr, W. (2000). Annual and interannual CO<sub>2</sub> exchanges of the
- 3216** terrestrial biosphere: process-based simulations and uncertainties. *Global*
- 3217** *Ecology and Biogeography* 9(3), 225–252.
- 3218** Knorr, W. and M. Heimann (2001). Uncertainties in global terrestrial biosphere
- 3219** modeling: 1. A comprehensive sensitivity analysis with a new photosynthesis
- 3220** and energy balance scheme. *Global Biogeochemical Cycles* 15(1), 207–225.
- 3221** Kulmatiski, A., P. B. Adler, J. M. Stark, and A. T. Tredennick (2017). Water
- 3222** and nitrogen uptake are better associated with resource availability than
- 3223** root biomass. *Ecosphere* 8(3), e01738.
- 3224** Lavergne, A., D. Sandoval, V. J. Hare, H. Graven, and I. C. Prentice (2020).
- 3225** Impacts of soil water stress on the acclimated stomatal limitation of pho-
- 3226** tosynthesis: Insights from stable carbon isotope data. *Global Change Biol-*
- 3227** *ogy* 26(12), 7158–7172.
- 3228** Lawrence, D. M., R. A. Fisher, C. D. Koven, K. W. Oleson, S. C. Swen-
- 3229** son, G. B. Bonan, N. Collier, B. Ghimire, L. Kampenhout, D. Kennedy,
- 3230** E. Kluzek, P. J. Lawrence, F. Li, H. Li, D. L. Lombardozzi, W. J. Riley,
- 3231** W. J. Sacks, M. Shi, M. Vertenstein, W. R. Wieder, C. Xu, A. A. Ali,

- 3232** A. M. Badger, G. Bisht, M. Broeke, M. A. Brunke, S. P. Burns, J. Buzan,  
**3233** M. Clark, A. Craig, K. M. Dahlin, B. Drewniak, J. B. Fisher, M. Flanner,  
**3234** A. M. Fox, P. Gentine, F. M. Hoffman, G. Keppel-Aleks, R. Knox, S. Ku-  
**3235** mar, J. Lenaerts, L. R. Leung, W. H. Lipscomb, Y. Lu, A. Pandey, J. D.  
**3236** Pelletier, J. Perket, J. T. Randerson, D. M. Ricciuto, B. M. Sanderson,  
**3237** A. Slater, Z. M. Subin, J. Tang, R. Q. Thomas, M. Val Martin, and X. Zeng  
**3238** (2019). The Community Land Model Version 5: description of new features,  
**3239** benchmarking, and impact of forcing uncertainty. *Journal of Advances in*  
**3240** *Modeling Earth Systems* 11(12), 4245–4287.
- 3241** LeBauer, D. S. and K. K. Treseder (2008). Nitrogen limitation of net primary  
**3242** productivity. *Ecology* 89(2), 371–379.
- 3243** Lefcheck, J. S. (2016). piecewiseSEM: Piecewise structural equation modelling  
**3244** in r for ecology, evolution, and systematics. *Methods in Ecology and Evolu-*  
**3245** *tion* 7(5), 573–579.
- 3246** Lenth, R. (2019). emmeans: estimated marginal means, aka least-squares  
**3247** means.
- 3248** Li, W., H. Zhang, G. Huang, R. Liu, H. Wu, C. Zhao, and N. G. McDowell  
**3249** (2020). Effects of nitrogen enrichment on tree carbon allocation: A global  
**3250** synthesis. *Global Ecology and Biogeography* 29(3), 573–589.
- 3251** Liang, J., X. Qi, L. Souza, and Y. Luo (2016). Processes regulating progressive  
**3252** nitrogen limitation under elevated carbon dioxide: a meta-analysis. *Bioge-  
osciences* 13(9), 2689–2699.
- 3254** Liang, X., T. Zhang, X. Lu, D. S. Ellsworth, H. BassiriRad, C. You, D. Wang,  
**3255** P. He, Q. Deng, H. Liu, J. Mo, and Q. Ye (2020). Global response patterns of

- 3256 plant photosynthesis to nitrogen addition: A meta-analysis. *Global Change*  
3257 *Biology* 26(6), 3585–3600.
- 3258 López, J., D. A. Way, and W. Sadok (2021). Systemic effects of rising atmo-  
3259 spheric vapor pressure deficit on plant physiology and productivity. *Global*  
3260 *Change Biology* 27(9), 1704–1720.
- 3261 Lu, J., J. Yang, C. Keitel, L. Yin, P. Wang, W. Cheng, and F. A. Dijkstra  
3262 (2022). Belowground carbon efficiency for nitrogen and phosphorus acqui-  
3263 sition varies between *Lolium perenne* and *Trifolium repens* and depends on  
3264 phosphorus fertilization. *Frontiers in Plant Science* 13, 1–9.
- 3265 Luo, X., T. F. Keenan, J. M. Chen, H. Croft, I. C. Prentice, N. G. Smith,  
3266 A. P. Walker, H. Wang, R. Wang, C. Xu, and Y. Zhang (2021). Global  
3267 variation in the fraction of leaf nitrogen allocated to photosynthesis. *Nature*  
3268 *Communications* 12(1), 4866.
- 3269 Luo, Y., W. S. Currie, J. S. Dukes, A. C. Finzi, U. A. Hartwig, B. A. Hungate,  
3270 R. E. McMurtrie, R. Oren, W. J. Parton, D. E. Pataki, R. M. Shaw, D. R.  
3271 Zak, and C. B. Field (2004). Progressive nitrogen limitation of ecosystem  
3272 responses to rising atmospheric carbon dioxide. *BioScience* 54(8), 731–739.
- 3273 Maire, V., P. Martre, J. Kattge, F. Gastal, G. Esser, S. Fontaine, and J.-F.  
3274 Soussana (2012). The coordination of leaf photosynthesis links C and N  
3275 fluxes in C<sub>3</sub> plant species. *PLoS ONE* 7(6), e38345.
- 3276 Makino, A. (2003). Rubisco and nitrogen relationships in rice: leaf photosyn-  
3277 thesis and plant growth. *Soil Science and Plant Nutrition* 49(3), 319–327.
- 3278 Makino, A., M. Harada, T. Sato, H. Nakano, and T. Mae (1997). Growth and N

- 3279** Allocation in Rice Plants under CO<sub>2</sub> Enrichment. *Plant Physiology* 115(1),  
**3280** 199–203.
- 3281** Markham, J. H. and C. Zekveld (2007). Nitrogen fixation makes biomass al-  
**3282** location to roots independent of soil nitrogen supply. *Canadian Journal of*  
**3283** *Botany* (9), 787–793.
- 3284** Marschner, H. and B. Dell (1994). Nutrient uptake in mycorrhizal symbiosis.  
**3285** *Plant and Soil* 159(1), 89–102.
- 3286** Matamala, R. and W. H. Schlesinger (2000). Effects of elevated atmospheric  
**3287** CO<sub>2</sub> on fine root production and activity in an intact temperate forest  
**3288** ecosystem. *Global Change Biology* 6(8), 967–979.
- 3289** Medlyn, B. E., E. Dreyer, D. S. Ellsworth, M. Forstreuter, P. C. Harley,  
**3290** M. U. F. Kirschbaum, X. Le Roux, P. Montpied, J. Strassmeyer, A. Wal-  
**3291** croft, K. Wang, and D. Loustau (2002). Temperature response of parameters  
**3292** of a biochemically based model of photosynthesis. II. A review of experimen-  
**3293** tal data. *Plant, Cell and Environment* 25(9), 1167–1179.
- 3294** Menge, D. N. L., S. A. Levin, and L. O. Hedin (2008). Evolutionary tradeoffs can  
**3295** select against nitrogen fixation and thereby maintain nitrogen limitation.  
**3296** *Proceedings of the National Academy of Sciences* 105(5), 1573–1578.
- 3297** Menne, M. J., I. Durre, R. S. Vose, B. E. Gleason, and T. G. Houston (2012).  
**3298** An overview of the global historical climatology network-daily database.  
**3299** *Journal of Atmospheric and Oceanic Technology* 29(7), 897–910.
- 3300** Meyerholt, J., K. Sickel, and S. Zaehle (2020). Ensemble projections elucidate  
**3301** effects of uncertainty in terrestrial nitrogen limitation on future carbon up-

- 3302** take. *Global Change Biology* 26(7), 3978–3996.
- 3303** Meyerholt, J., S. Zaehle, and M. J. Smith (2016). Variability of projected ter-
- 3304** restrial biosphere responses to elevated levels of atmospheric CO<sub>2</sub> due to
- 3305** uncertainty in biological nitrogen fixation. *Biogeosciences* 13(5), 1491–1518.
- 3306** Minocha, R., S. Long, A. H. Magill, J. D. Aber, and W. H. McDowell (2000).
- 3307** Foliar free polyamine and inorganic ion content in relation to soil and soil
- 3308** solution chemistry in two fertilized forest stands at the Harvard Forest,
- 3309** Massachusetts. *Plant and Soil* 222(1-2), 119–137.
- 3310** Moore, D. J., S. Aref, R. M. Ho, J. S. Pippen, J. G. Hamilton, and E. H. De
- 3311** Lucia (2006). Annual basal area increment and growth duration of Pinus
- 3312** taeda in response to eight years of free-air carbon dioxide enrichment. *Global*
- 3313** *Change Biology* 12(8), 1367–1377.
- 3314** Morgan, J. A., D. E. Pataki, C. Körner, H. Clark, S. J. Del Gross, J. M.
- 3315** Grünzweig, A. K. Knapp, A. R. Mosier, P. C. D. Newton, P. A. Niklaus,
- 3316** J. B. Nippert, R. S. Nowak, W. J. Parton, H. W. Polley, and M. R. Shaw
- 3317** (2004). Water relations in grassland and desert ecosystems exposed to ele-
- 3318** vated atmospheric CO<sub>2</sub>. *Oecologia* 140(1), 11–25.
- 3319** Muñoz, N., X. Qi, M. W. Li, M. Xie, Y. Gao, M. Y. Cheung, F. L. Wong, and
- 3320** H.-M. Lam (2016). Improvement in nitrogen fixation capacity could be part
- 3321** of the domestication process in soybean. *Heredity* 117(2), 84–93.
- 3322** Nadelhoffer, K. J. and J. W. Raich (1992). Fine root production estimates and
- 3323** belowground carbon allocation in forest ecosystems. *Ecology* 73(4), 1139–
- 3324** 1147.

- 3325 Niinemets, Ü. and J. D. Tenhunen (1997). A model separating leaf structural  
3326 and physiological effects on carbon gain along light gradients for the shade-  
3327 tolerant species *Acer saccharum*. *Plant, Cell and Environment* 20(7), 845–  
3328 866.
- 3329 Norby, R. J., J. Ledford, C. D. Reilly, N. E. Miller, and E. G. O'Neill  
3330 (2004). Fine-root production dominates response of a deciduous forest to  
3331 atmospheric CO<sub>2</sub> enrichment. *Proceedings of the National Academy of Sci-  
3332 ences* 101(26), 9689–9693.
- 3333 Norby, R. J., J. M. Warren, C. M. Iversen, B. E. Medlyn, and R. E. Mc-  
3334 Murtrie (2010). CO<sub>2</sub> enhancement of forest productivity constrained by  
3335 limited nitrogen availability. *Proceedings of the National Academy of Sci-  
3336 ences* 107(45), 19368–19373.
- 3337 Novick, K. A., D. L. Ficklin, P. C. Stoy, C. A. Williams, G. Bohrer, A. C.  
3338 Oishi, S. A. Papuga, P. D. Blanken, A. Noormets, B. N. Sulman, R. L.  
3339 Scott, L. Wang, and R. P. Phillips (2016). The increasing importance of  
3340 atmospheric demand for ecosystem water and carbon fluxes. *Nature Climate  
3341 Change* 6(11), 1023–1027.
- 3342 Noyce, G. L., M. L. Kirwan, R. L. Rich, and J. P. Megonigal (2019). Asyn-  
3343 chronous nitrogen supply and demand produce nonlinear plant allocation re-  
3344 sponses to warming and elevated CO<sub>2</sub>. *Proceedings of the National Academy  
3345 of Sciences* 116(43), 21623–21628.
- 3346 Onoda, Y., K. Hikosaka, and T. Hirose (2004). Allocation of nitrogen to  
3347 cell walls decreases photosynthetic nitrogen-use efficiency. *Functional Ecol-  
3348 ogy* 18(3), 419–425.

- 3349** Onoda, Y., I. J. Wright, J. R. Evans, K. Hikosaka, K. Kitajima, Ü. Niinemets,  
**3350** H. Poorter, T. Tosens, and M. Westoby (2017). Physiological and structural  
**3351** trade-offs underlying the leaf economics spectrum. *New Phytologist* 214(4),  
**3352** 1447–1463.
- 3353** Oren, R., J. S. Sperry, G. G. Katul, D. E. Pataki, B. E. Ewers, N. Phillips,  
**3354** and K. V. R. Schäfer (1999). Survey and synthesis of intra- and interspecific  
**3355** variation in stomatal sensitivity to vapor pressure deficit. *Plant, Cell and*  
**3356** *Environment* 22(12), 1515–1526.
- 3357** Oreskes, N., K. Shrader-Frechette, and K. Belitz (1994). Verification, vali-  
**3358** dation, and confirmation of numerical models in the Earth sciences. *Sci-  
ence* 263(5147), 641–646.
- 3360** Paillassa, J., I. J. Wright, I. C. Prentice, S. Pepin, N. G. Smith, G. Ethier,  
**3361** A. C. Westerband, L. J. Lamarque, H. Wang, W. K. Cornwell, and V. Maire  
**3362** (2020). When and where soil is important to modify the carbon and water  
**3363** economy of leaves. *New Phytologist* 228(1), 121–135.
- 3364** Parvin, S., S. Uddin, S. Tausz Posch, R. Armstrong, and M. Tausz (2020). Car-  
**3365** bon sink strength of nodules but not other organs modulates photosynthesis  
**3366** of faba bean (*Vicia faba*) grown under elevated [CO<sub>2</sub>] and different water  
**3367** supply. *New Phytologist* 227(1), 132–145.
- 3368** Paul, K. I., P. J. Polglase, A. M. O'Connell, J. C. Carlyle, P. J. Smethurst, and  
**3369** P. K. Khanna (2003). Defining the relation between soil water content and  
**3370** net nitrogen mineralization. *European Journal of Soil Science* 54(1), 39–48.
- 3371** Peng, Y., K. J. Bloomfield, L. A. Cernusak, T. F. Domingues, and I. C. Pre-  
**3372** nance (2021). Global climate and nutrient controls of photosynthetic capacity.

- 3373** *Communications Biology* 4(1), 462.
- 3374** Perkowski, E. A., E. F. Waring, and N. G. Smith (2021). Root mass carbon  
**3375** costs to acquire nitrogen are determined by nitrogen and light availability  
**3376** in two species with different nitrogen acquisition strategies. *Journal of*  
**3377** *Experimental Botany* 72(15), 5766–5776.
- 3378** Phillips, R. P., E. R. Brzostek, and M. G. Midgley (2013). The mycorrhizal-  
**3379** associated nutrient economy: a new framework for predicting carbon-  
**3380** nutrient couplings in temperate forests. *New Phytologist* 199(1), 41–51.
- 3381** Phillips, R. P., A. C. Finzi, and E. S. Bernhardt (2011). Enhanced root ex-  
**3382** udation induces microbial feedbacks to N cycling in a pine forest under  
**3383** long-term CO<sub>2</sub> fumigation. *Ecology Letters* 14(2), 187–194.
- 3384** Pinheiro, J. and D. Bates (2022). nlme: linear and nonlinear mixed effects  
**3385** models.
- 3386** Poggio, L., L. M. De Sousa, N. H. Batjes, G. B. M. Heuvelink, B. Kempen,  
**3387** E. Ribeiro, and D. Rossiter (2021). SoilGrids 2.0: Producing soil information  
**3388** for the globe with quantified spatial uncertainty. *Soil* 7(1), 217–240.
- 3389** Pons, T. L. and R. W. Pearcy (1994). Nitrogen reallocation and photosynthetic  
**3390** acclimation in response to partial shading in soybean plants. *Physiologia*  
**3391** *Plantarum* 92(4), 636–644.
- 3392** Poorter, H., J. Bühler, D. Van Dusschoten, J. Climent, and J. A. Postma (2012).  
**3393** Pot size matters: A meta-analysis of the effects of rooting volume on plant  
**3394** growth. *Functional Plant Biology* 39(11), 839–850.
- 3395** Poorter, H., O. Knopf, I. J. Wright, A. A. Temme, S. W. Hogewoning, A. Graf,

- 3396 L. A. Cernusak, and T. L. Pons (2022). A meta-analysis of responses of C<sub>3</sub>  
3397 plants to atmospheric CO<sub>2</sub>: dose-response curves for 85 traits ranging from  
3398 the molecular to the whole-plant level. *New Phytologist* 233(4), 1560–1596.
- 3399 Prentice, I. C., N. Dong, S. M. Gleason, V. Maire, and I. J. Wright (2014).  
3400 Balancing the costs of carbon gain and water transport: testing a new theo-  
3401 retical framework for plant functional ecology. *Ecology Letters* 17(1), 82–91.
- 3402 Prentice, I. C., X. Liang, B. E. Medlyn, and Y.-P. Wang (2015). Reliable, ro-  
3403 bust and realistic: The three R's of next-generation land-surface modelling.  
3404 *Atmospheric Chemistry and Physics* 15, 5987–6005.
- 3405 Priestley, C. H. B. and R. J. Taylor (1972). On the Assessment of Surface  
3406 Heat Flux and Evaporation Using Large-Scale Parameters. *Monthly Weather  
3407 Review* 100(2), 81–92.
- 3408 Querejeta, J. I., I. Prieto, C. Armas, F. Casanoves, J. S. Diémé, M. Diouf,  
3409 H. Yossi, B. Kaya, F. I. Pugnaire, and G. M. Rusch (2022). Higher leaf  
3410 nitrogen content is linked to tighter stomatal regulation of transpiration  
3411 and more efficient water use across dryland trees. *New Phytologist* 235(4),  
3412 1351–1364.
- 3413 R Core Team (2021). R: A language and environment for statistical computing.
- 3414 Raich, J. W., D. A. Clark, L. Schwendenmann, and T. E. Wood (2014). Above-  
3415 ground tree growth varies with belowground carbon allocation in a tropical  
3416 rainforest environment. *PLoS ONE* 9(6), e100275.
- 3417 Rastetter, E. B., P. M. Vitousek, C. B. Field, G. R. Shaver, D. Herbert, and  
3418 G. I. Ågren (2001). Resource optimization and symbiotic nitrogen fixation.

- 3419** *Ecosystems* 4(4), 369–388.
- 3420** Reich, P. B. (2014). The world-wide 'fast-slow' plant economics spectrum: a  
**3421** traits manifesto. *Journal of Ecology* 102(2), 275–301.
- 3422** Reich, P. B., S. E. Hobbie, T. Lee, D. S. Ellsworth, J. B. West, D. Tilman,  
**3423** J. M. H. Knops, S. Naeem, and J. Trost (2006). Nitrogen limitation con-  
**3424** strains sustainability of ecosystem response to CO<sub>2</sub>. *Nature* 440(7086), 922–  
**3425** 925.
- 3426** Reichman, G. A., D. L. Grunes, and F. G. Viets (1966). Effect of soil moisture  
**3427** on ammonification and nitrification in two Northern Plains soils. *Soil Science  
Society of America Journal* 30(3), 363–366.
- 3429** Rhine, E. D., R. L. Mulvaney, E. J. Pratt, and G. K. Sims (1998). Improving  
**3430** the Berthelot reaction for determining ammonium in soil extracts and water.  
**3431** *Soil Science Society of America Journal* 62(2), 473.
- 3432** Rogers, A. (2014). The use and misuse of  $V_{\text{cmax}}$  in Earth System Models. *Pho-*  
**3433** *tosynthesis Research* 119(1-2), 15–29.
- 3434** Rogers, A., B. E. Medlyn, J. S. Dukes, G. B. Bonan, S. Caemmerer, M. C.  
**3435** Dietze, J. Kattge, A. D. B. Leakey, L. M. Mercado, Ü. Niinemets, I. C.  
**3436** Prentice, S. P. Serbin, S. Sitch, D. A. Way, and S. Zaehle (2017). A roadmap  
**3437** for improving the representation of photosynthesis in Earth system models.  
**3438** *New Phytologist* 213(1), 22–42.
- 3439** Saathoff, A. J. and J. Welles (2021). Gas exchange measurements in the un-  
**3440** steady state. *Plant Cell and Environment* 44(11), 3509–3523.
- 3441** Sage, R. F. and R. W. Pearcy (1987). The nitrogen use efficiency of C<sub>3</sub> and C<sub>4</sub>

- 3442 plants: I. Leaf nitrogen, growth, and biomass partitioning in *Chenopodium*  
3443 *album* (L.) and *Amaranthus retroflexus* (L.). *Plant Physiology* 84(3), 954–  
3444 958.
- 3445 Saleh, A. M., M. Abdel-Mawgoud, A. R. Hassan, T. H. Habeeb, R. S. Yehia,  
3446 and H. AbdElgawad (2020). Global metabolic changes induced by arbuscular  
3447 mycorrhizal fungi in oregano plants grown under ambient and elevated levels  
3448 of atmospheric CO<sub>2</sub>. *Plant Physiology and Biochemistry* 151, 255–263.
- 3449 Saxton, K. E. and W. J. Rawls (2006). Soil water characteristic estimates by  
3450 texture and organic matter for hydrologic solutions. *Soil Science Society of  
3451 America Journal* 70(5), 1569–1578.
- 3452 Schaefer, K., C. R. Schwalm, C. Williams, M. A. Arain, A. Barr, J. M. Chen,  
3453 K. J. Davis, D. Dimitrov, T. W. Hilton, D. Y. Hollinger, E. Humphreys,  
3454 B. Poulter, B. M. Racza, A. D. Richardson, A. Sahoo, P. Thornton, R. Var-  
3455 gas, H. Verbeeck, R. Anderson, I. Baker, T. A. Black, P. Bolstad, J. Chen,  
3456 P. S. Curtis, A. R. Desai, M. C. Dietze, D. Dragoni, C. M. Gough, R. F.  
3457 Grant, L. Gu, A. K. Jain, C. Kucharik, B. E. Law, S. Liu, E. Lokipitiya,  
3458 H. A. Margolis, R. Matamala, J. H. McCaughey, R. Monson, J. W. Munger,  
3459 W. Oechel, C. Peng, D. T. Price, D. Ricciuto, W. J. Riley, N. Roulet,  
3460 H. Tian, C. Tonitto, M. Torn, E. Weng, and X. Zhou (2012). A model-  
3461 data comparison of gross primary productivity: Results from the North  
3462 American Carbon Program site synthesis. *Journal of Geophysical Research:  
3463 Biogeosciences* 117(G3), G03010.
- 3464 Schmitt, M. R. and G. E. Edwards (1981). Photosynthetic capacity and nitrogen  
3465 use efficiency of maize, wheat, and rice: A comparison between C<sub>3</sub> and C<sub>4</sub>

- 3466** photosynthesis. *Journal of Experimental Botany* 32(3), 459–466.
- 3467** Schneider, C. A., W. S. Rasband, and K. W. Eliceiri (2012). NIH Image to
- 3468** ImageJ: 25 years of image analysis. *Nature Methods* 9(7), 671–675.
- 3469** Scott, H. G. and N. G. Smith (2022). A Model of C<sub>4</sub> photosynthetic acclima-
- 3470** tion based on least-cost optimality theory suitable for Earth system model
- 3471** incorporation. *Journal of Advances in Modeling Earth Systems* 14(3), 1–16.
- 3472** Shi, M., J. B. Fisher, E. R. Brzostek, and R. P. Phillips (2016). Carbon cost
- 3473** of plant nitrogen acquisition: Global carbon cycle impact from an improved
- 3474** plant nitrogen cycle in the Community Land Model. *Global Change Biol-*
- 3475** *ogy* 22(3), 1299–1314.
- 3476** Shi, M., J. B. Fisher, R. P. Phillips, and E. R. Brzostek (2019). Neglecting
- 3477** plant–microbe symbioses leads to underestimation of modeled climate im-
- 3478** pacts. *Biogeosciences* 16(2), 457–465.
- 3479** Smith, B., D. Wärldin, A. Arneth, T. Hickler, P. Leadley, J. Siltberg, and
- 3480** S. Zaehle (2014). Implications of incorporating N cycling and N limitations
- 3481** on primary production in an individual-based dynamic vegetation model.
- 3482** *Biogeosciences* 11(7), 2027–2054.
- 3483** Smith, N. G. and J. S. Dukes (2013). Plant respiration and photosynthesis in
- 3484** global-scale models: incorporating acclimation to temperature and CO<sub>2</sub>.
- 3485** *Global Change Biology* 19(1), 45–63.
- 3486** Smith, N. G. and J. S. Dukes (2018). Drivers of leaf carbon exchange capacity
- 3487** across biomes at the continental scale. *Ecology* 99(7), 1610–1620.
- 3488** Smith, N. G. and T. F. Keenan (2020). Mechanisms underlying leaf photosyn-

- 3489      thetic acclimation to warming and elevated CO<sub>2</sub> as inferred from least-cost  
3490      optimality theory. *Global Change Biology* 26(9), 5202–5216.
- 3491      Smith, N. G., T. F. Keenan, I. C. Prentice, H. Wang, I. J. Wright, Ü. Niinemets,  
3492      K. Y. Crous, T. F. Domingues, R. Guerrieri, F. oko Ishida, J. Kattge, E. L.  
3493      Kruger, V. Maire, A. Rogers, S. P. Serbin, L. Tarvainen, H. F. Togashi,  
3494      P. A. Townsend, M. Wang, L. K. Weerasinghe, and S.-X. Zhou (2019).  
3495      Global photosynthetic capacity is optimized to the environment. *Ecology*  
3496      *Letters* 22(3), 506–517.
- 3497      Smith, N. G., D. L. Lombardozzi, A. Tawfik, G. B. Bonan, and J. S. Dukes  
3498      (2017). Biophysical consequences of photosynthetic temperature acclimation  
3499      for climate. *Journal of Advances in Modeling Earth Systems* 9(1), 536–547.
- 3500      Smith, N. G., S. L. Malyshev, E. Shevliakova, J. Kattge, and J. S. Dukes  
3501      (2016). Foliar temperature acclimation reduces simulated carbon sensitivity  
3502      to climate. *Nature Climate Change* 6(4), 407–411.
- 3503      Smith, S. E. and D. J. Read (2008). *Mycorrhizal Symbiosis*. Academic Press.
- 3504      Soil Survey Staff (2022). Web Soil Survey.
- 3505      Soudzilovskaia, N. A., J. C. Douma, A. A. Akhmetzhanova, P. M. van Bode-  
3506      gom, W. K. Cornwell, E. J. Moens, K. K. Treseder, and J. H. C. Cornelissen  
3507      (2015). Global patterns of plant root colonization intensity by mycorrhizal  
3508      fungi explained by climate and soil chemistry. *Global Ecology and Biogeogra-*  
3509      *phy* 24(3), 371–382.
- 3510      Stark, J. M. and M. K. Firestone (1995). Mechanisms for soil moisture ef-  
3511      fects on activity of nitrifying bacteria. *Applied and Environmental Microbi-*

- 3512       *ology* 61(1), 218–221.
- 3513       Stocker, B. D., H. Wang, N. G. Smith, S. P. Harrison, T. F. Keenan, D. San-
- 3514       doval, T. Davis, and I. C. Prentice (2020). P-model v1.0: An optimality-
- 3515       based light use efficiency model for simulating ecosystem gross primary pro-
- 3516       duction. *Geoscientific Model Development* 13(3), 1545–1581.
- 3517       Stocker, B. D., J. Zscheischler, T. F. Keenan, I. C. Prentice, J. Peñuelas, and
- 3518       S. I. Seneviratne (2018). Quantifying soil moisture impacts on light use
- 3519       efficiency across biomes. *New Phytologist* 218(4), 1430–1449.
- 3520       Sulman, B. N., D. T. Roman, K. Yi, L. Wang, R. P. Phillips, and K. A.
- 3521       Novick (2016). High atmospheric demand for water can limit forest car-
- 3522       bon uptake and transpiration as severely as dry soil. *Geophysical Research*
- 3523       *Letters* 43(18), 9686–9695.
- 3524       Sulman, B. N., E. Shevliakova, E. R. Brzostek, S. N. Kivlin, S. L. Malyshev,
- 3525       D. N. L. Menge, and X. Zhang (2019). Diverse mycorrhizal associations
- 3526       enhance terrestrial C storage in a global model. *Global Biogeochemical Cy-*
- 3527       *cles* 33(4), 501–523.
- 3528       Sweet, S. K., D. W. Wolfe, A. DeGaetano, and R. Benner (2017). Anatomy
- 3529       of the 2016 drought in the Northeastern United States: Implications for
- 3530       agriculture and water resources in humid climates. *Agricultural and Forest*
- 3531       *Meteorology* 247, 571–581.
- 3532       Taylor, B. N. and D. N. L. Menge (2018). Light regulates tropical symbiotic
- 3533       nitrogen fixation more strongly than soil nitrogen. *Nature Plants* 4(9), 655–
- 3534       661.

- 3535** Terrer, C., S. Vicca, B. A. Hungate, R. P. Phillips, and I. C. Prentice (2016).  
**3536** Mycorrhizal association as a primary control of the CO<sub>2</sub> fertilization effect.  
**3537** *Science* 353(6294), 72–74.
- 3538** Terrer, C., S. Vicca, B. D. Stocker, B. A. Hungate, R. P. Phillips, P. B. Reich,  
**3539** A. C. Finzi, and I. C. Prentice (2018). Ecosystem responses to elevated CO<sub>2</sub>  
**3540** governed by plant–soil interactions and the cost of nitrogen acquisition. *New*  
**3541** *Phytologist* 217(2), 507–522.
- 3542** Thieurmel, B. and A. Elmarhraoui (2019). suncalc: Compute sun position,  
**3543** sunlight phases, moon position, and lunar phase.
- 3544** Thomas, R. Q., E. N. J. Brookshire, and S. Gerber (2015). Nitrogen limita-  
**3545** tion on land: how can it occur in Earth system models? *Global Change*  
**3546** *Biology* 21(5), 1777–1793.
- 3547** Thomas, R. Q., S. Zaehle, P. H. Templer, and C. L. Goodale (2013). Global pat-  
**3548** terns of nitrogen limitation: confronting two global biogeochemical models  
**3549** with observations. *Global Change Biology* 19(10), 2986–2998.
- 3550** Thornton, P. E., J.-F. Lamarque, N. A. Rosenbloom, and N. M. Mahowald  
**3551** (2007). Influence of carbon-nitrogen cycle coupling on land model response  
**3552** to CO<sub>2</sub> fertilization and climate variability. *Global Biogeochemical Cy-*  
**3553** *cles* 21(4), GB4018.
- 3554** Tingey, D. T., D. L. Phillips, and M. G. Johnson (2000). Elevated CO<sub>2</sub> and  
**3555** conifer roots: effects on growth, life span and turnover. *New Phytolo-*  
**3556** *gist* 147(1), 87–103.
- 3557** Udvardi, M. and P. S. Poole (2013). Transport and metabolism in legume-

- 3558 rhizobia symbioses. *Annual Review of Plant Biology* 64, 781–805.
- 3559 USDA NRCS (2022). The PLANTS Database.
- 3560 Uselman, S. M., R. G. Qualls, and R. B. Thomas (2000). Effects of increased  
3561 atmospheric CO<sub>2</sub>, temperature, and soil N availability on root exudation  
3562 of dissolved organic carbon by an N-fixing tree (*Robinia pseudoacacia* L.).  
3563 *Plant and Soil* 222, 191–202.
- 3564 van Diepen, L. T. A., E. A. Lilleskov, K. S. Pregitzer, and R. M. Miller (2007).  
3565 Decline of arbuscular mycorrhizal fungi in northern hardwood forests ex-  
3566 posed to chronic nitrogen additions. *New Phytologist* 176(1), 175–183.
- 3567 Vance, C. P. and G. H. Heichel (1991). Carbon in N<sub>2</sub> fixation: Limitation or  
3568 exquisite adaptation. *Annual Review of Plant Physiology and Plant Molec-*  
3569 *ular Biology* 42(1), 373–392.
- 3570 Viet, H. D., J.-H. Kwak, K.-S. Lee, S.-S. Lim, M. Matsushima, S. X. Chang,  
3571 K.-H. Lee, and W.-J. Choi (2013). Foliar chemistry and tree ring δ<sup>13</sup>C of  
3572 *Pinus densiflora* in relation to tree growth along a soil pH gradient. *Plant*  
3573 *and Soil* 363(1-2), 101–112.
- 3574 Vitousek, P. M., K. Cassman, C. C. Cleveland, T. Crews, C. B. Field, N. B.  
3575 Grimm, R. W. Howarth, R. Marino, L. Martinelli, E. B. Rastetter, and  
3576 J. I. Sprent (2002). Towards an ecological understanding of biological nitro-  
3577 gen fixation. In *The Nitrogen Cycle at Regional to Global Scales*, pp. 1–45.  
3578 Springer Netherlands.
- 3579 Vitousek, P. M. and R. W. Howarth (1991). Nitrogen limitation on land and in  
3580 the sea: How can it occur? *Biogeochemistry* 13(2), 87–115.

- 3581 Vitousek, P. M., S. Porder, B. Z. Houlton, and O. A. Chadwick (2010).
- 3582 Terrestrial phosphorus limitation: mechanisms, implications, and nitro-
- 3583 gen–phosphorus interactions. *Ecological Applications* 20(1), 5–15.
- 3584 Walker, A. P., A. P. Beckerman, L. Gu, J. Kattge, L. A. Cernusak, T. F.
- 3585 Domingues, J. C. Scales, G. Wohlfahrt, S. D. Wullschleger, and F. I. Wood-
- 3586 ward (2014). The relationship of leaf photosynthetic traits -  $V_{cmax}$  and  $J_{max}$
- 3587 - to leaf nitrogen, leaf phosphorus, and specific leaf area: a meta-analysis
- 3588 and modeling study. *Ecology and Evolution* 4(16), 3218–3235.
- 3589 Walker, A. P., A. L. Johnson, A. Rogers, J. Anderson, R. A. Bridges, R. A.
- 3590 Fisher, D. Lu, D. M. Ricciuto, S. P. Serbin, and M. Ye (2021). Multi-
- 3591 hypothesis comparison of Farquhar and Collatz photosynthesis models re-
- 3592 veals the unexpected influence of empirical assumptions at leaf and global
- 3593 scales. *Global Change Biology* 27(4), 804–822.
- 3594 Wang, H., I. C. Prentice, T. F. Keenan, T. W. Davis, I. J. Wright, W. K.
- 3595 Cornwell, B. J. Evans, and C. Peng (2017). Towards a universal model for
- 3596 carbon dioxide uptake by plants. *Nature Plants* 3(9), 734–741.
- 3597 Wang, H., I. C. Prentice, I. J. Wright, D. I. Warton, S. Qiao, X. Xu, J. Zhou,
- 3598 Kikuzawa, and N. C. Stenseth (2023). Leaf economics fundamentals ex-
- 3599 plained by optimality principles. *Science Advances* 9(3), eadd566.
- 3600 Wang, J., J. M. Knops, C. E. Brassil, and C. Mu (2017). Increased productivity
- 3601 in wet years drives a decline in ecosystem stability with nitrogen additions
- 3602 in arid grasslands. *Ecology* 98(7), 1779–1786.
- 3603 Wang, W., Y. Wang, G. Hoch, Z. Wang, and J. Gu (2018). Linkage of root mor-
- 3604 phology to anatomy with increasing nitrogen availability in six temperate

- 3605** tree species. *Plant and Soil* 425(1-2), 189–200.
- 3606** Weatherburn, M. W. (1967). Phenol-hypochlorite reaction for determination of
- 3607** ammonia. *Analytical Chemistry* 39(8), 971–974.
- 3608** Wellburn, A. R. (1994). The spectral determination of chlorophylls a and b, as
- 3609** well as total carotenoids, using various solvents with spectrophotometers of
- 3610** different resolution. *Journal of Plant Physiology* 144(3), 307–313.
- 3611** Wen, Z., P. J. White, J. Shen, and H. Lambers (2022). Linking root exuda-
- 3612** tion to belowground economic traits for resource acquisition. *New Phytolo-*
- 3613** *gist* 233(4), 1620–1635.
- 3614** Westerband, A. C., I. J. Wright, V. Maire, J. Paillassa, I. C. Prentice, O. K.
- 3615** Atkin, K. J. Bloomfield, L. A. Cernusak, N. Dong, S. M. Gleason, C. Guil-
- 3616** herme Pereira, H. Lambers, M. R. Leishman, Y. Malhi, and R. H. Nolan
- 3617** (2023). Coordination of photosynthetic traits across soil and climate gradi-
- 3618** ents. *Global Change Biology* 29(3), 1–29.
- 3619** Wieder, W. R., C. C. Cleveland, W. K. Smith, and K. Todd-Brown (2015).
- 3620** Future productivity and carbon storage limited by terrestrial nutrient avail-
- 3621** ability. *Nature Geoscience* 8(6), 441–444.
- 3622** Wieder, W. R., D. M. Lawrence, R. A. Fisher, G. B. Bonan, S. J. Cheng, C. L.
- 3623** Goodale, A. S. Grandy, C. D. Koven, D. L. Lombardozzi, K. W. Oleson,
- 3624** and R. Q. Thomas (2019). Beyond static benchmarking: using experimental
- 3625** manipulations to evaluate land model assumptions. *Global Biogeochemical*
- 3626** *Cycles* 33(10), 1289–1309.
- 3627** Wright, I. J., P. B. Reich, and M. Westoby (2003). Least-cost input mixtures

- 3628 of water and nitrogen for photosynthesis. *The American Naturalist* 161(1),  
3629 98–111.
- 3630 Wright, I. J., P. B. Reich, M. Westoby, D. D. Ackerly, Z. Baruch, F. Bongers,  
3631 J. Cavender-Bares, T. Chapin, J. H. C. Cornelissen, M. Diemer, J. Flexas,  
3632 E. Garnier, P. K. Groom, J. Gulias, K. Hikosaka, B. B. Lamont, T. Lee,  
3633 W. Lee, C. Lusk, J. J. Midgley, M.-L. Navas, Ü. Niinemets, J. Oleksyn,  
3634 N. Osada, H. Poorter, P. Poot, L. Prior, V. I. Pyankov, C. Roumet, S. C.  
3635 Thomas, M. G. Tjoelker, E. J. Veneklaas, and R. Villar (2004). The world-  
3636 wide leaf economics spectrum. *Nature* 428(6985), 821–827.
- 3637 Xu-Ri and I. C. Prentice (2017). Modelling the demand for new nitrogen fixation  
3638 by terrestrial ecosystems. *Biogeosciences* 14(7), 2003–2017.
- 3639 Yahdjian, L., L. A. Gherardi, and O. E. Sala (2011). Nitrogen limitation in  
3640 arid-subhumid ecosystems: A meta-analysis of fertilization studies. *Journal  
3641 of Arid Environments* 75(8), 675–680.
- 3642 Yuan, W., Y. Zheng, S. Piao, P. Ciais, D. Lombardozzi, Y. Wang, Y. Ryu,  
3643 G. Chen, W. Dong, Z. Hu, A. K. Jain, C. Jiang, E. Kato, S. Li, S. Lienert,  
3644 S. Liu, J. E. Nabel, Z. Qin, T. Quine, S. Sitch, W. K. Smith, F. Wang,  
3645 C. Wu, Z. Xiao, and S. Yang (2019). Increased atmospheric vapor pressure  
3646 deficit reduces global vegetation growth. *Science Advances* 5(8), 1–12.
- 3647 Zaehle, S., B. E. Medlyn, M. G. De Kauwe, A. P. Walker, M. C. Dietze, T. Hick-  
3648 ler, Y. Luo, Y. P. Wang, B. El-Masri, P. Thornton, A. Jain, S. Wang,  
3649 D. Warlind, E. Weng, W. Parton, C. M. Iversen, A. Gallet-Budynek, H. Mc-  
3650 carthy, A. C. Finzi, P. J. Hanson, I. C. Prentice, R. Oren, and R. J. Norby  
3651 (2014). Evaluation of 11 terrestrial carbon-nitrogen cycle models against

- 3652** observations from two temperate Free-Air CO<sub>2</sub> Enrichment studies. *New*  
**3653** *Phytologist* 202(3), 803–822.
- 3654** Zaehle, S., S. Sitch, B. Smith, and F. Hatterman (2005). Effects of parame-  
**3655** ter uncertainties on the modeling of terrestrial biosphere dynamics. *Global*  
**3656** *Biogeochemical Cycles* 19(3), GB3020.
- 3657** Zhu, Q., W. J. Riley, J. Tang, N. Collier, F. M. Hoffman, X. Yang, and G. Bisht  
**3658** (2019). Representing nitrogen, phosphorus, and carbon interactions in the  
**3659** E3SM land model: development and global benchmarking. *Journal of Ad-*  
**3660** *vances in Modeling Earth Systems* 11(7), 2238–2258.
- 3661** Ziegler, C., M. E. Dusenge, B. Nyirambangutse, E. Zibera, G. Wallin, and  
**3662** J. Uddling (2020). Contrasting dependencies of photosynthetic capacity on  
**3663** leaf nitrogen in early- and late-successional tropical montane tree species.  
**3664** *Frontiers in Plant Science* 11, 1–12.
- 3665** Ziehn, T., J. Kattge, W. Knorr, and M. Scholze (2011). Improving the pre-  
**3666** dictability of global CO<sub>2</sub> assimilation rates under climate change. *Geophys-*  
**3667** *ical Research Letters* 38(10), L10404.

**3668      Appendix A: Supplemental material for "Structural carbon costs to**  
**3669      acquire nitrogen are determined by nitrogen and light availability in**  
**3670      two species with different nitrogen acquisition strategies"**

**Table A1.** Summary table containing volumes of compounds used to create modified Hoagland's solutions for each soil nitrogen fertilization treatment. All volumes are expressed as milliliters per liter (mL/L)

Compound	0 ppm N	70 ppm N	210 ppm N	630 ppm N
1 M NH <sub>4</sub> H <sub>2</sub> PO <sub>4</sub>	0	0.33	1	1
2 M KNO <sub>3</sub>	0	0.67	2	2
2 M Ca(NO <sub>3</sub> ) <sub>2</sub>	0	0.67	2	2
1 M NH <sub>4</sub> NO <sub>3</sub>	0	0.33	1	0
8 M NH <sub>4</sub> NO <sub>3</sub>	0	0	0	2
1 M KH <sub>2</sub> PO <sub>4</sub>	1	0.67	0	0
1 M KCl	4	1.33	0	0
1 M CaCO <sub>3</sub>	4	3	0	0
2 M MgSO <sub>4</sub>	1	1	1	1
10% Fe-EDTA	1	1	1	1
Trace Elements	1	1	1	1

**Table A2.** Analysis of variance results exploring species-specific effects of light availability, nitrogen fertilization, and their interactions on the ratio of whole plant biomass to pot volume (g L<sup>-1</sup>)\*

	df	Coefficient	$\chi^2$	p
<i>G. hirsutum</i>				
Intercept		0.740	-	-
Light (L)	1	-4.23E-03	189.581	<b>&lt;0.001</b>
Nitrogen (N)	1	7.86E-04	17.927	<b>&lt;0.001</b>
L*N	1	-6.61E-06	4.709	<b>0.030</b>
<i>G. max</i>				
Intercept		-0.233	-	-
Light (L)	1	-1.12E-02	69.500	<b>&lt;0.001</b>
Nitrogen (N)	1	8.29E-04	40.297	<b>&lt;0.001</b>
L*N	1	-8.51E-06	5.548	<b>0.019</b>

**3671** \*Significance determined using Wald's  $\chi^2$  tests ( $p=0.05$ ). P-values less than 0.05  
**3672** are in bold and p-values between 0.05 and 0.1 are italicized. Negative coefficients  
**3673** for light treatments indicate a positive effect of increasing light availability on  
**3674** all response variables, as light availability is treated as percent shade cover in all  
**3675** linear mixed-effects models.

**Table A3.** Slopes of the regression line describing the relationship between each dependent variable and nitrogen fertilization at each light level\*

Shade cover	Slope
<i>G. hirsutum</i>	
0%	<b>8.29E-04<sup>a</sup></b>
30%	<b>5.74E-04<sup>a</sup></b>
50%	<b>4.03E-04<sup>a</sup></b>
80%	1.48E-04 <sup>a</sup>
<i>G. max</i>	
0%	<b>7.86E-04</b>
30%	<b>5.87E-04</b>
50%	<b>4.55E-04</b>
80%	<i>2.57E-05</i>

**3676** \*Slopes represent estimated marginal mean slopes from linear mixed-effects models described in the Methods. Slopes  
**3677** were calculated using the ‘emmeans’ R package (Lenth 2019). Superscripts indicate slopes fit to natural-log (<sup>a</sup>) or  
**3678** square root (<sup>b</sup>) transformed data. Slopes statistically different from zero (Tukey:  $p < 0.05$ ) are indicated in bold.  
**3679** Marginally significant slopes (Tukey:  $0.05 < p < 0.1$ ) are italicized.

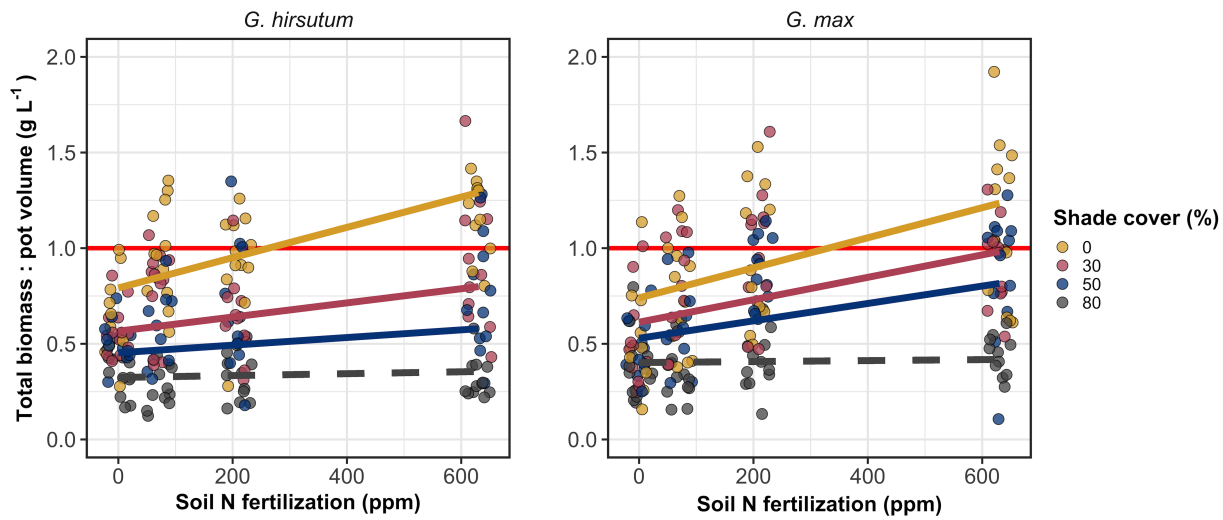


**Figure A1.** Effects of shade cover and nitrogen fertilization on the ratio of plant biomass to rooting volume in *G. hirsutum* (left panel) and *G. max* (right panel). The red horizontal line indicates the recommended  $1 \text{ g L}^{-1}$  threshold for BVR recommended by Poorter et al. (2012) to avoid pot size-induced growth limitation. Nitrogen fertilization treatments are represented on the x-axis. Shade cover treatments are represented through colored points and trendlines. Points are jittered for visibility. Yellow points and trendlines represent the 0% shade cover treatment, blue points and trendlines represent the 30% shade cover treatment, green points and trendlines represent the 50% shade cover treatment, and purple points and trendlines represent the 80% shade cover treatment. Solid trendlines indicate slopes that are significantly different from zero (Tukey:  $p < 0.05$ ), while dashed trendlines indicate slopes that are not statistically different from zero.

**3680      Appendix B: Supplemental material for "Soil nitrogen availability**  
**3681      modifies leaf nitrogen economies in mature temperate deciduous**  
**3682      forests: a direct test of photosynthetic least-cost theory"**

**Table B1.** Sample sizes of each species, abbreviated by their USDA NRCS PLANTS database code, within each plot at each site\*

	ACRU	ACSA	FAGR	FRAM	QURU	$N_{\text{plot}}$
Bald Hill						
+N; +S	0	6	1	0	1	8
+N; -S	1	2	2	0	1	6
-N; +S	2	2	0	0	2	6
-N; -S	2	3	3	0	2	10
Carter Creek						
+N; +S	0	6	1	2	0	9
+N; -S	0	4	0	2	0	6
-N; +S	0	5	1	4	0	10
-N; -S	0	7	0	0	0	7
Mount Pleasant						
+N; +S	3	2	1	0	3	9
+N; -S	0	5	4	1	0	10
-N; +S	1	2	4	0	0	7
-N; -S	3	3	1	2	1	10
$N_{\text{spp}}$	12	47	18	11	10	98

**3683** \*Plots within each site are represented based on nitrogen and sulfur addition  
**3684** status. The final column on the right depicts total sample size per plot in each  
**3685** site ( $N_{\text{plot}}$ ) and the final row on the bottom represents cumulative species sample  
**3686** size across all plots and all sites ( $N_{\text{spp}}$ ). Key: ACRU=*A. rubrum*; ACSA=*A.*  
**3687** *saccharum*; FAGR=*F. grandifolia*; FRAM=*F. americana*; QURU=*Q. rubra*

**Table B2.** Analysis of variance results exploring the linear effect of leaf temperature on net photosynthesis rate ( $A_{\text{net}}$ ;  $\mu\text{mol m}^{-2} \text{s}^{-1}$ ) and stomatal conductance ( $g_{\text{sw}}$ ;  $\mu\text{mol m}^{-2} \text{s}^{-1}$ ) measured at  $400 \mu\text{mol mol}^{-1} \text{CO}_2$

	df	$A_{\text{net}}$		$g_{\text{sw}}$	
		$\chi^2$	p	$\chi^2$	p
Leaf temperature	1	1.287	0.257	1.716	0.190

**3688** \*Results detail linear mixed effects model where temperature was regressed against  
**3689** net photosynthesis or stomatal conductance, with site and species designated as  
**3690** random intercept terms. Significance was determined using Type II Wald  $\chi^2$  tests  
**3691** ( $\alpha=0.05$ ).

**Table B3.** Second order log-polynomial regression coefficients that described the effect of leaf temperature on net photosynthesis ( $A_{\text{net}}$ ;  $\mu\text{mol m}^{-2} \text{s}^{-1}$ ) and stomatal conductance ( $g_s$ ;  $\mu\text{mol m}^{-2} \text{s}^{-1}$ ) measured at 400  $\mu\text{mol mol}^{-1} \text{CO}_2$ \*

	a	b	c
$A_{\text{net}}$	9.422	-0.573	0.010
$g_s$	-0.170	-0.186	0.003

**3692** \*Net photosynthesis and stomatal conductance values were fit to the log-polynomial  
**3693** equation  $\log(y) = a + bx + cx^2$ , where x is leaf temperature in °C.

**Table B4.** Mean, standard error, and 95% confidence interval ranges of soil nitrogen availability estimates across all measured plots. All units are expressed as  $\mu\text{g N g}^{-1}$  resin  $\text{d}^{-1}$

Site	Treatment	Mean	SE	Lower 95% CI	Upper 95% CI
Bald Hill	Ammonium sulfate	27.11	6.14	15.08	39.13
Bald Hill	Control	14.41	5.02	4.56	24.26
Bald Hill	Sodium nitrate	20.65	3.15	14.46	26.83
Bald Hill	Sulfur	6.33	2.19	2.04	10.62
Carter Creek	Ammonium sulfate	26.94	5.36	16.43	37.44
Carter Creek	Control	19.87	1.92	16.10	23.64
Carter Creek	Sodium nitrate	15.51	4.16	7.36	23.65
Carter Creek	Sulfur	5.50	1.40	2.75	8.25
Mount Pleasant	Ammonium sulfate	8.02	2.31	3.49	12.56
Mount Pleasant	Control	2.00	0.57	0.89	3.11
Mount Pleasant	Sodium nitrate	2.52	0.68	1.19	3.85
Mount Pleasant	Sulfur	2.42	0.39	1.66	3.17

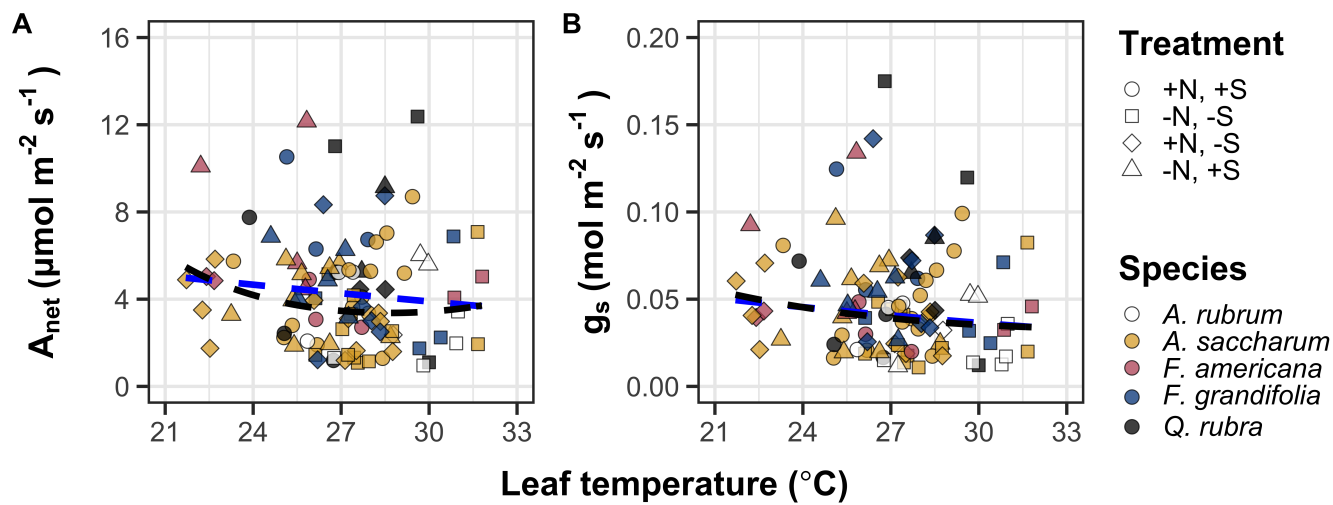


**Figure B1.** Effects of leaf temperature on net photosynthesis rate (A) and stomatal conductance (B) values when measured at  $400 \mu\text{mol mol}^{-1}$   $\text{CO}_2$ . Leaf temperature is represented on the x-axis, while species are represented as colored points. Colored points and shapes are as explained in Figure 3.1. The dashed blue trendline describes the linear relationship between leaf temperature and each response variable, while the dashed black trendline describes the same relationship with a log-polynomial regression equation.

**3694 Appendix C: Supplemental material for "The relative cost of resource  
3695 use for photosynthesis drives variance in leaf nitrogen content across a  
3696 climate and soil resource availability gradient"**

**3697 C.1 Calculations for soil water holding capacity**

**3698** Water holding capacity ( $\theta_{WHC}$ ; mm) was calculated as a function of the volumetric  
**3699** soil water storage at field capacity ( $W_{FC}$ ; m<sup>3</sup> m<sup>-3</sup>), and the volumetric soil water  
**3700** storage at wilting point ( $W_{PWP}$ ; m<sup>3</sup> m<sup>-3</sup>):

$$\theta_{WHC} = (W_{FC} - W_{PWP})(1 - f_{gravel}) * \min(z_{bedrock}, z_{max}) \quad (\text{C4.1})$$

**3701** where  $f_{gravel}$  (%) is the fraction of gravel content in soil,  $z_{bedrock}$  (mm) is the  
**3702** distance to bedrock, and  $z_{max}$  (mm) is the maximum allowable distance to bedrock,  
**3703** set to 2000mm.  $W_{FC}$  is calculated as:

$$\theta_{FC} = k_{fc} + (1.283 * (k_{fc})^2 - 0.374 * k_{fc} - 0.015) \quad (\text{C4.2})$$

**3704** where

$$\begin{aligned} k_{fc} = & -0.251 * f_{sand} + 0.195 * f_{clay} + 0.011 * f_{OM} \\ & + 0.006 * (f_{sand} * f_{OM}) - 0.027 * (f_{clay} \\ & * f_{OM}) + 0.452 * (f_{sand} * f_{clay}) + 0.299 \end{aligned} \quad (\text{C4.3})$$

**3705**  $W_{PWP}$  is calculated as:

$$W_{PWP} = k_{pwp} + (0.14 * k_{pwp} - 0.02) \quad (\text{C4.4})$$

**3706** where

$$\begin{aligned} k_{pwp} = & -0.024 * f_{sand} + 0.487 * f_{clay} + 0.006 * f_{OM} \\ & + 0.005 * (f_{sand} * f_{OM}) - 0.013 * (f_{clay} \\ & * f_{OM}) + 0.068 * (f_{sand} * f_{clay}) + 0.031 \end{aligned} \quad (\text{C4.5})$$

**3707** In Equations C4.4 and C4.5,  $f_{sand}$  (%) is the fraction of sand content in soil

**3708** (%),  $f_{clay}$  (%) is the fraction of clay content in soil (%), and  $f_{OM}$  is the fraction of

**3709** organic matter in soil (%). Organic matter in the soil was calculated by converting

**3710** soil organic carbon data extracted from SoilGrids 2.0 to soil organic matter using

**3711** the van Bemmelen factor (1.724 conversion factor).

**Table C1.** List of sampled species and their plant functional group assignment

Symbol	Species	Photo. pathway	Growth duration	Growth habit	N-fixer?	Plant functional group	Number sampled
ACAN11	<i>Acaciella angustissima</i>	c3	perennial	forb	yes	c3_legume	3
AMAR2	<i>Ambrosia artemisiifolia</i>	c3	annual	forb	no	c3_nonlegume	25
AMPS	<i>Ambrosia psilostachya</i>	c3	perennial	forb	no	c3_nonlegume	32
ARAL3	<i>Argemone albiflora</i>	c3	annual	forb	no	c3_nonlegume	3
ARPU9	<i>Aristida purpurea</i>	c4	perennial	graminoid	no	c4_nonlegume	2
ASAS	<i>Asclepias asperula</i>	c3	perennial	forb	no	c3_nonlegume	3
ASLA4	<i>Asclepias latifolia</i>	c3	perennial	forb	no	c3_nonlegume	3
ASSY	<i>Asclepias syriaca</i>	c3	perennial	forb	no	c3_nonlegume	18
BOIS	<i>Bothriochloa ischaemum</i>	c4	perennial	graminoid	no	c4_nonlegume	6
BOSA	<i>Bothriochloa saccharoides</i>	c4	perennial	graminoid	no	c4_nonlegume	6
CAPL3	<i>Carex planostachys</i>	c4	perennial	graminoid	no	c4_nonlegume	3
CAREX	<i>Carex</i> spp.	c4	perennial	graminoid	no	c4_nonlegume	16
CHFE3	<i>Chamaesyce fendleri</i>	c3	perennial	forb	no	c3_nonlegume	2
CHPI8	<i>Chrysopsis pilosa</i>	c3	annual	forb	no	c3_nonlegume	3
COCO13	<i>Conoclinium coelestinum</i>	c3	perennial	forb	no	c3_nonlegume	3
COER	<i>Commelina erecta</i>	c3	perennial	forb	no	c3_nonlegume	3
CRGLL	<i>Croton glandulosus</i>	c3	annual	forb	no	c3_nonlegume	22
CYDA	<i>Cynodon dactylon</i>	c4	perennial	graminoid	no	c4_nonlegume	15
DIAN	<i>Dichanthium annulatum</i>	c4	perennial	graminoid	no	c4_nonlegume	8
ENPE4	<i>Engelmannia peristenia</i>	c3	perennial	forb	no	c3_nonlegume	6
EUMA8	<i>Euphorbia marginata</i>	c3	annual	forb	no	c3_nonlegume	6
GAPU	<i>Gaillardia pulchella</i>	c3	annual	forb	no	c3_nonlegume	16
GLGO	<i>Glandularia gooddingii</i>	c3	perennial	forb	no	c3_nonlegume	2
HEAN3	<i>Helianthus annuus</i>	c3	annual	forb	no	c3_nonlegume	6

**Table C2.** List of sampled species and their plant functional group assignment (cont.)

Symbol	Species	Photo. pathway	Growth duration	Growth habit	N-fixer?	Plant functional group	Number sampled
HECA8	<i>Heterotheca canescens</i>	c3	perennial	forb	no	c3_nonlegume	2
HETE3	<i>Heliotropium tenellum</i>	c3	annual	forb	no	c3_nonlegume	3
IVAX	<i>Iva axillaris</i>	c3	perennial	forb	no	c3_nonlegume	4
LIAT	<i>Lilaeopsis attenuata</i>	c3	perennial	forb	no	c3_nonlegume	3
LIPU	<i>Liatris punctata</i>	c3	perennial	forb	no	c3_nonlegume	3
LOPE	<i>Lolium perenne</i>	c3	perennial	graminoid	no	c3_nonlegume	9
MIQU2	<i>Mimosa quadrivalvis</i>	c3	perennial	forb	yes	c3_legume	15
NALE3	<i>Nassella leucotricha</i>	c3	perennial	graminoid	no	c3_nonlegume	19
OECU2	<i>Oenothera curtiflora</i>	c3	annual	forb	no	c3_nonlegume	3
OENOT	<i>Oenothera</i> spp.	c3	annual	forb	no	c3_nonlegume	1
PAVI2	<i>Panicum virgatum</i>	c4	perennial	graminoid	no	c4_nonlegume	12
RACO3	<i>Ratibida columnifera</i>	c3	perennial	forb	no	c3_nonlegume	40
RHSET	<i>Rhynchosia senna</i>	c3	perennial	forb	yes	c3_legume	1
RUHI2	<i>Rudbeckia hirta</i>	c3	perennial	forb	no	c3_nonlegume	3
RUNU	<i>Ruellia nudiflora</i>	c3	perennial	forb	no	c3_nonlegume	15
RUTR	<i>Rubus trivialis</i>	c3	perennial	vine	no	c3_nonlegume	3
SAFA2	<i>Salvia farinacea</i>	c3	perennial	forb	no	c3_nonlegume	7
SCHIZ4	<i>Schizachyrium</i> spp.	c4	perennial	graminoid	no	c4_nonlegume	8
SCSC	<i>Schizachyrium scoparium</i>	c4	perennial	graminoid	no	c4_nonlegume	3
SODI	<i>Solanum dimidiatum</i>	c3	perennial	forb	no	c3_nonlegume	1
SOEL	<i>Solanum elaeagnifolium</i>	c3	perennial	forb	no	c3_nonlegume	53
SOHA	<i>Sorghum halapense</i>	c4	perennial	graminoid	no	c4_nonlegume	38
STTE3	<i>Stillingia texana</i>	c3	perennial	forb	no	c3_nonlegume	3
VEOC	<i>Verbesina occidentalis</i>	c3	perennial	forb	no	c3_nonlegume	3
VEST	<i>Verbena stricta</i>	c3	perennial	forb	no	c3_nonlegume	3

**Table C3.** Model selection results for soil moisture and vapor pressure deficit. Soil moisture was used in a bivariate regression against log-transformed  $\beta$ , while vapor pressure deficit was used in bivariate regressions against leaf  $C_l:C_a$

Day	Soil moisture		VPD	
	AICc	RMSE	AICc	RMSE
1	1431.77	0.8400	-772.71	0.0853
2	1431.76	0.8400	-775.47	0.0849
3	1431.78	0.8400	-770.86	0.0854
4	1431.79	0.8401	<b>-793.49</b>	<b>0.0839</b>
5	1431.79	0.8401	-771.66	0.0853
6	1431.78	0.8401	-771.66	0.0853
7	1431.78	0.8401	-771.05	0.0854
8	1431.76	0.8401	-770.94	0.0854
9	1431.75	0.8401	-770.11	0.0854
10	1431.74	0.8401	-770.08	0.0855
15	1431.54	0.8401	-768.64	0.0856
20	1431.40	0.8401	-769.77	0.0855
30	1431.23	0.8400	-772.18	0.0853
60	1429.84	0.8391	-779.06	0.0848
90	<b>1429.14</b>	<b>0.8385</b>	-773.99	0.0852

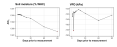


**Figure C1.** Model selection results exploring relevant timescales for soil moisture (left panel) and vapor pressure deficit (right panel). The x-axis indicates the number of days before each site visit and the y-axis notes the corrected Akaike Information Criterion value. The timescale with the lowest AICc value, and therefore most relevant timescale to include in statistical models, is noted as a red point.

**3712 Appendix D: Supplemental material for "Optimal resource investment  
 3713 to photosynthetic capacity maximizes nutrient allocation to whole  
 3714 plant growth under elevated CO<sub>2</sub>"**

**Table D1.** Summary table containing volumes of compounds used to create modified Hoagland's solutions for each soil nitrogen fertilization treatment. All volumes are expressed as milliliters per liter (mL/L)

Compound	0 ppm N	35 ppm N	70 ppm N	105 ppm N	140 ppm N
1 M NH <sub>4</sub> H <sub>2</sub> PO <sub>4</sub>	0	0.165	0.33	0.5	0.67
2 M KNO <sub>3</sub>	0	0.335	0.67	1	1.33
2 M Ca(NO <sub>3</sub> ) <sub>2</sub>	0	0.335	0.67	1	1.33
1 M NH <sub>4</sub> NO <sub>3</sub>	0	0.165	0.33	0.5	0.67
8 M NH <sub>4</sub> NO <sub>3</sub>	0	0	0	0	0
1 M KH <sub>2</sub> PO <sub>4</sub>	1	0.85	0.67	0.5	0.33
1 M KCl	3	2.45	2	1.5	1
1 M CaCO <sub>3</sub>	4	3.33	2.67	2	1.33
2 M MgSO <sub>4</sub>	1	1	1	1	1
10% Fe-EDTA	1	1	1	1	1
Trace elements	1	1	1	1	1

Compound	210 ppm N	280 ppm N	350 ppm N	630 ppm N
1 M NH <sub>4</sub> H <sub>2</sub> PO <sub>4</sub>	1	1	1	1
2 M KNO <sub>3</sub>	2	2	2	2
2 M Ca(NO <sub>3</sub> ) <sub>2</sub>	2	2	2	2
1 M NH <sub>4</sub> NO <sub>3</sub>	1	3.5	0	0
8 M NH <sub>4</sub> NO <sub>3</sub>	0	0	0.75	2
1 M KH <sub>2</sub> PO <sub>4</sub>	0	0	0	0
1 M KCl	0	0	0	0
1 M CaCO <sub>3</sub>	0	0	0	0
2 M MgSO <sub>4</sub>	1	1	1	1
10% Fe-EDTA	1	1	1	1
Trace elements	1	1	1	1

**Table D2.** Summary of the daily growth chamber growing condition program

Time	Air temperature (°C)	Light (%)
09:00	21	25
09:45		50
10:30	25	75
11:15		100
22:45	21	75
23:30		50
00:15	17	25
01:00		0

**Table D3.** Effects of CO<sub>2</sub>, fertilization, and inoculation on whole plant biomass: pot volume (BVR; g L<sup>-1</sup>)\*

	df	Coefficient	$\chi^2$	p
(Intercept)	-	1.33E-01	-	-
CO <sub>2</sub>	1	1.53E-01	146.004	<b>&lt;0.001</b>
Inoculation (I)	1	4.19E-01	19.320	<b>&lt;0.001</b>
Fertilization (N)	1	1.90E-03	279.387	<b>&lt;0.001</b>
CO <sub>2</sub> *I	1	1.03E-01	0.007	0.934
CO <sub>2</sub> *N	1	2.44E-03	49.725	<b>&lt;0.001</b>
I*N	1	-6.90E-04	9.006	<b>0.003</b>
CO <sub>2</sub> *I*N	1	-4.95E-04	0.640	0.424

**3715** \*Significance determined using Type II Wald  $\chi^2$  tests ( $\alpha=0.05$ ). P-values less  
**3716** than 0.05 are in bold. Key: df=degrees of freedom;  $\chi^2$ =Wald Type II chi-square  
**3717** test statistic.

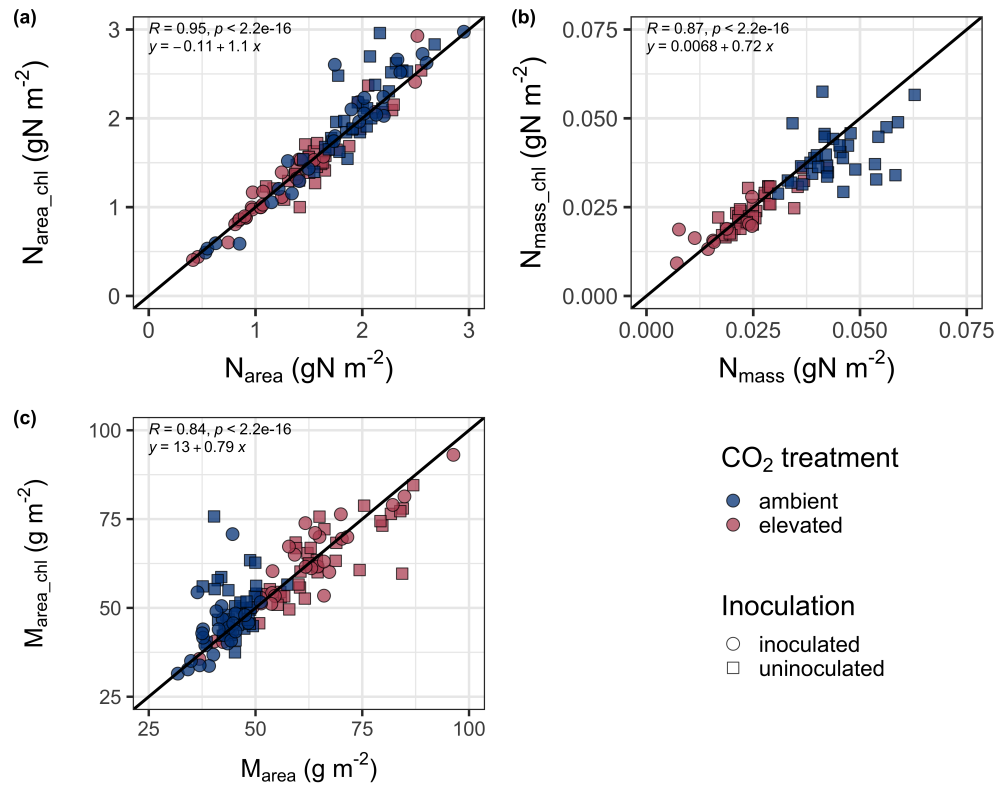


**Figure D1.** Relationships between area-based leaf nitrogen content (a), mass-based leaf nitrogen content (b), and leaf mass per unit leaf area (c) measured on the focal leaf used to generate  $A_{net}/C_i$  curves (x-axis) and leaf nitrogen content measured on the leaf used for chlorophyll extractions (y-axis). Blue points refer to leaves grown under ambient CO<sub>2</sub> and red points refer leaves grown under elevated CO<sub>2</sub>. Square points indicate uninoculated pots and circular points indicate inoculated pots. Pearson's correlation coefficient, associated *p*-values, and the line of the regression line that described each bivariate are included in the top left corner of each plot. The solid black line visualizes the trend given a 1:1 bivariate relationship.

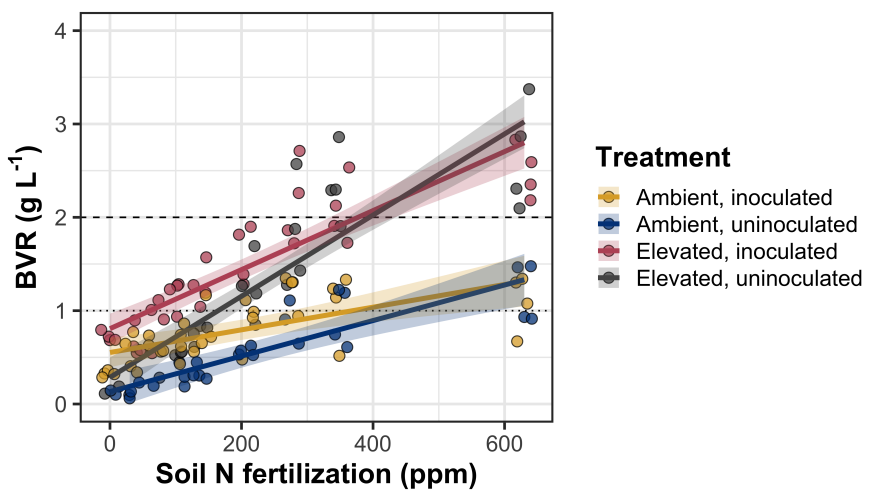


**Figure D2.** Effects of CO<sub>2</sub>, fertilization, and inoculation on the ratio of whole plant biomass to pot volume. Soil nitrogen fertilization is represented on the x-axis in all panels. Yellow points and trendlines indicate inoculated individuals grown under ambient CO<sub>2</sub>, blue points and trendlines indicate uninoculated individuals grown under ambient CO<sub>2</sub>, red points and trendlines indicate inoculated individuals grown under elevated CO<sub>2</sub>, and grey points indicate uninoculated individuals grown under elevated CO<sub>2</sub>. Solid trendlines indicate regression slopes that are different from zero ( $p<0.05$ ). The dotted horizontal line indicates the point where biomass:pot volume exceeds 1 g L<sup>-1</sup>, and the dashed line indicates the point where biomass:pot volume exceeds 2 g L<sup>-1</sup>.